

University of the Western Cape



**Functionalisation of electrospun
nanofibre for lanthanide ion
adsorption from aqueous solution**

by

Omoniyi Kolawole Perea

BSc Chemistry (Ondo State University, Ekiti State)
MSc Chemistry (Ekiti State University, Ekiti State)

A thesis submitted in fulfilment of the requirements for the degree of
Doctor of Philosophy in Chemistry

In the
Department of Chemistry
University of the Western Cape

Supervisor: Prof Leslie Petrik

Co-Supervisor: Dr Katri Laatikainen

March 2018

DECLARATION OF AUTHORSHIP

By submitting this thesis, I declare that “Functionalisation of electrospun nanofibre for lanthanide ion adsorption from aqueous solution” is my own original work and that it has not been submitted for any degree or examination in any other university and that all the sources I used or quoted have been indicated and acknowledged by appropriate references

PEREAO OMONIYI KOLAWOLE



Signature:

Date:

KEYWORDS

Adsorption

Cerium

Diglycolic acid

Electrospinning

Functionalisation

Lanthanide ion

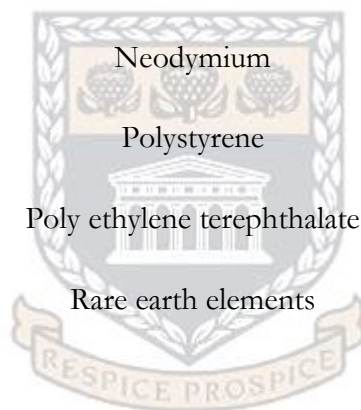
Nanofibre

Neodymium

Polystyrene

Poly ethylene terephthalate

Rare earth elements



ABSTRACT

Rare earth elements (REEs) have widespread use and importance for industrial applications due to their metallurgical, optical and electronic properties. Several typical hydrometallurgical techniques such as adsorption, chemical precipitation, filtration, ion exchange and solvent extraction techniques have been used for separation and recovery of the rare earth metals from aqueous solutions. Adsorption was recognised as one of the most promising methods due to its simplicity, high efficiency and availability. Many adsorbents are being investigated but there are few adsorbents containing specific functional groups in practical use for REEs recovery.

This aim of this study was to develop a nanofibre based adsorbent containing glycolic acid functional groups for the recovery of rare earth metals. Polystyrene (PS) and polyethylene terephthalate (PET) nanofibres were prepared by the electrospinning technique, glycolic acid functional groups were grafted onto the PS or PET nanofibres and the potential of the two modified nanofibre adsorbents for adsorption of Ce^{3+} or Nd^{3+} from aqueous solution were investigated and compared. The adsorption experiments were carried out to investigate the effect of different adsorption parameters such as pH, contact time and initial concentration in a batch system in order to achieve the objectives of this research.

Based on the electrospinning results, PET nanofibres obtained from process parameters of flow rate (1.0 mL/h), solution concentration (10 wt %), electric potential (17 kV) and distance (20 cm) respectively, generated very low average fibre diameters (20 – 150 nm) when compared with PS nanofibres with average fibre diameters of 200 – 600 nm. However, the adsorption tests revealed that polystyrene modified nanofibres (PS-DGA) highly adsorb Ce^{3+} and Nd^{3+} due to the introduction

of a greater number of glycolic acid groups on the surface of PS nanofibres compared to polyethylene terephthalate modified nanofibres (PET-DGA).

The results of different batch experiments conducted showed that PS-DGA equilibrium adsorption was achieved within approximately 20 minutes of contact time. The experimental results showed that the sorption isotherms were well fitted by the Langmuir equations for PS-DGA chelating nanofibre with the values of the correlation coefficient R^2 (>0.99) and a maximum adsorption capacity values of 152.5 mg/g (1.09 mmol/g) and 146.2 mg/g (1.01 mmol/g) for Ce^{3+} or Nd^{3+} respectively at pH 6. Ce^{3+} and Nd^{3+} were readily desorbed from loaded sorbents using 1 M solution of nitric acid and the adsorbents could be re-used with negligible loss in sorption performance for a minimum of 3 sorption/desorption cycles.

The maximum capacity of DGA on PS nanofibre was 0.827 g g^{-1} which is responsible for the better performance of the PS-DGA-3-3 nanofibre when compared with the PET-DGA-2-3 obtained with 0.449 g g^{-1} conversion of DGA groups on the surface of PET nanofibres after the optimum reaction time. PS-DGA-3-3 nanofibre therefore possess more abundant etheric oxygen and carbonyl ($>C=O$) groups which enhanced the removal and selectivity towards trivalent lanthanides.

PS-DGA and PET-DGA sorption properties were higher when compared with some other adsorbents because these nanofibre adsorbents with diglycolic acid ligands adsorbed REE ions due to the tridentate chelation which conferred high selectivity for REE ions. The other major advantage of the present adsorbent nanofibres is the fast kinetics of sorption associated with their nano size, large surface area and the easy recovery of the adsorbent and adsorbate at the end of the sorption process.

PUBLICATIONS FROM THE THESIS

- OK Pereo, C Bode-Aluko, G Ndayambaje, O Fatoba, LF Petrik. Electrospinning: Polymer Nanofibre Adsorbent Applications for Metal Ion Removal. *Journal of Polymers and the Environment*. Available at: <http://link.springer.com/article/10.1007/s10924-016-0896-y>
- Bode-Aluko, C.A., Pereo, O., Fatoba, O and Petrik, L. 2016. Surface-modified polyacrylonitrile nanofibres as supports. *Polymer Bulletin*, pp.1–12. Available at: <http://dx.doi.org/10.1007/s00289-016-1830-0>
- Bode-Aluko, C A., Pereo, O., Ndayambaje, G., Petrik, L. 2016. Adsorption of Toxic Metals on Modified Polyacrylonitrile Nanofibres: A Review: Water, Air, & Soil Pollution. Available at: <https://link.springer.com/article/10.1007/s11270-016-3222-3>
- O. Pereo, C. Bode-Aluko, K. Laatikainen and L. Petrik. Morphology, modification and characterisation of electrospun polymer nanofibre adsorbent material used in metal ion removal. Submitted to *International Journal of Environmental Science and Technology*.
- Omoniyi Pereo, Chris Bode-Aluko, Olanrewaju Fatoba, Katri Laatikainen and Leslie Petrik Rare Earth Elements removal techniques from water/wastewater: A review, Submitted to *Desalination and Water Treatment*.
- Omoniyi Pereo, Chris Bode-Aluko, Katri Laatikainen and Leslie Petrik. Adsorption of Ce^{3+} and Nd^{3+} by diglycolic acid functionalized polystyrene nanofibre from aqueous solutions. In preparation for submission to *Chemical Engineering Journal*.
- O. Pereo, C. Bode-Aluko, K. Laatikainen, Y. Kochnev, A.N. Nechaev and L. Petrik. Electrospun PET nanofibres functionalised with Diglycolic acid for the adsorption of rare earth metal ions. In preparation for submission to *Journal of Hazardous Materials*

- O. Perea, C. Bode-Aluko, K. Laatikainen, Y. Kochnev, A.N. Nechaev, L. Petrik and P. Apel. Preparation and characterization of hybrid nanofibres/track etch membrane for filtration and adsorption of dye in contaminated water. In preparation for submission to Science Bulletin
- Omoniyi Perea, Chris Bode-Aluko, Katri Laatikainen and Leslie F. Petrik. Removal of Rare Earth Metal ions by functionalised electrospun polystyrene nanofibers from aqueous solution. “Electrospin 2018 International Conference”. Conference proceedings, 16-18th January 2018, Wallenberg Research Centre at STIAS, Stellenbosch, South Africa.



DEDICATION

To my parents, late Mr Joshua Omotayo Pereo and Chief (Mrs) Bolatito Pereo, the entire Omotayo Pereo family, my darling wife Oluwaseyi Pereo and my lovely children Tomiwa, Tope, Tumise, Tobi and Tola Pereo



ACKNOWLEDGMENT

- God Almighty
- Prof Leslie Petrik (PhD supervisor) for the opportunity and resources to conduct fundamental research, valuable guidance, financial support and the generous investment of her time over the course of the project. This is greatly appreciated. I am indeed grateful for paving the way for me to understand independent dynamic research thinking.
- Dr Katri Laatikainen, PhD Co-supervisor, for the academic guidance.
- Financial support from Water Research Commission (WRC, South Africa) and the Environmental and Nanoscience Research group (ENS) of the University of the Western Cape, South Africa without which this study would not have been possible.
- Dr Yuri Kochnev; Prof A.N Nechaev and Prof P.Y Apel and the support from Joint Institute of Nuclear Research (JINR), Russia for water contact angle (WCA) measurements and the use of their laboratory in characterising composite nanofibres used for adsorption of cationic dyes and supply of track etched membranes
- ENS Research group colleagues, Dr O. Fatoba, Ilse Wells for BET and ICP analyses; and for administration duties, Vanessa Kellerman, Rallston Richards.
- The author is also grateful for the assistance of the following people; SEM analysis (Adrian Jacobs, Physics Dept, UWC); FTIR (Divian Robertson, Stellenbosch University); XRD (Remmy Bucher – ithemba labs); BET (Mohammed, SAIAMC, UWC); TGA(Yunus Kippie, Pharmacy, UWC).
- Prof O. Olaofe and Prof R. Akinyeye (MSc supervisors).

TABLE OF CONTENTS

Preface

Declaration of Authorship.....i

Keywordsii

Abstract iii

Publications from the thesis v

Dedication..... vii

Acknowledgment viii

Table of Contents ix

List of Figures..... xv

List of Tables xxii

List of equations..... xxiv

List of Schemes xxv

Abbreviations..... xxvi

Nomenclature..... xxvii

Chapter One 1

1 Introduction..... 1

1.1 Background 1

1.2 Problem statement 7

1.3 Aims and objectives of the study..... 8

1.4 Research questions 9

1.5 Hypothesis 10

1.6 Research approach and characterisation..... 10

1.7 Scope and delimitations of the study 12

1.8 Thesis outline 13

Chapter two	16
Literature review.....	16
2 Introduction.....	16
2.1 Background	16
2.2 Nanofibre.....	17
2.2.1 Electrospinning	19
2.2.2 Parameters affecting electrospinning process	21
2.2.3 Morphology of electrospun nanofibres.....	26
2.2.4 Solvents used for electrospinning	28
2.2.5 Polymers used in electrospinning and adsorption.....	30
2.3 Rare earths metals	37
2.3.1 Rare earth deposits and availability.....	37
2.3.2 Technological applications of rare earth metals.....	39
2.3.3 Environmental effects of Rare Earth Elements	42
2.3.4 Rare earth elements recovery technologies.....	43
2.3.5 Adsorbents in Use	46
2.3.6 Ligands in use.....	47
2.3.7 Nanofibre adsorbents.....	52
2.3.8 Modification of nanofibres.....	53
2.3.9 Desorption and regeneration processes	57
2.4 Characterisation techniques used in this study.....	58
2.4.1 Fourier transform infrared (FTIR) spectroscopy	59
2.4.2 Scanning electron microscopy (SEM)	60
2.4.3 Thermo - gravimetric analyser (TGA).....	61
2.4.4 Inductively coupled plasma-optical emission spectroscopy	62
2.4.5 X-ray diffraction (XRD)	63
2.4.6 Brunauer-Emmett-Teller (BET).....	64
2.4.7 pH.....	65

2.5	Summary	66
	Chapter three	68
3	Experimental details	68
3.1	Materials and chemicals.....	68
3.2	General electrospinning apparatus setup.....	69
3.2.1	Investigation of the effect of polymer concentration.....	70
3.2.2	Investigation of the effect of flow rate.....	71
3.2.3	Investigation of the effect of voltage.....	72
3.2.4	Investigation of the effect of needle tip to collector distance	73
3.3	Surface modification of the PS or PET nanofibres.....	75
3.3.1	Reaction scheme	75
3.3.2	Effect of ligand concentration on surface modification of the PS or PET nanofibre.....	78
3.3.3	Effect of reaction time on surface modification of the PS or PET nanofibre...79	
3.3.4	Material stability in nitric acid (HNO ₃) and ethylene diamine tetra acetic acid (EDTA).....	80
3.4	Characterisation techniques used in this study.....	81
3.4.1	Fourier transform infrared (FTIR) spectroscopy	81
3.4.2	Scanning electron microscopy (SEM)	82
3.4.3	Thermo-gravimetric analyser (TGA).....	82
3.4.4	X-ray diffraction (XRD)	83
3.4.5	Brunauer-Emmett-Teller (BET).....	83
3.4.6	Water contact angle (WCA) Measurement	83
3.4.7	Inductively coupled plasma-optical emission spectroscopy	84
3.5	Adsorption experiments.....	84
3.5.1	Procedure for adsorption and desorption experiments.....	85
3.5.2	Effect of pH	86
3.5.3	Effect of contact time	86
3.5.4	Effect of equilibrium concentration	88

3.5.5	Desorption and regeneration of metal ions from nanofibre mats.....	90
3.5.6	The selective adsorption of Ce(III) and Nd(III) onto PS-DGA or PET-DGA nanofibre.....	91
Chapter Four		92
Effect of process parameters on electrospun polystyrene (PS) and polyethylene terephthalate (PET) nanofibres		92
4 Introduction.....		92
4.1	Effect of polymer solution concentration on PS nanofibre morphology.....	93
4.2	Effect of polymer solution concentration on PET nanofibre morphology	97
4.3	Effect of flow rate on PS nanofibre.....	101
4.4	Effect of flow rate on PET nanofibre	106
4.5	Effect of applied voltage on PS nanofibre morphology.....	111
4.6	Effect of applied voltage on PET nanofibre morphology	114
4.7	Effect of needle tip to collector distance on PS nanofibre morphology.....	117
4.8	Effect of needle tip–collector distance on PET nanofibre morphology.....	119
4.9	Water contact angle (WCA) measurements	125
4.10	Summary	129
Chapter Five		131
Characterisation of starting materials and surface modified nanofibre adsorbents		131
5 Introduction.....		131
5.1	Surface modification of PS and PET nanofibres.....	132
5.1.1	Effect of the concentration of DGA ligand on the surface modification of PS nanofibres	133
5.1.2	Effect of the reaction time on the surface modification of PS	136
5.1.3	Effect of the concentration of DGA ligand on the surface modification of PET nanofibres.....	138
5.1.4	Effect of the reaction time on the surface modification of PET.....	142

5.1.5	Morphology of modified PS as a function of concentration of DGA ligand and reaction time	144
5.1.6	Morphology of modified PET as a function of DGA ligand concentration and reaction time	149
5.1.7	Structural properties of PS-DGA-3-3	154
5.1.8	Structural properties of PET-DGA-2-3.....	156
5.1.9	Thermal profile of modified PS-DGA-3-3.....	158
5.1.10	Thermal profile of modified PET-DGA-2-3	161
5.1.11	Nitrogen adsorption–desorption of PS-DGA-3-3.....	164
5.1.12	Nitrogen adsorption–desorption of PET-DGA-2-3	166
5.1.13	Material stability of PS-DGA-3-3 adsorbent in HNO ₃ and EDTA	168
5.1.14	Material stability of PET-DGA-2-3 nanofibre in HNO ₃ and EDTA	171
5.2	Summary	173
Chapter Six.....		176
Adsorption study of Ce ³⁺ and Nd ³⁺ on the chelating PS-DGA-3-3 or PET-DGA-2-3 nanofibres.....		176
6 Introduction.....		176
6.1 Determination and optimisation of adsorption parameters of Ce ³⁺ and Nd ³⁺ binding capacity on modified nanofibre adsorbents.....		177
6.1.1	Effect of solution pH using PS-DGA-3-3 nanofibre adsorbent.....	177
6.1.2	Effect of solution pH using PET-DGA-2-3 nanofibre adsorbent.....	179
6.1.3	Effect of contact time on PS-DGA-3-3.....	182
6.1.4	Effect of contact time on PET-DGA-2-3.....	184
6.1.5	Effect of equilibrium concentration of Ce ³⁺ or Nd ³⁺ on PS-DGA-3-3	187
6.1.6	Effect of equilibrium concentration of Ce ³⁺ or Nd ³⁺ on PET-DGA-2-3.....	189
6.2 Adsorption isotherm models.....		190
6.2.1	Adsorption isotherm models for PS-DGA-3-3.....	191
6.2.2	Adsorption isotherm models for PET-DGA-2-3	195

6.3	Comparison of the functionalised nanofibre absorption capacity with other adsorbents.....	198
6.4	Kinetic study of nanofibre adsorbent (PS-DGA-3-3 and PET-DGA-2-3).....	201
6.4.1	Kinetic studies for PS-DGA-3-3.....	202
6.4.2	Kinetic studies for PET-DGA-2-3.....	205
6.5	Desorption and regeneration studies.....	208
6.6	Selective adsorption.....	210
6.7	Chapter Summary.....	212
	Chapter Seven.....	215
	Conclusions, Novelty and Recommendations.....	215
7	Introduction.....	215
7.1	Conclusions.....	215
7.2	Novelty.....	220
7.3	Recommendations.....	221
	References.....	223
	Appendix A.....	274
	Appendix B.....	275

LIST OF FIGURES

Figure 2.1 Schematic diagram of electrospinning apparatus set up..... 21

Figure 2.2 A classification of the fibre diameter..... 27

Figure 2.3 Polystyrene 34

Figure 2.4 Polyethylene terephthalate 36

Figure 2.5 Structure of diglycolic acid (DGA)..... 49

Figure 2.6. Bite angle between the metal and the coordinating atoms of the ligand..... 51

Figure 4.1 SEM micrographs and frequency distribution of PS fibres at various polymer weight percentage (a) 10, (b) 15, (c) 20, (d) 25 and (e) 30 wt % (flow rate - 1.0 mL/h; voltage - 20 kV and distance - 17 cm)..... 94

Figure 4.2 The effect of solution concentration on fibre diameter of electrospun PS nanofibres at various polymer weight percentage (a) 10, (b) 15, (c) 20, (d) 25 and (e) 30 wt % (flow rate - 1.0 mL/h; voltage - 20 kV and distance - 17 cm).... 96

Figure 4.3 SEM micrographs and distribution of PET nanofibres at various polymer weight percentage (a) 8, (b) 10, (c) 15 and (d) 20 wt % (flow rate - 0.8 mL/h; voltage - 20 kV and distance - 20 cm)..... 98

Figure 4.4 Trend of fibre diameter as a function of concentration for PET samples (polymer weight percentage (a) 8, (b) 10, (c) 15 and (d) 20 wt % (flow rate - 0.8 mL/h; voltage - 20 kV and distance - 20 cm)..... 100

Figure 4.5 SEM micrographs and distribution of electrospun PS nanofibres at different flow rates (a) 0.2, (b) 0.4, (c) 0.8 and (d) 1.0 mL/h (polymer concentration - 15 wt %; voltage - 20 kV and distance - 17 cm)..... 102

Figure 4.6. Cross section of SEM micrographs of electrospun PS nanofibre mat after 2 hrs (flow rates - 0.8 mL/h; polymer concentration - 15 wt %; voltage - 20 kV and distance - 17 cm)..... 103

Figure 4.7. Trend of fibre diameter as a function of flowrate for PS at different flow rates (a) 0.2, (b) 0.4, (c) 0.8 and (d) 1.0 mL/h (polymer concentration - 15 wt %; voltage - 20 kV and distance - 17 cm)..... 105

Figure 4.8. SEM micrographs and distribution of electrospun PET nanofibres at different flow rates (a) 0.2, (b) 0.4, (c) 0.8 and (d) 1.0 mL/h (polymer concentration - 10 wt %; voltage - 20 kV and distance - 20 cm)..... 107

Figure 4.9. Cross section of SEM micrographs of electrospun PET nanofibre mat after 2 hrs (flow rate - 1.0 mL/h; polymer concentration - 10 wt %; voltage - 20 kV and distance - 20 cm)..... 108

Figure 4.10. Trend of fibre diameter as a function of flow rate for PET at different flow rates (a) 0.2, (b) 0.4, (c) 0.8 and (d) 1.0 mL/h (polymer concentration - 10 wt %; voltage - 20 kV and distance - 20 cm)..... 110

Figure 4.11. SEM micrographs and distribution of electrospun PS nanofibres at different applied voltage (a) 15, (b) 17 (c) 20 kV (flow rate - 0.8 mL/h; polymer concentration - 15 wt % and distance - 17 cm)..... 112

Figure 4.12. Trend of fibre diameter as a function of voltage for PS samples at different applied voltages (a) 15, (b) 17 (c) 20 kV (flow rate - 0.8 mL/h; polymer concentration - 15 wt % and distance - 17 cm)..... 113

Figure 4.13. SEM micrographs and distribution of electrospun PET nanofibres at different applied voltage (a) 10, (b) 15 (c) 17 (d) 20 kV (flow rate - 1.0 mL/h; polymer concentration - 10 wt % and distance - 20 cm)..... 115

Figure 4.14. Trend of fibre diameter as a function of voltage for PET samples at different applied voltage (a) 10, (b) 15 (c) 17 (d) 20 kV (flow rate - 1.0 mL/h; polymer concentration - 10 wt % and distance - 20 cm)..... 116

Figure 4.15. SEM micrographs and distribution of electrospun PS nanofibres on needle tip–collector distance (a) 10, (b) 15 and (c) 20 cm (flow rate - 0.8 mL/h; voltage - 17 kV and polymer concentration - 15 wt %). 118

Figure 4.16. Trend of fibre diameter as a function of needle tip–collector distance at (a) 10, (b) 15 and (c) 20 cm (flow rate - 0.8 mL/h; voltage 17 kV and polymer concentration - 15 wt %) 119

Figure 4.17. SEM micrographs and distribution of electrospun PET nanofibres on needle tip–collector distance (a) 10, (b) 15 (c) 20 and (d) 25 cm (flow rate - 1.0 mL/h; voltage - 17 kV and polymer concentration - 10 wt %). 121

Figure 4.18. Trend of fibre diameter as a function of needle tip–collector distance at (a) 10, (b) 15 (c) 20 and (d) 25 cm (flow rate - 1.0 mL/h; voltage - 17 kV and polymer concentration - 10 wt %). 123

Figure 4.19. Contact angle of PS-D2 nanofibre (polymer concentration - 15 wt %; voltage - 17 kV; solution flow rate - 0.8 mL/h and collector distance - 15 cm).127

Figure 4.20. Contact angle of PET-D3 nanofibre (polymer concentration - 10 wt %; voltage - 17 kV; solution flow rate - 1.0 mL/h and collector distance - 20 cm). 128

Figure 5.1. Modification of PS nanofibre with DGA chelating ligand 133

Figure 5.2. FTIR spectra of a) Pristine PS b) PS-DGA-1 (1 g), c) PS-DGA-1.5 (1.5 g), d) PS-DGA-2 (2 g), e) PS-DGA-3 (3 g), f) PS-DGA-4 (4 g), and g) DGA (time - 240 mins; PS fibre weight - 0.109 g; temp – 43 °C; 5mL acetic acid; 40 mL 99% methanol). 134

Figure 5.3. FTIR spectra of a) Pristine PS b) PS-DGA-3-1 (1 hr), c) PS-DGA-3-2 (2 hr), d) PS-DGA-3-3 (3 hr), e) PS-DGA-3-4 (4 hr) and f) DGA (conc -3 g (0.026 mol); fibre weight - 0.109 g)..... 137

Figure 5.4. (a) PET modification with DGA chelating ligand and (b) graphical representation of surface modification of PET nanofibres using DGA chelating ligand..... 139

Figure 5.5. FTIR spectra of a) PET; b) PET-DGA-1 (1 g), c) PET-DGA-1.5 (1.5 g), d) PET-DGA-2 (2 g) e) PET-DGA-3 (3 g) and f) DGA (time - 4 h; fibre weight - 0.102 g)..... 140

Figure 5.6. FTIR spectra of a) PET, b) PET-DGA-2-1 (1 hr), c) PET-DGA-2-2 (2 hr), d) PET-DGA-2-3 (3 hr), e) PET-DGA-2-4 (4 hr), (conc - 2 g (0.017 mol); fibre weight - 0.102 g)..... 143

Figure 5.7. SEM micrograph of pristine PS nanofibre (concentration - 15 wt %; voltage - 17 kV; flow rate - 0.8 mL/h; collector distance - 15 cm)..... 145

Figure 5.8. SEM micrograph of PS nanofibre after surface modification with different DGA concentrations (a) PS-DGA-2 (2 g) and (b) PS-DGA-3 (3 g) (time - 4 h; fibre weight - 0.109 g)..... 146

Figure 5.9. SEM micrograph of PS nanofibre modified at 2, 3, and 4 hr time intervals (a) PS-DGA-3-2, (b) PS-DGA-3-3 and (c) PS-DGA-3-4 (conc - 3 g; fibre weight - 0.109 g) 148

Figure 5.10. SEM micrograph of pristine PET nanofibre (PET concentration - 10 wt %; voltage - 17 kV; solution flow rate - 1.0 mL/h; collector distance - 20 cm) 150

Figure 5.11. SEM micrograph of (a) PET-DGA-1.5 (1.5 g) (b) PET-DGA-2 (2 g) and (c) PET-DGA-3 (3 g) (time - 3 h; fibre weight - 0.102 g)..... 151

Figure 5.12. SEM micrograph of (a) PET-DGA-2-2 (2 hr), (b) PET-DGA-2-3 (3 hr) and (c) PET-DGA-2-4 (4 hr) (DGA conc - 2 g (0.017 mol); fibre weight - 0.102 g).....	153
Figure 5.13. XRD of (a) PS and (b) PS-DGA-3-3	155
Figure 5.14. XRD graphs of (a) PET and (b) PET-DGA-2-3	156
Figure 5.15. (a) TGA profile (b) TGA derivatives of pristine PS and PS-DGA-3-3	159
Figure 5.16. (a) TGA profile (b) TGA derivatives of PET and PET-DGA-2-3 ...	162
Figure 5.17. N ₂ adsorption–desorption isotherm for (a) PS and (b) PS-DGA-3-3. (Inset) Pore size distribution of PS and PS-DGA-3-3	164
Figure 5.18. N ₂ adsorption–desorption isotherm for (a) PET and (b) PET-DGA-2-3.	167
Figure 5.19. FTIR Spectra of a) Pristine PS nanofibre, b) PS-DGA-3-3, c) 1 M HNO ₃ , d) 1.5 M HNO ₃ , and e) 2 M HNO ₃ . (Vol – 10 mL; time - 1 hr; rpm - 240)	169
Figure 5.20. FTIR Spectra of a) PS-DGA-3-3 b) 0.05 M EDTA, c) 0.1 M EDTA and d) 0.25 M EDTA (vol – 10 mL; time - 1 hr; rpm - 240)	170
Figure 5.21. FTIR Spectra of a) Pristine PET; b) PET-DGA-2-3; c) 0.5 M HNO ₃ , d) 1 M HNO ₃ , e) 1.5 M HNO ₃ and f) 2M HNO ₃ . (Vol - 10 mL HNO ₃ ; time - 1 hr; rpm -240).....	171
Figure 5.22. FTIR Spectra of a) PET-DGA-2-3, b) 0.05 M EDTA d) 0.1 M EDTA and f) 0.25 M EDTA (vol - 10 mL EDTA; time - 1 h; rpm - 240).....	172
Figure 6.1. Effect of pH on the removal efficiency (%) of Nd ³⁺ ; Ce ³⁺ from aqueous solution by PS-DGA-3-3 nanofibres (Ce ³⁺ or Nd ³⁺ concentration - 100 mg/L; contact time - 120 min; adsorbent dosage - 0.0075 g).....	178

Figure 6.2. Effect of pH on the removal efficiency (%) of Nd ³⁺ ; Ce ³⁺ from aqueous solution by PET-DGA-2-3 nanofibres (Ce ³⁺ or Nd ³⁺ concentration - 100 mg/L; contact time - 60 min; adsorbent dosage - 0.0075 g).....	180
Figure 6.3. Effect of contact time on the removal efficiency of Ce ³⁺ ; Nd ³⁺ from aqueous solution by Pristine PS and PS-DGA-3-3 nanofibre (Ce ³⁺ or Nd ³⁺ concentration - 100 mg/L; pH – 6; adsorbent dosage - 0.0075 g).....	183
Figure 6.4. Effect of contact time on the removal efficiency of Ce ³⁺ ; Nd ³⁺ from aqueous solution by Pristine PET and PET-DGA-2-3 nanofibre (Ce ³⁺ or Nd ³⁺ concentration - 100 mg/L; pH – 6; adsorbent dosage - 0.0075 g).....	185
Figure 6.5. Effect of equilibrium metal concentrations on adsorption of Nd ³⁺ ; Ce ³⁺ onto PS-DGA-3-3 nanofibre (contact time - 90 min; pH - 6; adsorbent dosage - 0.0075 g /10 mL)	188
Figure 6.6. Effect of equilibrium metal concentrations on adsorption of Ce ³⁺ ; Nd ³⁺ onto PET-DGA-2-3 nanofibre (contact time - 100 min; pH – 6; adsorbent dosage - 0.0075 g /10 mL).....	189
Figure 6.7. Adsorption isotherm of PS-DGA-3-3 nanofibre adsorbent for Ce ³⁺ ; Nd ³⁺ linearised according to Langmuir equations.	192
Figure 6.8. Adsorption isotherm of PS-DGA-3-3 nanofibre adsorbent of Nd ³⁺ ; Ce ³⁺ linearised according to the Freundlich equation.	193
Figure 6.9. Adsorption isotherm of PET-DGA-2-3 nanofibre adsorbent of Ce ³⁺ ; Nd ³⁺ linearised according to Langmuir equations.....	196
Figure 6.10. Adsorption isotherm of PET-DGA-2-3 nanofibre adsorbent for Nd ³⁺ ; Ce ³⁺ linearised according to the Freundlich equation.	197
Figure 6.11. Adsorption kinetics of Nd ³⁺ ; Ce ³⁺ based on the pseudo-first-order model for PS-DGA-3-3	203

Figure 6.12. Adsorption kinetics of Nd^{3+} ; Ce^{3+} based on the pseudo-second-order model for PS-DGA-3-3 204

Figure 6.13. Adsorption kinetics of Nd^{3+} ; Ce^{3+} based on the pseudo-first-order model for PET-DGA-2-3..... 206

Figure 6.14. Adsorption kinetics of Nd^{3+} ; Ce^{3+} based on the pseudo-second-order model for PET-DGA-2-3..... 206



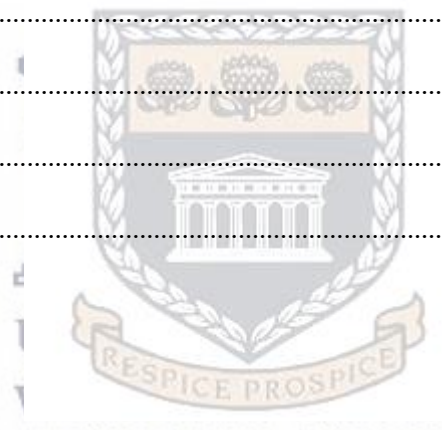
LIST OF TABLES

Table 2.1. Properties of different solvents used in electrospinning process	29
Table 2.2. Typical examples of polymers used in electrospinning, solvents and the nanofibre applications.....	31
Table 2.3. Estimated supply and demand of rare earth elements in 2014 and the commercial pricing of REEs.....	39
Table 2.4. REE uses and applications by industry	41
Table 3.1. List of the chemicals used in the present study.....	69
Table 3.2. Electrospinning conditions for PS at different polymer concentrations	70
Table 3.3. Electrospinning conditions for PET at different polymer concentrations	71
Table 3.4. Electrospinning conditions for PS at different flow rates.....	72
Table 3.5. Electrospinning conditions for PET at different flow rates	72
Table 3.6. Electrospinning conditions for PS at different voltages.....	73
Table 3.7. Electrospinning conditions for PET at different voltages	73
Table 3.8. Electrospinning conditions for PS at different collector distances.....	74
Table 3.9. Electrospinning conditions for PET at different collector distances	74
Table 3.10. List of the sample name and codes used in the surface modification ..	75
Table 3.11. The experimental parameters used in nanofibre surface modification (fixed amount of 0.10 g) with different mass concentrations of DGA for 240 min	79
Table 3.12. The experimental parameters used in nanofibre surface modification (fixed amount of 0.10 g) as a function of reaction time.....	80

Table 4.1. Comparison of flow rate and fibre mass (polymer concentration - 15 wt %; voltage - 20 kV and distance - 17 cm).....	104
Table 4.2. Comparison of flow rate and fibre mass (polymer concentration - 10 wt %; voltage - 20 kV and distance - 20 cm).....	109
Table 5.1. Electrospinning conditions used for the nanofibres used as support for DGA.....	132
Table 5.2. TG analysis data of PS and PS-DGA-3-3.....	159
Table 5.3. TG analysis data of PS and PET-DGA-2-3.....	162
Table 6.1. Parameters obtained from the plot of Langmuir and Freundlich isotherms for Ce ³⁺ or Nd ³⁺ adsorption using PS-DGA-3-3.....	194
Table 6.2. Parameters obtained from the plot of Langmuir and Freundlich isotherms for Ce ³⁺ or Nd ³⁺ adsorption for PET-DGA-2-3.....	198
Table 6.3. Comparison of sorption capacities of different sorbents for Nd ³⁺	199
Table 6.4. Comparison of sorption capacities of different sorbents for Ce ³⁺	200
Table 6.5. Comparison of the kinetics constants for the sorption of for Ce ³⁺ or Nd ³⁺ on PS-DGA-3-3.....	204
Table 6.6. The kinetics constants for the sorption of Ce ³⁺ or Nd ³⁺ on PET-DGA207	
Table 6.7. Desorption efficiency for Ce ³⁺ or Nd ³⁺ from PS-DGA-3-3 and PET-DGA-2-3 for three cycles of adsorption–desorption (initial concentration - 100 mg/L; adsorbent dosage - 0.0075 g; stripping agent - 1 M HNO ₃ ; desorption time - 60 min).....	208
Table 6.8. Adsorption capacity of different metal ions in solution on PS-DGA-3-3 and their selectivity coefficients (S).....	210
Table 6.9. Adsorption capacity of different metal ions in solution on PET-DGA-2-3 and their selectivity coefficients.....	211

LIST OF EQUATIONS

Equation 3.1.....	85
Equation 3.2.....	87
Equation 3.3.....	87
Equation 3.4.....	89
Equation 3.5.....	89
Equation 3.6.....	90
Equation 3.7.....	91
Equation 4.1.....	126
Equation 6.1.....	191
Equation 6.2.....	193
Equation 6.3.....	202
Equation 6.4.....	202



LIST OF SCHEMES

Scheme 1.1. Scheme of the research protocol 11

Scheme 3.1. Ring opening of diglycolic anhydride under acidic conditions..... 76

Scheme 3.2. Mechanism for PS electrophilic aromatic substitution..... 77

Scheme 3.3. Mechanism for PET electrophilic aromatic substitution 77



ABBREVIATIONS

ATR	Attenuated Total Reflectance
BET	Brunauer-Emmet-Teller
DGA	Diglycolic anhydride
DMF	N,N dimethylformamide
DDI	Doubly deionised water
EDTA	Ethylene diamine tetra acetic acid
FTIR	Fourier Transform Infrared
HR-SEM	High Resolution Scanning Electron Microscopy
ICP-OES	Inductively Coupled Plasma-Optical Emission Spectroscopy
PET	Polyethylene terephthalate
PS	Polystyrene
REE	Rare earth element
TFA	Trifluoroacetic acid
TGA	Thermogravimetric analysis
THF	Tetrahydrofuran
WCA	Water contact angles
XRD	X-ray powder diffraction
PEO	poly (ethylene oxide)
PVA	poly (vinyl alcohol)
PDLA	poly (D,L-lactic acid)

NOMENCLATURE

b	constant related to the energy of adsorption (L/mg)
C_0	initial concentration in aqueous solution (mol L ⁻¹)
C_t	concentration in solution at any time t (mol L ⁻¹)
C_e	equilibrium concentration of the adsorbate (mg/L)
K_f	Freundlich constant
k_1	adsorption rate constant for first-order kinetic equation (min ⁻¹)
k_2	adsorption rate constant second-order kinetic equation (g/mg min)
M	mass of adsorbent (g)
n	measure of the deviation of the adsorption from linearity
q_e	equilibrium concentration of metals ions on adsorbent (mg/g)
q_t	the amount of metals ions adsorbed at any time, t (mg/g)
q_m	Langmuir monolayer capacity of the adsorbent (mg/g)
R^2	linear regression coefficient
t	time (s)
V	volume of solution

CHAPTER ONE

1 INTRODUCTION

This chapter is the introduction to the study and provides a brief overview of the study, giving the problem statement, research aims and objectives, research questions, research approach, research hypothesis and the research scope with the delimitations (sections 1.1 to 1.7). The chapter ends in section 1.8 with an outline of all the subsequent chapters in the thesis.

1.1 Background

Rare earth elements (REEs) are surface active elements which play an important role in metallurgy, such as alloying and purification of metals, refinement of microstructure, and metamorphosis of inclusions (Xiong et al. 2009). REEs have widespread use and importance for industrial applications due to their metallurgical, optical and electronic properties. They have been used to enhance the properties of materials in different fields, such as petrogenetic tracers in geochemistry, superconductors, and super magnets in industry (Çelik et al. 2015). The REEs group are comprised of the lanthanide series plus scandium and yttrium. The REEs physicochemical properties are very close because of their close electronic configurations, and their most thermodynamically stable form is the trivalent, M(III) form (Galhoum et al. 2015). Therefore, the development of new sources of REEs is important to ensure a secure supply of these elements.

For individual REEs, the most widely used are cerium (Ce) and neodymium (Nd) (Naumov 2008) and the increase in the industrial usage, economic and environmental benefits of the REEs have resulted in an increased demand and price. The increase has similarly led to the development of technologies and processes for the separation

of the metallic ions from various sources. The growing demand for the REEs has led to an increased environmental impact and water pollution from numerous REE commercial products and rare earth metal mines. The main pathways of human exposure to REEs include inhalation, dermal contact, and ingestion of foods and beverages. Studies have reported that environmental exposure to high levels of REEs could result in harmful effects, such as pneumoconiosis, acute myocardial infarction, abnormal blood biochemical indices, leukaemia, lower Intelligence Quotient (IQ) scores in children, low total protein content of serum, itching, sensitivity to heat, and skin lesions (Guo et al. 2015). As a result, the recovery of REEs is a significant issue that requires appropriate consideration.

Cerium (Ce) is the most abundant of the rare earth metals and can be extracted from allanite, bastnasite and monazite minerals (Koskenmaki and Gschneidner 1978). Very pure cerium is used in the production of nuclear power and as a catalyst in nuclear industries; the automotive catalyst industry also consumes significant REEs by weight as cerium carbonate and cerium oxide in the catalyst substrate and as a component of the converter's oxidising catalyst system; in microwave devices; television sets; lasers; as an alloy with chromium, besides other important uses in environmental pollution assessment or agronomy and biochemistry (Khan et al. 2015; Sahu et al. 2013). Substantial amounts of cerium concentrates and cerium oxide are used in glass-polishing applications. Many cerium compounds have also found important uses in biomedical applications (Castor and Hedrick 2006; Sahu et al. 2013).

Neodymium (Nd) is the second most abundant rare earth element and an important member of the rare earth family (Manoochchri and Khalesi 2012). It has been

extensively used in electronics components, optic filters, artistic glasses, steel modifiers and hydrogen storage (Park and Tavlarides 2010). It plays an important role in the electronic instrument and laser equipment manufacturing industries and the global demand for Nd is expected to rise by 700% over the next 25 years (Alonso et al. 2012). Neodymium was acknowledged by the U.S. Department of Energy (DOE) in their medium-term criticality matrix as one of the five most critical REEs (Bauer et al. 2010) while in its landmark report *Critical Raw Materials for the European Union* (2010), the European Commission considered REEs as the most critical raw materials group, with the highest supply risk (EC-European Commission 2010). The most widely used form of Nd is “sintered Nd-Fe-B permanent magnetic material” due to its excellent magnetic properties (Horikawa et al. 2004).

Rare earth elements recovery from solid waste or minerals may involve pyrometallurgy (Galhoum et al. 2015), an energy intensive process, using high temperatures to chemically convert feed materials and separate them so that the valuable metals can be recovered (Yoon et al. 2014; Zhang et al. 2013). Alternatively, hydrometallurgy (chemical leaching or bioleaching) may be used (Galhoum et al. 2015) and is the most common chemical extraction method of separating individual REEs from the mineral concentrate (El-Didamony et al. 2012; Qu and Lian 2013). Hydrometallurgical processes such as adsorption, chemical precipitation, coagulation–flocculation, electrochemical, filtration, flotation, ion exchange, membrane processes, reverse osmosis, and solvent extraction techniques are available for the removal or extraction of REEs from solution with varying levels of successes (Abreu and Morais 2014; Das and Das 2013; Foo and Hameed 2010; Vander Hoogerstraete and Binnemans 2014).

Precipitation is the easiest method of recovering REEs, but its disadvantages, including the large amount of chemical reagents required, sludge generation, and its ineffectiveness for low concentrations of metals makes it less attractive (Van Nguyen et al. 2016). Solvent extraction is well-established for recovery of metals from various effluents. Many types of extractant have been investigated for the extraction of rare earth metals, including Cyanex 301 and Cyanex 302 (Miaomiao et al. 2013; Tong et al. 2009), di-(2-ethylhexyl) phosphoric acid (HDEHP) (Wang et al. 2006b), Ethyl-bis-triazinylpyridine (Et-BTP) (Bhattacharyya et al. 2009), and Cyanex 272 and Cyanex 921 /Cyanex 923 (Panda et al. 2013). However, the available extractants also extract other base metals, making it difficult to obtain the required rare earth metal purity.

Naganawa et al. (2007) developed a new extractant containing the glycol amic acid group which was selective for extraction of rare earth metals. Thereafter, several researchers (Kubota et al. 2011; Naganawa et al. 2007; Sakaki et al. 2015; Shimojo et al. 2007; Shimojo et al. 2014) have carried out recovery of rare earth elements from aqueous solutions using the new extractants and in these investigations, extractants containing glycol amic acid showed effective and selective extraction of rare earth metals from mixtures of diverse metals. Narita and Tanaka (2013) synthesised N-N'-dimethyl-N,N'-dioctyl diglycol amide (MODGA) for separation of rare elements from base metals and reported that MODGA preferentially extracted rare earth metal cations over those of the base metals. However, Van Nguyen et al. (2013) pointed out the disadvantages of solvent extraction which include loss of extractant, emulsion and third-phase formation, phase separation and use of inflammable diluents.

These developed processes have indeed accelerated the advancement of knowledge but a key interest, the adsorption process, being a surface phenomenon, is recognised as the most efficient, promising and most widely used fundamental approach in hydrometallurgy and wastewater treatment processes (Demirbas 2008; Foo and Hameed 2009; Gupta and Bhattacharyya 2012) due to being simple, economically viable, technically feasible and socially acceptable (Nouri et al. 2007). The adsorption process offers flexibility in design and operation and in many cases will produce high-quality treated effluent. In addition, since adsorption is sometimes reversible, adsorbents can be regenerated by suitable desorption process (Fu and Wang 2011; Lakherwal 2014).

The recovery of rare earth metals from aqueous solutions using adsorbents has been studied by several researchers (Gasser and Aly 2013; Korovin and Shestak 2009; Moldoveanu and Papangelakis 2012), but there are no adsorbents containing special functional groups for selective adsorption of rare earth metals in practical use. Therefore, an idea was generated to develop an adsorbent containing the glycol amic acid group for recovery of rare earth metals. Ogata et al. (2015) have published research on the adsorption of the rare earth metals using this adsorbent, which was prepared by modification of silica gel with the diglycol amic acid group. These authors found that it selectively adsorbed dysprosium and neodymium from a mixture containing copper, iron, zinc, dysprosium, and neodymium. Researchers in Kuraray Company, Japan (Morikawa et al. 2015) have also successfully synthesised a resin containing glycol amic acid which was also used in a study by Van Nguyen et al. (2016) to explore the separation and recovery of the rare earth metals from model solutions containing scandium, cerium, lanthanum, and aluminium.

As various adsorbents are being investigated for metal ion removal (Galhoum et al. 2017), researchers are further investigating and developing the use of polymeric nanofibres to remove metal ions from different sources (Dong et al. 2013; Li et al. 2016; Wang and Hsiao 2016) because nanofibres have interesting structural characteristics such as high surface area to volume ratio, high porosity and interconnectivity, good structural stability and controllable thickness of the electrospun scaffold which are suited for adsorption of metals. Nanofibres can therefore provide an effective backbone for anchoring functional ligands on their high surface area in a feasible and cost effective manner (Hong et al. 2014; Hong et al. 2015).

Electrospinning has been recognised as an efficient technique for the fabrication of polymer nanofibres and is currently the most promising technique used for the production of continuous nanofibres on a large scale where the fibre diameter can be adjusted from nanometres to microns (Pereao et al. 2017). This process of electrospinning has gained much consideration in the last decade not only due to its versatility in spinning a wide variety of polymeric nanofibres but also due to its ability to consistently produce fibres in the submicron range which is difficult to achieve by using other standard mechanical fibre-spinning technologies (Reneker et al. 2000; Schreuder-Gibson et al. 2002).

The surface properties of polymer nanofibres are crucial to their application and therefore, the surface functionality engineering of nanofibres is expected to provide new systems for materials science (Wan et al. 2009). Therefore the control of surface properties is achieved by surface modification through various chemical or physical processes (Ahad et al. 2014) and the strategies for modifying nanofibre surfaces

include co-electrospinning (He et al. 2005), plasma treatment (Hegemann et al. 2003), chemical modification (Yuan et al. 2003), and surface graft polymerisation (Wang and Chen 2007).

Polystyrene (PS) has been widely used as the basic polymer for functional polymers as used in the ion exchange process, which are mostly available in beaded form and not in fibre form (Shimamura et al. 1989). However, the fibre form is generally considered to be one of the most practical and suitable forms for functional polymers to display their special functions, such as the large specific surface area (Lewin 1984).

Poly (ethylene terephthalate) (PET) is a strong, stiff synthetic fibre and a member of the polyester family of polymers (Strain et al. 2015; Wang et al. 2012). PET fibres are one of the most important synthetic fibres used in the textile industry and have superior fibre forming properties (Coşkun 2008). PET has a wide application ranging from functional fibres to automotive parts because of its excellent mechanical properties and thermal stability (Bartolome et al. 2012) and modified PET fibres have been applied for the efficient extraction of heavy metals from the aquatic environment (Moghimi and Abdouss 2012; Sereshti et al. 2015).

Therefore, this study focused on the chemical modification of the surface of PS and PET nanofibres with high REEs metal selective glycolic acid chelating ligand in order to produce chelating nanofibre adsorbents.

1.2 Problem statement

The adsorption of metal species in the aqueous phase is an essential step in various fields such as hydrometallurgy, or recovery of metals from waste. Most of the

methods used are not economical when used with dilute solutions due to the large volumes of liquid which must be handled, high reagent and energy requirement and production of large amounts of toxic sludge which requires careful disposal. It is therefore necessary to develop improved materials for the removal of metals which will have high capacity and will be selective and also stable in solution. Furthermore, from the study of the reported literature (Bode-Aluko et al. 2017; Bode-Aluko et al. 2017a; Ndayambaje et al. 2016; Perea et al. 2017), some significant points can be concluded namely that (1) achieving stability of the ligand on functionalised adsorbents has been difficult using polymer nanofibrous adsorbents and (2) the various modification techniques reported on electrospun nanofibre adsorbents have not resulted in an efficient long term performance in the removal of metal ions from water. Finding new functionalised nanofibre chelating materials for adsorption with increased performance in the removal of Ce^{3+} and Nd^{3+} from aqueous solutions is therefore the focus of interest in this study.

1.3 Aims and objectives of the study

The study aim is to determine and compare the selectivity, adsorption capacity and stability of polystyrene and polyethylene terephthalate nanofibres functionalised with diglycolic anhydride (DGA) for adsorption of rare earth metals of Ce^{3+} and Nd^{3+} from aqueous solution.

The specific objectives of the study include:

- investigate the effects of electrospinning parameters on PS or PET nanofibre diameter
- incorporate the ligand into the PS or PET nanofibre and gain an understanding of the nature of ligand bond on the support

- utilise preparation conditions such as time, concentration and ligand ratio to obtain optimal modification properties for functionalised materials
- determine the stability of the ligand attached to the nanofibre
- investigate the influence of surface properties and pore structure of the nanofibre supports on the adsorbent
- remove rare earth metals ions from aqueous model solutions by the different functionalised nanofibres
- determine the effect of pH, time and initial concentration on the adsorption of REEs by the new functionalised nanofibres.
- determine the effectiveness of the adsorbents' desorption and regeneration conditions.

1.4 Research questions

This study will attempt to provide answers to the following questions;

- What are the optimum conditions for the PS or PET polymers to be electrospun into nanofibres?
- Can these nanofibres be successfully functionalised with the selected ligand?
- How can the ligand binding be enhanced on the PS or PET nanofibres?
- How stable is the ligand on the PS or PET nanofibres after modification?
- What is the PS or PET modified nanofibre adsorbents' capacity?
- Which combination of polymer/ligand will be most effective for REE metal removal?
- How effectively will these functionalised nanofibres recover different REE metals from the model aqueous solution?

- What is the effect of a change in pH, time, and concentration on the adsorption of REEs by the functionalised nanofibres?
- Can these adsorbents be regenerated?

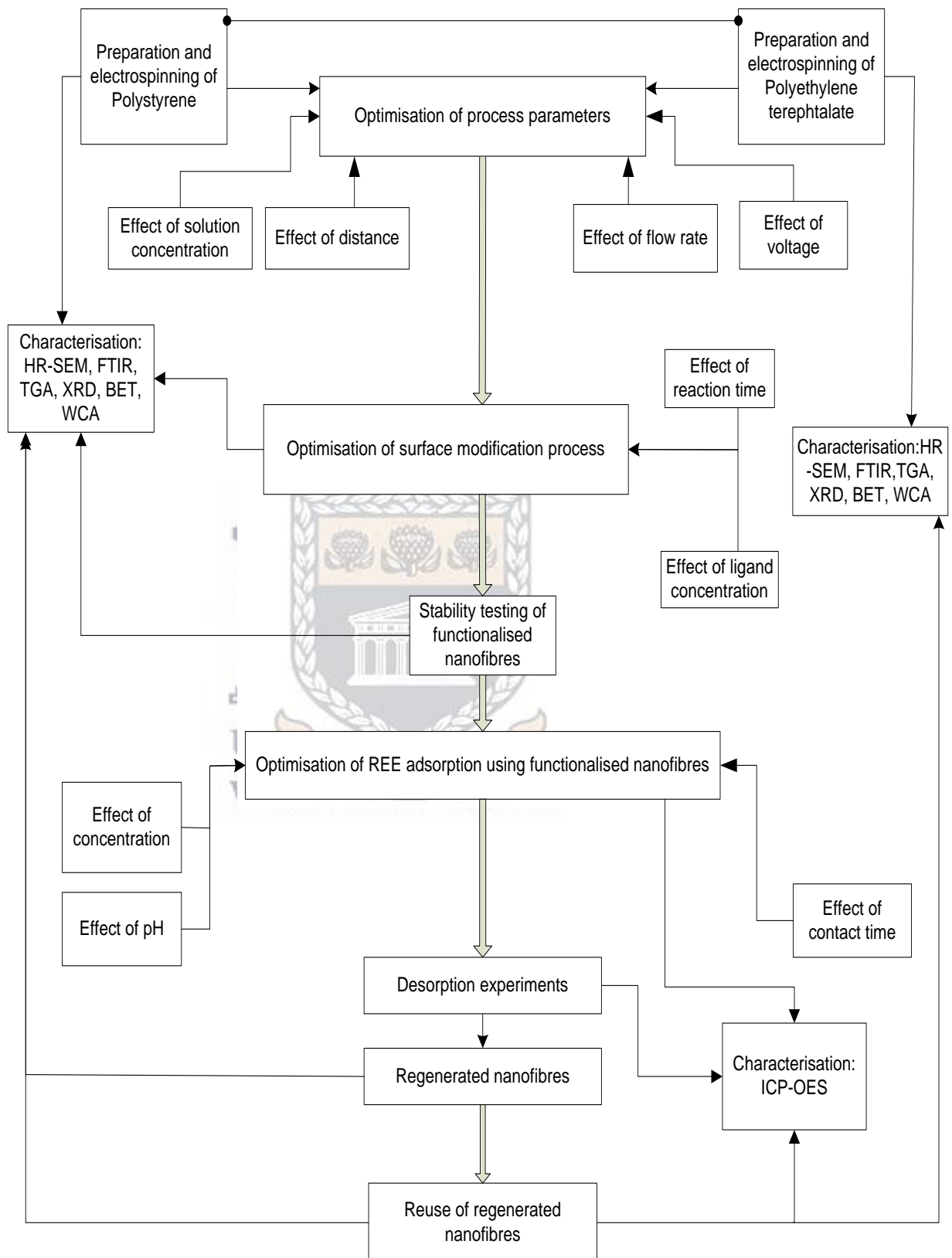
1.5 Hypothesis

The diglycolic acid surface-modified nanofibres will be stable after modification and therefore suitable for rare earth metal ion recovery and will also be selective for the separation of metal ions (Ce or Nd) from other metals in aqueous solutions.

1.6 Research approach and characterisation

In order to achieve the aims and objectives of this study, PS and PET were electrospun and characterised using FTIR, WCA, HRSEM and TGA. The surface of PS and PET nanofibres were modified with diglycolic anhydride and their efficiency as a nanofibre adsorbents were investigated. The process of surface modification of PS and PET nanofibres was done by varying experimental parameters such as reaction contact time and the concentration of the ligand. The grafted DGA chelating moieties on the chelating nanofibre were tested for their stability under acidic and basic medium in order to confirm the adsorbent regeneration ability. The produced PS-DGA and PET-DGA nanofibres were then applied in batch adsorption experiments to adsorb Ce^{3+} or Nd^{3+} from model aqueous solutions. Cerium (Ce) and neodymium (Nd) are abundant and the most widely used of the REE's and were therefore used as model adsorbates for the study. The adsorption experiments were conducted by varying the experimental parameters such as solution pH, reaction contact time and the metal initial concentration in order to optimise the system. The schematic diagram shown in Scheme 1.1 briefly describes all the experimental processes of this study.

Scheme 1.1. Scheme of the research protocol



The reusability of nanofibre for the removal of Ce^{3+} or Nd^{3+} was also determined over three sorption–desorption cycles while the selectivity experiments were carried out with model solutions containing aqueous solution of Ce^{3+} , Co^{2+} , Ni^{2+} and Sr^{2+} metal ions. Characterisation of the structure of the grafted surface is crucial for a better understanding of the grafted surface. The physical characteristics and chemical compositions of the various polymer and functionalised polymer were determined with the aid of various techniques. Fourier transform infrared spectroscopy coupled with attenuated total reflection (ATR-FTIR) was used for determining the molecular structure and chemical bonding of the synthesised nanofibre samples. It provided information regarding the constituent components and chemical structure near the surface region and any structural and conformational changes. High Resolution Scanning Electron Microscope (HR-SEM) was used for the morphology and fibre diameter of functionalised and pristine nanofibre. Surface areas and pore characteristics of the fibres were determined by N_2 adsorption and the associated Brunauer-Emmett-Teller (BET) isotherms. X-ray powder diffraction (XRD) was used for crystalline phase determination of modified nanofibre surfaces. Thermal behaviour of the fibres and stability of the immobilised ligands were investigated by thermogravimetric analyser (TGA). The water contact angles (WCA) was used to determine the hydrophilicity or hydrophobicity of the nanofibres while Inductively Coupled Plasma-Optical Emission Spectroscopy (ICP-OES) was used to determine the concentration of the metal ions in solutions before and after the adsorption experiments.

1.7 Scope and delimitations of the study

Laboratory synthesising methods were used for the production of the different kinds of polymeric nanofibres that were evaluated as adsorbents. Investigation of the effect

of electrospinning conditions on fibre diameter was conducted on PS and PET. Due to the nature of surface modification optimisation, the parameters investigated during the functionalisation included reaction time and concentration of the ligand. Polystyrene (PS) and polyethylene terephthalate (PET) were the two different types of polymers that were electrospun as nanofibre support of the ligands used as adsorbent in this study. Diglycolic anhydride (DGA) was tested as ligand on the nanofibre supports. Stability of the grafted chelating moieties was investigated by testing if it can withstand nitric acid or EDTA as regenerant for lanthanide extractions. Batch adsorption and desorption experiments were conducted to identify the optimum operating conditions for removal and recovery of Ce^{3+} or Nd^{3+} rare earth metals using the functionalised nanofibres and their capacity for rare earth metal removal were verified. All the adsorption optimisation parameters were conducted on the adsorption of light REE Ce^{3+} or Nd^{3+} and not on other rare earth metal ions due to budgetary constraints. Advanced characterisations techniques such as FTIR, HR-SEM, TGA, BET, WCA and XRD were performed for all the synthesised materials and the adsorption mechanisms were studied with ICP-OES.

1.8 Thesis outline

The remaining chapters of the thesis are structured as follows:

Chapter two: Literature review

Chapter two contains the review of literature focusing on polymer nanofibres and supports, nanofibre modification types, electrospinning, metal removal techniques, chelating ligands and rare earth elements. The principles behind the analytical techniques used in this study are also reviewed.

Chapter three: Sampling, experimental and analytical methods

Detailed methodological information on the preparation of different adsorbent nanofibres and the adsorbate solutions are given. Analytical methods are detailed for nanofibre characterisation before and after modification. Sample measurements are introduced including rare earth metal ion measurement before and after adsorption determinations. The experimental design and procedures for the batch studies are also described in this chapter.

Chapter four: Electrospinning and investigation of solution and process parameters on PS and PET nanofibres

This chapter discusses the results of optimisation of polystyrene and polyethylene terephthalate nanofibres' electrospinning process parameters to be used for the nanofibre production in the study.

Chapter five: Surface modification and characterisation of functionalised PS and PET nanofibres

This chapter discuss the results of surface modification of polystyrene and polyethylene terephthalate nanofibres. The functionalised nanofibres were characterised and stability tests conducted on the adsorbent material to probe their ligand stability prior to the studies on the selective removal of rare earth elements in batch systems. The success of the grafting process was confirmed by FTIR spectrometry, while the physical properties of the derivatives were characterised by BET, XRD, WCA and TGA.

Chapter six: REE adsorption using functionalised PS and PET nanofibre

This chapter discusses the results of adsorption studies using polystyrene or polyethylene terephthalate nanofibre adsorbent in a synthetic batch adsorption system for selective removal of rare earth elements Ce^{3+} or Nd^{3+} . The sorption properties were carried out by investigating the effect of the pH, studying the uptake kinetics and evaluating the sorption isotherms described by the Freundlich and the Langmuir equation. The reusability of nanofibres for the removal of Ce^{3+} or Nd^{3+} was also determined after three sorption–desorption cycles. The selectivity experiments were investigated with model solutions containing aqueous solution of Ce^{3+} , Co^{2+} , Ni^{2+} and Sr^{2+} metal ions.

Chapter seven: Conclusion and recommendations

This chapter summarises the findings of the present study. The conclusions reached from the investigation of the electrospun nanofibres; their functionalisation and uses as adsorbent are presented in this chapter. The knowledge and experience acquired from this study are used to make appropriate recommendations for future work and the possibilities for future research and applications on this subject are outlined.

CHAPTER TWO

LITERATURE REVIEW

2 INTRODUCTION

This chapter will review the literature related to this study. This chapter is divided into six sections. Section 2.1 is the literature review background while section 2.2 describes nanofibres, their fabrication processes, morphology, solvents and polymers in use. Section 2.3 describes the rare earths elements, mineral deposits and availability, technological application, environmental effects and removal technologies while Section 2.4 introduce adsorption and adsorbents in use, synthesis and modification of nanofibre adsorbent including the desorption and regeneration process. Section 2.5 describes the principles of the characterisation techniques and Section 2.6 is the summary of the literature review that informed this study

2.1 Background

The search for novel materials appears to be a never ending pursuit as new challenges will always surface to drive innovations. Nanofibres are emerging as new materials suited for adsorption of toxic and other metals with a great variety of new fibre materials that have been developed for industrial applications based on their excellent mechanical properties and / or special functions (Shimamura et al. 1989). Nanofibres containing functionalised surfaces have a wide range of interesting and useful properties and can provide an effective backbone for anchoring functional ligands which are decorated on the high surface area support in a feasible and cost effective manner. The adsorption properties of the ligands could then be utilised and because of these advantages, electrospun nanofibres have been widely investigated in

the last few years for their use in metal ion removal (Bhardwaj and Kundu 2010; Jayaraman et al. 2004).

Chelating resins and polymers are widely used for wastewater treatment and selective concentration, removal and recovery of metal ions from a wide variety of sources (Shin et al. 2004a; Tabarzadi et al. 2009). Fabrication of chelating fibrous materials by introducing functional groups to the chemical structure of commercial fibres is a relatively new approach for producing novel high efficiency metal adsorbents (Chang et al. 2001; Shoushtari et al. 2006; Tahaei et al. 2008). Chelating fibres contain functional groups which are able to complex with metal ions and their sorption mechanism is by chelation rather than ion exchange and consequently, they are highly selective. Chelating fibres possess high specific surface area which is at least five times larger than that of porous beads (Lian et al. 2005) and the functional groups on the fibres are more accessible for metal ions, which are the reasons they present better kinetic characteristics (Abdous et al. 2012; Lian et al. 2005).

There are many types of fibres or modified fibres, including activated carbon fibre, cotton fibre, glass fibre, and synthetic fibres (polyester, polypropylene, polyethylene terephthalate, polystyrene), that have been used to adsorb metal ions or to enrich trace amount of metals from aqueous solutions (Deng et al. 2003). This literature review will highlight the emerging progress and use of electrospun nanofibres for metal ion adsorption with emphasis on the current scientific efforts which inform the background for the choices made in this study.

2.2 Nanofibre

Fibres with diameters below 100 nm are generally classified as nanofibres (MacDiarmid et al. 2001). Nanofibres provide a connection between the nanoscale

and the macro scale world, they possess unique properties that distinguish them from other non-woven fibres, like high surface area per unit mass, high porosity, layer thinness, high permeability, low basis weight, cost effectiveness, superior directional strength. It is these unique properties of nanofibres that make them promising materials for a variety of applications from medical to consumer products and industrial to high-tech applications (Fang et al. 2008; Fayemi et al. 2013; Reneker and Yarin 2008).

An advantage of electrospun polymeric nanofibres is the benefit of surface chemistry modifications in order to accommodate various functionalities for adsorption applications (Jayaraman et al. 2004; Reneker and Yarin 2008; Yoon et al. 2008). There are several approaches for generating fibres at nanometre scale and these include template synthesis (Feng et al. 2002), drawing (Huang et al. 2003; Xing et al. 2008), phase separation (Huang et al. 2003; Liu and Ma 2009), and self-assembly (Huang et al. 2003; Sargeant et al. 2008; Whitesides and Grzybowski 2002) and electrospinning. Electrospinning is a novel process for forming superfine fibres by forcing a polymer melt or solution through a spinneret with an electric field. Electrospinning is currently the most widely used method for the production of polymeric nanofibres, due to its simplicity, low cost, and suitability to yield very long fibres from various polymers (Mokhena et al. 2015). It has been shown for instance that nanofibres with a diameter of 100 nm have a ratio of geometrical surface area to mass of approximately 100 m²/g (Frenot and Chronakis 2003) and this can be a very good characteristic for an adsorbent and an interesting aspect of using functionalised electrospun nanofibres.

2.2.1 Electrospinning

Electrospinning or otherwise called electrostatic spinning is a unique synthetic method which has received much attention lately. This is the process of spinning fibres with the help of electrostatic forces, which has been found to be a viable technique to produce nanofibres with diameters in the range of 40–200 nm (Pereao et al. 2017; Sharma 2013). Electrospinning has gained much attention due to its versatility in spinning a wide variety of polymeric fibres and for its consistency in producing fibres in the submicron range (Ramakrishna et al. 2006). In fact, the major advantages of the electrospinning process are the technical simplicity and its easy adaptability (Subbiah et al. 2005). This process was patented by Antonin Formhals in 1934 and has become an attractive technique for the preparation of polymeric and composite nanofibres (Huang et al. 2003).

Electrospinning is a process by which polymer nanofibres can be produced using an electrostatically driven jet of polymer solution (or polymer melt). This approach has been used successfully to spin a number of synthetic and natural polymers into fibres many kilometres in length (Frenot and Chronakis 2003). Electrospinning has gained popularity in recent years due in large part to an increased interest in nanoscale properties and technologies. This technique allows for the production of polymer nanofibres with diameters varying diameters in the range of 40 - 200 nm or higher (Pham et al. 2006). One attractive feature of electrospinning is the simplicity and inexpensive nature of the setup.

The origin of electrospinning as a viable fibre spinning technique dates back to the early 1930s. In 1934, Formhals patented his first invention relating to the process and the apparatus for producing artificial filaments using electric charges. The method of

producing artificial threads using an electric field had been explored for a long time but it gained importance after Formhals's invention due to some technical difficulties of earlier spinning methods, such as fibre drying and collection. Formhals developed several innovative set-ups to produce yarns made out of electrospun fibres including designs that do not require the use of a spinneret (Teo and Ramakrishna 2006).

Electrospinning can simply be carried out by applying a high voltage (several thousand volts/cm) to a capillary tube filled with polymer fluid (solution or melt), which is ejected out toward a counter electrode serving as the collector. The liquid jet undergoes a whipping process and splaying occurs in a region where the repulsive force from the electric charges carried by the jet becomes larger than its cohesive force. Splaying and solvent evaporation, together with a large elongation (because of the acceleration of the polymer jet by the electric force) are responsible for formation of the nanometre-sized polymeric fibres (Hohman et al. 2001). Electrospinning is a direct extension of electrospraying, as both processes are based on the same physical and electrical mechanisms. The main difference is that continuous fibres are formed in electrospinning whereas small droplets are produced in electrospraying (Kanani and Bahrami 2011).

There are basically two electrospinning set-ups; vertical and horizontal and with the expansion of this technology, several research groups have developed more sophisticated systems that can fabricate more complex nanofibrous structures in a more controlled and efficient manner (Kidoaki et al. 2005; Stankus et al. 2006). The electrospinning process offers many advantages over traditional nanofibre fabrications (drawing, template synthesis, phase separation, and self-assembly) such as control over morphology, porosity and the possibility to develop continuous

nanofibres from various polymers for mass production. Electrospinning is currently the only technique that allows the fabrication of continuous fibres with diameters down to a few nanometres. An additional advantage of this nanofibre technology is that electrospinning has been up-scaled for nanofibre production on a commercial scale (Fayemi et al. 2013). Figure 2.1 illustrate a scheme of electrospinning set up.

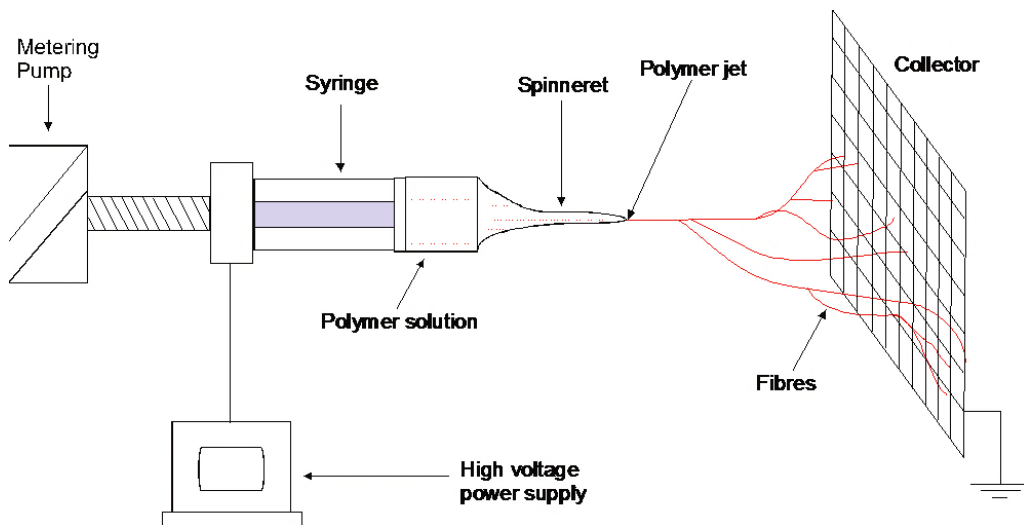


Figure 2.1 Schematic diagram of electrospinning apparatus set up

2.2.2 Parameters affecting electrospinning process

The production of nanofibres by the electrospinning procedure is influenced by the electrostatic forces and the viscoelastic behaviour of the polymer (Frenot and Chronakis 2003; Garg and Bowlin 2011). The parameters that affect the electrospinning process and the morphology and diameter of electrospun fibres can be divided into three main categories: (1) the processing conditions, (2) the intrinsic properties of the polymer solution, and (3) the ambient parameters (Haghi and Akbari 2007; Ramakrishna et al. 2005) and significant efforts have been made to characterise the properties of fibres as a function of process and material parameters (Subbiah et al. 2005). It is very important to understand and be able to control the electrospinning working parameters, as they affect fibre morphologies. It is possible

to obtain desired fibre diameters and morphologies through control of parameters such as applied voltage, distance between the nozzle tip and the collector, polymer flow rate, solution concentration, spinning environment (Li and Wang 2013). The ideal targets in electrospinning of a polymer into nanofibre are consistent and controllable fibre diameters, bead-free or defect-controllable fibre surface and collectable continuous aligned and/or single nanofibres (Raghavan et al. 2012).

Solution viscosity is considered the most important in determining the final diameter of as-spun fibres among all these process parameters (Garg and Bowlin 2011). An investigation of the effects of electrospinning parameters on the nanofibre diameter and length showed that continuous individual polycaprolactone (PCL) nanofibres with diameters in the range of approximately 350 nm to 1 μm could be collected at lengths of 35 to 50 cm, and that polymer concentration, voltage, and plate size had significant effects on maximum fibre length, fibre diameter, and fibre uniformity (Beachley and Wen 2009). However, an electrospinning solution with entangled chain network is generally required in producing bead-free nanofibres (Wang et al. 2015).

2.2.2.1 Applied voltage

Most researchers agreed that when higher voltages are applied, there is more polymer ejection and this facilitates the formation of a larger diameter fibre (Demir et al. 2002; Zhang et al. 2005). However, other authors (Lee et al. 2004; Megelski et al. 2002) have reported that an increase in the applied voltage (i.e., by increasing the electric field strength) increased the electrostatic repulsive force on the fluid jet which ultimately favoured the decrease of fibre diameter. Generally, an increase in the applied voltage increases the deposition rate of nanofibre due to higher mass flow

from the needle tip. The charge transport due to the applied voltage is mainly due to the flow of the polymer jet towards the collector, and the increase or decrease in the current is attributed to the mass flow of the polymer from the nozzle tip. Therefore an increase in applied voltage causes a change in the shape of the jet initiating point, and hence the structure and morphology of fibres (Deitzel et al. 2001a; Zong et al. 2002). Thus, voltage influences fibre diameter, but the level of significance varies with the polymer solution concentration and on the distance between the tip and the collector (Yördem et al. 2008).

There are different arguments by researchers; Reneker and Chun (1996) showed that applied voltage does not have a significant effect on fibre diameter in electrospinning of polyethylene oxide while Pawlowski et al. (2003) demonstrated that drier fibres could be obtained if the voltage is increased because of the faster evaporation of the solvent. Zhang et al. (2005) showed that there is more polymer ejection at higher voltages, facilitating the formation of larger fibre diameters when they studied the effect of voltage on fibre morphology and diameter distribution with poly(vinyl alcohol) (PVA)/water solution.

2.2.2.2 Distance between the nozzle tip and the collector

The structure and morphology of electrospun fibres is easily affected by the nozzle to collector distance because of their dependence on the deposition time, evaporation rate, and whipping or instability interval (Buchko et al. 1999; Megelski et al. 2002). The effect of tip and the collector distance on fibre morphology is not as significant as other parameters such as applied voltage, flow rate and solution concentration (Ki et al. 2005; Zhang et al. 2005; Zhao et al. 2005) but it has been reported that flatter fibres can be produced at closer distances while rounder fibres

were observed with an increase in distance (Buchko et al. 1999). However, average fibre diameters tend to decrease with an increase in collector distance (Chase and Reneker 2004; Fong et al. 1999; Zuo et al. 2005) and on the other hand authors such as Geng et al. (2005) and Lee et al. (2004) established that a minimum distance is required to give the fibres sufficient time to dry before reaching the collector, otherwise beads could be observed with distances that are either too close or too far. The function of a collector is also to form a conductive substrate for the collection of nanofibres. Aluminium foil is mostly used; however rotating rods on wire mesh, conductive paper as well as cloth and parallel or gridded bars are also used (Bhardwaj and Kundu 2010).

An investigation of mesoporous poly (vinyl alcohol) / tetraethylorthosilicate/aminopropyltriethoxysilane (PVA/TEOS/APTES) composite nanofibre prepared by sol-gel/electrospinning showed that beaded fibres were formed when the distance between needle tip and collector was 7.5 cm, and by increasing the needle tip-collector distance to 10 cm, the stability of the jet was increased resulting in the formation of fibres with fewer beads (Irani et al. 2012). When the needle tip-collector distance was increased to 12.5 cm, the fibres with the smallest diameters (average diameter equal to 196 nm) without beads formed on the collector. The strength of electrical force on the spinning solution was decreased by further increasing the needle tip-collector distance to 15 cm or greater than 15 cm which resulted in the formation of fibres with larger diameters (Irani et al. 2012).

2.2.2.3 Polymer flow rate

An increase in the polymer flow rate increases the fibre diameter and the pore diameter (Fong et al. 1999; Zuo et al. 2005). The polymer flow rate from the syringe

influences the jet velocity and the material transfer rate (Megelski et al. 2002). A slower feed rate is recommended in order to offer sufficient time for the evaporation of the solvent but too low flow rate of spinning solution may cause blockages of nozzles when pendant droplets form on the tip of the needle (Baumgarten 1971) and the drops may dry up and thus be sealed by solidified polymer residue. On the other hand, too high a flow rate of the spinning solution may cause an excess of solution which causes beaded fibres to be formed due to unavailability of proper drying time prior to reaching the collector (Kim et al. 2005b; Wannatong et al. 2004; Yuan et al. 2004; Zuo et al. 2005). In a dynamic liquid support system for continuous electrospun yarn fabrication, Teo et al. (2007) showed that with increased feed rate, there was a corresponding increase in the diameter of the individual fibres.

2.2.2.4 Solution concentration

The concentration of the polymer solution influences the spinning of fibres and controls the fibre structure and morphology. Low concentration polymer solutions form droplets due to the influence of surface tension, while higher concentrations prohibit fibre formation due to higher viscosity. Undulating morphologies in fibres were attributed to the delayed drying and the stress relaxation behaviour of the fibres at lower concentrations (Zong et al. 2002). The more viscous the solution becomes (lower than the process limiting concentration), the more uniform the fibres that are formed, and the diameters of the beads become bigger whilst the average distance between the beads increased as the solution viscosity increased.

When a solid polymer is dissolved in a solvent, the solution viscosity is proportional to the polymer concentration (Pereao et al. 2017). A higher viscosity leads to larger fibre diameter and higher polymer concentrations will also result in larger nanofibre

diameters (Fakirov 2016). It has been found that at low solution concentrations, a mixture of beads and fibres is obtained and as the solution concentration increases the shape of the beads changes from spherical to spindle-like and finally uniform fibres with increased diameters are formed because of the higher viscosity resistance (Haghi and Akbari 2007). The presence of beads in electrospun fibres is a common problem (Garg and Bowlin 2011; Gugliuzza 2014). The occurrence of beading depends on the various processing variables. When the applied voltage is increased, jet velocity is increased and the solution is removed from the tip more quickly. When the volume of the droplet on the tip becomes smaller, the Taylor cone shape oscillates and becomes asymmetrical. This leads to the formation of beads (Garg and Bowlin 2011).

2.2.3 Morphology of electrospun nanofibres

Electrospinning provides the opportunity to produce nanofibres with different structures and morphologies by varying the processing parameters. A number of methods have been employed in different contexts to fabricate polymeric nanofibres with different morphologies; beaded (Fong et al. 1999), branched (Koombhongse et al. 2001), helical fibres (Ramakrishna et al. 2006), ribbon (Koombhongse et al. 2001; McCann et al. 2006), porous (Ramakrishna et al. 2006; Zhang et al. 2006), smooth and core-shell nanofibres (Forward et al. 2013; Sun et al. 2003), and aligned nanofibres (Nguyen et al. 2016; Teo and Ramakrishna 2006).

The morphology of the electrospun nanofibre as well as fibre diameter can be changed by varying the electrospinning parameters to fit desired applications (Beachley and Wen 2009). Polymeric fibre can have nanosized diameter and Figure. 2.2 (Kim et al. 2005a) showed the classification of fibre diameters.

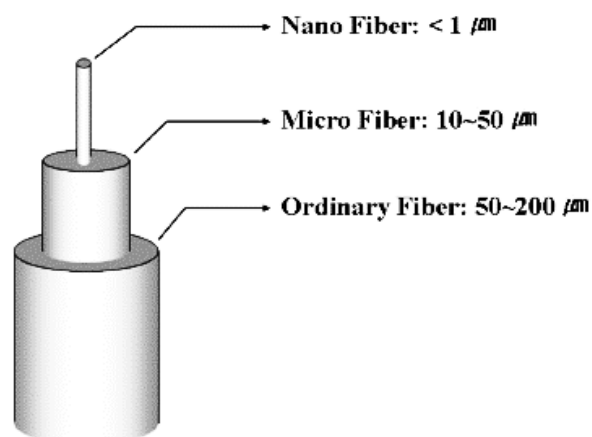


Figure 2.2 A classification of the fibre diameter

Nowadays, almost all adsorbents developed for the removal of toxic metal ions rely on the interactions of targeted compounds with functional groups that are present on the surface of the adsorbents (Amin et al. 2014), therefore, a large surface area and many adsorption sites of the matrix are essential properties for adsorbents to remove the contaminants from wastewater, and the specific surface area is one of the most important considerations for the adsorption capacity of the adsorbents.

In order to obtain a nanofibre membrane with ultra-high specific surface area, it is desirable to introduce a rough surface or pore structure on the fibre surface (Han et al. 2014). In the study by Min et al. (2012) who fabricated affinity membranes, electrospun fibres made of mixtures of poly (ether sulfones)/poly (ethyleneimine) (PES / PEI) were treated by solvent etching in a crosslinking solution of PEI. A unique fibre morphology was reported with significant PEI surface area per unit mass, with high effectiveness for toxic metal ions removal from water. Their experimental results showed that the main adsorption sites for the toxic metal ions were amino and imino groups on the PEI macromolecular chains which had

bifunctional properties that enabled them to adsorb cationic target compounds at different pH values in aqueous solutions.

2.2.4 Solvents used for electrospinning

The solvent used for preparing a polymer solution has a substantial influence on its spinnability, because the initial step in the electrospinning process is the dissolution of the polymer in a suitable solvent (Sarkar et al. 2010). Deitzel et al. (2001a) and Mahalingam et al. (2015) reported that solvent properties such as boiling point, density, surface tension and viscosity influence nanofibre morphology. Thus for successful electrospinning the selection of an appropriate solvent system is indispensable (Bhardwaj and Kundu 2010; Zhang et al. 2002b).

Solvent selection is pivotal in determining the critical minimum solution concentration to allow the transition from electro spraying to electrospinning, thereby significantly affecting solution spinnability and the morphology of the electrospun fibres (Luo et al. 2010). Solvent volatility plays a key role in the formation of nanofibres by influencing the phase separation process and the properties of solvents also have a profound effect on fibre diameter. In Table 2.1 below, Bhardwaj and Kundu (2010) described some typical solvents used in the electrospinning process and their different properties such as surface tension, dielectric constant and boiling point which should be kept in mind during solvent selection for the electrospinning process.

Table 2.1. Properties of different solvents used in electrospinning process

Solvents	Surface tension (mN/m)	Dielectric constant	Boiling point (°C)	Density (g/ml)
Chloroform	26.5	4.8	61.6	1.498
Dimethyl formamide	37.1	38.3	153	0.994
Hexafluoro isopropanol	16.1	16.7	58.2	1.596
Tetrahydrofuran	13.5	8.4	72.4	1.525
Trifluoro ethanol	26.4	7.5	66	0.886
Acetone	21.1	27	78	1.393
Water	25.2	21	56.1	0.786
Methanol	72.8	80	100	1
Acetic acid	22.3	33	64.5	0.791
Formic acid	26.9	6.2	118.1	1.049
Dichloro methane	37	58	100	1.21
Ethanol	27.2	9.1	40	1.326
Tri fluoro acetic acid	21.9	24	78.3	0.789

Basically, solvents perform two crucial roles in electrospinning: firstly to dissolve the polymer molecules for forming the electrified jet and secondly to carry the dissolved polymer molecules towards the collector (Ohkawa et al. 2004). Several studies, Son et al. (2004); Veleirinho, (2008) and Wannatong et al. (2004) have investigated the effect of solvents such as chloroform, ethanol, dimethylformamide (DMF), mixtures of trifluoroacetic acid, dichloromethane and water for electrospinning of poly (ethylene oxide) (PEO), PS and PET. The studies investigated the solvent properties and polymer concentration on the morphology, structure, mechanical and thermal properties during electrospinning. Trifluoroacetic acid (TFA), for instance, was found to be an excellent solvent for PET electrospinning to produce fine diameters because of the advantages which include its high dielectric constant (42.1), low

boiling point (72.4 °C), viscosity (η_s) (0.81cP) and low surface tension (13.4 dyn/cm) which favoured the production of fine fibres by electrospinning (Wang et al. 2012).

2.2.5 Polymers used in electrospinning and adsorption

The electrospinning process is applicable to many polymers, as a melt or a solution (Pereao et al. 2017). Polymers are amorphous, except for a minority of thermoplastics. Due to the bonding, polymers are typically electrical and thermal insulators (Chung 2013). Polymers in the form of thermoplastics (e.g., nylon, polyethylene, polyvinyl chloride, rubber) consist of molecules which have covalent bonding within each molecule and van der Waals forces between the molecules. Polymers in the form of thermosets (e.g., epoxy, phenolics) consist of a network of covalent bonds.

Polymers are well known for their wide availability and low cost and have been used for a myriad of product applications. They are being used in an increasingly wider range of applications such as wastewater treatment, toxic metal removal and enrichment of precious metals from hydrometallurgical liquids (Moloney 2008; Reddy and Reddy 2003). Up to now, it is reported that nearly one hundred different polymers, mostly dissolved in solvents (yet some heated into melts) have been successfully spun into ultrafine fibres using the electrospinning technique (Bhardwaj and Kundu 2010; Huang et al. 2003). In Table 2.2, some examples of these polymers, solvents used and their perspective applications are given.

Table 2.2. Typical examples of polymers used in electrospinning, solvents and the nanofibre applications.

Polymers	Applications	solvent	References
Collagen/chitosan	Biomaterials	hexafluoro-2-propanol/Trifluoroacetic acid (HFP/TFA)	Chen et al. 2007
PS	Skin tissue engineering	tetrahydrofuran (THF)	Sun et al. 2005
Cellulose acetate	Adsorptive membranes/felts	acetone, N,N-dimethylacetamide (DMAc)	Zhang et al. 2008
Chitosan	metal ions adsorption	acetic acid	Li et al. 2015
PET	metal ions adsorption	Trifluoroacetic acid/methylene chloride (TFA/CH ₂ Cl ₂)	Dong et al. 2013
Polyacrylonitrile	metal ions adsorption	Dimethylformamide (DMF)	Neghlani et al. 2011
Gelatin	Scaffold for wound healing	trifluoroethanol (TFE)	Huang et al. 2004
Polyarylene ether nitrile (PEN)	metal ions adsorption	dimethylformamide (DMF)	Zheng et al. 2015
Nylon 66	metal ions adsorption	formic acid/chloroform	Shahram et al. 2016
Nafion-polyvinyl alcohol (PVA)	metal ions adsorption	dimethylacetamide (DMAc)	Sharma et al. 2014
poly(ethersulfones) /poly(ethyleneimine)	adsorption	dimethylacetamide (DMAc)	Min et al. 2012

Electrospun nanofibres have been reported as being made from various synthetic polymers, natural polymers or a blend of both polymers (Bhardwaj and Kundu 2010; Ramakrishna et al. 2006). Regarding polymer source therefore, it can be distinguished between natural and synthetic polymers and these are further discussed.

2.2.5.1 Synthetic polymers

Synthetic polymers are generally named based on the monomer it is synthesised from, for example, ethylene is used to produce poly (ethylene) (Mohammad 2007). Synthetic polymers may be either semicrystalline or amorphous. Semicrystalline polymers have regular repeating units that allow the chains to fold into dense regions called crystallites. These act as crosslinks giving the polymer higher tensile strengths and higher modulus (stiffness) compared to an amorphous analog. No polymer can completely organize into a fully crystalline material so there are still amorphous areas in semicrystalline polymers (Middleton and Tipton 2000).

Most synthetic polymers have been synthesised by ring-opening polymerisation and there exists a thermodynamic equilibrium between the polymerisation reaction and the reverse reaction that will result in monomer formation. Excessively high processing temperatures can push the equilibrium to depolymerisation, resulting in monomer formation during the molding or extrusion process. The presence of excess monomer may act as a plasticiser changing the mechanical properties and may catalyse the hydrolysis of the device resulting in altered degradation kinetics (Middleton and Tipton 2000). Synthetic polymers can also be produced by modifications of natural polymers or by coupling of synthetic polymer such as polyethylene glycol (PEG) to naturally occurring substances such as fatty acids (Werle 2008).

Synthetic polymers offer many advantages over natural polymers as they can be tailored to give a wider range of properties, such as necessary mechanical properties (viscoelasticity and strength), and desired degradation rate (Hakkarainen 2002). Synthetic polymers have good mechanical properties and thermal stability, much

better than several naturally occurring polymers. There is also a limitation in the performance of several natural polymers in comparison to synthetic polymers. Synthetic polymers can be processed into a wide range of shapes, whereas for natural polymers several shapes are not easily obtained; for example, high temperatures imposed in processing can destroy their native structure (Sionkowska 2011). From the list of various polymers used for electrospinning, polystyrene and polyethylene terephthalate, typical polymers used for electrospinning process in this study will be discussed.

2.2.5.1.1 Polystyrene

Polystyrene, a hydrophobic-oleophilic material, is a popular plastic that can be chemically modified by sulfonation (Roth 1954), acylation (Blanchette and Cotman Jr 1958), amination (Dharanivasan et al. 2015), amidomethylation (Shimamura et al. 1989; Teramoto and Nakamoto 2002), nitration (Bachman et al. 1947) and chloromethylation (Teramoto 1991) by preparing the polystyrene polymer as a carrier for immobilisation of various compounds for adsorbing capacity. The benzene ring of the polystyrene is quantitatively substituted by any of these groups and can be further converted into various functional groups (Teramoto and Nakamoto 2002). Polystyrene has a hydrophobic surface, and to obtain a better surface contact with the aqueous solution being extracted an activating solvent such as acetone, methanol, or acetonitrile is used to pre-treat the nanofibre. Another strategy is to make the surface of the nanofibre permanently hydrophilic through a chemical reaction (León-González and Pérez-Arribas 2000).

The use of polystyrene as an adsorption support is not recent because of its outstanding physical and reactive properties (Bessbousse et al. 2009). Polystyrene

(Figure 2.3) remains the most popular organic polymer support, and has proven to be a versatile support due to the large number of ligands that can be covalently bound to it (Alexandratos and Crick 1996). With a careful choice of ligands, immobilised ligands which include amines, pyridines, imidazoles, oximes, hydroxylamines, Schiff bases, thiols, crown ethers, and a variety of phosphorus ligands can lead to the synthesis of polymer-supported extractants that can be used for the recovery of metal ions from aqueous solution (Alexandratos and Crick 1996; Helfferich 1965).

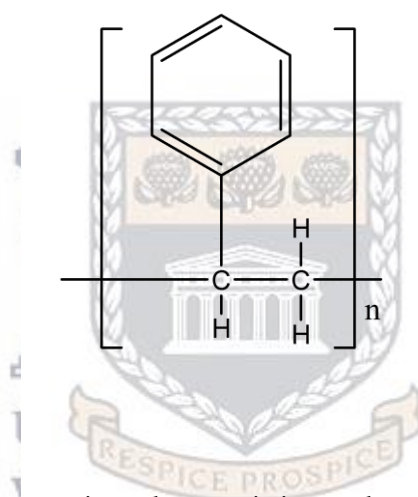


Figure 2.3 Polystyrene

PS possesses widely appropriate characteristics such as good mechanical properties and chemical resistance, ease of electrospinning, and low cost, but cannot individually adsorb metal ions efficiently. Chemical modification often affords an easy access route to polymers which are normally difficult to prepare by a direct route. The chemical modification of PS has continued to attract much attention due to the numerous applications of functionalised polymers in areas as varied as ion exchange, polymeric protecting groups, peptide synthesis and other polymer-supported reactions. Feng et al. (2011) did a comparison between electrospun PS and styrene–butadiene–styrene (SBS)/PS blend nanofibres for copper ion (Cu^{2+}) adsorption. They showed that PS/SBS blend nanofibrous samples have more rapid

adsorption rate for Cu^{2+} than that of those samples consisted of pure PS because there were more exposed functional groups for the metal ion onto the surface of the samples.

Polystyrene has been chemically modified by Friedel-Crafts acylation with cis-1,2,3,6 tetrahydrophthalic anhydride in the presence of anhydrous aluminium chloride (Biswas and Chatterjee 1983). It was also shown that electrophilic substitution of polystyrene with aromatic anhydrides including phthalic anhydride, pyromellitic dianhydride and trimellitic anhydride modifies the properties of the parent polystyrene (Biswas and Chatterjee 1982). Saadeh et al. (2012) synthesised a new PS-based terpyridine polymer for the adsorption of Ni^{2+} , Cu^{2+} , Pb^{2+} , and Zn^{2+} ions. Darko et al. (2011) incorporated potassium salts of pyrazole-1-carbodithioate and imidazole-1-carbodithioate into electrospun polystyrene fibres as sorbents for toxic metals of Cu^{2+} , Pb^{2+} and Ni^{2+} from aqueous environments.

2.2.5.1.2 Polyethylene terephthalate

Electrospun polyethylene terephthalate is a strong, stiff synthetic fibre, and a member of the polyester family of polymers (Strain et al. 2015; Wang et al. 2012). Poly(ethylene terephthalate) (PET) polymer is one of the most important synthetic polymer fibres used in the textile industry and has superior fibre forming properties such as the easy packaging of polymer chains with orientation, and resistance against microorganisms, erosion, stretching and acidic media (Coşkun 2008). PET fibre's structures contain benzene rings, alkane chains and ester groups (Figure 2.4). Poly(ethylene terephthalate) is one of the most common synthetic polymers used to produce fibres, textile, beverage containers, package and engineering materials

(Kuczenski and Geyer 2010; Wang et al. 2012) and has a high resistance toward weak mineral acids, even at high temperature, and to most strong acids at room temperature as well as oxidising agents, sunlight and micro-organisms (Monier and Abdel-Latif 2013b).

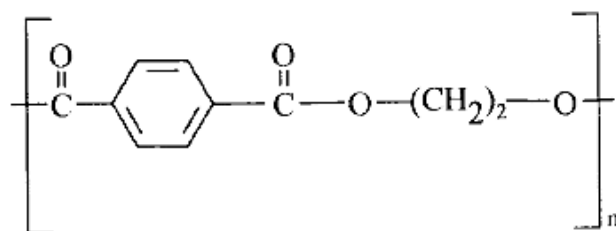


Figure 2.4 Polyethylene terephthalate

PET fibres do not contain chemically reactive functional groups, showing resistance to moisture, dye anions or cations (Monier and Abdel-Latif 2013a) but possess desirable fibre properties such as strength, high resistance to stretching, shrinkage, and abrasions, as well as undesirable features such as low moisture regain, difficulty of dyeing, due to its crystalline structure, hydrophobic character, and lack of chemically reactive groups. Certain desirable properties could be imparted to PET fibres by grafting onto it a number of different hydrophilic and other vinyl monomers such as 4-vinyl pyridine (4-VP), 2-hydroxyethylmethacrylate (HEMA), acrylic acid, methacrylic acid, acrylamide, and acrylonitrile (Abdolahifard et al. 2011; Kaur et al. 2013).

Modified Poly(ethylene terephthalate) (PET) fibres have been applied for the efficient extraction of metals from aquatic environment, for instance, Sereshti et al. (2015) fabricated electrospun polyethylene terephthalate (PET) nanofibre films which were used as novel adsorbent for the extraction of chromium (VI) in water

samples. The prospects for rare earth elements removal and the revolution and advancement of various opportunities using electrospun nanofibres are emerging as a better choice for potential adsorbent applications. The modification of nanofibres for rare earth elements will be further reviewed in Section 2.3.8 while the ligands in use are discussed in Section 2.3.6.

2.3 Rare earths metals

Rare earth elements denote a group of seventeen chemically similar metallic elements, including scandium, yttrium, and the lanthanoids (Ogata et al. 2014). The lanthanide element electronic configuration is constituted of an inner shell with electrons in the $4f^n$ orbital, shielded by an outer shell composed of electrons in orbitals $5s^2$, $5p^6$, $5d^{1-10}$ and $6s^2$ (Galhoum et al. 2015). The demand for rare earth metals and their compounds are crucial due to a broad and rapidly expanding range of applications that rely upon their chemical, catalytic, electrical, magnetic, and optical properties which has equally led to the development of technologies and processes for the separation of the metallic ions from various sources. Rare earth deposits and availability, technological applications of rare earth metals, environmental effects of REEs and different prospects for rare earth elements recovery technologies will be further discussed in the following subsections.

2.3.1 Rare earth deposits and availability

The main commercial sources of rare earths are bastnasite $(La, Ce)FCO_3$, monazite, $(Ce, La, Y, Th)PO_4$, and xenotime, YPO_4 . Four rare earth metals, viz. cerium, lanthanum, neodymium, and yttrium, constitute more than 85% of the global production. Recoveries for each of these metals are possible, but it still remains a challenge (Du and Graedel 2011). Over 90% of the world's economically recoverable

rare earth elements are found in primary mineral deposits in bastnaesite ores located in China and at Mountain Pass in California (USA) while monazite deposits in Australia, Brazil, China, India, Malaysia, Russia and South Africa contain the second largest concentrations of rare earth elements (Kołodzyńska and Hubicki 2012).

Rare earth mines have operated in Brazil, India and South Africa in the 1950s, but from the 1960s to the 1980s, the largest global producer was a mine in Mountain Pass, California (Xie et al. 2014). In the 1990s, China began large scale production and exported cheaper rare earths. Invariably, other producers were unable to compete economically, and they began to close down in the 1990s and later, Mountain Pass mine shut down in 2002 (Tse 2011). Consequently, China became the world's largest producer of rare earth elements, providing more than 95% of the world's total supply from its mines in Inner Mongolia (Chen 2011). Presently, the major mining and extraction processes from primary ore are highly energy intensive and require sufficient concentration of the metal of interest (Dodson et al. 2012).

The result of an analysis of 14 raw materials defined as critical at a European Union level with respect to the politico-economic stability of the producing country, their geographical concentration, their substitution potential, and their rate of recycling showed that rare earth elements (REEs) (15 lanthanides plus yttrium and scandium) were included on this list from the forty-one raw materials analysed (Blissett et al. 2014; Seredin et al. 2013). Therefore, rare earth elements' demand will continue to grow and depending on price and availability, global demand could increase to 160-200,000 t.p.a. by 2020 and magnet based applications will continue to grow at the highest rate.

Despite the name, REEs are not actually rare, especially the light rare earth elements group (LREEs) containing elements from lanthanum to europium (Z from 57 to 63), which are extracted in a more common and easier way than the toxic rare earth elements group (HREEs) which contain elements from gadolinium to lutetium (Z from 64 to 71) (Charalampides et al. 2016; Drost and Wang 2016). The only elements that are really scarce (upper crust abundance ≤ 1 ppm) and difficult to find, are europium, lutetium and thulium (Massari and Ruberti 2013). The forecast supply and demand of rare earths for 2014 (Jha et al. 2016; Seaman 2010) is presented in Table 2.3 as well as the commercial pricing of REEs in dollars (Frontier Rare Earths 2015).

Table 2.3. Estimated supply and demand of rare earth elements in 2014 and the commercial pricing of REEs

Elements	Supply (REO in tonnes)	Demand (REO in tonnes)	Surplus/Deficit (REO in tonnes)	REE price (\$/kg)
Lanthanum	54,750	51,050	3700	5
Cerium	81,750	65,750	16,000	5
Praseodymium	10,000	7900	2100	117
Neodymium	33,000	34,900	- 1900	58
Samarium	4000	1390	2610	5
Europium	850	840	10	705
Gadolinium	3000	2300	700	47
Terbium	350	590	- 240	615
Dysprosium	1750	2040	- 290	340
Erbium	1000	940	60	0
Yttrium	11,750	12,100	- 350	13
Ho-Tm-Yb-Lu	1300	200	1100	0
Total	203,500	180,000	23,500	-

2.3.2 Technological applications of rare earth metals

The availability of rare earth metals and their compounds are often crucial due to a broad and rapidly expanding range of applications that rely upon their chemical,

catalytic, electrical, magnetic, and optical properties (Koltun and Tharumarajah 2014; Xie et al. 2014). The REEs are increasingly important in the transition to a green, low-carbon economy due to their usefulness in catalysts, permanent magnets, rechargeable nickel–metal hydride (NiMH) batteries and lamp phosphors. The increasing popularity of hybrid and electric cars, wind turbines and compact fluorescent lamps is also triggering an increase in the demand and price of REEs (Binnemans et al. 2013). The commercial significance of REEs is not reflected in the volume in which they are used or produced as their annual primary production tonnage is approximately two orders of magnitude less than copper and four orders of magnitude less than iron.

However, they are more important than bulk metals because they provide critical functionality in a widespread variety of applications and are used in relatively large amounts in key technologies being developed to provide sustainable mobility and energy supplies (Alonso et al. 2012). Another major reason why lanthanides are expensive is because they have similar fundamental chemical properties which make them difficult to separate into individual elements (Shimojo et al. 2007). High-technology industries are demanding increasing amounts of precious (noble metals, platinum group metals) and strategic metals, especially rare earth elements (comprising lanthanides plus yttrium and scandium), which are used in metallurgy, electronic devices and the nuclear power industry (Tao and Huiqing 2009). They are becoming indispensable in many high-tech industries as shown in Table 2.4 by Castor and Hedrick (2006).

Table 2.4. REE uses and applications by industry

Industry	Applications
Automotive	Catalysts for pollution control; catalytic converter catalyst substrate; rechargeable batteries; fuel cells; coloured plastics
Ceramics	Oxygen sensors; structural ceramics for bearings; jet engine coatings; investment molds; refractories; pigments
Chemicals	Oil refinery fluid cracking catalysts; pharmaceuticals; water treatment; catalysts; moisture control, dryers, and detection
Defence	Lasers; missile guidance and control; visual displays; radar; electronic countermeasures; communication; shielding
Electronics	Capacitors; cathodes; electrodes; semiconductors; thermistors; traveling wave tubes (TWTs); radio frequency circulators; yttrium iron garnet (YIG) ferrites
Glass	Polishing compounds; decolourizing; colourizing; increase refraction; decrease dispersion; radiation stabilization; absorber
Illumination	Trichromatic fluorescent lamps; mercury lamps; carbon arc lamps; gas mantles; auto headlamps; long-glow phosphors
Magnets	Speakers and headphones; linear motors; antilock braking systems; tape and disk drives; gauges; electric motors; pumps; ignition
Magnetostrictive	Sonar systems; precise actuators; precision positioning; vibratory screens; speakers; ultrasonic to kill bacteria
Medical	Contrast agents; magnetic resonance imaging (MRI); positron emission tomography (PET); radioisotope tracers and emitters
Metallurgy	Alloying agents in aluminium, magnesium, iron, nickel, and steel alloys; super alloys; pyrophoric alloys; lighter flints; armaments
Phosphors	Cathode-ray tubes (CRTs); fluorescent lighting; radar and cockpit displays; x-ray intensifying screens; temperature sensors
Others	Simulated gemstones; textiles; magnetic refrigeration; hydrogen fuel storage; lubrication; photography; nuclear uses

Therefore new metal removal processes from dilute effluents (uranium leachates, metallurgy effluents) and from secondary resources (coal and phosphate ore residues) are being developed (Galhoum et al. 2015). Four rare earth metals, viz. cerium, lanthanum, neodymium, and yttrium, constitute more than 85% of the global production. Generally cerium is the most abundant lanthanide on earth with a comparable crustal concentration to the lighter Ni and Cu (Cotton 2006) while Neodymium (Nd) is the second most abundant rare earth element (Manoochehri and Khalesi 2012) with wide use in advanced technologies such as electronic and communication devices, high-performance alloys, magnets, glasses, ceramics and catalysts (Galhoum et al. 2017). Cerium and neodymium are two important member of the rare earth family. Cerium plays an important role in three-way catalysis and fluid catalytic cracking, two catalytic processes that are significant because of their economic relevance and tonnage.

2.3.3 Environmental effects of Rare Earth Elements

The growing demand for REEs has led to an increased environmental exposure and water pollution from numerous REEs commercial products and rare earth metal mines. The main pathways of human exposure to rare earth oxides (REO) include inhalation, dermal contact, and ingestion of foods and beverages. Studies have reported that environmental exposure to high levels of REO could result in harmful effects, such as pneumoconiosis, acute myocardial infarction, abnormal blood biochemical indices, leukaemia, lower IQ scores in children, low total protein content of serum, itching, sensitivity to heat, and skin lesions (Guo et al. 2015). Zhenggui and co-workers (Zhenggui et al. 2001) reported higher solubility and bioavailability of REEs in mining area soils compared to those in normal soils. REE ores and commodities, as well as by-products and waste materials from REE processing, are

naturally radioactive, mostly because of the contained thorium (Castor and Hedrick 2006). The thorium content of monazite for instance, typically ranges from 4% to 10% ThO₂ therefore thorium produced during REE processing presents an expensive disposal problem for the industry (Castor and Hedrick 2006).

2.3.4 Rare earth elements recovery technologies

Rare earth element recovery from solid waste or minerals may involve pyrometallurgy or hydrometallurgy (chemical leaching or bioleaching) (Galhoum et al. 2015; Zhang et al. 2013). A significant challenge is the selectivity of the materials and their capacity to separate target metals from complex effluents. A wide range of technologies such as adsorption (Foo and Hameed 2009), ion exchange (Reddy et al., 2009), ionic imprinted polymers (Rao et al. 2006), chemical precipitation (Ku and Jung 2001), electrocoagulation (Parga et al. 2005), flotation (Polat and Erdogan 2007), electrodialysis (Marder et al. 2004), reverse osmosis (Fu and Wang 2011), membrane filtration (Vigneswaran et al. 2005), nanofiltration (Yang et al. 2001), membrane electrolysis (Janssen and Koene 2002) and solvent extraction (Rydberg 2004; Vander Hoogerstraete et al. 2013), are available for the removal or extraction of metals from leachates or waste streams with varying levels of success (Foo and Hameed 2010; Galhoum et al. 2015).

The recovery of metal ions and more specifically REEs can involve many different processes depending on the concentration of valuable or toxic metals, the composition of the solution and the economics of the process and target metals (Tolba et al. 2017). Ion-exchange and chelating resins are more appropriate for concentrating and separating metals ions from dilute effluents, playing with the

affinity of their specific functional groups towards REEs (Esma et al. 2014; Jain et al. 2002; Jain et al. 2007; Maheswari and Subramanian 2004; Tolba et al. 2017).

2.3.4.1 Adsorption

Adsorption is an alternative treatment technique for recovering valuable elements or toxic metals from wastewaters. Adsorption is a mass transfer process where a substance is transferred from the liquid phase to the surface of a solid, and becomes bound by either physical and/or chemical interactions which results in the transfer of metals from the aqueous phase to the solid phase (Foo and Hameed 2009; Freeman 1989; Voice 1989; Watson 1999). The adsorption process advantages make it a promising alternative to costly removal methods for the separation and removal of various metals from polluted water. Studies on the treatment of effluents containing toxic metals have shown adsorption to be a highly effective technique and it could be used for the removal of REEs from aqueous environments (Wang et al. 2010; Younis et al. 2014).

Adsorption has been recognised as one of the most efficient, promising and widely used fundamental approaches in hydrometallurgy and wastewater treatment processes (Foo and Hameed 2009; Gładysz-Plaska et al. 2014; Ogata et al. 2016; Zhao et al. 2016), mainly due to being simple, economically viable, technically feasible and socially acceptable (Nouri et al. 2007) even from low-concentration sources (Ogata et al. 2015). Several adsorbents such as those used in biosorption (Yan and Viraraghavan 2003), magnetic nanoparticle adsorbent (Zhao et al. 2015a; Goon et al. 2010; Ren et al. 2013), silica based sorbents (Jal et al. 2004; Matoso et al. 2003; Xie et al. 2008) have been used for the removal of metal ions.

In practice, adsorption commonly involves passing a fluid over a bed of adsorbent particles, onto which components (sorbate) are sorbed. The process continues until the sorbent is saturated and the adsorbate components can no longer be removed from solution effectively. The sorbent may be disposed of or regenerated. Regeneration is commonly carried out by passing a solvent (often strong acid) through the used adsorbent, releasing sorbed components into a regenerant solution which is collected. The sorbent material may then be reused. Regeneration also recovers the metals so they can be disposed of properly or purified for reuse (Zander 2009).

In the processes of adsorption, adsorbents with porous structure and enormous surface areas are significant. Small pores, such as micropores (pore size < 2 nm) and mesopores (2 nm < pore size < 50 nm), result in high porosity and surface area which are responsible for adsorption (Zhao et al. 2015b). Adsorption capacity is an essential parameter for the estimation of process costs. Regeneration of the sorbent is important in cyclic processes when the used sorbents are expensive while kinetic parameters are used to determine the rate of the sorption process (Keller and Staudt 2005).

In adsorption technology, it is widely known that two adsorbent materials (even for the same pollutant) cannot be compared without maintaining similar experimental conditions. Some of the considerations which strongly influence the whole procedure are (i) the adsorbent's dosage; (ii) agitation speed; (iii) contact time; (iv) initial pollutant concentration; (v) ionic strength of solution; (vi) temperature; (viii) the pH solution; (ix) volume of adsorbate. It is clear that if any of the aforementioned conditions vary, the experiment will not be the same and consequently no

comparison will be correct. Having the above in mind, the only comparisons that can be realised are those for adsorbent/adsorbate systems of the same study (Kyzas and Bikiaris 2015).

2.3.5 Adsorbents in Use

There are many types of adsorbents, including activated carbon, zeolites, bentonite, peat, sawdust, and biomaterials, that have been studied for the adsorption of metals from aqueous solutions (Kobyas 2004; Nakajima and Baba 2004). The adsorbent must also have good mechanical properties such as strength and resistance to attrition and it must have good kinetic properties, that is, it must be capable of transferring adsorbing molecules rapidly to the adsorption sites. In most applications, the adsorbent must be regenerated after use and therefore it is desirable that regeneration can be carried out efficiently and without damage to mechanical and adsorptive properties. The raw materials and methods for producing adsorbents must ultimately be inexpensive for adsorption to compete successfully on economic grounds with alternative separation processes (Crittenden and Thomas 1998; Neto et al. 2013; Olafadehan et al. 2012).

A number of different materials with increasing complexity have been tested for Ce^{3+} and Nd^{3+} ; inorganic sorbents (Iannicelli-Zubiani et al. 2015; Kozhevnikova and Tsybikova 2008; Ponou et al. 2014), hydrous ferric oxide (HFO) (Dubey and Rao 2011), granulated zeolites (Subotić and Bronić 1986), plant leaves (Kütahyalı et al. 2010; Sert et al. 2008), agriculture wastes (Paudyal et al. 2012), composite inorganic/organic materials (Roosen et al. 2014; Roosen et al. 2015), algal or yeast biomass (Oliveira et al. 2012; Palmieri et al. 2000; Vlachou et al. 2009), biopolymers (Konishi et al. 1992; Konishi et al. 1998), chemically-modified biopolymers

(Galhoum et al. 2016), imprinted polymers (Dolak et al. 2015), cellulose and chitosan polymers bearing hydroxyl/carboxyl groups and amine groups, respectively (Galhoum et al. 2017).

Many of these adsorbents are reported to have low selectivity and poor removal efficiencies for low concentrations of metal ions. Also, the slow removal rates often fail to meet pollution control requirements (Ruparelia et al. 2008). Thus, the need arises for exploring alternative adsorbents, with better metal removal efficiency for low aqueous concentrations initiating the research to exploit the unusual and unique properties of nanomaterials. More recently nanofibres have attracted a great deal of attention due to their unique properties, such as high surface area, high porosity and adsorption capacity. The nanometre material is a new functional material, which has attracted much attention due to its special properties. Nanofibres have high adsorption capacity; besides, the operation is simple, and the adsorption process rapid. So there is a growing interest in the application of nanofibres as adsorbents (Rahmani et al. 2010).

2.3.6 Ligands in use

For increasing adsorption efficiency, surface modifications of synthetic and semi-natural polymers by using functional groups of carboxylic, sulfonic, amide, and amine have been abundantly developed (Bahramzadeh et al. 2016; Dharanivasan et al. 2015; Huang et al. 2012; Leonor et al. 2007; Li, Feng, Huang 2009; Li et al. 2009; Lü et al. 2007; Shin et al. 2004b).

Several polymer-supported ligands used in REEs separations include: EDTA and DTPA (Dupont et al. 2014; Rahal et al. 2015), 8-hydroxyquinoline (8-HQ) (Kajiya et al. 2004; Sohrin et al. 1998), hydroxamic acid (Agrawal et al. 1999; Kumar et al.

2011a), tetramethylmalonamide (TMMA) (Nogami et al. 2003; Yang and Alexandratos 2010), 2,6-diacetylpyridine (Karadaş et al. 2011), phosphorus ligands (Wu et al. 2013), o-vanillinsemicarbazone (OVSC) (Jain et al. 2001). Selectivity can be increased with ligands that can coordinate or chelate with the target metal ion. The grafting of amino and carboxylic acid groups on cellulose increased La(III) sorption efficiency of cellulose and maximum sorption capacity increased from 38 mg La g⁻¹ (0.273 mmol/g) for cellulose to 101 (0.727 mmol/g) and 170 mg La g⁻¹ (1.22 mmol/g) for amino derivative (PAC) and amino-carboxylic derivative (PCMC) (Tolba et al. 2017).

Macro porous cross-linked polystyrene functionalised with iminodiacetic and aminomethylphosphonic acid groups have been used in the sorption of La(III) metal (Esma et al. 2014). Calix[4]arene-o-vanillinsemicarbazone was immobilised on a polymeric matrix and used for the preconcentration and separation of lanthanum(III) and cerium(III) (Jain et al. 2007). Cellulose and chitosan intrinsic sorption properties for Nd(III) and their efficiency for metal recovery was improved by the grafting of aspartic acid thus allowing increased sorption capacities due to the specific reactivity of carboxylate groups (Galhoum et al. 2017).

2.3.6.1 Diglycolic acid (DGA)

Diglycolic acid (DGA), a dicarboxylic acid, can be employed as ligand for the extraction and pre-concentration of valuable actinide and lanthanide metal ions from aqueous solution. DGA (Figure 2.5) is a tridentate ligand and possesses a great tendency to bind with REEs (Ogata et al. 2014; Ogata et al. 2015). Diglycolic acid is similar to diglycol amic acids which are both regarded as promising task specific ligands suitable for the removal of lanthanides (Selvan et al. 2017). For instance,

diglycol amic acid was chemically immobilised onto the surface of silica gel particles in order to investigate the adsorption behaviour of rare earth metal ions (Dy and Nd) and base metal ions (Cu, Fe(III), and Zn) (Ogata et al. 2014) while iron oxide (Fe_3O_4) particles functionalised with diglycolamic acid (Fe-DGAH) were used for the mutual separation of Am(III) and Eu(III) from dilute nitric acid medium (Suneesh et al. 2015).

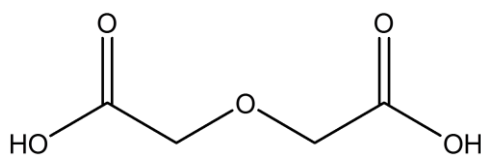


Figure 2.5 Structure of diglycolic acid (DGA)

Diglycolamide (containing ether linkages between two amide groups) which is a kind of diamide derivative has been employed as a ligand for the extraction and pre-concentration of valuable actinide and lanthanide metal ions from aqueous solution (Deb et al. 2011; Kannan et al. 2008). Several studies have described extractants, based on alkyl diglycolamides, that show unusually effective extraction of trivalent actinides and lanthanides from nitric acid (Horwitz et al. 2005; Sasaki and Tachimori 2002; Suneesh et al. 2012). The diglycolamide compounds as extractants have been studied in the field of nuclear energy for the separation of actinoids from high-level waste (Ansari et al. 2011) and for the separation of rare earth elements from base metals (Narita and Tanaka 2013).

The challenge in separating REEs from environmental and industrial samples resides in the fact that REEs and more specifically the lanthanides (Ln) have very similar physical and chemical properties (Florek et al. 2015) and, while other oxidation states are synthetically available for the REEs, they tend to exist in environmental

conditions as trivalent ions (Schweitzer and Pesterfield 2010). In addition, all of the REEs have similar radii ranging from 74.5 (Sc³⁺) to 103.2 pm (La³⁺) and also have coordination numbers ranging from 6 to 9, and sometimes more (Cotton 2006).

In order to satisfy their coordination spheres, REE's tend to coordinate different solvent molecules and have a predilection for chelating ligands (Abbasi et al. 2005; Cossy et al. 1989; Meier et al. 1990). However, the Ln³⁺ cations are strong Lewis acids and easily coordinate nucleophiles to form stable complexes and they show a clear tendency towards oxygen donors, both in acidic and basic conditions, which can be advantageous for their efficient extraction (Hart 1987). It is documented that the best ligands used for extraction of REEs are mostly oxygen donors (e.g., carboxylic acids, ketones, phosphoric acids) (Rabie 2007; Singh et al. 2006; Xie et al. 2014). In particular, the derivatives of DGA are used industrially for the selective extraction of REEs from aqueous solutions, as they are commonly recognised as effective and size selective binders of trivalent f-elements. They show high and rapid extraction even in strongly acidic conditions (104 to 100 M in HNO₃) (Narita et al. 1998; Sasaki et al. 2001; Sasaki et al. 2007; Zhu et al. 2004).

2.3.6.2 Adsorption mechanism of rare earth elements by adsorbents with diglycolamic acid ligands

The structural analysis of complexes bearing the DGA ligands shows that REEs bind traditionally in a tridentate fashion, where each metal ion is coordinated by the three oxygen atoms of DGA-type ligands. The lanthanide ions (e.g., La, Yb, Ce) are sterically saturated in their nine-coordinate geometry with three DGA ligands (Matloka et al. 2005; Tian et al. 2005; Zhang et al. 2002a). The angle formed by

chelate ligands, known as the bite angle, can greatly affect the binding properties of these ligands in the complexes (Figure. 2.6) (Birkholz et al. 2009; Jover et al. 2012).

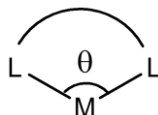


Figure 2.6. Bite angle between the metal and the coordinating atoms of the ligand.

Ligands with large bite angles will have a higher affinity for larger ions whereas smaller bite angles will favour coordination to smaller ions (Freixa and Van Leeuwen 2003). However, it is expected that a chelating ligand bound to a solid surface by more than one anchor point will possess a rigid conformation and will exhibit less flexibility to adapt itself to the metal electronic requirements than in solution. Therefore, by the right tailoring of chemically similar chelating ligands and their grafting on solid supports, it should be possible for functional materials to exhibit selective affinities for smaller or larger ions (Florek et al. 2015).

Adsorbents with diglycolamic acid ligands adsorb REE ions via three oxygen atoms and this tridentate chelation confers high selectivity for REE ions. Even though the high REE selectivity seems to be attributed to chelation of the metal ions by the tridentate diglycolamic acid framework, the details of the adsorption mechanism remained to be properly clarified. Ogata et al. (2016) elucidated the adsorption mechanism, by preparing some derivatives of DGA and investigating the differences in their adsorption behaviours with respect to REE ions. It was concluded that the adsorbents modified with diglycolamic acid adsorbed REE ions because diglycolamic acid contains ether oxygen atoms whereas succinamic and glutaramic acids do not. These results indicated that the ether oxygen atoms in the diglycolamic acid framework played a crucial role in adsorption of the REE ions.

On the basis of these, it was concluded that adsorbents with diglycolamic acid ligands adsorb REE ions via three oxygen atoms (that is, the ether, amide, and carboxylic acid oxygen atoms of the diglycolamic acid ligands). However, Van Nguyen et al. (2016) held a contrary view. They believed that the dissociation of the terminal carboxylic acid functional groups was responsible for adsorption and that when the pH increases, dissociation of the resin increases to provide more ion-exchange sites and the existence of the cation exchange species eventually become dominant and increased the adsorption efficiency.

2.3.7 Nanofibre adsorbents

Polymeric nanofibres are a class of materials having a diameter in the range of the nanometre. Fibres with diameters below 100 nm are generally classified as nanofibres (MacDiarmid 2001). Nanometre scale materials are new functional materials, which have attracted much consideration due to their special properties. Nanofibres possess unique properties that distinguish them from other non-woven fibres, like high surface area per unit mass, high porosity, layer thinness, high permeability, low basis weight, cost effectiveness, superior directional strength. It is these unique properties of nanofibres that make them a promising material for a variety of applications from medical to consumer products and industrial to high-tech applications (Fang et al. 2008). Nanoparticles have high adsorption capacities; the operation is simple, and the adsorption process is rapid. There is an emergent and growing interest in the application of these nanomaterials as adsorbents (Rahmani et al. 2010).

Nanofibres provide an attractive solution to the removal of toxic metals from water (Thavasi et al. 2008). Electrospun polymeric nanofibres have a vast potential for deposition and support of other materials on their surfaces due to the high surface

area, high porosity, and high inter-fibres connections (Reneker and Yarin 2008). To date, a variety of synthetic and natural polymers have been electrospun (Huang et al. 2003), and applied to adsorption of metals. The research and development of nanofibres for adsorption is still emerging and more investigations are expected to increase the knowledge in this new area especially for removal of REEs from aqueous solutions.

In recent years, the use of electrospun polymeric nanofibres for adsorption of heavy metals has increased (Abbasizadeh et al. 2013; Aliabadi et al. 2014; Kampalanonwat and Supaphol 2014; Ki et al. 2007; Li et al. 2011; Lu et al. 2014; Musyoka et al. 2011; Ndayambaje et al. 2016; Razzaz et al. 2016; Sharma et al. 2014; Tian et al. 2011; Wang et al. 2011; Wu et al. 2010) and some applications of electrospun nanofibres as adsorbent were summarised elsewhere (Pereao et al. 2017).

2.3.8 Modification of nanofibres

Different schemes can be used to produce nanofibres bearing different functional groups and the functionalisation of a preformed nanofibre only requires setting the conditions for the functionalisation reaction, since the base fibre is the same. The approaches to the preparation of functional fibres are essentially of three different types, namely by (1) pre-electrospinning - synthesis of a functional polymer followed by spinning into a fibre or by (2) blending and co-electrospinning by special spinning techniques or by (3) post-functionalisation-fibre preparation followed by introduction of functional groups (Shimamura et al. 1989).

Electrospun nanofibres have great potential as adsorbents when modified for collecting metal ions from a solution because of their high specific surface area, high

porosity and controllable surface functionality. The functionalised electrospun nanofibres have a great prospect when functionalised via incorporation of functional materials into the fibres, or via surface chemistry or coating techniques, and may be able to collect small molecules or metal ions from a solution (Fang et al. 2008). Generally, the polymer support can be modified either chemically (by covalent bonding of the ligand to the matrix) or physically (by sorption of a chelant into the matrix) (Rao et al. 2004; Yang and Alexandratos 2009). A number of chemical processes have been established for introduction of functional groups, and are discussed below.

2.3.8.1 Pre-functionalisation and electrospinning

Due to the abundance of functional groups on the surface of polymers, different chemical modifications can be carried out before electrospinning to enable the adsorption of metal ions from aqueous solutions. The modification methods may be through monomer-grafting or direct modification which enables an attachment of a wide range of specific groups to the nanofibre backbone (Ngah et al. 2008; O'Connell et al. 2008). Grafting of monomers onto cellulose is an important tool for the modification of cellulose. In this process, side chain grafts are covalently attached to a main chain of a polymer backbone to form a branched copolymer. Depending on the monomer grafted onto cellulose, it gains new properties. The grafting can be performed in a heterogeneous or homogeneous medium (Hokkanen et al. 2016; Wojnárovits et al. 2010) and subsequently electrospun into nanofibres. Zhao et al. (2004) prepared ethyl - cyanoethyl cellulose from ethyl-cellulose and acrylonitrile. The ethyl-cyanoethyl cellulose was then dissolved in tetrahydrofuran (THF) and successfully electrospun into porous fibres. In 2005, Shukla et al. (2005) demonstrated that hydroxypropyl cellulose (derivative of cellulose) could be

electrospun utilising two different solvents at a variety of applied voltages and two different tip-to-collector distances (10 and 15 cm).

2.3.8.2 Blending and co-electrospinning

Blending is another process of surface functionalisation; the molecules can be incorporated into the bulk material of nanofibres during the fabrication process. The two most common methods of bulk molecule incorporation into polymer nanofibres are direct blending or mixing into a polymer solution, and co-axial electrospinning. It has been shown that the direct incorporation technique can allow for a greater amount of molecule incorporation and improved activity when compared to the surface modification techniques (Koh et al. 2008). In addition, molecules incorporated by this technique are embedded into the bulk material of the fibres and can facilitate extended adsorption throughout the nanofibres and not just the surface. However, the approach for controlling surface properties through the incorporation of small molecules or oligomeric additives, which migrate to the polymer surface and which can be removed after washing, may not be very effective. Such additives may compromise the polymer's bulk physical properties and because they are not strongly bound to the polymeric matrix, may be removed by evaporation, dissolution, wear or leaching out of the adsorbent. Many of these kinetically governed reaction mechanisms allow relatively little control over the equilibrium surface composition and structure. Additionally, such processes may be expensive and difficult (Jeoung et al. 2015).

2.3.8.3 Post - functionalisation

Different methods like plasma treatment (Ladizesky and Ward 1995), UV irradiation and UV-induced grafting polymerisation have been employed to surface modify

polymers. However, for surface modification of polymer nanofibres, strong reaction conditions should be avoided because the ultrafine polymeric nanofibres are not as strong as bulk materials and therefore can easily be destroyed (Ramakrishna et al. 2005). For example, in their work, Ma et al., (2005b) showed plasma treatment could damage PET nanofibres severely and therefore, Ce(IV) was used in their work to initiate grafting polymerisation of methacrylic acid (MAA) on PET surfaces and the results showed that the morphology of the PET nanofibre was very well preserved after the gelatin grafting (Ma et al. 2005b).

Fibre preparation followed by introduction of functional groups offers a significant advantage in that a variety of functional fibres can readily be prepared from one common precursor fibre by employing such reactions. The post-functionalisation method is more popular due to the varieties of functional fibres that can readily be produced from one common precursor fibre by employing suitable chemical reactions established for introduction of functional groups to the polymer matrix. Several chelating ligands such as catechol, iminodiacetic acid, EDTA and DETPA (and similar functional groups), iminodimethylphosphonic acid, phenylarsonic acid or serine, and amino acid moieties (glycine, valine, leucine and serine) have been used to functionalise cross-linked polymer for the sorption of REEs and associated metal ions (Galhoum et al. 2015).

However, the post functionalisation approach requires fibres with an acceptably high mechanical strength as a prerequisite and electrospun nanofibres offer an approach to improving the mechanical strength while the resulting fibre can be further subjected to crosslinking to an adequate extent (Shimamura et al. 1989). Depending on the molecular configuration of the specific polymer requiring modification,

functional groups may already be present, or can be added to the surface by chemical treatments.

2.3.9 Desorption and regeneration processes

The environmental regulations prohibiting the discharge of toxic pollutants from industrial activities, coupled with the need for conservation of raw materials has led to consideration of the recycling, recovery, and reuse of waste products. The choice between recovery of valuable materials from waste and disposal of waste seems to depend mainly on two factors: economics and technology. Economics is probably the most important factor that limits the recycling, recovery and reuse of industrial waste products. In certain applications, it may be economic to discard the used adsorbent in which case it may be necessary to describe it as a waste. Clearly, the nature and concentration of the adsorbates will dictate the disposal or recycling route to be followed.

Disposal would be favoured when the adsorbent is of low cost and very difficult to regenerate (perhaps because adsorbates are held by chemical forces) and the adsorbed products of the adsorptive separation are not of very high value. In the majority of process applications, disposal of the adsorbent as a waste is not an economic option and therefore regeneration is carried out either in situ or external to the adsorption vessel to an extent sufficient that the adsorbent can be reused (Schmidt and Kodukula 1985). The regeneration of the modified adsorbent and the stability of any moiety attached to the surface of nanofibre are very important in adsorption in order to promote their reusability, its potential practical application and also improve the process economics. Desorption studies help to elucidate the nature of adsorption processes and to recover the metal ions from sorbents. Moreover, it is

essential to be able to regenerate the sorbents so that they can be used again to adsorb metal ions.

There are a number of regeneration methods that have been applied for various metal ions and adsorbents. The regeneration methods used in adsorption include solvent washing, chemical, thermal (Shah et al. 2007), and electrochemical regeneration. These methods have limited applications depending upon the sorbates of interest. Solvent washing is considered very effective and advantageous from an environmental point of view when compared to other methods (Velu et al. 2003). The removal of metal ions adsorbed on solid materials such as the polymer matrix is usually done using acidic or basic solutions (Jeon and Kwon 2012; Pakade et al. 2011).

There are several useful desorption agents currently being explored for desorption and regeneration of modified nanofibres after adsorption. The desorbing agents can be NaOH, NaCl, HCl, H₂SO₄ and H₃PO₄. For instance, experiments for desorption efficiency were carried out with 0.05 M EDTA and 0.05 M NaOH solutions for heavy metal ions in poly(ether sulfones)/poly(ethyleneimine) nanofibrous affinity membranes (Min et al. 2012).

2.4 Characterisation techniques used in this study

Various characterisation techniques have been used to investigate the structure changes and properties of the surface of nanofibre materials. The techniques used include FTIR, SEM, TGA, ICP-OES, XRD and BET and a brief review on the characterisation techniques are presented in the following section.

2.4.1 Fourier transform infrared (FTIR) spectroscopy

The principle of FTIR spectroscopy is to submit the sample to an infrared beam and the absorption of this radiation will promote the excitation of its molecular vibrations by depositing quanta of energy into vibrational modes (Sacksteder and Barry 2001). The chemical bonds absorb the infrared energy at specific frequencies (or wavelengths) corresponding to its molecular modes of vibration in the region of the electromagnetic spectrum (Rodríguez 2000). This absorption corresponds specifically to the bonds present in the molecule and the resulting spectrum is characteristic of the molecules structures present in the sample.

Fourier Transform Infrared spectroscopy (FTIR) is a method to deduce the structure of a sample by irradiating the sample with infrared (IR) radiation and measuring the radiation which is transmitted (or absorbed) by the sample. The sample absorbs radiation when the frequency of the radiation is equal to the frequency of the vibrations between the atoms of the sample (Nicolet 2001). A spectrum which indicates the intensity versus the frequency of an absorption peak is generated. Since every structure has its own unique spectrum, the spectrum can be compared to a molecular fingerprint of the sample. Not only does the spectrum give information about which molecule(s) is/are present, also the amount of material present is indicated by the intensity of the absorption peaks (Nicolet 2001).

Fourier transform infrared (FTIR) spectroscopy is a very selective analytical technique useful for investigating the conformation, inter and intra-molecular interactions in polymers (Koenig 1999). Olmos et al., (2014) also proposed the use of FTIR spectroscopy to understand the changes that take place along the dynamic behaviour of polystyrene (PS) with temperature (Olmos et al. 2014). Fourier

Transform infrared spectroscopy coupled with attenuated total reflection (ATR-FTIR) provides very valuable information regarding the constituent elements and chemical structure near the surface region (Kansiz et al. 2007)

2.4.2 Scanning electron microscopy (SEM)

Scanning electron microscopy (SEM) has been used in polymer research to get a better understanding of structure property correlations in polymers. Moreover, SEM considered being the most popular of the microscopic techniques because of the ease of specimen preparation, and the general simplicity of image interpretation (Michler 2008). It is a type of electron microscope that images the sample surface by scanning it with a high energy beam of electrons. Morphological details at length scales from the visible (0.1 mm) up to a few nm can be detected by using SEM.

Basically, the coated sample is placed into the SEM chamber and the air is pumped out of the chamber creating a vacuum. Then, a high energy electrons beam is emitted by an electron gun positioned at the top of the set-up which travels down the column through a series of magnetic lenses in order to focus the beam to a very fine spot. The focused beam hits the sample surface producing secondary electrons which are attracted and collected by a detector and then translated into signals. These signals are then amplified, analysed, and translated into images for the surface topography of the sample (Michler 2008).

High resolution scanning electron microscopy (HRSEM) is a versatile imaging technique capable of producing three-dimensional profiles of material surface (Bruckenstein and Miller 1977). HRSEM produces an image by probing the specimen with a focused electron beam that is scanned across a rectangular area of the specimen (raster scanning) (Kumar et al. 2011b; Tseng et al. 2006). Conductivity

of specimen is a requirement for HRSEM analysis operating in conventionally high vacuum. Thus, non-conductive specimens have to be coated in order to be used in an HRSEM. This is because non-conductive specimens tend to charge when scanned by the electron beam, especially in secondary electron imaging mode and these charging causes scanning faults and other image artifacts. The conductive materials currently used to coat specimen include, gold/palladium alloy, gold, carbon, chromium, tungsten, osmium, and indium (Bruckenstein and Miller 1977).

2.4.3 Thermo - gravimetric analyser (TGA)

It is important to check the thermal characteristics of the electrospun nanofibres with the modified nanofibre for comparison. The thermal degradation is a sign of structural change which might have occurred after electrospinning and modification. Thermogravimetric analysis (TGA) is a method of thermal analysis in which changes in physical and chemical properties of materials are measured as a function of increasing temperature (with constant heating rate), or as a function of time (with constant temperature and/or constant mass loss) (El-Naggar 2013). TGA is commonly used to determine selected characteristics of materials that exhibit either mass loss or gain due to decomposition, oxidation, or loss of volatiles (such as moisture). Chaúque and co-workers (Chaúque et al. 2016) surface modified polyacrylonitrile (PAN) nanofibres obtained by the electrospinning technique with polyethylenediaminetetraacetic acid (EDTA) using ethylenediamine (EDA) as the cross-linker. The TGA thermograms of the nanofibres elucidated the degradation steps observed during modification.

2.4.4 Inductively coupled plasma-optical emission spectroscopy

Inductively coupled plasma/optical emission spectrometry (ICP/OES) is a powerful tool for the determination of metals in a variety of different sample matrices (Hou et al. 2000; Wu et al. 2009) and various studies determined the concentration of the metal ions in solutions from adsorption and desorption of metal ions from modified nanofibre adsorbent (Ndayambaje et al. 2016; Saeed et al. 2011; Sharma, 2014) using the technique.

With this technique, liquid samples are injected into a radiofrequency (RF)-induced argon plasma using one of a variety of nebulisers or sample introduction techniques. The sample mist reaching the plasma is quickly dried, vaporised, and energised through collisional excitation at high temperature. The atomic emission emanating from the plasma is viewed in either a radial or axial configuration, collected with a lens or mirror, and imaged onto the entrance slit of a wavelength selection device (Hou et al. 2000). The instrumentation associated with an ICP/OES system is relatively simple. A portion of the photons emitted by the ICP is collected with a lens or a concave mirror. This focusing optic forms an image of the ICP on the entrance aperture of a wavelength selection device such as a monochromator. The particular wavelength exiting the monochromator is converted to an electrical signal by a photodetector. The signal is amplified and processed by the detector electronics, then displayed and stored by a personal computer.

The characteristics of the ICP as an analytical atomic emission source are so impressive that virtually all other emission sources (such as the flame, microwave induced plasma (MIP), direct current plasma (DCP), laser-induced plasma (LIP), and electrical discharge) have been relegated to specific, narrowly defined application niches. Also, the application field originally assigned to atomic absorption

spectrometry (AAS), using both the flame and graphite furnace atomic absorption spectrometry (GFAAS), has been relinquished to the ICP. Compared to these other techniques, ICP/OES enjoys a higher atomisation temperature, a more inert environment, and the natural ability to provide simultaneous determinations for up to 70 elements. This makes the ICP less susceptible to matrix interferences, and better able to correct for them when they occur (Hou et al. 2000).

2.4.5 X-ray diffraction (XRD)

X-ray diffraction (XRD) is a powerful non-destructive technique for characterising crystalline materials. It provides information on structures, phases, preferred crystal orientation, and other structural parameters such as, crystalline or grain size, crystallinity, and crystal defects (Maass et al. 2008). It is therefore, an indispensable tool for material characterisation and thus, forms an integral part of a comprehensive characterisation study of modified fibres. XRD in this study was utilised for the direct examination of crystalline structure, phase identification.

In a typical XRD analysis, X-rays are generated in a cathode ray tube by heating the filament to produce electrons. The produced electrons are then accelerated toward the target material by applying voltage and bombarding the target material with electrons. When the electrons have enough energy to dislodge the inner shell electrons of the target material, characteristic X-ray spectra are produced. Copper is generally the most used target material for single-crystal diffraction, with a $\text{CuK}\alpha$ radiation of 1.5418\AA . These X-rays are collimated and directed onto the sample. As the sample and detector are rotated, the intensity of the reflected X-rays is recorded.

Based on the principle of X-ray diffraction, a wealth of structural, physical and chemical information about the material being investigated can therefore be acquired

(Danafar et al. 2009; Maass et al. 2008; Rodriguez-Reinoso 1998). Crystalline size determination is performed by measuring the broadening of a particular peak in a diffraction pattern associated with a particular planar reflection from within the crystal unit cell (Danafar et al. 2009). Typically the narrower and more intense the peak, the more crystalline the sample is. A broad peak is usually associated with small particle size on an amorphous material.

The X-ray diffraction (XRD) analysis of prepared Phosphine-functionalised PVA/SiO₂ (pgf-PVA/SiO₂) composite nanofibre showed XRD peak was somewhat broadened with lowered intensity by the addition of SiO₂, on pgf-PVA/SiO₂ which implied an increase in the amorphous character of the composite nanofibres (Islam, Rahaman, Yeum 2015). XRD was also used to elucidate the modification pattern of electrospun polyvinylpyrrolidone/silica/3-aminopropyltriethoxysilane (PVP/SiO₂/APTES) composite nanofibre adsorbents which showed no diffraction peak for the corresponding modified nanofibre adsorbent (Keshtkar et al. 2016).

2.4.6 Brunauer-Emmett-Teller (BET)

The nitrogen-adsorption technique is based on the concept conceived by Brunauer, Emmett and Teller. Brunauer–Emmett–Teller (BET) theory aims to explain the physical adsorption of gas molecules on a solid surface and serves as the basis for an important analysis technique for the measurement of the specific surface area of a material. The BET theory refers to multi-layer adsorption, and usually adopts non-corrosive gases (like nitrogen, argon, carbon dioxide) as adsorbates to determine the surface area data. It usually uses static volumetric data and also has gas flowing technology that can determine surface area data (Brunauer et al. 1938; Davis and Davis 2012). In general, porous materials can be classified according to their pore

sizes: microporous materials (less than 2 nm), mesoporous materials (2–50 nm), macroporous materials (50–200 nm), and gigaporous materials (more than 200 nm).

The surface area and pore size of functionalised cellulose nanofibres modified with oxolane-2,5-dione were compared to the bare cellulose fibres using BET with results showing the fibre integrity and porosity were maintained during deacetylation and functionalisation (Musyoka et al. 2011) but BET analysis in another study revealed that the surface area of TiO₂ coated chitosan nanofibres did not significantly change by coating of TiO₂ on the surface of chitosan nanofibres when compared with pure chitosan nanofibres (Razzaz et al. 2016). (Brunauer et al. (1938) classified sorption isotherms according to their shape and processes, establishing five different types of sorption isotherms while the mechanisms of hysteresis remain crucial for obtaining an accurate pore size distribution and information about the texture of complex porous materials.

2.4.7 pH

The measurement of pH is possibly the most widely performed test in the chemical laboratory which reflects the importance of water as an ubiquitous reactant and solvent. pH is used to specify the degree of acidity or basicity of an aqueous solution. Generally, pH was first defined as the negative logarithm of the hydrogen ion concentration (pondus Hydrogenii, i.e. hydrogen exponent), to simplify the handling of the very small concentrations (on the order of 10⁻⁷ moles liter⁻¹) encountered most commonly in nature (Galster 1991; Sheppard et al. 1999).

In practice, the routine measurement of pH is not accomplished by the direct determination of the hydrogen ion activity but determined relative to one or more standard solutions of known pH. The addition of acids or bases to pure water

increases or decreases the hydrogen ion activity respectively and the resulting pH depends on a number of factors, such as the concentration of the added acid or base and the strength as quantified by its dissociation constant (Skoog et al. 2013).

2.5 Summary

Rare earth elements have unique properties and are essentially becoming valuable in many high-technology applications such as catalysts for petroleum refining, high-strength permanent magnets, metal and glass additives and phosphors used in electronic displays. The review described nanofibres, their fabrication processes, morphology, solvents and polymers in use. This literature review highlighted significant developments in the selective adsorption of rare earth elements from aqueous solutions with emphasis on the current progress in the use of electrospun nanofibres as an adsorbent material. A brief review of the various characterisation techniques (FTIR, SEM, TGA, ICP-OES, XRD and BET) used to investigate the structural changes and properties of the surface of nanofibre materials was presented.

Although the reviewed literature demonstrated the high efficiency of polymeric adsorbents for the removal of toxic metals, there are still some gaps to be filled in order to introduce these materials as an ideal solution for adsorption applications. The combination of electrospun nanofibres and incorporated functional nanomaterials by blending and co-electrospinning approach of preparation of functional fibres showed most modifications were removed by wear or leaching out of the adsorbent and led to the drawback of small adsorption capacity for the adsorbent. Another gap is that recovering REE from complex aqueous media is challenging because existing separation technologies for REE are not adequately

selective or involve many chemical steps which increase the overall cost of the process. There is also inadequate information on suitable strategies for separating REE from a mixture selectively.

Another gap is the selectivity and regeneration of existing separation techniques which makes them unfeasible, time consuming, costly and therefore limits their practical application. Another drawback is the lack of systematic research on the appropriate adsorbent or functional group that has rapid kinetics. This study, therefore, seeks to fill these gaps and to further enhance the performance of polymer nanofibre adsorbents for the removal of metals ions in order to introduce them as an efficient, feasible and cost-effective technique.

The anticipated alternative would be a functionalising system that could be applied to a large range of electrospun polymers and permits direct chemical modification under mild conditions using inexpensive reagents to functionalise the nanofibres as an adsorbent. This study reports the modification of polystyrene and polyethylene terephthalate nanofibres with diglycolic anhydride by direct surface chemical modification for the introduction of adsorbent function and aims to demonstrate that the adsorbent can be used to remove rare earth metal ions from aqueous solution selectively.

CHAPTER THREE

3 EXPERIMENTAL DETAILS

This chapter contains the experimental details of this thesis and is subdivided according to the objectives of this work:

- Fabrication and investigation of nanofibre process parameters through electrospinning.
- Functionalisation of the surface of the electrospun nanofibres and their characterisation using different methods.
- Application of the obtained fibres as adsorbent material for rare earth metal ion removal

This chapter is divided into five sections. Section 3.1 describes the materials and chemicals used. Section 3.2 describes the methods for electrospinning of nanofibres and Section 3.3 describes the procedure for fibre modifications carried out in this study. The adsorption methodologies, adsorption isotherms, kinetic models, desorption and regeneration studies and selectivity experiments are described in Section 3.4 while Section 3.5 describes the characterisation techniques used in this study. Scheme 1.1 in chapter 1 describes all the experimental processes in this study and how the different experiments are related.

3.1 Materials and chemicals

In this work, two polymers (polystyrene and polyethylene terephthalate) and different solvents were used to fabricate electrospun nanofibres. Several analytical grade chemicals were used to modify the surface of the nanofibres for adsorbent application and two different rare earth metals were used in the adsorption experiments. The list of the chemicals, polymers and their solvents are shown in

Table.3.1. All the analytical grade reagents were purchased from Sigma-Aldrich (South Africa).

Table 3.1. List of the chemicals used in the present study

Reagents	Purity	Supplier
Acetic acid	100%	Sigma-Aldrich
Cerium(III) nitrate hexahydrate (99.99%)	99.90%	Sigma-Aldrich
Diglycolic anhydride (DGA)	90%	Sigma-Aldrich
EDTA solution	-	Kimix
Ethanol	99.99%	Sigma-Aldrich
Methanol	99.99%	Sigma-Aldrich
Neodymium(III) nitrate hexahydrate	99.90%	Sigma-Aldrich
N,N-dimethylformamide (DMF)	≥99.8%	Sigma-Aldrich
Nitric acid	70.00%	Sigma-Aldrich
Polyethylenenaphthalene(granular)	-	Sigma-Aldrich
Polystyrene(Mw ~192,000)	-	Sigma-Aldrich
Tetrahydrofuran (THF)	≥99.0%	Sigma-Aldrich
Sulfuric acid	95.0-98.0%	Sigma-Aldrich
Trifluoroacetic acid (TFA)	99%	Sigma-Aldrich

3.2 General electrospinning apparatus setup

The instrument setup used in this work was a horizontal double nozzle spinning configuration (Chapter 2, Figure. 2.1). Electrospinning was carried out using an infusion pump (Harvard Apparatus 33 Twin Syringe Pump) and applied voltages were driven by a high voltage power supply. Polymer solution was prepared by dissolving an appropriate polymer mass in a solvent system and stirring consistently. The polymer solution prepared was filled in two 5 mL syringe attached to a steel needle with a 0.8 mm inner diameter filed flat and mounted on the programmable syringe pump. A square glass plate covered with aluminium foil acting as a counter electrode as well as collector was placed at specific distances away from the needle tips. After electrospinning, the fibre mats were air dried at room temperature for 24 h to remove residual solvent and subsequently prepared for analysis. All samples were

spun for sufficient time to ensure that a substantial amount of fibres could be obtained for SEM and FT-IR-spectroscopy analysis. The fibre diameter analysis was evaluated from SEM images using Image J® software. Flow rate, applied voltage, tip to collector distance and concentration were the parameters optimised in the electrospinning process.

3.2.1 Investigation of the effect of polymer concentration

This experiment was performed to investigate the effect of polymer concentration on the electrospinning process and the electro-spinnability of the polymer solution to generate beadless nanofibres. Firstly, concentration was varied while all other parameters such as flow rate, applied voltage and tip to collector distance were fixed for the two polymers. The optimisation plan used different solvent system for the two different polymers to determine the concentration and electro-spinnability while other parameters were fixed. The experimental conditions are shown in Table 3.2 and 3.3 for polystyrene and polyethylene terephthalate respectively.

Table 3.2. Electrospinning conditions for PS at different polymer concentrations

Sample code	fixed			varied
	voltage (kV)	Distance (cm)	Flow rate (mL/h)	Concentration (wt %)
PS- C1	20	17	1.0	10
PS- C2	20	17	1.0	15
PS- C3	20	17	1.0	20
PS- C4	20	17	1.0	25
PS- C5	20	17	1.0	30

Table 3.2 shows the electrospinning conditions used to determine the optimised polymer concentration (wt %) for PS prepared at different polymer weight percentages of (a) 10, (b) 15, (c) 20, (d) 25 and (e) 30 wt % by dissolving approximately 1.04, 1.65, 2.33, 3.11 and 4.00 g of PS in a 10 mL dimethylformamide

and tetrahydrofuran (DMF:THF) (4:1 v/v) solvent system. The PS polymer solution was stirred continuously for 12 h using a magnetic stirrer to form a homogeneous solution. The viscous solution was loaded into two 5 mL syringe and mounted on the programmable syringe pump. Table 3.3 shows the electrospinning conditions used to determine the PET optimised polymer concentration.

Table 3.3. Electrospinning conditions for PET at different polymer concentrations

Sample code	fixed		varied	
	voltage (kV)	Distance (cm)	Flow rate (mL/h)	Concentration (wt%)
PET-C1	20	20	0.8	8
PET-C2	20	20	0.8	10
PET-C3	20	20	0.8	15
PET-C4	20	20	0.8	20

Different polymer concentration of (a) 8, (b) 10, (c) 15, and (d) 20 of polyethylene terephthalate (PET) were prepared by dissolving approximately 1.30, 1.66, 2.63 and 3.73 g PET in a 10 mL Trifluoroacetic acid (TFA) solvent system. The mixture was stirred continuously for 24 hr using a magnetic stirrer to obtain a homogeneous solution. The viscous solution was loaded into two 5 mL syringe and mounted on the programmable syringe pump.

3.2.2 Investigation of the effect of flow rate

This experiment was performed to investigate the effect of flow rate on the electrospinning process. In this experiment, flow rate was varied while all other parameters were fixed. The optimised polymer concentration was obtained as detailed in section 3.2.1. The experimental parameters used in these experiments are listed in Table 3.4 and 3.5 for polystyrene and polyethylene terephthalate respectively.

Table 3.4. Electrospinning conditions for PS at different flow rates

Sample code	fixed			varied
	Concentration (wt%)	Voltage (kV)	Distance (cm)	Flow rate (mL/h)
PS- F1	15	20	17	0.2
PS- F2	15	20	17	0.4
PS- F3	15	20	17	0.8
PS- F4	15	20	17	1

Table 3.4 depicts the electrospinning conditions used to determine the optimised flow rate for PS. Polystyrene solution of 15 wt % previously optimised was used for the electrospinning.

Table 3.5. Electrospinning conditions for PET at different flow rates

Sample code	fixed			varied
	Concentration (wt%)	voltage (kV)	Distance (cm)	Flow rate (mL/h)
PET-F1	10	20	20	0.2
PET-F2	10	20	20	0.4
PET-F3	10	20	20	0.8
PET-F4	10	20	20	1

Table 3.5 showed the electrospinning conditions used to determine the optimised flow rate for PET obtained previously from a polymer solution prepared by dissolving 1.66 g in a 10 mL Trifluoroacetic acid (TFA) solvent system (Section 3.2.1) after the optimisation process.

3.2.3 Investigation of the effect of voltage

These experiments were performed to investigate the effect of voltage on the electrospinning process; voltage was varied while all other parameters were fixed. Optimised concentration was described in Section 3.2.1 and flow rate in Section 3.2.2. The experimental parameters used in this experiment are listed in Table 3.6 and 3.7 for polystyrene and polyethylene terephthalate respectively.

Table 3.6. Electrospinning conditions for PS at different voltages

Sample code	fixed			varied
	Concentration (wt%)	Distance (cm)	Flow rate (mL/h)	voltage (kV)
PS- V1	15	17	0.8	*
PS- V2	15	17	0.8	15
PS- V3	15	17	0.8	17
PS- V4	15	17	0.8	20

Table 3.6 shows the electrospinning conditions used to determine the optimised voltage for PS. There are no electrospinning results for +10 kV because no fibres were deposited and denoted with (*). Concentration (15 wt%) and flow rate (0.8 mL/h) were previously optimised in Section 3.2.1 and 3.2.2

Table 3.7. Electrospinning conditions for PET at different voltages

Sample code	fixed			varied
	Concentration (wt%)	Distance (cm)	Flow rate (mL/h)	voltage (kV)
PET- V1	10	20	1.0	10
PET- V2	10	20	1.0	15
PET- V3	10	20	1.0	17
PET- V4	10	20	1.0	20

Table 3.7 shows the electrospinning conditions used to determine the optimised flow rate for PET. Concentration (10 wt %) and flow rate (1.0 mL/h) were previously optimised in Section 3.2.1 and 3.2.2.

3.2.4 Investigation of the effect of needle tip to collector distance

This experiment was performed to investigate the effect of collector distance on the electrospinning process. In this experiment, needle tip to collector distance was varied while all other parameters were fixed. Optimised concentration was obtained as described in Section 3.2.1, flow rate in Section 3.2.2 and voltage in Section 3.2.3.

The experimental parameters used in this experiment are listed in Table 3.8 and 3.9 for polystyrene and polyethylene terephthalate respectively.

Table 3.8. Electrospinning conditions for PS at different collector distances

Sample code	fixed			varied
	Concentration (wt%)	voltage (kV)	Flow rate (mL/h)	Distance (cm)
PS- D1	15	17	0.8	10
PS- D2	15	17	0.8	15
PS- D3	15	17	0.8	20
PS- D4	15	17	0.8	*

Table 3.8 shows the electrospinning conditions used to determine the optimised collector distance for PS. There are no electrospinning results for 25 cm because no fibres were deposited for analysis and denoted with (*). Concentration (15 wt%), flow rate (0.8 mL/h) and voltage (17 kV) for PS were previously optimised in Sections 3.2.1, 3.2.2 and 3.2.3

Table 3.9. Electrospinning conditions for PET at different collector distances

Sample code	fixed			varied
	Concentration (wt%)	voltage (kV)	Flow rate (mL/h)	Distance (cm)
PET-D1	10	17	1	10
PET-D2	10	17	1	15
PET-D3	10	17	1	20
PET-D4	10	17	1	25

Table 3.9 shows the electrospinning conditions used to determine the optimised flow rate for PET. Concentration (10 wt%), flow rate (1.0) and voltage (17 kV) for PET were previously optimised in Section 3.2.1, 3.2.2 and 3.2.3.

3.3 Surface modification of the PS or PET nanofibres

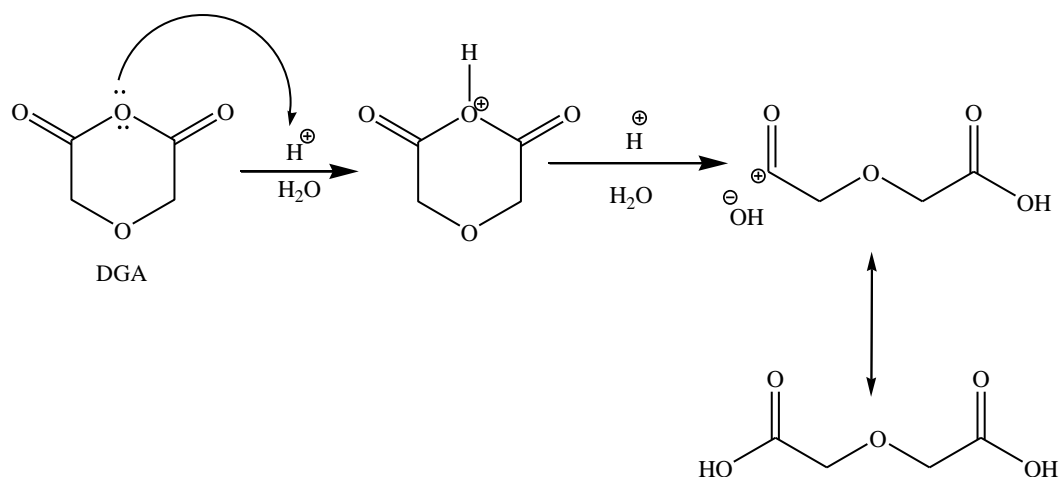
The following experiments were used to modify the surface of polystyrene (PS) or polyethylene terephthalate (PET) nanofibres with diglycolic anhydride which was utilised as an adsorbent for REE metal ions from aqueous solutions. The reaction was undertaken according to the chemical grafting modification procedure described by Repo et al. (2010); Teramoto and Nakamoto (2002) and Zaugg and Martin (2004) with little modification. Table 3.10 shows the sample names and the codes used in the surface modification of the PS and PET nanofibres.

Table 3.10. List of the sample name and codes used in the surface modification

Material	Code
Pristine polystyrene nanofibre	PS
Pristine poly(ethylene terephthalate) nanofibre	PET
Polystyrene nanofibre after surface modification with Diglycolic anhydride	PS -DGA
Poly(ethylene terephthalate) nanofibre after surface modification with Diglycolic anhydride	PET -DGA

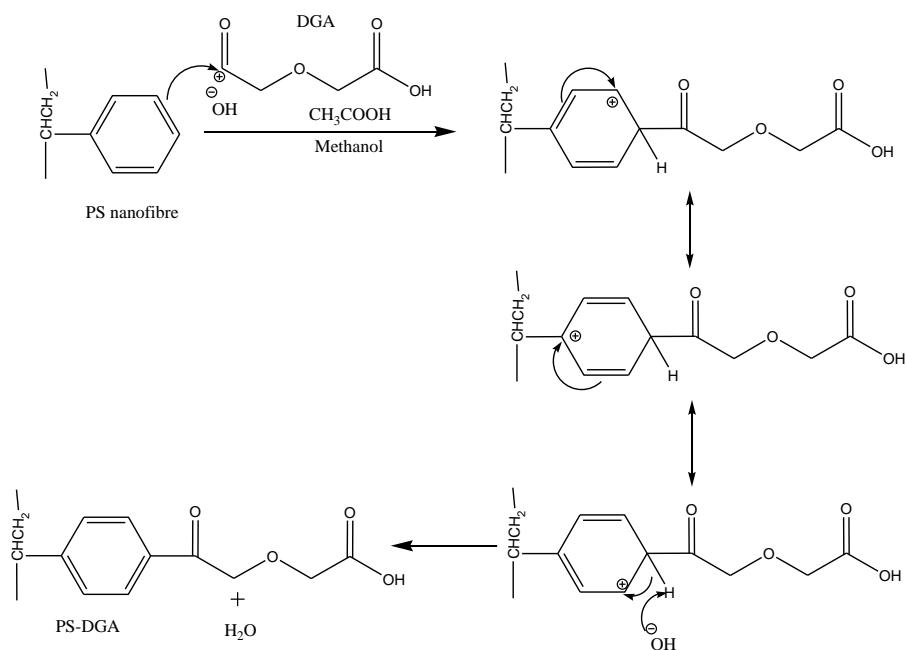
3.3.1 Reaction scheme

The proposed reactions for the surface modifications was an electrophilic aromatic substitution method of introducing functional groups from the ligand directly into the polymer nanofibre to form a new carbon-carbon bond which is expected to be strong. Scheme 3.1 illustrates the ring opening of diglycolic anhydride by suitable acid.

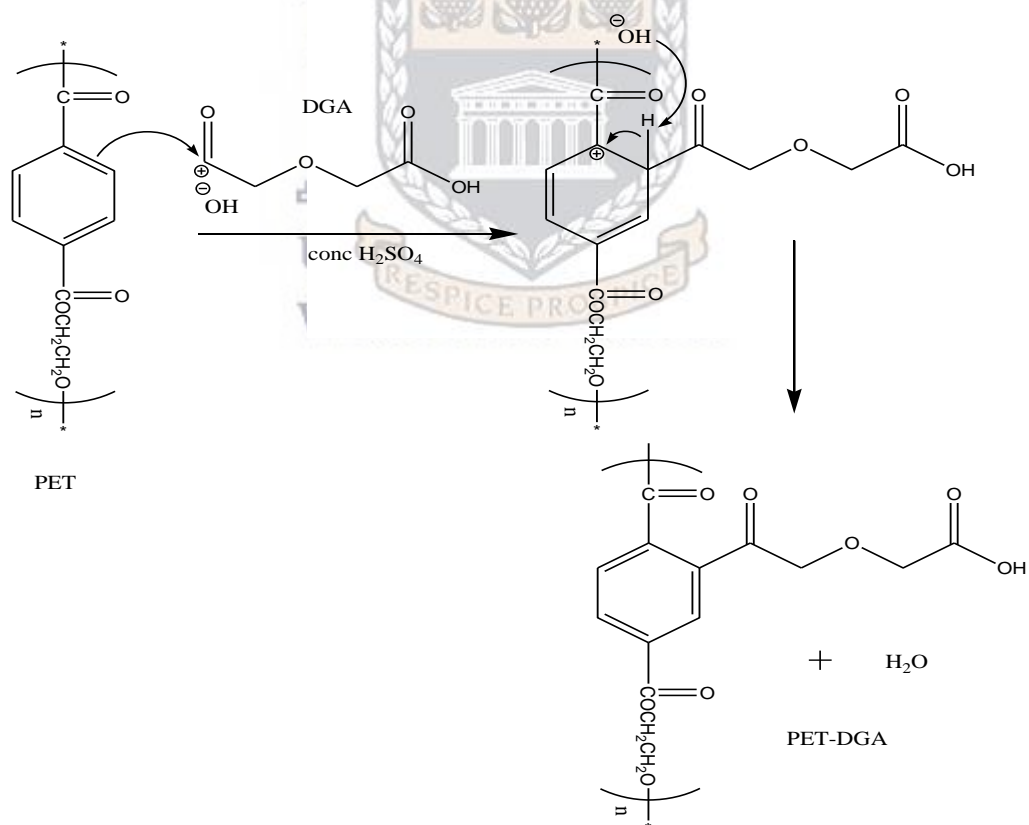


Scheme 3.1. Ring opening of diglycolic anhydride under acidic conditions

In scheme 3.1, the anhydride is protonated in the first step, to yield a diglycolic acid moiety which the nucleophile can attack at the most substituted position which is an established reaction scheme. The proposed reaction design in this study now utilise the benzene ring (Scheme 3.2) which behaves as the nucleophile in this reaction and the substitution on this benzene occurred by the addition of an electrophile from the ligand, the conjugate base of the initial electrophile then assists in removing the now-extraneous proton, and restores aromaticity. In this case, the electrophile was substituted for hydrogen (nucleophile) in the polymer support as depicted in Scheme 3.2 and Scheme 3.3.



Scheme 3.2. Mechanism for PS electrophilic aromatic substitution



Scheme 3.3. Mechanism for PET electrophilic aromatic substitution

Electrophilic substitution of the OH radical to the aromatic ring was the dominant reactive pathway in the two systems studied. The reaction is an acid-catalysed process. For PS, acetic acid was used while H₂SO₄ was used for PET. H₂SO₄ altered the surface properties of the PS nanofibre during the modification process.

3.3.2 Effect of ligand concentration on surface modification of the PS or PET nanofibre

PS electrospun nanofibres (PS-D2) were cut into square shapes weighing 0.109 g and were immersed in a mixture of different masses of 1, 1.5, 2, 3 and 4 g diglycolic anhydride and 10 mL of 5 % (v/v) aqueous acetic acid solution in 40 mL methanol (99.9%) and shaken for 4 hours at 43 °C in a beaker. In the case of the PET (PET-D3) nanofibre, (0.100 g) was first pre-wetted with ethanol (10 mL) and then immersed into 50 mL deionised water to exchange the ethanol with water. Thereafter, the functionalisation of the PET nanofibre with diglycolic anhydride was undertaken. The strip of PET nanofibre was immersed in 50 mL of a solution containing different masses of 1, 1.5, 2 and 3 g diglycolic anhydride and 5 mL of 5 M concentrated sulfuric acid at 60 °C and the beaker was placed in a shaker for 4 h to allow the reaction with the PET nanofibre to proceed. The experimental parameters are listed in Table 3.11

Table 3.11. The experimental parameters used in nanofibre surface modification (fixed amount of 0.10 g) with different mass concentrations of DGA for 240 min

Sample -code	DGA, (mol)	DGA, (g)	Fibre weight (g)	Reaction time (hr)	Temp (°C)
PS-DGA-1	0.0086	1	0.108	240	43
PS-DGA-1.5	0.012	1.5	0.11	240	43
PS-DGA-2	0.017	2	0.103	240	43
PS-DGA-3	0.026	3	0.102	240	43
PS-DGA-4	0.034	4	0.102	240	43
PET-DGA-1	0.0086	1	0.99	240	60
PET-DGA-1.5	0.012	1.5	0.1	240	60
PET-DGA-2	0.017	2	0.112	240	60
PET-DGA-3	0.026	3	0.108	240	60

Table 3.11 shows the experimental parameters used in the surface modification (fixed amount of 0.10 g nanofibre) with different mass concentrations of DGA for 240 min. Modified PS or PET nanofibre were washed with deionised water. The final products were air dried for 24 h and later dried in a vacuum oven at 60 °C for 5 h.

3.3.3 Effect of reaction time on surface modification of the PS or PET nanofibre

The electrospun PS nanofibre (PS-D2), weighing 0.109 g was immersed in a mixture of the optimum weight of 3 g of diglycolic anhydride solution and 5 mL aqueous acetic acid solution in 40 mL methanol at different time intervals of 1, 2, 3, 4 hours at 43 °C. In the case of the PET nanofibre (PET-D3), (0.100 g) was first pre-wetted with ethanol (10 mL) and then immersed into 50 mL deionised water to exchange the ethanol with water. Thereafter, the functionalisation of the PET nanofibre with diglycolic anhydride was undertaken. The strip of PET nanofibre was immersed in 50 mL of a solution containing optimised 2 g of DGA and 5 mL of 5 M concentrated sulfuric acid at 60 °C and the beaker was placed in a shaker for different time

intervals of 30 mins, 1, 2, 3 and 4 hr to allow the reaction with the PET nanofibre to proceed. The experimental parameters are listed in Table 3.12

Table 3.12. The experimental parameters used in nanofibre surface modification (fixed amount of 0.10 g) as a function of reaction time.

Sample -code	DGA, (mol)	DGA, (g)	Fibre weight, (g)	Contact time (min)
PS-DGA-3-1	0.026	3	0.1	60
PS-DGA-3-2	0.026	3	0.0998	120
PS-DGA-3-3	0.026	3	0.101	180
PS-DGA-3-4	0.026	3	0.108	240
PET-DGA-2-1	0.017	2	0.107	60
PET-DGA-2-2	0.017	2	0.113	120
PET-DGA-2-3	0.017	2	0.111	180
PET-DGA-2-4	0.017	2	0.103	240

Table 3.12 shows the experimental parameters used in the surface modification (fixed amount of 0.10 g nanofibre) with different mass concentrations of DGA as a function of reaction time. Modified PS or PET nanofibres were washed with deionised water, with 0.1 M HCl, and then again with deionised water. The final products were air dried for 24 h and later dried in a vacuum oven at 60 °C for 5 h.

3.3.4 Material stability in nitric acid (HNO₃) and ethylene diamine tetra acetic acid (EDTA)

Stability experiments were performed to determine if the optimised materials (PS-DGA-3-3), (PET-DGA-2-3) obtained in Section 3.31 and 3.32, can withstand short term contact with HNO₃ or EDTA as regenerant for lanthanide extractions on a lab-scale. Functionalised nanofibres were contacted with 0.1, 0.5, 1, 1.5 and 2 M concentrations of HNO₃ and with 0.25, 0.1 and 0.05 M concentrations of EDTA for 1 hour to simulate the conditions that would be used for batch desorption

experiments. The fibre samples were then washed with deionised water, air dried and then prepared for FTIR analysis. It was expected that the IR spectra of the pristine functionalised nanofibre and the acid-contacted functionalised nanofibre would be nearly identical indicating that the ligand had remained intact after the short-term contact.

3.4 Characterisation techniques used in this study

Characterisation of the morphology of the nanofibres and nanofibre grafted surface is vital for understanding of the changes of the grafted surface which was a key factor for further development and application. The nanofibre samples were characterised before and after ligand functionalisation. To investigate the effects of the applied parameters on the fibre morphology and diameter, a range of techniques were selected. The following sections describe in detail the conditions used for each of the characterisation techniques applied in this study.

3.4.1 Fourier transform infrared (FTIR) spectroscopy

FTIR spectra were measured and used to determine the change in the functional groups of unmodified and modified nanofibre mats and ligand samples. The spectra of the pure electrospun fibres and modified samples were obtained using Thermo Scientific-Nicolet iS10 Fourier Transform Infrared Spectrophotometer (FT-IR) equipped with diamond Attenuated Total Reflectance (ATR) in this study. Each sample to be analysed was placed on the ATR sample holder. The nanofibre sample was recorded in the range of $4000 - 650 \text{ cm}^{-1}$ with a resolution of 4 cm^{-1} and at 64 scans, the baseline was corrected and the spectra smoothed. The use of a diamond crystal allowed adjustment of the thickness of the sample by squeezing which enables analysis of microgram samples to be performed.

3.4.2 Scanning electron microscopy (SEM)

The Scanning Electron Microscopy (SEM) was utilised to determine the surface morphological changes and diameter of the materials. The morphology of the nanofibres was investigated using the Zeiss Gemini Auriga high resolution scanning electron microscope (HRSEM) equipped with a CDU-lead detector at 25 kV with tungsten filament. The dried samples were placed on a carbon adhesive tape attached onto an aluminium stub. The samples on the aluminium stubs were coated by EMITECH K950X gold coater machine. Each sample was then mounted into specimen holders and the morphology and chemistry of the samples were analysed from backscattered electrons as well as secondary electron images. The fibre size distribution and fibre diameter were evaluated by measuring over 20 fibres selected randomly from the SEM images using Image J® analysis software.

3.4.3 Thermo-gravimetric analyser (TGA)

Thermo-gravimetric analyser (TGA) was employed to determine the useful temperature range of the sample material, as well as to determine the stability of immobilised ligands that might have bonded to the material chemically. The thermal gravimetric analysis (TGA) of PS and PET nanofibres was conducted in order to determine the thermal behaviour of the fibres before and after their surface modification with DGA. The TGA instrument was calibrated before each analysis session in order to stabilise the instrumental baseline. The TGA was performed using STA 6000 (Perkin-Elmer Instrument Model, USA). About 5.0 mg of the samples were placed in ceramic pans and heated from 30 to 800 °C at a heating rate of 10 °C min⁻¹ under nitrogen (N₂) flow. The reproducibility of the thermogram was confirmed by performing duplicate determinations.

3.4.4 X-ray diffraction (XRD)

XRD measurement was conducted using a Bruker AXS (Karlsruhe, Germany) X-ray diffractometer (model D8 Advance) with $\text{CuK}\alpha$ radiation ($\lambda = 0.15406 \text{ nm}$) accelerated at voltage and current of 40 kV and 40 mA, respectively and with LynxEye PSD detector. At 25 °C, the XRD patterns were collected from 4° to 60° 2 θ at an increment of 0.034° 2 θ per 0.5 sec/step. The data evaluation was done with EVA software from BRUKER (ICDD: PDF database 1998).

3.4.5 Brunauer-Emmett-Teller (BET)

Surface areas and pore characteristics of the fibres were determined using the Brunauer-Emmett-Teller (BET) isotherms. The nitrogen adsorption/desorption isotherms were measured at -196 °C using a Micromeritics Tristar surface area and porosity analyser fitted with a Micromeritics flowprep 060 sample degas system. The samples were out-gassed at 120 °C for 10 h to obtain a residual pressure of less than 10⁻³ torr. The amount of N₂ adsorbed at a relative pressure of P/P₀=0.98 was used to determine the total pore volume, which corresponded to the sum of the pore size and pore volume.

3.4.6 Water contact angle (WCA) Measurement

The water contact angles (WCA) of electrospun nanofibres samples were determined with a DSA 100 drop shape analyser (Kruss, Germany) by using doubly deionised water (DDI) as wetting liquid at 25°C with a relative humidity of about 32 ± 1%. To ensure the validity of measurements, both Teflon (PTFE) and glass (standard hydrophobic and hydrophilic materials) were used. For calculating the average contact angles of the samples with P-value < 0.05, 10 data points of water drops for each sample were recorded.

3.4.7 Inductively coupled plasma-optical emission spectroscopy

ICP-OES was used to determine the concentration of metal ions. Elemental analysis of the metal solution collected before and after the adsorption experiments was done in order to gain a better understanding of the metal species and concentrations in the filtrates obtained from the adsorption experiments. The instrument used for determining the metal ions was a Varian Radial ICP-OES using a High Matrix Introduction (HMI) accessory and He as collision gas. External calibration of the instrument was performed daily, and a quality control standard verifying accuracy was included with every batch of samples analysed. During ICP-OES analysis, internal standards were used to correct the matrix effects and instrument drift. Samples were diluted by a factor of a hundred depending on the concentration solution that was available since some samples contained high metal concentration. Triplicate samples were considered in order to achieve reproducibility of the analysis results.

3.5 Adsorption experiments

Adsorption experiments were conducted to compare the capacity of the two prepared nanofibre adsorbents (PS-DGA-3-3), (PET-DGA-2-3) for the removal of rare earth metals from aqueous solutions. The surface-modified adsorbents were applied in batch studies to investigate the performance of each adsorbent in the removal of the following rare earth metals from solution.

- Cerium (III) (Ce^{3+})
- Neodymium (III) (Nd^{3+})

At least two replicates were run in parallel for each experiment. The experiments were generally carried out at $22 \pm 1^\circ\text{C}$. Chemical stock solutions were prepared from

reagent-grade chemicals using high-purity 18 MΩ cm⁻¹ water (Milli-Q UV Plus, Millipore). For the batch tests, 1000 mg/L stock solutions of Cerium (III) (Ce³⁺) or Neodymium (III) (Nd³⁺) each, were first prepared by dissolving the reagent-grade metal compounds in ultrapure water. For the adsorption experiments, the synthetic metal solutions were then freshly prepared by diluting from the stock solutions (Ce³⁺ or Nd³⁺) to target concentrations with ultrapure water. The pH was adjusted using drops of NaOH or HNO₃ depending on the counter ions desired. The solutions were filtered with 20-25 μm filters (Whatman® qualitative filter paper, Grade 4) before analysis. The ICP OES was used to determine the concentration of REEs in the aqueous stock, and in used solutions. The difference between the initial and the final concentrations of the solutions was considered to be the concentration of metal ions adsorbed.

3.5.1 Procedure for adsorption and desorption experiments

Batch mode adsorption studies were carried out by immersing 0.0075 g of the respective nanofibre adsorbent sample in 10 mL of Cerium (III) (Ce³⁺) or Neodymium (III) (Nd³⁺) of 100 mg/L. Adsorption and desorption experiments for all rare earth metal ions were carried out in a batch system. A typical adsorption experimental procedure was as follows: the adsorbent (0.0075 g, dry basis) was added to 10 mL of a solution containing metal ions, and the mixture was shaken for at least 60 minutes (except the time course test). After filtration, the concentration of each metal ion remaining in the filtrate was determined with ICP-OES analysis. The amount of metal ion adsorbed onto functionalised nanofibres was expressed as the adsorption capacity and computed by the following equation.

$$q_e = \frac{(C_0 - C_e)V}{M} \dots \dots \dots \text{Equation 3.1}$$

where: q_e is the amount of metals ions adsorbed by the nanofibre adsorbent (mg/g). C_0 and C_e are the initial and equilibrium concentrations of metal ions, respectively, in solution. V and M are volume of solution and weight of adsorbent, respectively. All the batch experiments were performed in duplicate and the negative controls (with no adsorbent) were simultaneously carried out to determine metal ion loss during the adsorption due to the glassware and determine the actual concentration of the working solution.

3.5.2 Effect of pH

Adsorption experiments of pH values ranging from 1 to 6 in 100 mg/L standard solutions of the metals were investigated for determining the optimal pH for the metal ion adsorption. This experiment investigated the pH range of 1.0; 2.0; 3.0; 4.0; 5.0 and 6.0. The amount of 0.0075 g (of the same size) of the adsorbent mat was immersed into either the 10 mL of Ce^{3+} or Nd^{3+} (100 mg/L) solution respectively, which was adjusted to the desired pH. It was then shaken for a period of 2 hr and the solution was then filtered from the adsorbents. The respective metal (Ce^{3+} or Nd^{3+}) filtrate was then prepared for metal analysis using the ICP-OES to determine the adsorbed amount of Ce^{3+} or Nd^{3+} after the equilibrium.

3.5.3 Effect of contact time

Uptake of metal ions in 100 mg/L metal ion solutions in batch experiments was carried out at various contact time intervals. To study the effect of contact time, batch experimental procedures were conducted over different shaking times of 1,2,3,4, 5, 10, 15, 20, 40 and 60 min at optimised pH value obtained in Section 3.5.2 with sampling at each interval while the other parameters such as sorbent dosage

(0.0075 g) and concentration of metals in solution (100 mg/L) were kept constant. Samples were measured using the ICP-OES analysis.

3.5.3.1 Kinetic models

In order to clarify the adsorption process and to investigate the mechanism of sorption and potential rate controlling steps such as mass transport and chemical reaction processes, kinetic models have been used to test experimental data. Two reaction-based kinetic models can be used to describe the transient behaviour of a batch adsorption process. The models are known as pseudo-first-order and pseudo-second-order as regards reaction-based kinetic models. In the pseudo-first-order model, all phases of the adsorption process involving external diffusion, internal diffusion and adsorption are integrated. It is also supposed that the driving force for the adsorption is the changing rate of occupation of adsorption sites which is directly proportional to the number of unoccupied sites. The linear form of the pseudo-first-order kinetic model is known as the Lagergren equation (Lagergren 1898):

$$\ln(q_e - q_t) = \ln q_e - K_1 t \dots \dots \dots \text{Equation 3.2}$$

where q_t and q_e , are the amounts of ion adsorbed at time t and at equilibrium (mg/g), respectively, and k_1 is the rate constant of pseudo-first-order adsorption process (min^{-1}) which can be calculated from the slope of the linear plot of $\ln(q_e - q_t)$ versus t (slope is K_1 , while q_e is the intercept) while the linearised form of the pseudo-second-order kinetic model is:

$$\frac{t}{q_t} = \frac{1}{k_2 q_e^2} + \frac{1}{q_e} t \dots \dots \dots \text{Equation 3.3}$$

where k_2 is the equilibrium rate constant of pseudo-second-order sorption (g/mg min) and can be calculated from the slope and intercept of the plot of t/q_t against t

(Ho 2006; Özacar and Şengül 2004). The pseudo-second-order also considers the same assumptions as the pseudo-first-order model, but the rate of occupation of adsorption sites is proportional to the square of the number of unoccupied sites, while the overall rate of adsorption process is controlled by chemisorption. The kinetics of metal ions sorption is an important parameter for designing sorption systems and is required for selecting the optimum operating conditions for full-scale batch metal removal processes. Any observed rapid kinetics has significant practical importance as it will facilitate the scale up of the process to smaller reactor volumes ensuring efficiency and economy (Aksu 2002; Krishnani et al. 2008).

3.5.4 Effect of equilibrium concentration

The effect of the equilibrium concentrations of the metal ions was investigated for a range of standard solution concentrations. A typical experimental procedure was conducted by shaking the different nanofibre adsorbents with different initial concentrations of Ce^{3+} or Nd^{3+} ranging from 40 to 180 mg/L at optimised pH using a mass of 0.0075 g nanofibre adsorbent and agitated at 200 rpm for 60 min. Samples were withdrawn at fixed time intervals, filtered and the final concentrations of metal ions in the respective metal solutions were measured using the ICP-OES analysis.

3.5.4.1 Adsorption isotherms

There are several isotherm equations available for analysing experimental sorption equilibrium parameters, the most common being the Langmuir and Freundlich models which were used in this study.

The Langmuir model is probably the best known and most widely applied sorption isotherm. It has produced good agreement with a wide variety of experimental data (Gerente et al. 2007). The derivation of the Langmuir adsorption isotherm involves

four implicit assumptions: a) the adsorption is at a fixed number of definite, localised sites; b) monolayer adsorption is formed on the surface of adsorbent; c) the surface is homogeneous, that is, the affinity of each binding site for adsorbed molecules is the same; d) there is no lateral interaction between adsorbate molecules (Oscik 1982).

The commonly expressed form is:

$$q_e = \frac{q_m b C_e}{1 + b C_e} \dots \dots \dots \text{Equation 3.4}$$

Where q_e is the amount adsorbed at equilibrium (mg/g), C_e is the equilibrium concentration of the adsorbate (mg/L), q_m is Langmuir monolayer capacity of the adsorbent (mg/g) and constant b is related to the energy of adsorption (L/mg). The Langmuir adsorption model is probably the most useful among all isotherms describing adsorption, and often serves as a basis for more detailed developments (Noll 1991).

The Freundlich isotherm model applies to adsorption on heterogeneous surfaces with interaction between the adsorbed molecules and is not restricted to the formation of a monolayer. This model assumes that as the adsorbate concentration increases, the concentration of adsorbate on the adsorbent surface also increases and, correspondingly, the sorption energy exponentially decreases (Vijayakumar et al. 2012). The well-known expression for the linear form of Freundlich model is given as (Freundlich 1906b):

$$q_e = K_f C_e^n \dots \dots \dots \text{Equation 3.5}$$

Where q_e is the amount adsorbed at equilibrium (mg/g), K_f is the Freundlich constant and C_e is the equilibrium concentration (mg/L). The other Freundlich constant (n) is a measure of the deviation of the adsorption from linearity. If the

value of n is equal to unity, the adsorption is linear. If the value of n is below unity, it implies that the adsorption process is unfavourable, and if the value of n is above unity, adsorption is favourable (Rouliia and Vassiliadis 2008).

3.5.5 Desorption and regeneration of metal ions from nanofibre mats

This experiment was carried out to de-adsorb and regenerate the nanofibre adsorbent materials so that the metal ions could be recovered and the adsorbent reused. The loaded sorbent was filtered out, washed 3 times with 10 mL portions of ultrapure water and dried on a filter using vacuum suction. The dried adsorbent fibres were placed in 15 mL containers each containing 10 mL aliquots of 1 M HNO₃ solution and stirred for 1 hour in order to desorb the metal ions taken up on the adsorbent. After shaking, the solution was filtered and 5 mL of the recovered aliquot was prepared for metal analysis (Ce³⁺ or Nd³⁺) using ICP-OES. The concentration obtained from ICP analysis was considered as the metal desorbed from the used functionalised adsorbent. The regenerated nanofibre mats were dried at 40 °C overnight for further analyses. This experiment was repeated three times under the same adsorption and desorption conditions to determine how many regeneration cycles were possible.

The desorption efficiency (D_E) was determined from the following equation:

$$D_E = \frac{c \times v}{q \times m} \times 100 \% \quad \dots\dots\dots \text{Equation 3.6}$$

where C (mg/L) is the concentration of adsorbates in the desorption solution, V is the volume of the desorption solution, q (mg/g) is the amount of adsorbates adsorbed on the nanofibre before desorption experiment, and m (mg) is the amount of the adsorbent used in the desorption experiments.

3.5.6 The selective adsorption of Ce(III) and Nd(III) onto PS-DGA or PET-DGA nanofibre.

The selectivity of PS-DGA and PET-DGA nanofibre was examined in 15 mL plastic containers containing 10 mL aqueous solution containing selected metal ions (Ce^{3+} , Co^{2+} , Ni^{2+} and Sr^{2+}) with the same concentration of each (100 mg/L) and a piece of nanofibre (0.0075 g) was dipped into the solution. The flask was equilibrated in a shaker operated at 200 rpm for 1 h. After the adsorption experiments, the nanofibres were taken out and rinsed with deionised water twice, and then dried in vacuum at 40 °C till constant weight for later analysis. The concentrations of mixed metal ions in solution before and after adsorption were determined. The amount of metal ions absorbed on the nanofibre sample at adsorption equilibrium (q_e , mg/g) was calculated according to Equation 3.7, and the selective coefficient of $K_{\text{REE}/\text{M}}$ could be calculated with the following equation (Dorfner 1991; Hong et al. 2015; Laatikainen et al. 2015; Toutianoush et al. 2005; Wang et al. 2014):

$$K_{\text{REEM}} = \frac{q_{\text{REE}} \cdot C_{\text{M}}}{q_{\text{M}} \cdot C_{\text{REE}}} \quad \dots \dots \dots \text{Equation 3.7}$$

where q_{REE} and q_{eM} is the amount of REE ion and metal ions adsorbed onto PS-DGA and PET-DGA nanofibre at equilibrium, respectively.

CHAPTER FOUR

EFFECT OF PROCESS PARAMETERS ON ELECTROSPUN POLYSTYRENE (PS) AND POLYETHYLENE TEREPHTHALATE (PET) NANOFIBRES

4 INTRODUCTION

Chapter four discusses the results of the investigation and optimisation of process parameters for electrospun polystyrene (PS) and polyethylene terephthalate (PET) nanofibres on the morphology and average fibre diameter (AFD). The electrospinning process parameters such as the concentration of polymer solutions, applied voltage, flow rate, and the distance between needle tip–collector screens were investigated.

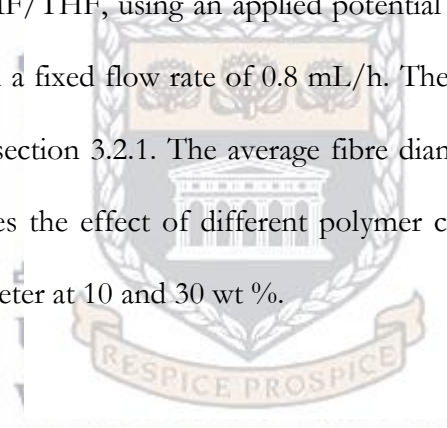
The emphasis of this chapter was to exploit several parameters which affect electrospinning such as polymer solution properties, process and ambient conditions to determine the appropriate conditions for electrospinning polystyrene or polyethylene terephthalate polymers into nanofibres for metal ion adsorption. It is important to note that the nature of the electrospun fibres is different from the polymer itself and therefore, the ultrafine nanofibres can exhibit or be used in a variety of potential applications (Yuan et al. 2004).

Nanofibre diameter influence the performance of some specific applications, for instance, nanofibre filtration membranes require a more uniform and smaller fibre diameter, better diffusion interception, and inertial compaction efficiencies (Lin et al. 2007). In the electrospinning process, it is very important to produce electrospun nanofibres with minimum diameter, because the thinner and more homogeneous fibres are, the more they provide the maximum surface area and porosity, which results in higher efficiency adsorbents (Keshtkar et al. 2013) and this study should

obtain low fibre diameters with smooth and beadless morphologies through the control of factors such as the concentration of polymer solutions, applied voltage, flow rate, and the distance between needle tip–collector screens.

4.1 Effect of polymer solution concentration on PS nanofibre morphology

This experiment investigated the effect of the polymer solution concentration on the morphology of polystyrene nanofibres. The effect of concentration was tested to determine the best concentration for the nanofibre morphology. This experiment was conducted at different weight percentage concentration of polystyrene (a) 10, (b) 15, (c) 20, (d) 25 and (e) 30 wt %. These fibres were spun from solutions of 10 - 30 % (w/v) of PS in DMF/THF, using an applied potential of 17 kV over a collection distance of 15 cm and a fixed flow rate of 0.8 mL/h. The experimental procedure is detailed in chapter 3 section 3.2.1. The average fibre diameters are shown in Figure 4.1 (a - e) to illustrate the effect of different polymer concentrations on the fibre morphology and diameter at 10 and 30 wt %.



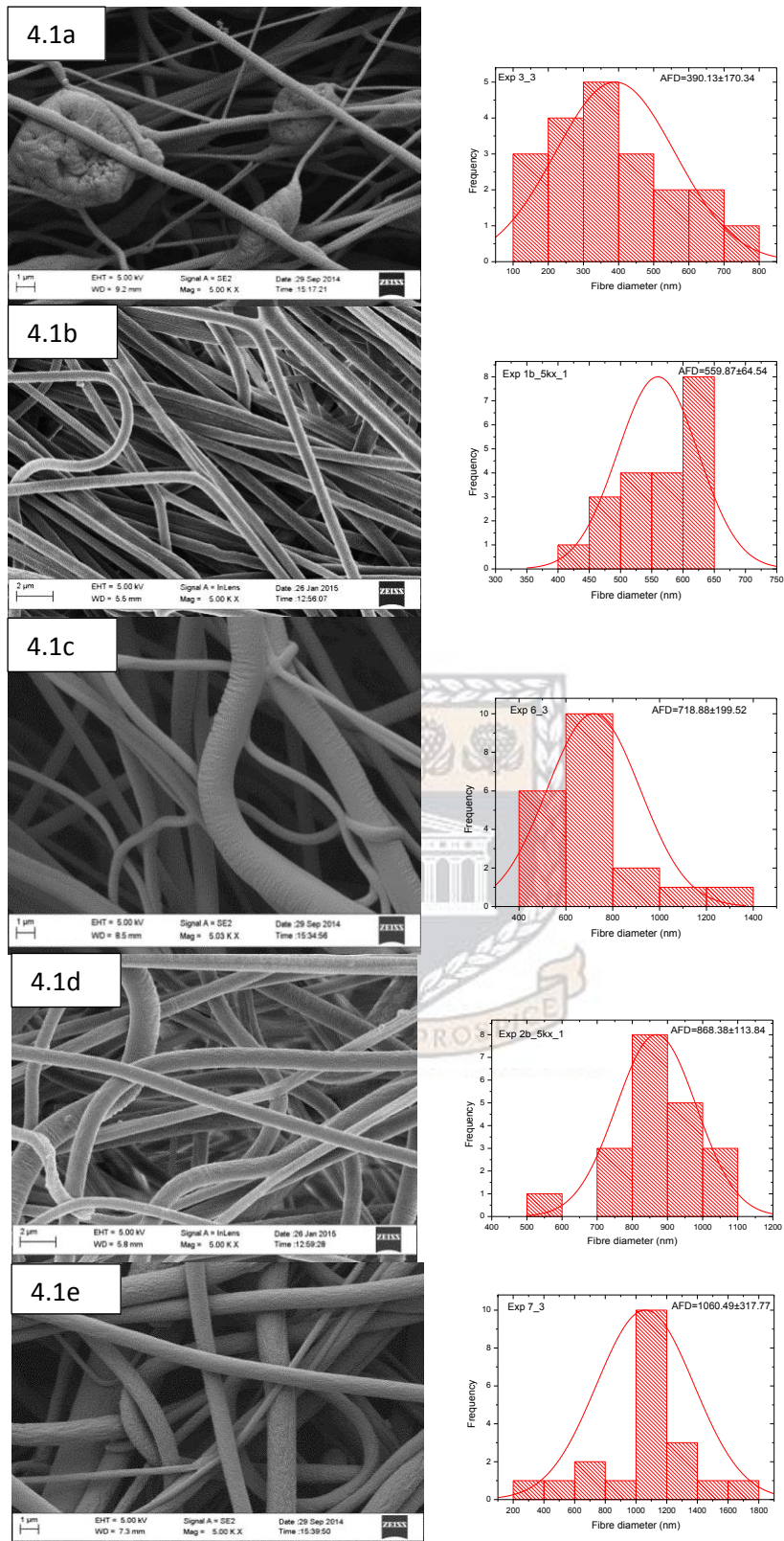


Figure 4.1 SEM micrographs and frequency distribution of PS fibres at various polymer weight percentage (a) 10, (b) 15, (c) 20, (d) 25 and (e) 30 wt % (flow rate - 1.0 mL/h; voltage - 20 kV and distance - 17 cm).

Figure 4.1 (a) represents the surface morphologies of 10 wt % electrospun nanofibre which exhibited bead-on-string structures while Figure 4.1 (b - e) depicts that the spherical beaded structure disappeared with the use of higher concentrations of PS polymer solution. All the electrospun nanofibres showed cylindrical and non uniform diameters for all fibres at the different concentrations. The low concentration polymer solutions formed droplets due to the influence of surface tension, while excessively high concentrations prohibited fibre formation due to higher solution viscosity. The effect of fibre alignment on the as-spun nonwoven fibres was only noticeable at 15 wt % PS concentration but the surface structure of other fibres were not so aligned but big, round and smoother owing to increasing PS concentration due to stable interfacial conditions during electrospinning.

The PS electrospun nanofibres fabricated in this study were cotton-like fibres; especially the lower weight concentration (10 % wt) and they were unable to be detached easily from the collector foil to preserve the fibre mat in its original form. This occurrence was probably due to insufficient entanglement of polymer chains, generating a skin layer on the surface of fibres before they reach the collector which reduced the fibre-fibre bonding, thus, demonstrating a poor fibre adhesion.

The fibres produced at the low polymer weight percentage of 10 wt% showed that the bead-on-string morphology turned into blobs of polymer but by increasing the concentration of PS in solution, a morphological transformation of electrospun products was seen from the beaded fibres with low average fibre diameters slightly lower than 400 nm to more cylindrical fibres with increased average fibre diameters of 900 nm at higher concentrations as depicted by the plot of this trend in Figure 4.2.

Figure 4.2 shows the trend of fibre diameter as a function of solution concentration for PS nanofibres.

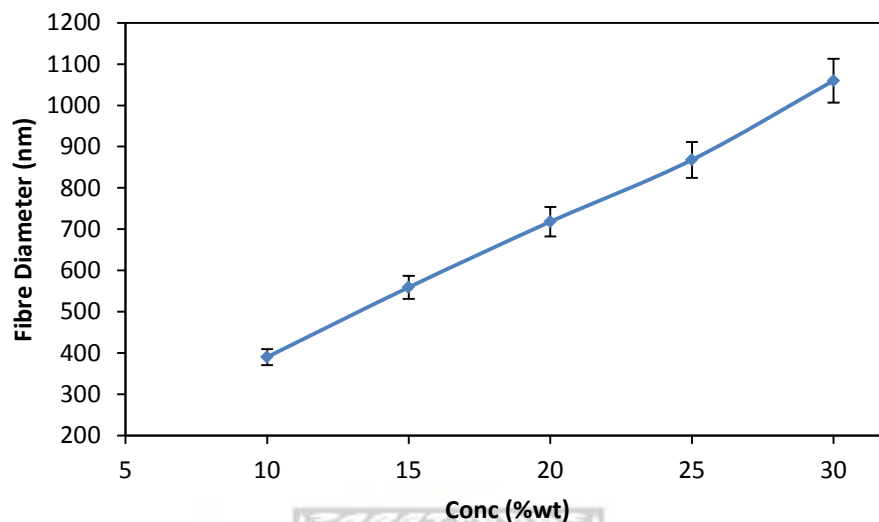


Figure 4.2 The effect of solution concentration on fibre diameter of electrospun PS nanofibres at various polymer weight percentage (a) 10, (b) 15, (c) 20, (d) 25 and (e) 30 wt % (flow rate - 1.0 mL/h; voltage - 20 kV and distance - 17 cm)

Figure 4.2 shows a trend of increasing solution concentration on fibre diameter. With the increase in polymer weight percentage, the bead formation was reduced but then, there was an increase in the average fibre diameter. Therefore, 15 wt % concentration of PS was selected as the best concentration for fabrication of non-woven PS nanofibre mats for further functionalisation experiments. The fibre diameter which increased due to an increase in polymer concentration was attributed to inadequate elongation and stretching of ejected jets with higher viscosity of the electrospinning solution. The formation of beads and beads on strings in the electrospinning process is attributed to lower polymer concentration, higher surface tension and lower viscosity of the polymer solution (Lee et al. 2016; Zheng et al. 2006).

These findings are consistent with previous findings in the literature where bead-free PS fibres were obtained at the high concentration range of 20% (w/v) through 30% (w/v) (Uyar and Besenbacher 2008) even though conductivity of the solvent was the key factor for the reproducible electrospinning of uniform polystyrene (PS) fibres from DMF solutions. Low polymer concentration can also lead to insufficient entanglement of polymer chains, resulting in the polymer solution breaking down into droplets and not fibres during the electrospinning process (Koski et al. 2004). These observations were similar to those observed in an earlier work (Wu et al. 2016) where the surface morphologies of the PS15 and PS20 electrospun sorbents, respectively, exhibited bead-on-string structures but the spherical bead structure disappeared in the PS25 and PS30 electrospun nanofibres sorbent.

4.2 Effect of polymer solution concentration on PET nanofibre morphology

This experiment investigated the effect of polyethylene terephthalate (PET) polymer concentration in Trifluoroacetic acid (TFA) solvent on the morphology of PET nanofibres. This experiment was conducted at different weight percentage (a) 8, (b) 10, (c) 15, and (d) 20 % (w/v) concentration of PET in TFA and the morphology and fibre diameter size results are shown in Figure 4.3 (a - d) below.

Figure 4.3 (a - d) illustrates the effect of different PET weight percentages in solution on the fibre morphology and diameter spun from the solution of (a) 8, (b) 10, (c) 15 and (d) 20 % (w/v) polymer concentration in TFA using an applied potential of 17 kV over a collection distance of 20 cm and a fixed flow rate of 1.0 mL/h. The experimental procedure for the SEM technique is detailed in Chapter 3 Section 3.2.1.

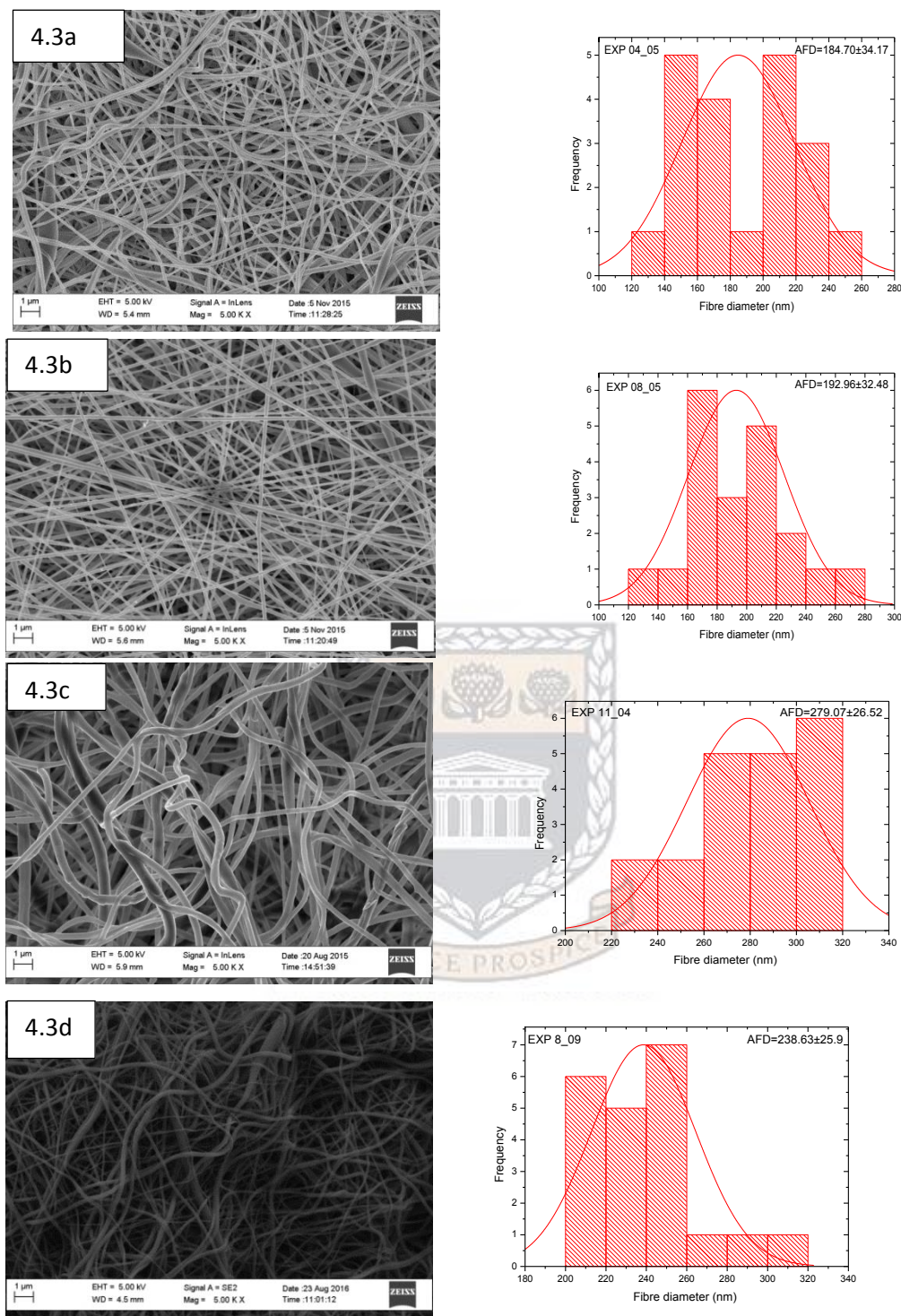


Figure 4.3 SEM micrographs and distribution of PET nanofibres at various polymer weight percentage (a) 8, (b) 10, (c) 15 and (d) 20 wt % (flow rate - 0.8 mL/h; voltage - 20 kV and distance - 20 cm).

The fibres observed at low polymer concentration (Figure 4.3 (a)) are essentially independent of each other and not interconnected and showed a well-defined

cylindrical morphology. For concentrations less than 10 wt %, droplet spray occurred and a continuous jet of polymer, (i.e., spinning) was not really formed. The jet from low viscosity solutions broke up into droplets due to the lower amount of polymer and lower entanglement density than what was needed to form a stable jet. The electrospun nanofibre alignment appeared to increase up to 10 wt % but thereafter fibres remained unaligned even with an increased PET concentration. In addition, there were more entanglements as the concentration was increased (Figure 4.3 b). The fibre diameters also slightly increased with an increase in the concentration.

Only a small amount of fibres were formed at the low PET concentration (< 10 %) and some droplets were still present. Continuous nanofibre structures were obtained for 10 % (w/v) PET and higher concentration, until the solubility limit of the polymer was reached, at about 20 % (w/v). As shown from the micrographs, the concentration of the polymer solution influenced the spinning of fibres as well as the structure and morphology, as the chain conformation of PET changed from the linear conformation to a coiled structure causing the fibres to stick together during the formation and deposition process as shown in Figure 4.3 (c) and the surface morphology change could be attributed to the localised charge effects on the surface of the fibres. As shown in Figure 4.4 an increase in the polymer concentration up to 15 wt % led to an increase in diameter which reduced slightly at a higher concentration of 20 wt %.

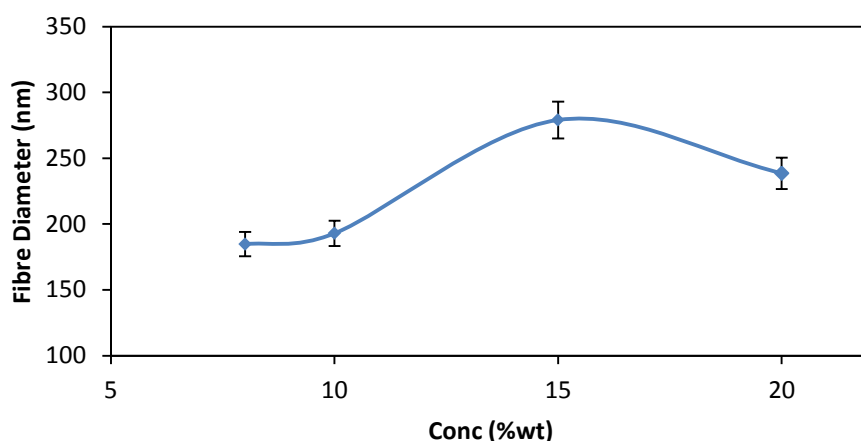


Figure 4.4 Trend of fibre diameter as a function of concentration for PET samples (polymer weight percentage (a) 8, (b) 10, (c) 15 and (d) 20 wt % (flow rate - 0.8 mL/h; voltage - 20 kV and distance - 20 cm).

The maximum fibre length and fibre diameter were obtained when increasing the polymer concentration and the optimum concentration was therefore determined to be 10 wt % for PET in this study. When polymer concentration increased, the influence of the solution viscosity and elasticity also increased, the average fibre diameter (AFD) also increased and the fibre defects (i.e., beaded fibres) decreased for the samples. It was difficult to electrospin nanofibres above 20 wt % because of the high polymer viscosity. The AFD of PET at 10 wt % was lower when compared to fibres generated by Hadjizadeh et al. (2011) when they electrospun PET in dichloromethane (CH_2Cl_2) and trifluoroacetic acid (TFA) using 9 % solution concentration, fibres with 0.7 μm were obtained and fibres with 2 μm were produced using 12.5 % in their study.

Studies have shown that there is no general rule for selecting the optimal polymer concentration because it depends on the polymer and solvent characteristics. For example, in the case of poly (ethylene oxide)(PEO), the optimum concentration was 3 % (w/w) (Rošić et al. 2012) and in the case of poly (vinyl alcohol)(PVA) it was

found to be between 8 and 12 % (w/w) (Rošic et al. 2013). In addition, it was confirmed that a higher solution concentration caused an increase in the fibre diameter, which can be explained by the higher number of entanglements between polymer chains, as well as opposing jet stretching under the applied electric field (Cramariuc et al. 2013; Veleirinho et al. 2008). Zong et al. (2002) were able to show that at concentrations higher than 40 wt % of poly(D,L-lactic acid) (PDLA), the electrospinning process was hard to maintain due to the high viscosity of the solution, i.e. the droplet was dried out before the constant jet could be formed but the more viscous the solution becomes (lower than the process limiting concentration), the more uniform the fibres that were formed, and the diameters of the beads become bigger while the average distance between the beads increased as the solution viscosity increased.

4.3 Effect of flow rate on PS nanofibre

This experiment was carried out to investigate the effect of flow rate during electrospinning on fibre diameter for polystyrene (PS). The purpose was to determine and optimise conditions necessary for the low average fibre diameter needed when the electrospun nanofibre is used for adsorption. Nanofibres of polystyrene (PS) were prepared by electrospinning of PS solutions in a mixture of N,N-dimethylformamide (DMF) and tetrahydrofuran (THF) at high voltages as detailed in chapter 3 section 3.2.2. The morphology of the electrospun PS nanofibres was investigated by scanning electron microscopy. The experimental procedure for the SEM technique is detailed in Chapter 3 Section 3.4.2 and the fibre diameter analysis was evaluated using Image J® software. The results for the generated PS SEM microgram images and average fibre diameter of these investigations are shown in Figure 4.5 below.

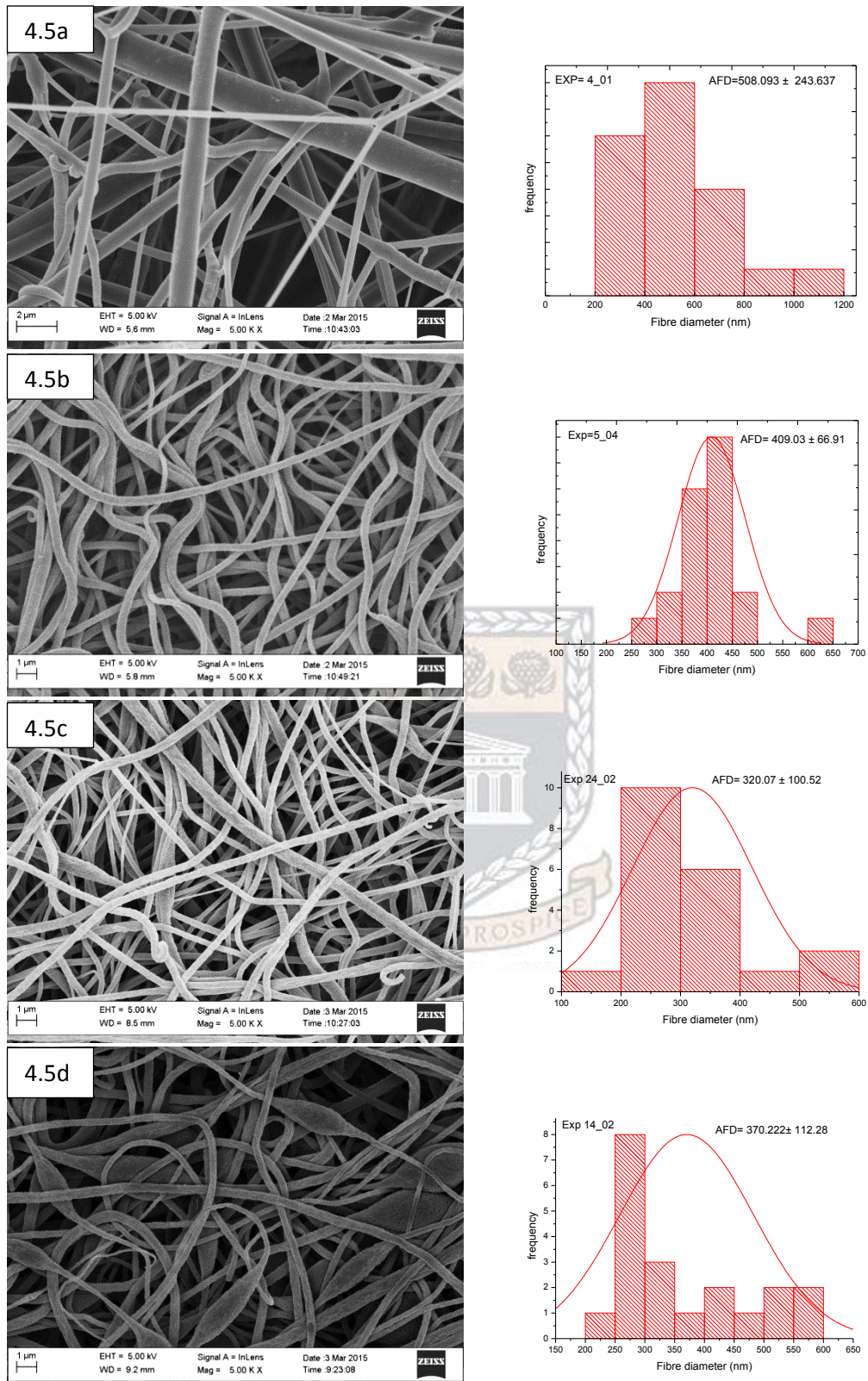


Figure 4.5 SEM micrographs and distribution of electrospun PS nanofibres at different flow rates (a) 0.2, (b) 0.4, (c) 0.8 and (d) 1.0 mL/h (polymer concentration - 15 wt %; voltage - 20 kV and distance - 17 cm).

Figure 4.5 (a - d) presents the result of SEM micrographs and average fibre distribution (AFD) of electrospun polystyrene (PS) nanofibres at 0.2 and 1.0 mL/h flow rates and at a polymer concentration of 15 wt %; using an applied electrostatic potential of 20 kV over a collection distance of 20 cm. At the low flow rate of 0.2 mL/h, the spinning solution was drying quickly and the electrospinning process was not progressing as expected, giving rise to very large fibre diameters, but when the flow rate of the spinning solution was increased, fibres were deposited on the collector in greater abundance with an increased fibre mass and the average diameter of fibres decreased. The fibres produced at the highest flow rate of 1.0 mL/h (Figure 4.5 d) showed the bead-on-string morphology and an increased fibre diameter.

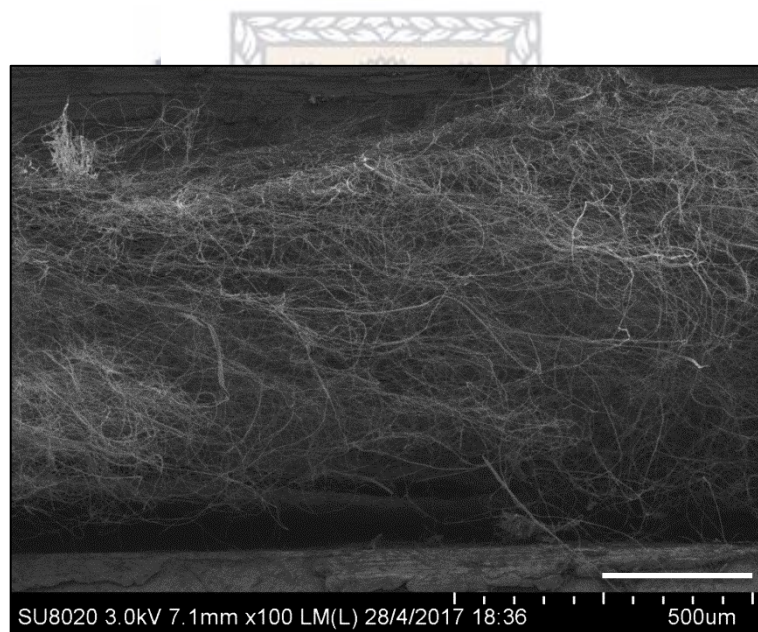


Figure 4.6. Cross section of SEM micrographs of electrospun PS nanofibre mat after 2 hrs (flow rates - 0.8 mL/h; polymer concentration - 15 wt %; voltage - 20 kV and distance - 17 cm).

A large amount of nanofibres in the form of thin hair - like structures (Figure 4.6) was achieved by increasing the flow rate. The thickness of nanofibre mats was increased by appropriately prolonging the electrospinning time. Table 4.1 shows the

fibre mass when time was prolonged. The relative distribution of fibre diameters for PS show greater variation as the flow rate was increased.

Table 4.1. Comparison of flow rate and fibre mass (polymer concentration - 15 wt %; voltage - 20 kV and distance - 17 cm).

Sample code	Flow rate (mL/h)	Time (min)	Fibre mass (g)
PS-F1	0.2	60	0.0074
PS-F2	0.4	60	0.0342
PS-F3	0.8	60	0.0676
PS-F3	0.8	120	0.1256
PS-F3	0.8	180	0.1847
PS-F4	1.0	60	0.0033

From Table 4.1, deposition at a flow rate of 1.0mL/h decreased because too high flow rate of spinning solution may cause dropping of solution and less deposition on the collector. It can also be due to decreasing of electrostatic density which led to fabrication of the beaded fibres with increased diameters at higher flow rate. Fibre deposition increased with increasing flow rate and therefore 0.8 mL/h was determined to be the appropriate optimisation flow rate in the PS electrospinning process.

The PS fibre diameter decreased as the flow rate increased contrary to the views held by Fong et al. (1999) and Zuo et al. (2005) when they investigated electrospinning of poly (ethylene oxide) (PEO) and poly(hydroxybutyrate-co-valerate (PHBV).

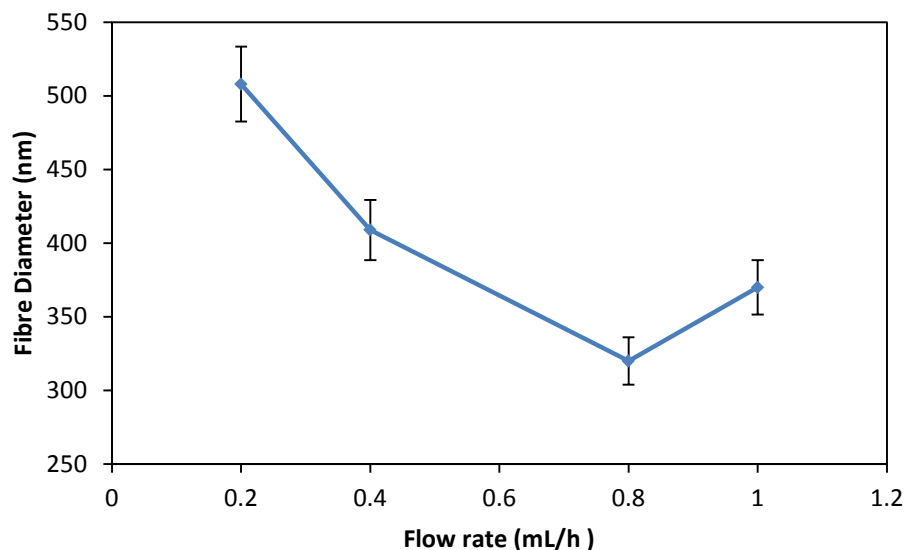


Figure 4.7. Trend of fibre diameter as a function of flowrate for PS at different flow rates (a) 0.2, (b) 0.4, (c) 0.8 and (d) 1.0 mL/h (polymer concentration - 15 wt %; voltage - 20 kV and distance - 17 cm).

Figure 4.7 showed that despite the observed decrease of fibre diameter up to an optimum of 0.8 mL/h, there was an increase in fibre diameter when the flow rate was increased to 1.0 mL/h. For this study, too low a flow rate (0.2 mL/h) of the spinning solution caused blockages of the nozzles when pendant droplets disappeared from the tip of the needle and dried up, thus sealing the nozzle with the solidified polymer residue. On the other hand, too high a flow rate (1.0 mL/h) of the spinning solution caused droplets of solution to be ejected which resulted in a bead-on-string fibre morphology (Figure 4.5d). Considering the average diameter sizes for the fibres (508.09, 409.03, 320.07 and 370.02 nm) which were generated for 0.2, (b) 0.4, (c) 0.8 and (d) 1.0 mL/h flow rates respectively, the optimum solution flow rate for fabrication of PS composite fibres was determined as 0.8 mL/h and electrospun time of 180 mins for further experiments and was suitable for fabricating an adsorbent nanofibre.

4.4 Effect of flow rate on PET nanofibre

This experiment was carried out to investigate the effect of flow rate during electrospinning on fibre diameter for polyethylene terephthalate (PET) to determine the optimum conditions necessary for low average fibre diameters needed when the electrospun nanofibre is used for adsorption. Figure 4.8 (a - d) presents the SEM micrographs and average fibre distribution (AFD) of electrospun polyethylene terephthalate (PET) nanofibres at different flow rates (a) 0.2, (b) 0.4, (c) 0.8 and (d) 1.0 mL/h (polymer concentration 10 %; using applied voltage of 25 kV; distance 17 cm). The electrospinning process is detailed in Chapter 3 Section 3.2.2.



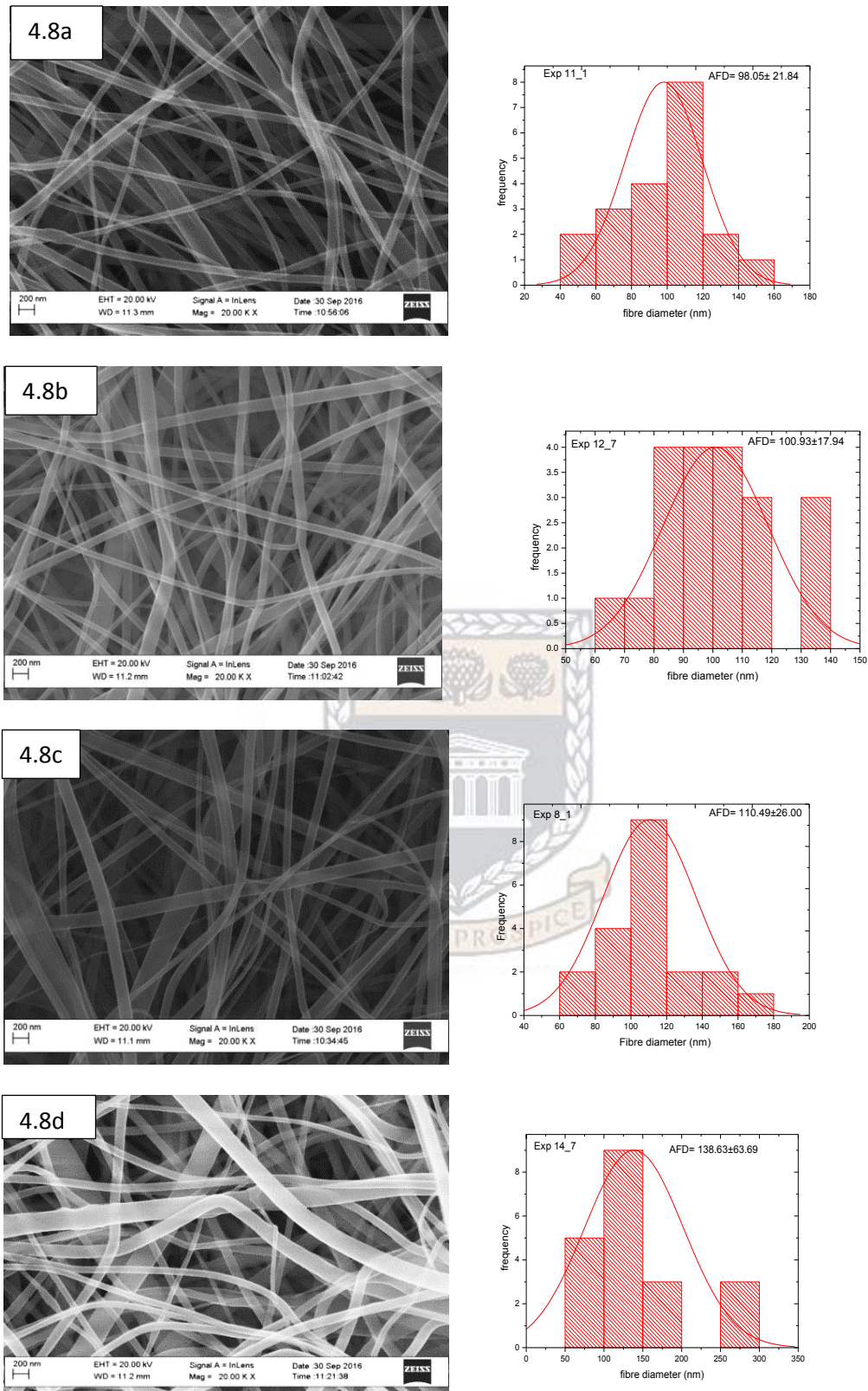


Figure 4.8. SEM micrographs and distribution of electrospun PET nanofibers at different flow rates (a) 0.2, (b) 0.4, (c) 0.8 and (d) 1.0 mL/h (polymer concentration - 10 wt %; voltage - 20 kV and distance - 20 cm).

From the SEM observations, the fibre diameters were in a range from about 50 to 150 nm (see Figure 4.8), which is thinner than the average fibre diameter obtained for the PS nanofibres.

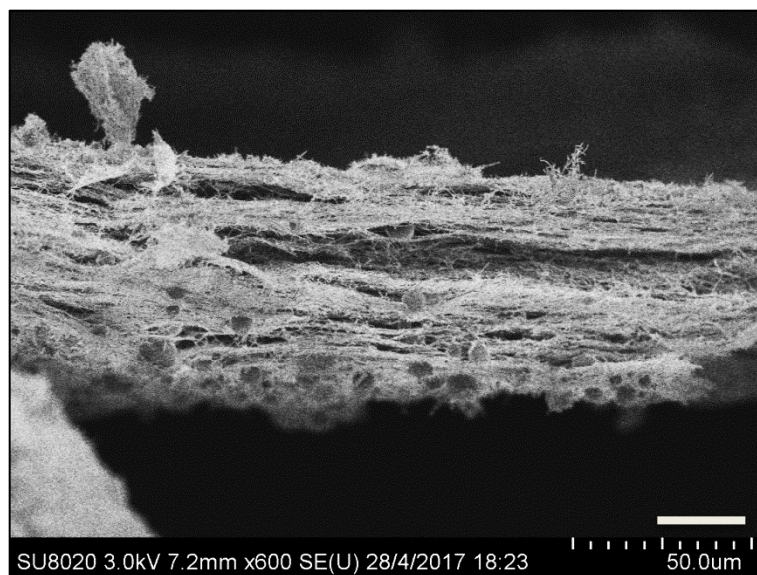


Figure 4.9. Cross section of SEM micrographs of electrospun PET nanofibre mat after 2 hrs (flow rate - 1.0 mL/h; polymer concentration - 10 wt %; voltage - 20 kV and distance - 20 cm).

Figure 4.9 show the dimension of PET nanofibre mats which was realised without prolonging the electrospinning time and the deposition was uniform. Table 4.2 depicts the fibre mass when the flow rate was varied under constant time.

Table 4.2. Comparison of flow rate and fibre mass (polymer concentration - 10 wt %; voltage - 20 kV and distance - 20 cm).

Sample code	Flow rate (mL/h)	Time (min)	Fibre mass (g)
PET-F1	0.2	60	0.0795
PET-F2	0.4	60	0.0944
PET-F3	0.8	60	0.111
PET-F4	1.0	60	0.1298
PET-F4	1.0	120	0.1823
PET-F4	1.0	180	0.1711

Table 4.2 depicts the flow rate and fibre mass as a function of deposition time and shows that as the flow rate is increased, fibre deposition also increased, however, prolonged deposition at a specific flow rate did not increase the fibre productivity which could be due to a decrease of electrostatic density at a high flow rate. The optimum solution flow rate for fabrication of PET fibers was determined to be 1.0 mL/h and 120 mins which compared favourably with obtained results by Ignatova et al. (2008) in their study of PET polymer concentration using 11 wt % which achieved 0.0242 g after 150 mins of deposition time.

The fibres deposition and diameters were however, not uniform in relative distribution as shown in Figure 4.8. For instance, the major distribution region (over 95%) of nanofibre diameters was in the range of 60-120 nm for the flow rate of 0.4 mL/h with an average diameter of 100 nm, which was nearly three times thinner than that of PS electrospun nanofibres of the same flow rate. Beading was not present at any of the flow rates even though there was increased non alignment of fibres as flow rate increased. The fibre diameter distribution was broader, more matted and non aligned as the flow rate increased (Figure 4.8 b). Fibres were deposited more randomly and intersected each other. From the investigation, the

flow rate correlated with PET fibre diameter as shown in Figure 4.10, indicating an increased average fibre diameter as the flow rate increased from 0.2 to 1.0 mL/h.

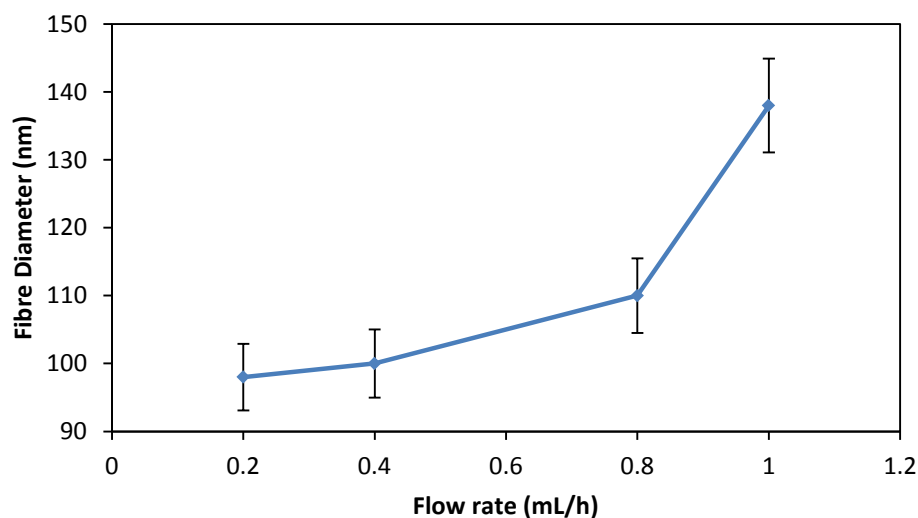


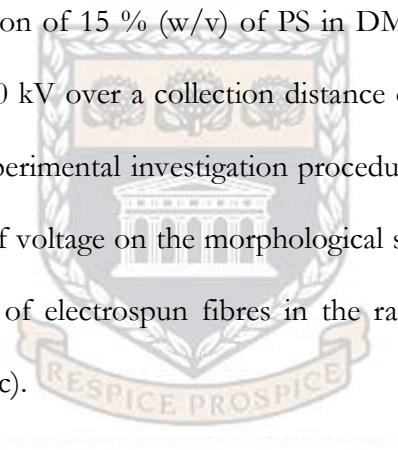
Figure 4.10. Trend of fibre diameter as a function of flow rate for PET at different flow rates (a) 0.2, (b) 0.4, (c) 0.8 and (d) 1.0 mL/h (polymer concentration - 10 wt %; voltage - 20 kV and distance - 20 cm).

The PET nanofibres were smooth and cylindrical in shape, which indicated that the PET polymer was substantially miscible in Tetrahydrofuran (THF) solution. The optimum solution flow rate for fabrication of PET nanofibres was determined to be 1.0 mL/h and 120 mins for further experiments due to the increased deposition flow rate and thickness of the nanofibre mat that could be spun per unit of time which was important for the adsorption experiments. Beachley and Wen (2009) reported that the feed rate may not have a significant effect on the maximum fibre length, diameter or uniformity over all parameter variations when he investigated polycaprolactone (PCL) nanofibres. They claimed that once the feed rate was sufficient for forming fibres, higher feed rates only provided more polymer solution than needed, and it was observed that the amount of excess polymer solution formed at the needle tip increased with an increased feed rate. However, other investigations,

Poly(DL-lactide) (Cui et al. 2007), poly (acrylic acid) (Li and Hsieh 2005), poly(l-lactid-co-caprolactone) (Tan et al. 2005) showed that as the flow rate of the spinning solution increased, the average fibre diameter increased and the fibre diameter distribution spread. Generally, an increase in the PET polymer flow rate increases the fibre diameter (Fong et al. 1999; Zuo et al. 2005).

4.5 Effect of applied voltage on PS nanofibre morphology

This experiment was carried out to investigate the effect of voltage on fibre diameter and the morphological alignment of the electrospun polystyrene (PS) nanofibre. The results and average fibre diameters are illustrated in Figure 4.11 (a - c). These fibres were spun from the solution of 15 % (w/v) of PS in DMF/THF, using an applied potential range of 15 to 20 kV over a collection distance of 20 cm and a fixed flow rate of 0.8 mL/h. The experimental investigation procedure is detailed in Chapter 3 Section 3.2.3. The effect of voltage on the morphological structure, average diameter and diameter distribution of electrospun fibres in the range of 15 and 20 kV are shown in Figures 4.11 (a - c).



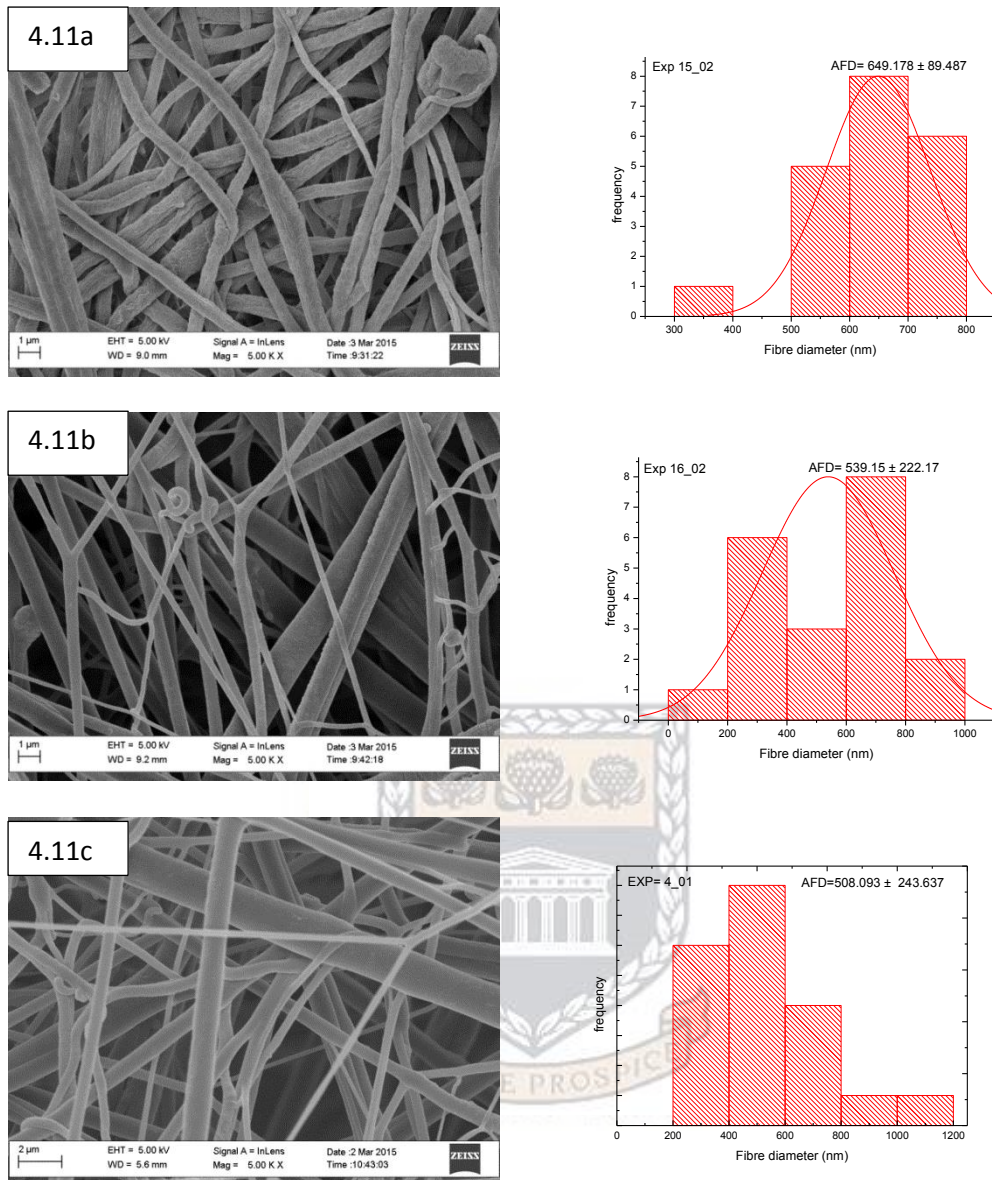


Figure 4.11. SEM micrographs and distribution of electrospun PS nanofibres at different applied voltage (a) 15, (b) 17 (c) 20 kV (flow rate - 0.8 mL/h; polymer concentration - 15 wt % and distance - 17 cm).

Figure 4.11 showed that at a very low voltage, fibres with a weak, flat and irregular morphology were observed which may have resulted from the structures of a collapsed fibre because the applied electrical force was not sufficient to form the perfect fibres (Figure 4.11a) but as the applied potential was increased, the fibres become cylindrical in nature. The average fibre distribution for applied voltages of

15, 17 and 20 kV also depicts that very high fibre diameters were obtained up to a maximum of 800, 1000 and 1200 nm respectively.

The distribution of the fibre diameters was broad with some fibre entanglements when the applied potential was 17 kV, and fibres became more elongated at the higher applied potential of 20 kV (Figure 4.11c). Despite the poor morphology with fibres markedly inferior in the case of 15 kV (Figure 4.11a), the average fibre diameter was high but as voltage was increased, the fibres became more non-uniform because the high strength of the electrical field increased the instabilities of jet solution. Ultrafine fibres which were cylindrical in shape with smooth surfaces were observed with the increased voltage. Moreover, the average diameter of the nanofibres decreased and the morphology of the as-spun fibres was improved. It can also be observed that the fibres have many junctions showing poor fibre uniformity at 20 kV voltage. However, the fibre diameters were found to slightly decrease with increasing applied potential from 649 nm at 15 kV to 508 nm at 20 kV as shown in Figure 4.12.

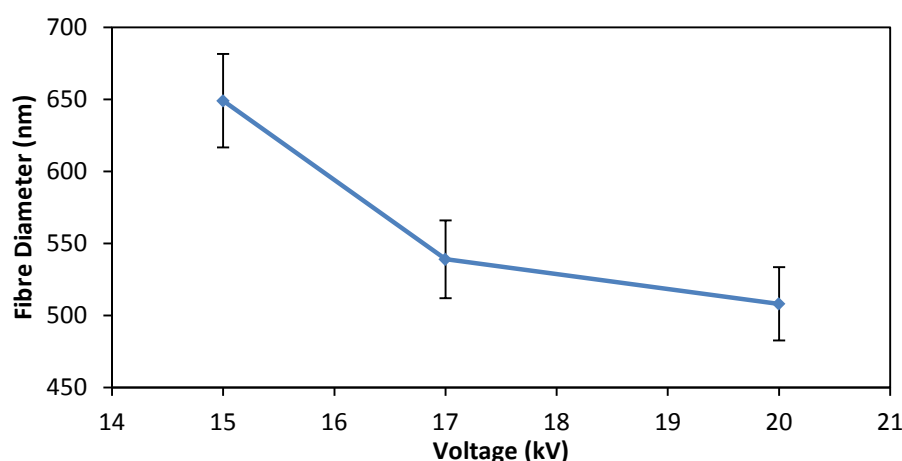


Figure 4.12. Trend of fibre diameter as a function of voltage for PS samples at different applied voltages (a) 15, (b) 17 (c) 20 kV (flow rate - 0.8 mL/h; polymer concentration - 15 wt % and distance - 17 cm).

Below an applied voltage of 15 kV, the fibres were not ejecting nor depositing on the collector, and as can be seen at average voltage (15 kV), the electrical field strength for the formation of homogenous fibres was weak and very weak fibres were observed, but by increasing the voltage, uniform thinner fibres were obtained. Therefore, the optimum applied voltage was determined to be 17 kV for further experiments due to the greater uniformity of the fibres. Fibre diameter decreased with increasing voltage over all data points but there was no uniformity of the fibre's diameters with increasing voltage.

4.6 Effect of applied voltage on PET nanofibre morphology

The results of the experiment performed to investigate the effect of the applied potential during electrospinning on both the diameters and the morphological alignment of the as-spun polyethylene terephthalate (PET) nanofibres are illustrated in Fig 4.13 (a and d). These fibres were spun from the solution of 10 % (w/v) of PET in TFA, using an applied potential range from (a) 10 (b) 15 (c) 17 (d) 20 kV over a collection distance of 17 cm and a fixed flow rate of 1.0 mL/h. The experimental investigation procedure is detailed in Chapter 3 Section 3.2.3.

Figure 4.13 (a - d) showed that fibre alignment was not uniform at a voltage of 15 kV and nanofibre diameters were diverse, with different diameter sizes. Some beads on strings were noticed in the case of the low voltage electrospun fibres, however, the morphology was much improved with an increased potential.

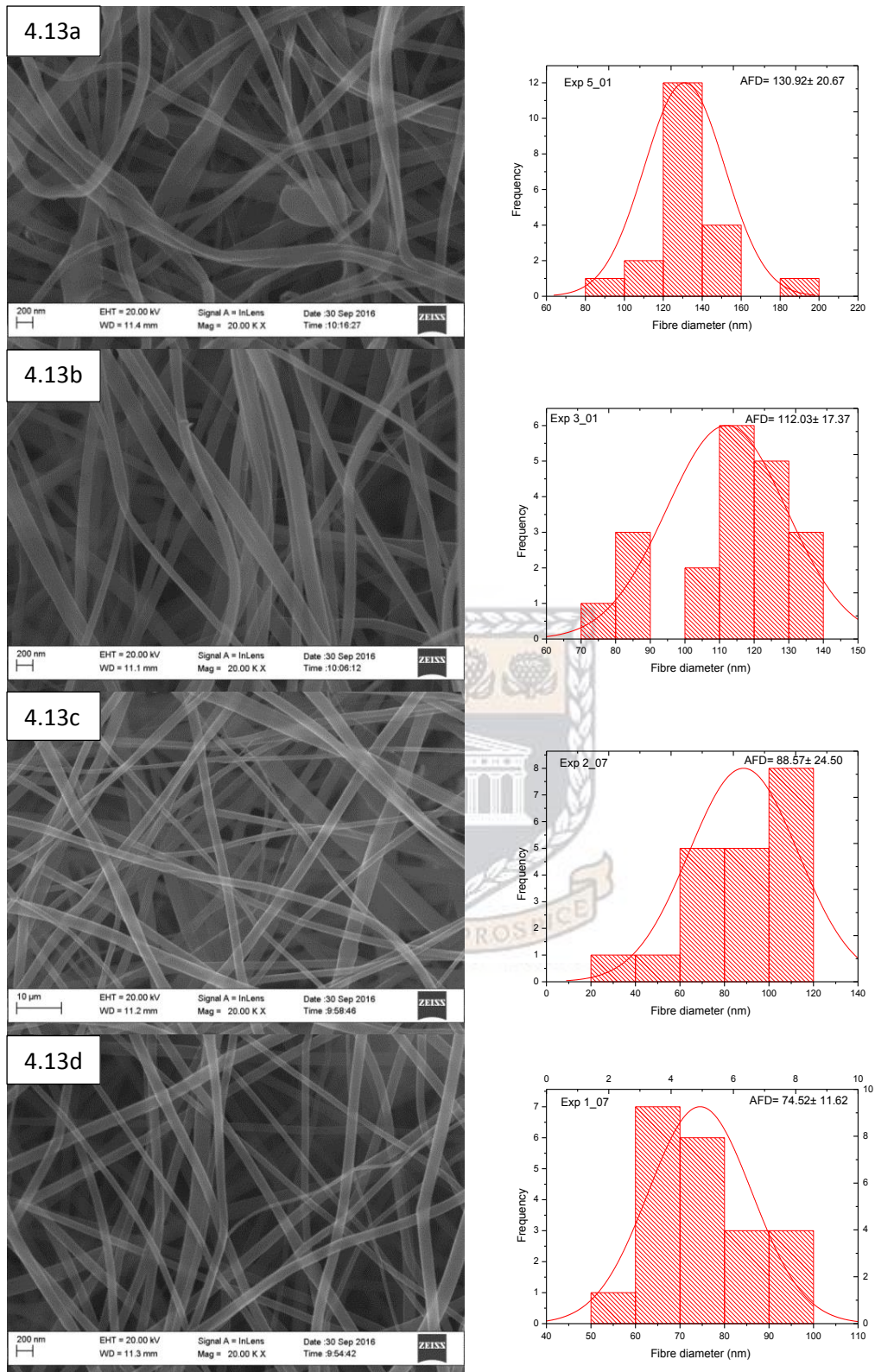


Figure 4.13. SEM micrographs and distribution of electrospun PET nanofibres at different applied voltage (a) 10, (b) 15 (c) 17 (d) 20 kV (flow rate - 1.0 mL/h; polymer concentration - 10 wt % and distance - 20 cm).

Figure 4.13 (b) shows the alignment of the as-spun fibres in the machine direction when the electrostatic potential of 15 kV was applied but for higher potentials there were no alignment due to the increased strength of the electrical field which increased the instabilities of the jet solution. Electrostatic potential of 17 kV was adopted because of the low fibre diameter, fibre thickness and smooth morphology. Generally, the fibre diameters were found to decrease in diameter sizes with some slight changes in morphology as the voltage was increased. The fibre diameters were found to decrease from 130 nm at 10 kV to 74 nm at 20 kV as shown in Figure 4.14.

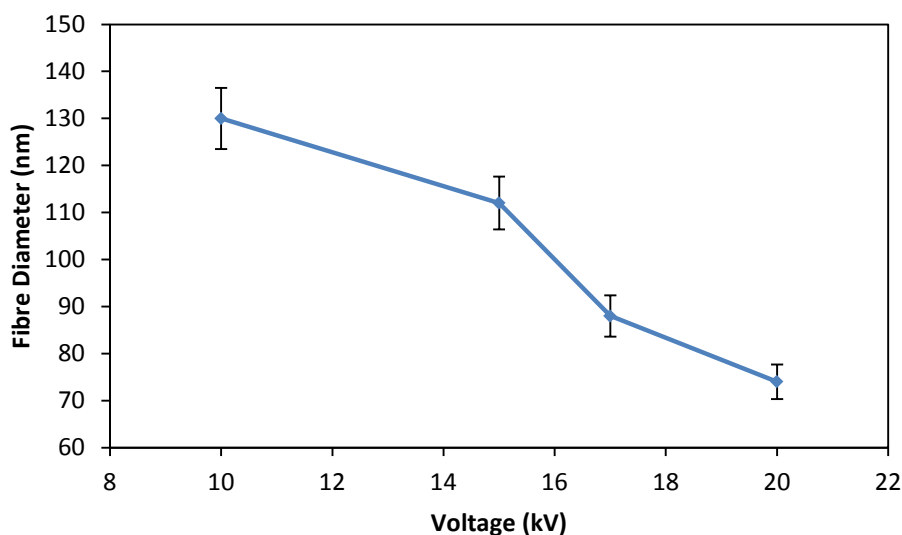


Figure 4.14. Trend of fibre diameter as a function of voltage for PET samples at different applied voltage (a) 10, (b) 15 (c) 17 (d) 20 kV (flow rate - 1.0 mL/h; polymer concentration - 10 wt % and distance - 20 cm).

For the two polymers used, polystyrene (Figure 4.12) and polyethylene terephthalate (Figure 4.14), there was a decrease in fibre diameter when the voltage was increased and this may be attributed to the influences of the polymer solution concentration due to its viscosity as well as the distance between the tip and the collector. The applied voltage in the electrospinning process is an essential parameter that affects

the formation of fibres and there were no change in nanofibre yield per unit time with increased voltage.

Demir et al. (2002) and Zhang et al. (2005) electrospun polyurethane and poly(vinyl alcohol) (PVA) respectively and agreed that when higher voltages are applied, there is more polymer ejection and this facilitates the formation of a larger diameter fibre. However, other authors Lee et al. (2004); Megelski et al. (2002); Gu and Ren (2005) and Kim et al. (2005) reported that an increase in the applied voltage (i.e., by increasing the electric field strength), increased the electrostatic repulsive force on the fluid jet which ultimately favoured the decrease of fibre diameter. Cui et al. (2007) and Kim et al. (2005) argued that too high applied voltages may also cause the acceleration of charge on the spinning solution which leads to an increase in the fibre diameters. Generally, high voltage is able to generate more charges in the solution or droplet surface located at the tip of the needle as well as larger electrostatic forces, both of which stretch the jets fully for the favourable formation of the thinner fibres (Theron et al. 2004).

4.7 Effect of needle tip to collector distance on PS nanofibre morphology

The results of the experiment investigating the effect of needle tip to collector distance during electrospinning of PS nanofibres are presented in this section. The experimental details are in Chapter 3 Section 3.2.4. Figure 4.15 (a - c) below illustrates the effect of different needle tip–collector distances on PS fibre morphology and diameter. These fibres were spun from the solution of 15 % (w/v) of PS in DMF/THF, using an applied potential of 17 kV over a collection distance between 10 and 20 cm and a fixed flow rate of 0.8 mL/h.

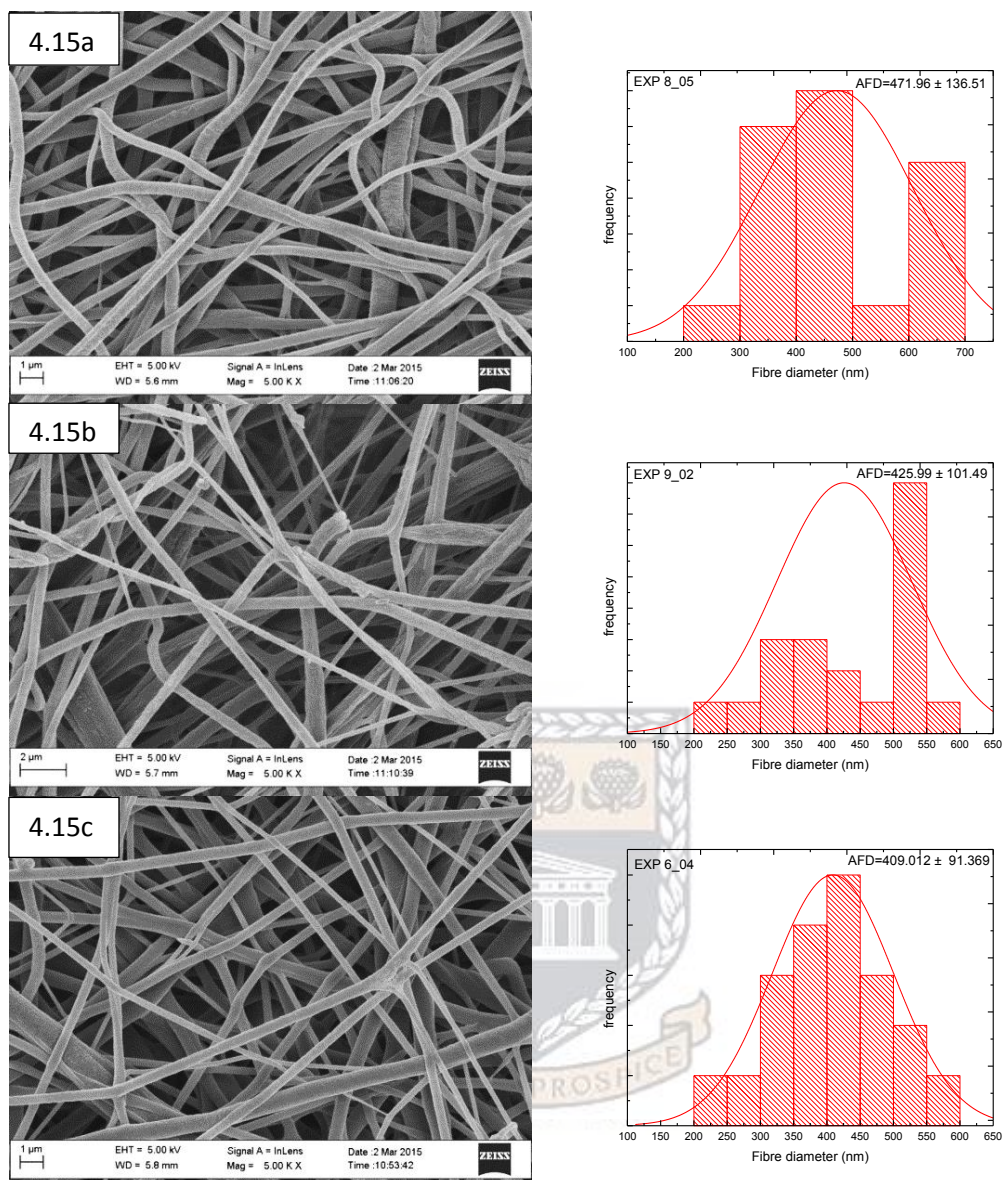


Figure 4.15. SEM micrographs and distribution of electrospun PS nanofibres on needle tip–collector distance (a) 10, (b) 15 and (c) 20 cm (flow rate - 0.8 mL/h; voltage - 17 kV and polymer concentration - 15 wt %).

Fig. 4.15 (a-c) depicts the morphology, average diameter and distribution of PS electrospun fibres at different needle tip–collector distances. All the fibres were not aligned but matted and there was not much difference between the fibre morphology showing little effect of tip to collector distance on PS electrospinning. However, flatter fibres were noticed at short distances while rounder fibres were seen when the distance was increased.

By increasing the collector distance, the stability of the jet solution was increased and this resulted in the formation of non-woven homogeneous fibres with lower diameters. The fibre alignment of the as-spun fibres was not too improved with increasing distance, but the fibre diameters were found to reduce slightly from 471 nm to 400 nm with the increase in the distance as shown in Figure 4.16.

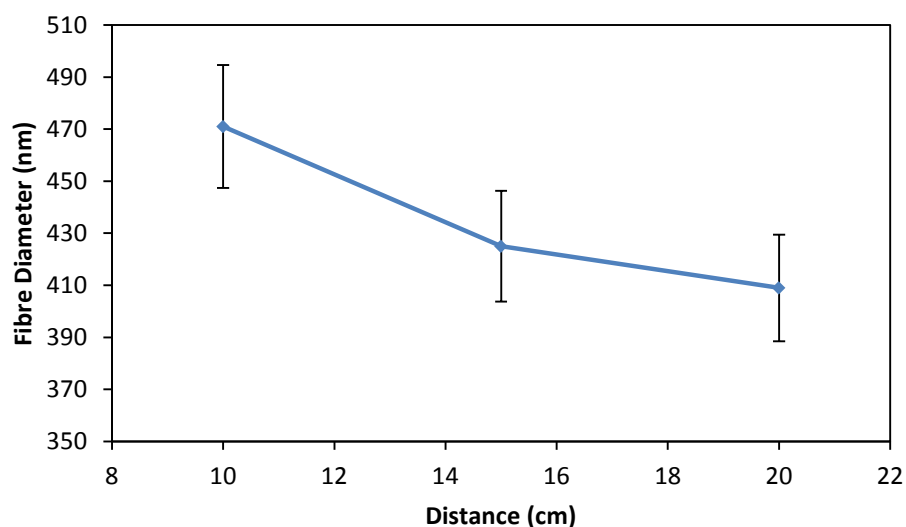


Figure 4.16. Trend of fibre diameter as a function of needle tip-collector distance at (a) 10, (b) 15 and (c) 20 cm (flow rate - 0.8 mL/h; voltage 17 kV and polymer concentration - 15 wt %)

The structure and morphology of electrospun fibres is easily affected by the nozzle to collector distance because of their dependence on the deposition time, evaporation rate, and whipping or instability interval (Buchko et al. 1999; Megelski et al. 2002). The optimum needle tip-collector distance for fabrication of PS composite fibres was determined as 15 cm for further experiments because of the minimal average diameter of the nanofibres.

4.8 Effect of needle tip-collector distance on PET nanofibre morphology

This experiment was conducted to investigate the effect of needle tip – collector distance during electrospinning on PET nanofibre morphology and the average fibre

diameter. The experimental protocol is detailed in chapter 3 sub section 3.2.4. These fibres were spun from a solution of 10 % (w/v) of PET in TFA using an applied potential of 17 kV over a collection distance of (a) 10, (b) 15 (c) 20 and 25 cm at a fixed flow rate of 1.0 mL/h. Figure 4.17 (a - d) illustrates the effect of needle tip– collector distance on (PET) on fibre morphology and diameter.



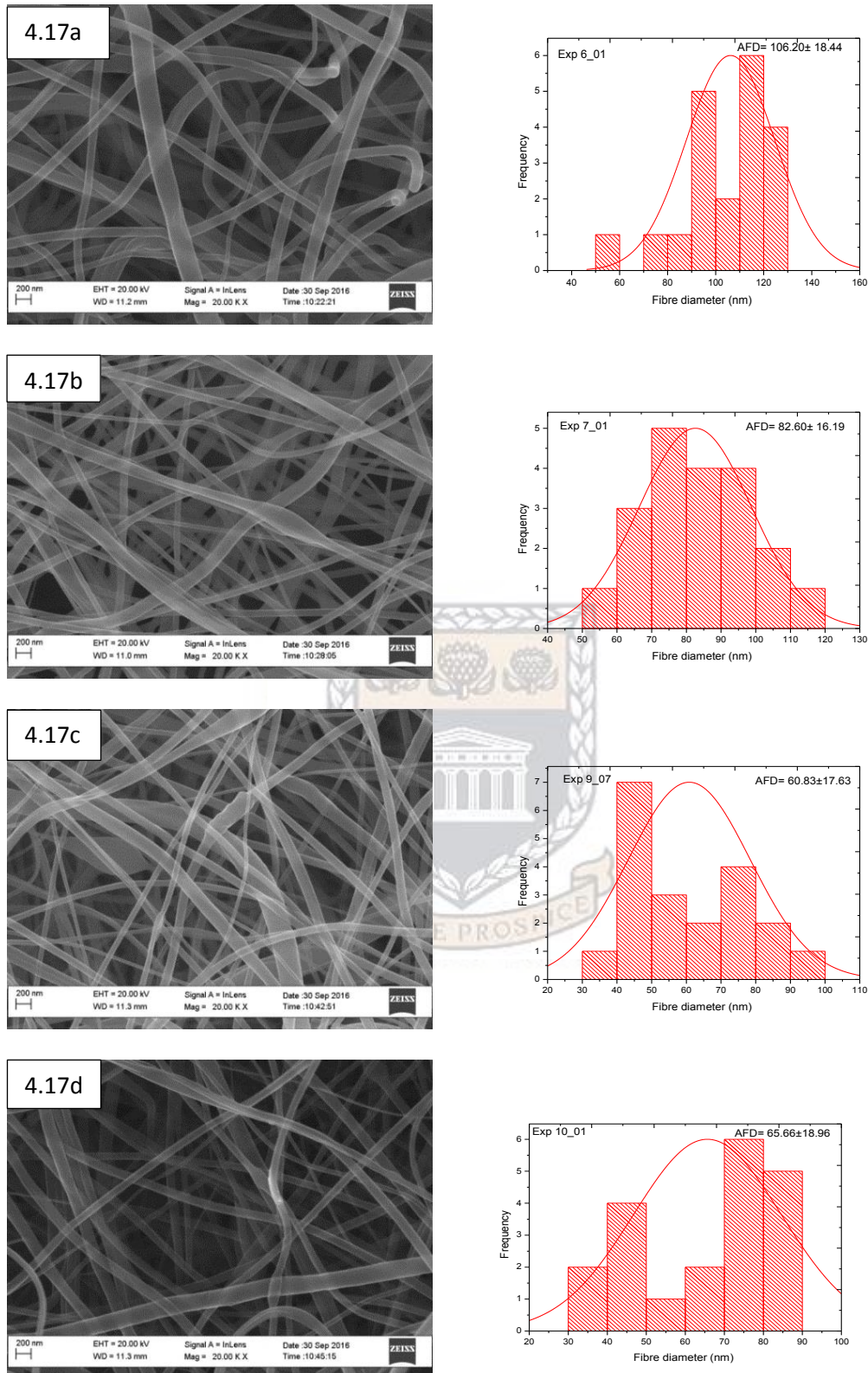
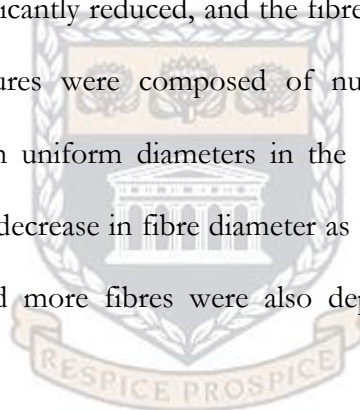


Figure 4.17. SEM micrographs and distribution of electrospun PET nanofibres on needle tip–collector distance (a) 10, (b) 15 (c) 20 and (d) 25 cm (flow rate - 1.0 mL/h; voltage - 17 kV and polymer concentration - 10 wt %).

The average PET fibre diameters were found to decrease with an increase in the needle tip–collector distance. Broken fibres were noticed at short distances and the diameter decreased with an increased distance. Beads on string that were initially noticed up to the distance of 20 cm disappeared as the needle tip–collector distance increased to 25 cm. When the distance between the spinnerets and the collecting device was short, spun fibres tended to stick to the collecting device as well as to each other, due to incomplete solvent evaporation.

From these results, 20 cm was determined as the needle tip–collector distance to use for further experiments with PET. At this distance, the PET fibres' diameter and bead formation were significantly reduced, and the fibre mats were denser and more aligned. The fibre structures were composed of numerous, randomly oriented nonwoven nanofibres with uniform diameters in the range of 30 - 100 nm. The obtained results showed a decrease in fibre diameter as the distance was increased as shown in Figure 4.18 and more fibres were also deposited as the distance was increased.



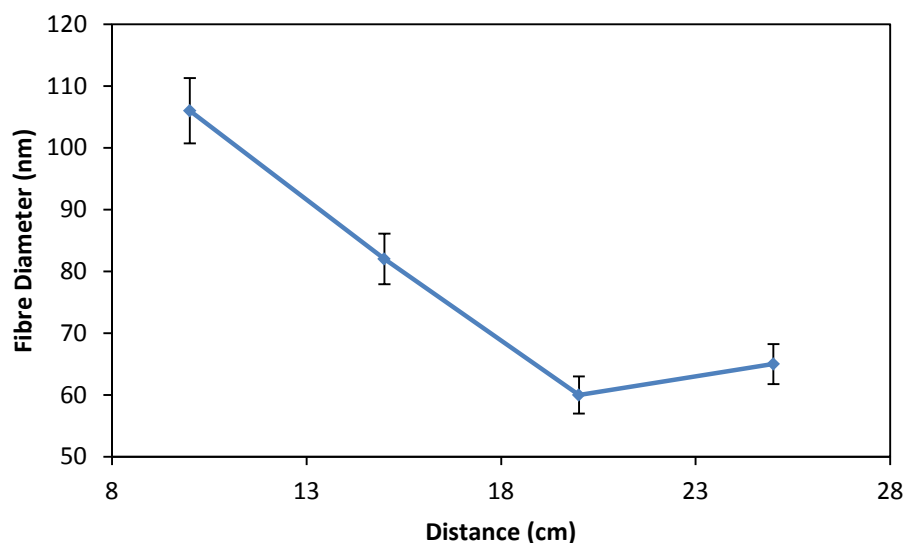


Figure 4.18. Trend of fibre diameter as a function of needle tip–collector distance at (a) 10, (b) 15 (c) 20 and (d) 25 cm (flow rate - 1.0 mL/h; voltage - 17 kV and polymer concentration - 10 wt %).

The optimisation of distance between needle tip and collector has a very important role in formation of homogeneous and fine fibres. The distance between the needle tip and collector affects the deposition time, evaporation rate of solvent and instability interval (Subbiah et al. 2005) because over very short distances, the electrical field becomes very strong which increases the instability of the jet solution and may multiply the jets emerging from the nozzle resulting in the formation of beaded fibres (Doshi and Reneker 1995).

The increase in the tip–collector distance leads to formation of fibres without the presence of beads. Over very long distances, the strength of the electrical field becomes weak resulting in an increase in fibre diameters (Deitzel et al. 2001; Zong et al. 2002). Average fibre diameters tend to decrease with an increase in collector distance (Chase and Reneker 2004; Zuo et al. 2005) and (Geng et al. 2005; Lee et al. 2004) established that a minimum distance is required to give the fibres sufficient time to dry before reaching the collector, otherwise beads could be observed with

distances that are either too close or too far during their investigation of chitosan dissolved in concentrated acetic acid solution and Poly(vinyl alcohol) respectively.

The optimum electrospinning conditions for the experiments were therefore obtained under the following operating conditions using PS-D2 and PET-D3:

	PS-D2	PET-D3
Concentration (wt %)	15	10
Voltage (kV)	17	17
Solution flow rate (mL/h)	0.8	1
Collector distance (cm)	15	20
Average fibre diameter (nm)	425.99	60.83
Range (nm)	200 - 600	20 - 150

The obtained PS-D2 nanofibres in this study (as described in Chapter 3 Table 3.8) achieved average fibre diameter (425.99 nm) at solution concentration of 15 wt % and 17 kV after 180 mins of deposition time and when compared with Jarusuwannapoom et al. (2005) who investigated the effects of solvents on electrospinnability of polystyrene solutions on morphological appearance. Their results using dimethylformamide (DMF) solvent showed that smooth as-spun fibres were observed at 30% (w/v) only. Investigations by electrospinning of polystyrene/poly(2-methoxy-5-(2'-ethylhexyloxy)-1,4-phenylene vinylene) (PS/MEH-PPV) blends solutions in chloroform, 1,2-dichloroethane, and tetrahydrofuran (THF) studied by Wutticharoenmongkol et al. (2005) showed that smooth fibres were only observed from 23.5% (w/v) PS/MEH-PPV solution in chloroform and the average diameters of the as-spun PS/MEH-PPV fibres were between 0.30 and 5.11 μm .

Uyar and Besenbacher (2008) also investigated the electrospinning of uniform polystyrene (PS) fibres from dimethylformamide (DMF) solutions and the

conductivity of the solvent was considered as the key factor. Bead-free PS fibres between 1500 and 4000 nm were obtained from PS solutions in the range of 20% (w/v) through 30% (w/v) depending on the DMF grade used while investigation of morphology of porous and wrinkled fibres of polystyrene electrospun from dimethylformamide by Pai et al. (2009) showed that 30 wt % solution of PS dissolved in DMF in air at 29% relative humidity and room temperature produced as-spun PS fibres with a smooth surface and cylindrical shape while the average fibre diameter was $3.52 \pm 0.2 \mu\text{m}$.

PET-D3 (as described in Chapter 3 Table 3.9) yielded a comparable fibre diameter to Ignatova et al. (2008) who obtained PET nanofibres with an average diameter of 170 nm with the distribution range of fibre diameter between 80 – 280 nm. PET-D3 also produced a lower fibre diameter compared to that using Atactic poly (vinyl alcohols) (a-PVAs) (Lee et al. 2004) prepared by electrospinning with an average diameters of 300 and 240 nm. Their study identified that the molecular weight of a-PVA had a marked influence on the structure and properties of nanofibres produced, however the PET-D3 was much bigger in AFD when compared to Atactic poly(vinyl alcohols). In the melt-electrospinning of PET by Ogata et al. (2007), the minimum value of average fibre diameter obtainable was about $1.7 \mu\text{m}$ irrespective of the different intrinsic viscosities (IV) values which suggests that the obtainable fibre diameter was not influenced by the molecular weight of the PET contrary to the solution concentration effect on PET in this study.

4.9 Water contact angle (WCA) measurements

This experiment investigated the effect of wettability on the morphology of PS and PET electrospun nanofibres. The experiment determined the water contact angle

(WCA) properties of the nanofibres which require hydrophilic surface modification for desired responses. Only the optimised samples (PS-D2 and PET-D3, determined in Chapter 3, Section 3.2.4), which are to be used in modification were therefore investigated to ascertain their suitability for further modification. This analysis was conducted by using doubly deionised water (DDI) as wetting liquid at 25°C on the PS-D2 and PET-D3 sample morphology and the results are shown in Figure 4.19 and 4.20 below. The sample WCA were measured according to the process described in Chapter 3 Section 3.4.6 and the results are shown in Figure 4.19 and 4.20 below. The contact angle values (equation 4.1) were calculated using the Wenzel equation (Wenzel 1936)

$$\cos \theta^* = r \cos \theta_Y \dots\dots\dots \text{Equation 4.1}$$

where θ^* is the apparent contact angle and θ_Y is the equilibrium contact angle from Young's equation on an ideal solid without roughness, which took into account the surface roughness and the penetration of the liquid into the grooves. Figure 4.19 presents the contact angle values for PS-D2 nanofibre.

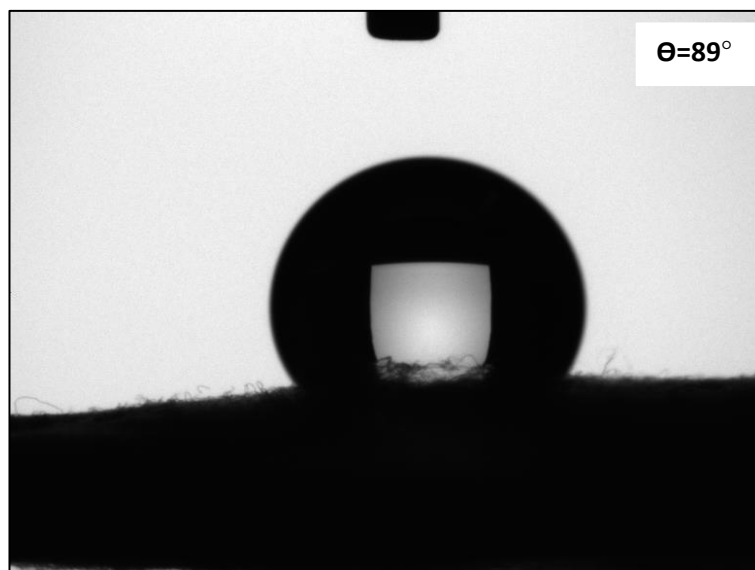


Figure 4.19. Contact angle of PS-D2 nanofibre (polymer concentration - 15 wt %; voltage - 17 kV; solution flow rate - 0.8 mL/h and collector distance - 15 cm).

The WCA of the electrospun PS-D2 nanofibre was 89° and can be attributed to the surface roughness after electrospinning and bead-free nanofibre morphology. The presence of beads on the fibres could contribute to higher water contact angle which make the bead-on-string structure a favorable one for increasing the hydrophobicity (Lee et al. 2013; Ma et al. 2005). The PS-D2 result was near the WCA of an atactic PS ($\sim 85^\circ$) (Chan et al. 1996) and also comparable to results obtained by Bahramzadeh et al. (2016) (WCA = 86°) in their study but different from results of studies by Wu et al. (2016) which exhibited very high water repelling capability (WCA = 127.4°). The change in surface morphology of PS from polymer to nanofibre can lead to a change in contact angle (CA) value, which means that the wettability of the PS surface could be changed distinctly with modification (Zheng et al. 2006). The WCA of PET-D3 is shown in the Figure 4.20 below.

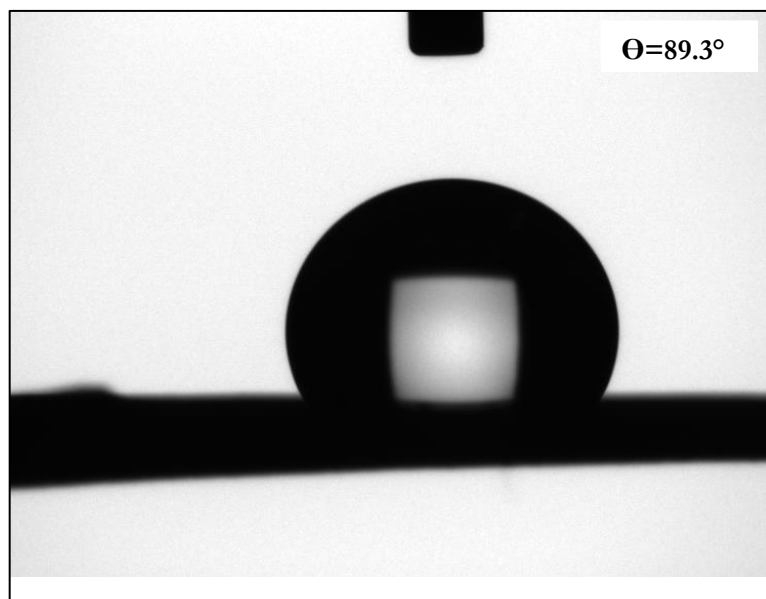


Figure 4.20. Contact angle of PET-D3 nanofibre (polymer concentration - 10 wt %; voltage - 17 kV; solution flow rate - 1.0 mL/h and collector distance - 20 cm).

The contact angle (WCA = 89.3°) which was observed for PET-D3 nanofibres is also attributed to the surface roughness after electrospinning and lack of nanofibre beading. Beading could result in enhanced hydrophobicity of the electrospun mats (Lee et al. 2013; Ma et al. 2005). The electrospinning process obviously increased the hydrophilicity of the polymer surface based on the WCA result and may therefore be further functionalised. The water contact angle of a solid surface is affected by surface roughness in such a manner as explained by Ma et al. (2005), that if the material is intrinsically hydrophobic, the water will not be able to penetrate into the hollows and pores on the rough surface and can be regarded as resting on a semi-solid and semi-air plane surface, which will increase the contact angle significantly. In contrast, the water will penetrate and fill up most of the hollows and pores formed by an intrinsically hydrophilic material, forming a surface which is partly solid and partly liquid and therefore leading to a low water contact angle.

4.10 Summary

Electrospinning is a process of electrostatic fibre formation which uses electrical forces to produce polymer nanofibres from polymer solutions. The aim of this study was to produce beadless nanofibres with a minimum diameter since the thinner and more homogeneous fibres would provide the maximum surface area and porosity which may result in higher efficiency adsorbents. The optimum electrospinning conditions for the experiments were obtained under the following operating conditions: PS (concentration - 15 wt %; voltage - 17 kV; solution flow rate - 0.8 mL/h and collector distance - 15 cm) and PET (concentration - 10 wt %; voltage - 17 kV; solution flow rate - 1.0 mL/h and collector distance - 20 cm).

In the PS nanofibre electrospinning process, it was observed that when the solution jet was placed in a strong electric field, the competition between electrical forces and surface tension decided the morphology of the product while solution concentration and flow rate had the most influence on the quality and quantity of the PET nanofibre. From this investigation, for PS, a solvent ratio of DMF:THF (4:1) was adopted and the flow rate (0.8 mL/h), solution concentration (15 wt %), electric potential (17 kV) and distance (15 cm) were selected as the best electrospinning process parameter for PS electrospinning in this study (PS-D2) which are to be used for further study.

In the case of PET nanofibres, trifluoroacetic acid (TFA) was used as solvent to prepare the electrospinning solution. It generated a nanofibre with very low average fibre diameter. From this study, the flow rate (1.0 mL/h), solution concentration (10 wt %), electric potential (17 kV) and distance (20 cm) were selected as the best electrospinning process parameter for PET electrospinning to produce the desired

nanofibre diameter and morphology (PET-D3) which are to be used for further experiments.

The optimised PS-D2 nanofibres diameter was in the range between 200 - 600 nm for PS which yielded 0.1847 g after 180 mins. PET nanofibres yielded 0.1823 g after electrospinning for 120 mins with an average fibre diameter range of 20 - 100 nm for the adsorption process. From this investigation, PET nanofibres had smaller fibre diameter and the electrospinning productivity at 120 mins yielded sufficient nanofibre mats (0.1823 g) for further use than PS. The results of this study achieved low average fibre diameters for the two polymers studied when compared with some reported work on PS and PET with smooth and bead less nanofibres.



CHAPTER FIVE

CHARACTERISATION OF STARTING MATERIALS AND SURFACE MODIFIED NANOFIBRE ADSORBENTS

5 INTRODUCTION

This chapter presents and discusses the results of the characterisation of the starting materials used in the experiments and the optimisation of the surface modification of nanofibres with diglycolic anhydride (DGA) chelating moieties to yield polystyrene – diglycolic acid (PS-DGA) and polyethylene terephthalate – diglycolic acid (PET-DGA) nanofibre adsorbents. The aim of the surface modification of polymer nanofibres was to improve and enhance the nanofibre binding capacity towards rare earth metal ions after grafting the ligand on the surface of polymer nanofibres to create specific functional groups useful for separation and selectivity of rare earth metal ion.

The previous chapter discussed the electrospinning of polystyrene (PS) nanofibre and polyethylene terephthalate (PET) nanofibres which were the starting raw materials for the modification procedure. Table 5.1 shows the electrospinning conditions used for the experiments which was achieved in Chapter 4. The PS electrospinning process parameters used to prepare fibres for diglycolic acid modification were flow rate (0.8 mL/h), solution concentration (15 wt %), electric potential (17 kV) and distance (15 cm), while PET nanofibres were electrospun using a flow rate of (1.0 mL/h), solution concentration (10 wt %), electric potential (17 kV) and collector distance (20 cm). The chelating ligand used to modify the surface of the nanofibres was diglycolic anhydride (DGA). To achieve an optimum amount of the functional ligand on the surface of the nanofibres, different experiments were conducted by considering experimental parameters such as the reaction time and the

initial concentration of the chelating ligand (DGA) required to be grafted on the surface of polymer nanofibres.

Table 5.1. Electrospinning conditions used for the nanofibres used as support for DGA

	PS	PET
Concentration (wt %)	15	10
Voltage (kV)	17	17
Solution flow rate (mL/h)	0.8	1.0
Collector distance (cm)	15	20

The stability of the surface-modified nanofibres after functionalisation was also investigated and the results of the stability studies on the DGA chelating moieties grafted on the surface of the two polymer nanofibres is also presented. The aim of the stability study was to determine the regeneration ability of the synthesised nanofibre adsorbents for further adsorption cycles and to determine how strongly the grafted DGA moieties were attached onto the surface of the nanofibres. The stability of the chelating adsorbents were tested with different acidic and basic solutions of different concentrations to determine which solution would be ideal for the regeneration of the DGA modified chelating nanofibre adsorbents.

5.1 Surface modification of PS and PET nanofibres

The surfaces of electrospun PS nanofibres were modified using diglycolic anhydride (DGA) as a selective chelating ligand for rare earth metal ion separation from aqueous solution as shown by the reaction scheme depicted in Chapter 3 Section 3.3.1. The optimum conditions of the surface modification process of nanofibres were examined with a target to determine whether the DGA moieties can be successfully grafted on the surface of the nanofibres. The parameters considered in the modification process were the reaction contact time and the initial concentration

of the chelating ligand DGA. The sample names and the codes used in the surface modification of the PS and PET nanofibres were previously presented in Chapter 3 Section 3.3.2.

5.1.1 Effect of the concentration of DGA ligand on the surface modification of PS nanofibres

This experiment was carried out to investigate the effect of the concentration of DGA chelating ligand content which is required for the modifications of electrospun PS nanofibre in order to confirm the optimum concentration of DGA required to modify the surface of PS nanofibre for further adsorption applications. Electrospun polystyrene (PS) nanofibre (0.109 g) made according to the optimum conditions in Chapter 4 was immersed in a mixture of different mass content of diglycolic anhydride solution as described in Chapter 3 Section 3.3.2. Figure 5.1 illustrates the scheme of modification of PS nanofibre with DGA.

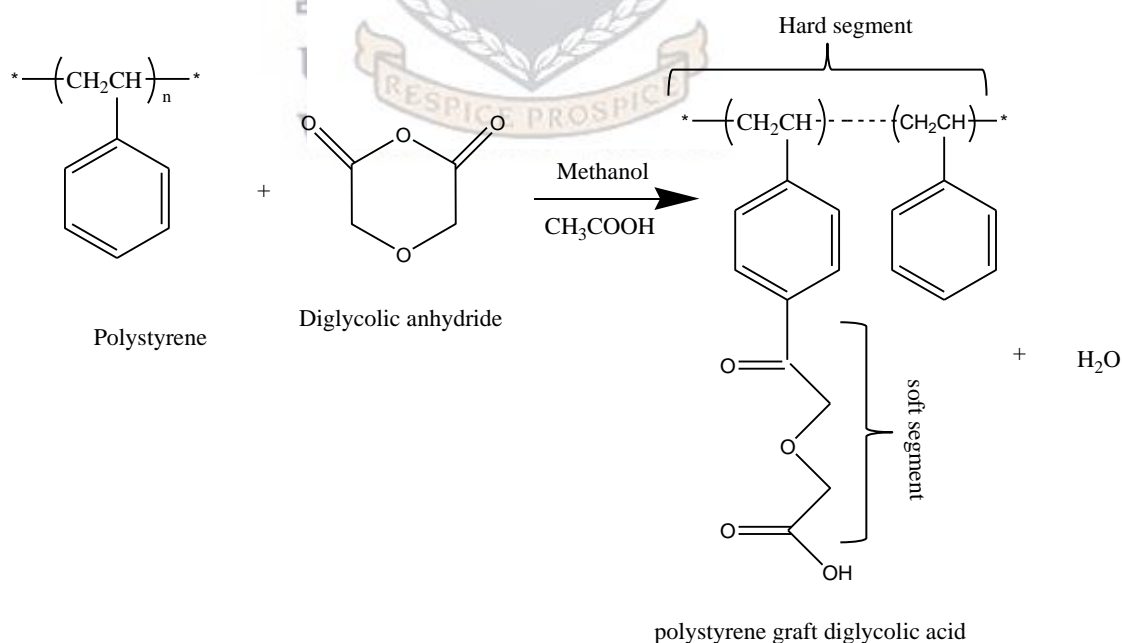


Figure 5.1. Modification of PS nanofibre with DGA chelating ligand

The modification reaction was carried out using triplicate samples for each considered parameter. The obtained FTIR results of PS, DGA and the surface modification of PS nanofibres using DGA solution of different concentrations (1, 1.5, 2, 3 and 4 g) are shown in Figure 5.2 (a – g). It is necessary to modify the surface of the adsorbent to enhance the selectivity towards trivalent lanthanides. Diglycolic acid is similar to diglycolamic acid which is regarded as promising task specific ligands suitable for the removal of lanthanides (Selvan et al. 2017). Since diglycolic acid possesses two carbonyl groups and an etheric oxygen atom, it is expected to exhibit high extraction of trivalent lanthanides. As shown in Figure 5.1, diglycolic anhydride contains etheric oxygen and a couple of $>C=O$ groups and during the reaction of diglycolic anhydride with PS, it is likely that diglycolic anhydride undergoes a reaction with PS leading to the formation of diglycolic acid over the surface of PS to form PS-DGA.

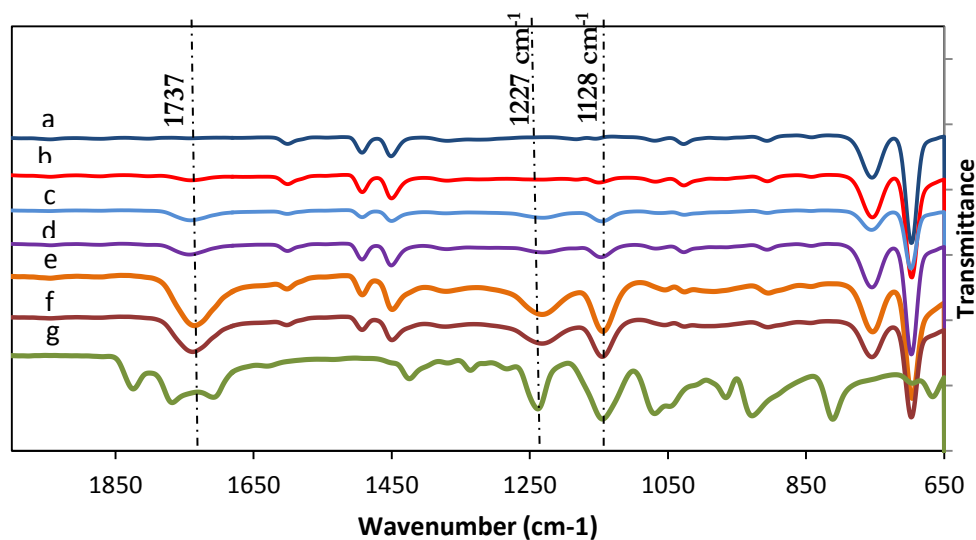


Figure 5.2. FTIR spectra of a) Pristine PS b) PS-DGA-1 (1 g), c) PS-DGA-1.5 (1.5 g), d) PS-DGA-2 (2 g), e) PS-DGA-3 (3 g), f) PS-DGA-4 (4 g), and g) DGA (time - 240 mins; PS fibre weight - 0.109 g; temp – 43 °C; 5mL acetic acid; 40 mL 99% methanol).

The FTIR spectrum in Figure 5.2 (a) confirms the presence of the main absorption characteristic peaks of PS. The following were identified; aromatic C-H bond stretching vibration; (1601; 1493; 1453 cm^{-1}), deformation CH_2 and C=C of the aromatic ring; (1026 cm^{-1} ; 756 cm^{-1}). Moreover, the peaks at 1601, 1493 and 1453 cm^{-1} all belong to the characteristic peaks of benzene ring of the polystyrene backbone. The spectrum of PS shown in Figure 5.2 (a) is in agreement with previously published spectra and bands of the IR spectrum for polystyrene (León-Bermúdez and Salazar 2008; Liang and Krimm 1958; Wu et al. 2001). Chemical studies have also indicated that the monomeric units in polystyrene occur predominantly in a head-to-tail arrangement, i.e., the phenyl groups are attached to alternate carbon atoms (Liang and Krimm 1958; Su 2013). Figure 5.2 (g) depicts the FTIR spectrum of DGA by itself and the identified band at 1800 -1700 cm^{-1} is associated with the stretching vibration of the two C=O groups. The bands due to the scissoring vibrations of CH_2 groups are observed in the 1425 cm^{-1} range. These identified peaks are in agreement with previous studies on DGA by Breda et al. (2008); Jarmelo et al. (2008).

Figure 5.2 (b-f) depicts the spectra of the functionalised nanofibres and the presence of C=O groups on the polymer matrix, which can interact with metal ions in solution chelation and complexation reactions, can be noticed initially after 1.5 g (0.012 mol). The increased content of C=O groups confirmed the presence of the DGA chelating ligand on the nanofibres. As shown from the relative intensity of the spectra peaks of PS-DGA-3 in Fig. 5.2 (e), the stretching vibration peak of the carbonyl (-C=O) group was seen at 1737 cm^{-1} , 1128 cm^{-1} and 1227 cm^{-1} while the peak at 1454 cm^{-1} which is the -CH_2 bending peak of the polymer support, remained intact confirming the presence of PS nanofibre support, this indicates that introduction of diglycolic

acid in PS did not alter the structure of PS to any significant extent, indicating the matrix is intact. When the spectra of the PS-DGA-3 was further compared with that of pristine PS, it could be seen that there was no available absorption band of the carbonyl group (C=O) on the PS (Figure 5.2a) whereas the PS-DGA-3 had stretching vibrations of the carbonyl group at 1737 cm^{-1} which is due to the diglycolic anhydride grafted to the PS backbone.

PS nanofibre modification with DGA concentration of 3 g (0.026 mol) was selected as the concentration to work with since the characteristic bands and peaks for DGA are already present and increasing DGA concentration may result in a waste of ligands. From this investigation, an optimum amount of 3 g (0.026 mol) of the ligand allowed for the effective functionalisation of 0.109 g of PS nanofibre and therefore PS-DGA-3 was selected as the appropriate nanofibre sample to be used for further functionalisation and testing.

5.1.2 Effect of the reaction time on the surface modification of PS

The experiments to determine the optimum reaction time for the surface modification of PS nanofibres were carried out as set out in Chapter 3 Section 3.3.1.2. The experiments were carried out by immersing 0.109 g samples of electrospun polystyrene (PS) nanofibre mats made as set out in Chapter 3, Section 3.3.3, Table 3.11. where a mixture of 3 g of diglycolic anhydride solution in 5 mL glacial acetic acid solution and 40 mL methanol was held at $43\text{ }^{\circ}\text{C}$ and the reaction time was varied over different time intervals of 1, 2, 3 or 4 (hrs) in order to determine the optimum contact time for the surface modification of PS nanofibre with DGA without destroying the nanofibre morphology. The modification reaction was carried out using triplicate samples for each considered parameter and the FTIR

spectra obtained after surface modification of PS nanofibres with DGA at different reaction times (1, 2, 3 or 4 hr) are shown in Figure 5.3 (a – f).

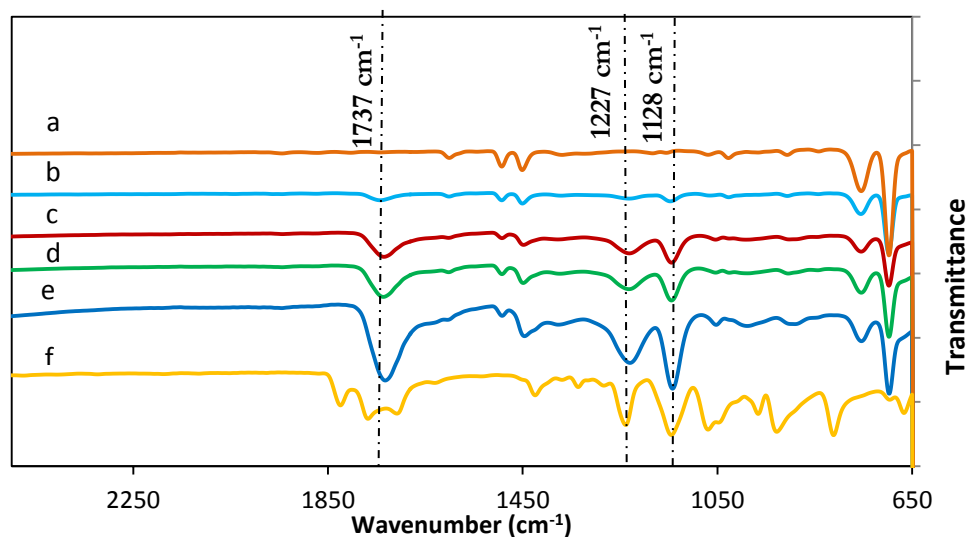


Figure 5.3. FTIR spectra of a) Pristine PS b) PS-DGA-3-1 (1 hr), c) PS-DGA-3-2 (2 hr), d) PS-DGA-3-3 (3 hr), e) PS-DGA-3-4 (4 hr) and f) DGA (conc -3 g (0.026 mol); fibre weight - 0.109 g).

Figure 5.3 (a) represents the FTIR spectrum of PS while Figure 5.3 (f) represents the spectrum of DGA as baselines. As shown from the spectra in Figure. 5.3 (c – e), the stretching vibration peak of the carbonyl (-C=O) group was seen at 1737 cm^{-1} , the characteristic absorption band of the carbonyl group (C-O stretch) of diglycolic acid was also observed at 1134 cm^{-1} and 1236 cm^{-1} . The peak at 1454 cm^{-1} which is the -CH_2 bending peak of the polymer support remained intact after 2 hrs and up to 4 hrs of modification reaction time with the DGA ligand. All these bands were absent in the pristine PS nanofibre (Figure 5.3 (a)), and the modification at 1 hr of contact time (PS-DGA-3-1) as depicted in Figure 5.3(b) showed little binding of DGA moieties to the polystyrene backbone due to insufficient contact time and this implies that modification of PS appeared to begin only after 1 hr of contact time.

The modification and spectral peaks which appeared after 2 hr of contact time (Figure 5.3 (c)) were consistent up to 3 hrs (Figure 5.3 (d)), but after 4 hrs (Figure 5.3 (e)) of modification time, the peak at 1450 cm^{-1} which is the $-\text{CH}_2$ bending peak of the polymer support disappeared. The contact time of three hours (PS-DGA-3-3) for fibre modification was therefore selected as the appropriate time to be used for further adsorption studies because this time had afforded sufficient time for the modification without denaturing the nanofibre.

The modified adsorbent (PS-DGA-3-3) therefore contained the O-CO group, which gave rise to three strong infrared bands that appeared at approximately 1700 , 1200 , and 1100 cm^{-1} (Van Nguyen et al. 2013; Van Nguyen et al. 2016). The PS-DGA-3-3 spectra exhibit a strong band at 1737 cm^{-1} , which represents the CO stretch. The band at 1227 cm^{-1} may be assigned to the asymmetric stretching of the C-C and C-O bonds attached to the carbonyl carbon while the band at 1128 cm^{-1} may be due to vibration involving the oxygen and the two carbons attached to it in the chain.

5.1.3 Effect of the concentration of DGA ligand on the surface modification of PET nanofibres

This experiment was carried out to investigate the optimum concentration of the DGA chelating ligand required for the modifications of electrospun PET nanofibres to be used in further applications. This experiment was carried out as set out in Chapter 3 Section 3.3.2. The strip of PET nanofibre mat (0.102 g) was immersed in 50 mL of an aqueous solution containing different masses of 1 g (0.0086 mol), 1.5 g (0.012 mol), 2 g (0.017 mol), 3 g (0.026 mol) of diglycolic anhydride and 5 mL of 5M concentrated sulphuric acid at $60\text{ }^\circ\text{C}$ according to the conditions shown in Chapter 3, Section 3.3.2, Table 3.10 and the beaker was placed in a shaker for 3 hrs to allow the

reaction with the PET nanofibre to proceed in triplicates. Figure 5.4 illustrates the scheme of modification of PET nanofibre with DGA.

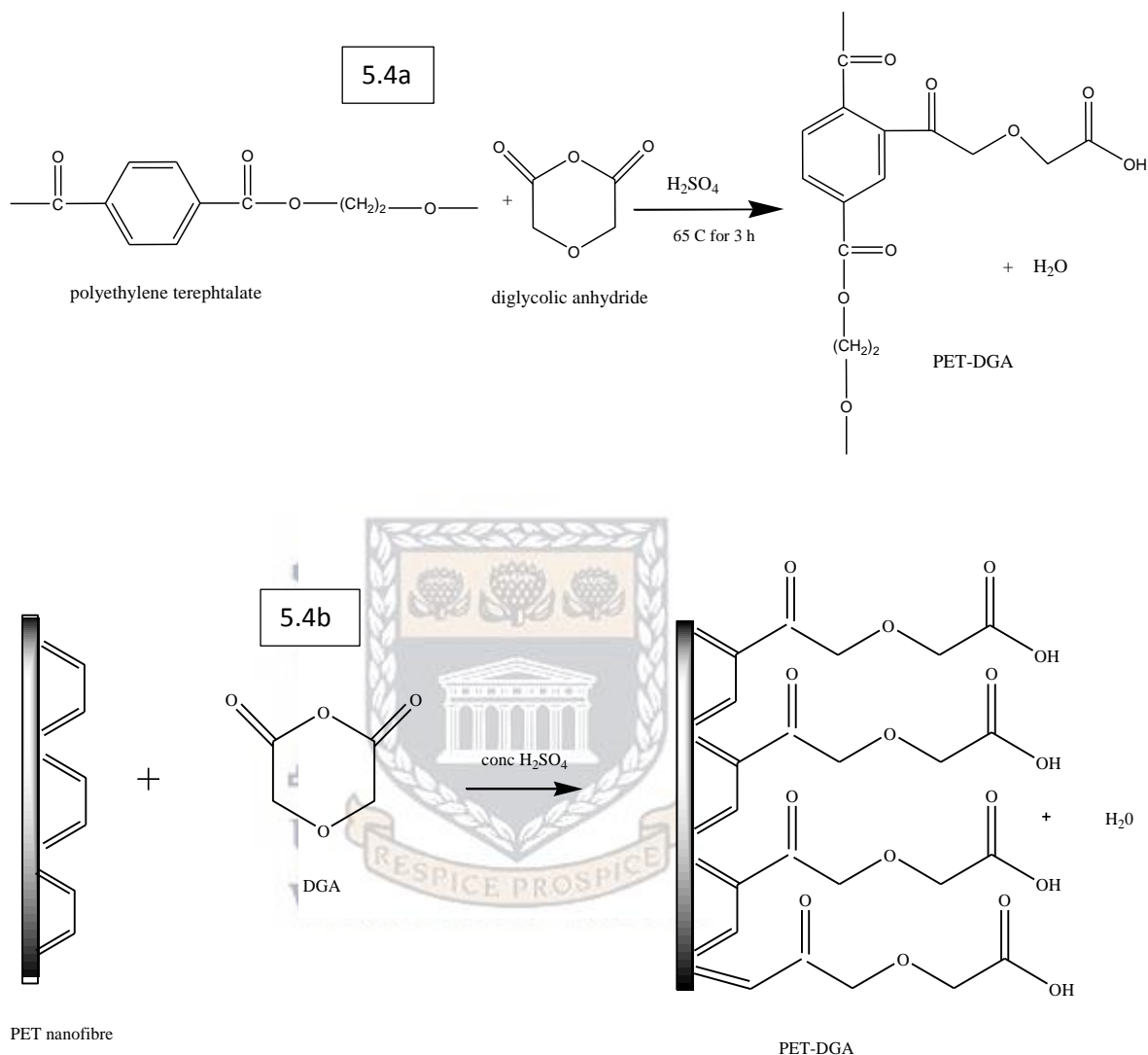


Figure 5.4. (a) PET modification with DGA chelating ligand and (b) graphical representation of surface modification of PET nanofibres using DGA chelating ligand

The graphical representation of surface modification of PET nanofibres is shown in Figure 5.4 (b) while Figure 5.4 (a) presents the grafted DGA moieties on the surface of PET nanofibres during the surface modification process (previously shown in Scheme in 3.3).

The modification reaction was carried out using triplicate samples for each considered parameter. The obtained FTIR results of the surface modification of PET nanofibres using DGA solution of different concentrations (1, 1.5, 2, 3 and 4g) are shown in Figure 5.5.

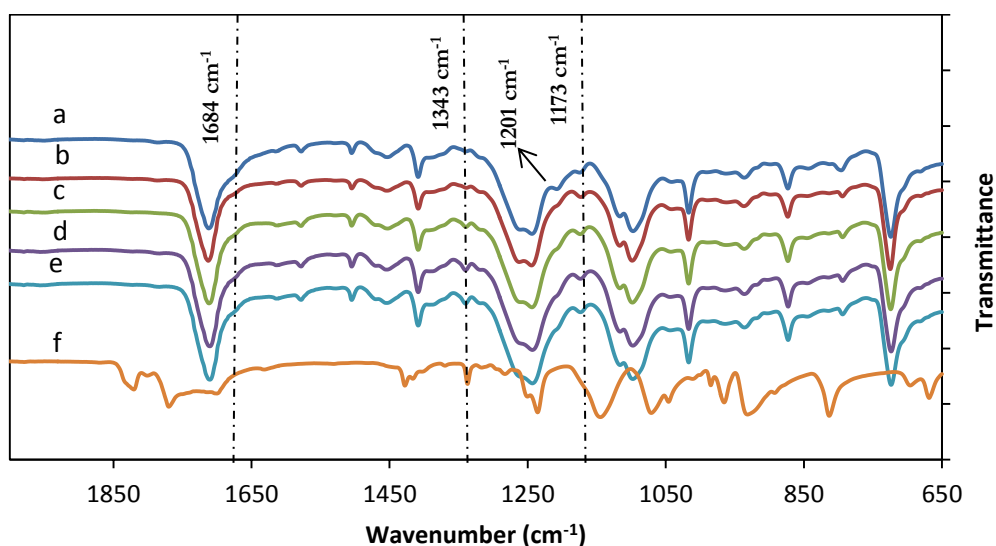


Figure 5.5. FTIR spectra of a) PET; b) PET-DGA-1 (1 g), c) PET-DGA-1.5 (1.5 g), d) PET-DGA-2 (2 g) e) PET-DGA-3 (3 g) and f) DGA (time - 4 h; fibre weight - 0.102 g).

The peak assignments shown in Figure 5.5 (a) depicts the FTIR of PET with bands at 1712 cm^{-1} attributed to the ester carbonyl bond stretching, and the band at 1245 cm^{-1} to the ester group stretching. The band at 1092 cm^{-1} is assigned to the methylene group. The band at 1452 cm^{-1} is assigned to a CH_2 bending mode while the band near 1409 cm^{-1} is assigned to a CH_2 wagging mode of the ethylene glycol segment. The band near 1016 cm^{-1} is assigned to an O-CH_2 stretching mode and the band near 827 cm^{-1} has been assigned to the C=O out-of-plane bending mode coupled with a ring CH out-of-plane bending mode. Other sharp bands at $1400 - 1600\text{ cm}^{-1}$ and $950 - 1250\text{ cm}^{-1}$ are assigned to C - C stretching and C - H in plane

bending of benzene rings (Liu et al. 2013). The assignments for PET are virtually identical to those reported previously (Boerio et al. 1976; Chen et al. 2012; Djebara et al. 2012; Chen et al. 2013) and the absorption bands are assigned according to the groups in the monomeric unit of PET.

FTIR spectra depicted in Figure 5.5 (b - e) show the changes observed in PET structures when functionalised with DGA. A new peak at 1343 cm^{-1} was noticed in the modified nanofibres which were assigned to the vibration peak of the carbonyl (C-O) group from DGA. The IR spectrum of PET (Figure 5.5 a) did not exhibit this adsorption band at 1343 cm^{-1} . The new C-O bond shows that diglycolic groups have been successfully added to the PET skeleton of PET-DGA modified adsorbent. The C-O groups with tension and bending absorption peaks broadened the C-O shoulder at 1684 cm^{-1} . The disappearance of the weak absorption peak of 1201 cm^{-1} while increasing the weak peak at 1173 cm^{-1} was attributed to DGA modification of PET surface. This weak peak (1201 cm^{-1}) was observed clearly in PET, but the intensity was decreased in modified PET nanofibres (PET-DGA) and was attributed to removing H atoms from CH group of benzene.

PET-DGA-1 (Figure 5.5 b) did not indicate any noticeable changes from the pristine PET indicating that 1 g of chelating ligand was insufficient to functionalise PET after 3 h of modification time. The peak at 1343 cm^{-1} was first noticed after 1.5 g of the chelating ligand (Figure 5.5 c) had been added but the band peak intensity grew with an increase in the DGA ligand concentration. It was concluded that in order to improve the minimum chelating ligand required for immobilisation, PET-DGA-2 (Figure 5.5 d) with 2 g chelating ligand was sufficient to graft anchor the chelating

moieties on the nanofibre supports and was therefore selected for further functionalisation and testing.

5.1.4 Effect of the reaction time on the surface modification of PET

The experiments to determine the optimum reaction time for the surface modification of PET nanofibres were carried out as set out in Chapter 3 Section 3.3.3. The experiments were carried out by immersing ethanol pre-wetted PET nanofibre (0.102 g) into 50 mL of a aqueous solution containing the optimised value of 2 g of DGA and 5 mL of 5 M concentrated sulphuric acid held at 60 °C and varying the reaction time over different time intervals of 60, 120, 180 and 240 mins in order to determine the optimum reaction time for the surface modification of PET nanofibres made according to the conditions shown in Chapter 3, Section 3.3.3, Table 3.11.

The modification reaction was carried out using triplicate samples for each considered parameter. The obtained FTIR spectra after surface modification of PET nanofibres at different reaction times are shown in Figure 5.6.

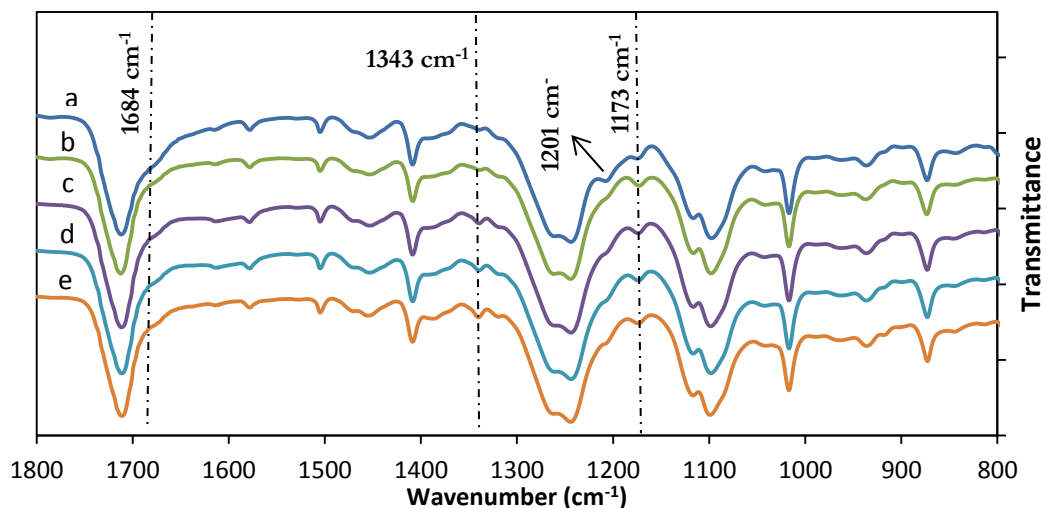


Figure 5.6. FTIR spectra of a) PET, b) PET-DGA-2-1 (1 hr), c) PET-DGA-2-2 (2 hr), d) PET-DGA-2-3 (3 hr), e) PET-DGA-2-4 (4 hr), (conc - 2 g (0.017 mol); fibre weight - 0.102 g).

An investigation of the reaction time needed for immobilisation of DGA on PET showed that after one hour (Figure 5.6 c), the FTIR spectrum remained unchanged and this showed that no functionalisation had been achieved on the nanofibre yet. From this FTIR results, it could be seen that the PET nanofibre was only functionalised with DGA after 2 hours (Figure 5.6 d), and the nanofibre was thereafter allowed to react for 2 more hours of reaction time for an effective modification to take place. The PET peaks remained even after 4 h of reaction time (Figure 5.6 e) without changes in the PET major assignment peak bands at 1343 cm^{-1} . The peaks at 1201 cm^{-1} on PET are ascribed to C-H aromatic and aliphatic vibrational stretching, and out of plane C-H bending on PET and are missing in the modified PET (Figure 5.6 b - e), however, the bands at 1173 cm^{-1} are due to C - O stretches which increased slightly after modification.

The weak C-O stretching peak seen at 1343 cm^{-1} was due to the C-O bond in the DGA ring which confirms that diglycolic groups (Figure 5.4) had been successfully grafted or anchored on to the PET skeleton of the PET-DGA modified adsorbent.

Figure 5.6 (d) shows that 3 hrs modification time will assure an appropriate modification while 2 hrs of modification remains the minimum time required for functionalisation because the peak was first noticed after 2 hours of modification. As the peak intensity was increasing with an increase in time of reaction and to afford sufficient modification time, 3 hrs modification time (PET-DGA-2-3) was therefore selected as the appropriate reaction time and this sample was selected as the nanofibre mat to use for testing and for further adsorption studies.

5.1.5 Morphology of modified PS as a function of concentration of DGA ligand and reaction time

In the practical use of functionalised nanofibres, it is important that nanofibres should retain their morphology substantially after modification. The surface morphology of nanofibres was determined using the HRSEM technique described in the experimental procedure in Chapter 3, Section 3.4.2. This characterisation technique was performed in order to monitor changes in morphology of the surface of nanofibres during their functionalisation steps with DGA chelating moieties. The PS nanofibres mats analysed in this case were those obtained after surface modification as a function of ligand concentration as described in Chapter 3, Section 3.3.2 and 3.3.3 where electrospun polystyrene (PS) nanofibre (0.109 g), was immersed in a mixture of different mass concentration of 1, 1.5, 2, 3 and 4 g diglycolic anhydride at different time interval of 1, 2, 3, 4 hours. Morphologies were determined by HRSEM of the neat and the modified PS nanofibre PS-DGA mats treated with different DGA concentrations and Figure. 5.7 shows SEM micrograph of pristine PS nanofibre while Figure. 5.8 illustrates PS nanofibres modified with different concentrations of DGA ligand respectively.

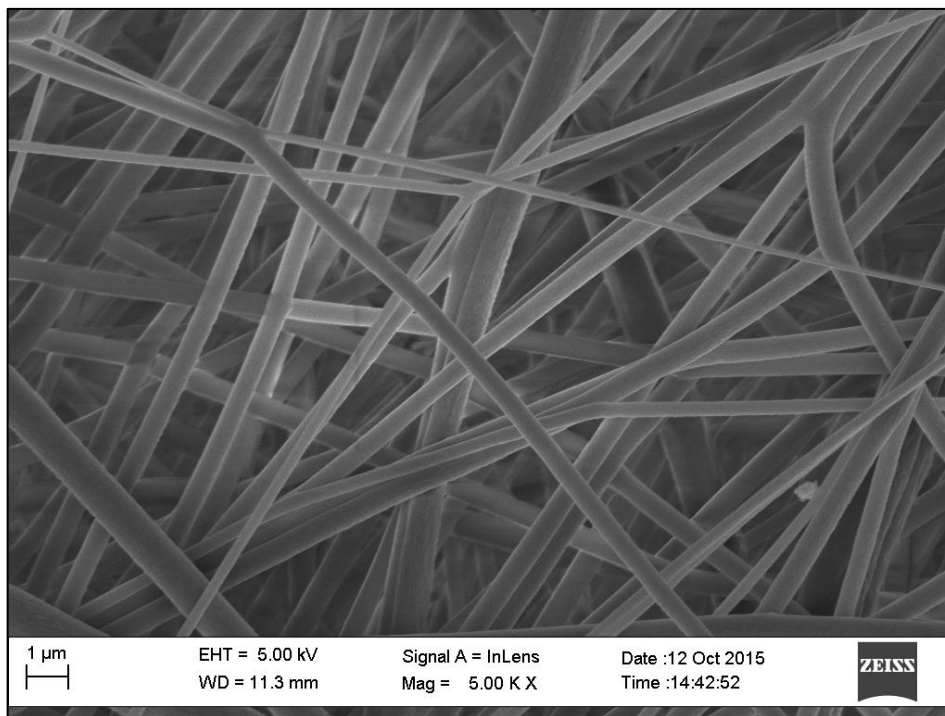
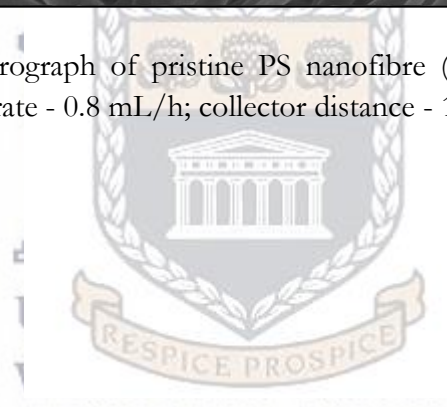


Figure 5.7. SEM micrograph of pristine PS nanofibre (concentration - 15 wt %; voltage - 17 kV; flow rate - 0.8 mL/h; collector distance - 15 cm)



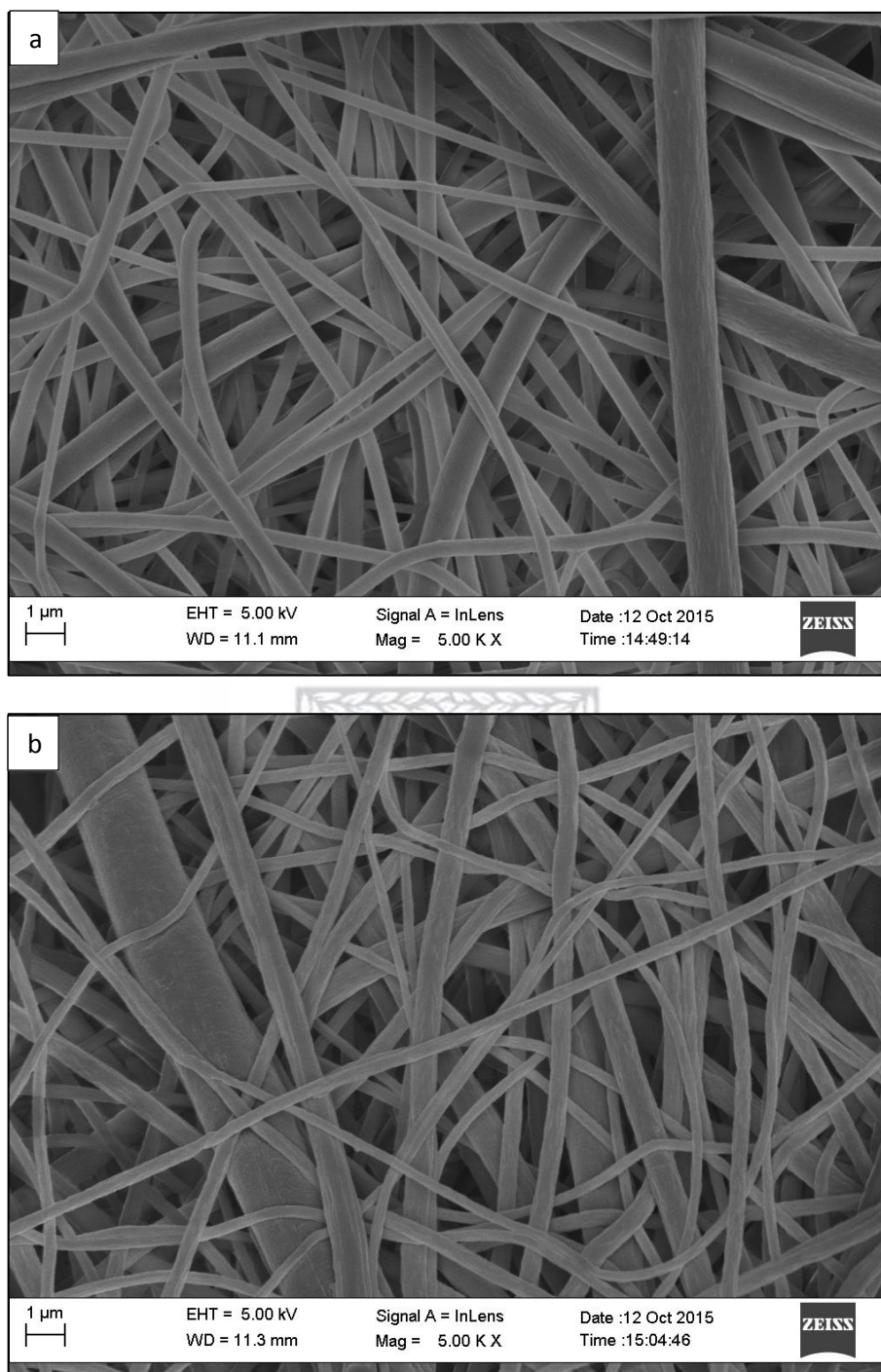


Figure 5.8. SEM micrograph of PS nanofibre after surface modification with different DGA concentrations (a) PS-DGA-2 (2 g) and (b) PS-DGA-3 (3 g) (time - 4 h; fibre weight - 0.109 g)

Figure 5.8 depicts PS nanofibres modified with (a) 2 g or (b) 3 g of the DGA chelating ligand while the pristine PS nanofibres (Figure 5.7) used showed smooth fibres with no beads or beads-on-strings prior to modification, with a diameter of

392 nm. PS-DGA-2 (456 nm) and PS-DGA-3 (481 nm) showed no morphological changes or damage after the functionalisation steps (Figure 5.7 (a) and (b)). The SEM images of the nanofibres which were synthesised with the DGA functional groups showed fibre diameters in the range 426 - 481 nm compared with an average of 392 nm for the pristine nanofibres and implied an increase in nanofibre diameter after functionalisation. The DGA modification therefore increased the nanofibre diameter and the PS-DGA-3 was selected for further adsorption studies as it still presented a smooth morphology as shown in Figure 5.8 (b) but increased only in fibre diameter from the pristine PS. This result supports the obtained results in the FTIR analysis in Section 5.2.1.

There was no significant change of the surface morphology of any of the PS nanofibre samples after modification with DGA which is comparable to the report of Dong et al. (2015) who electrospun poly(vinyl alcohol) (PVA), followed by chemical cross-linking with glutaraldehyde and surface modification via low surface energy fluoroalkylsilane (FAS) and they suggested that the direct grafting or anchoring of a ligand only changes the surface chemical compositions of the nanofibre without altering its fibre structure. Further HRSEM analyses were done on the nanofibre samples to determine the effect of the reaction time on the nanofibre morphology. Morphologies by SEM image of the neat and the modified PS nanofibre modified with 3 g of DGA chelating ligand mats at different time intervals of 2, 3, 4 h are shown in Figure. 5.9 below.

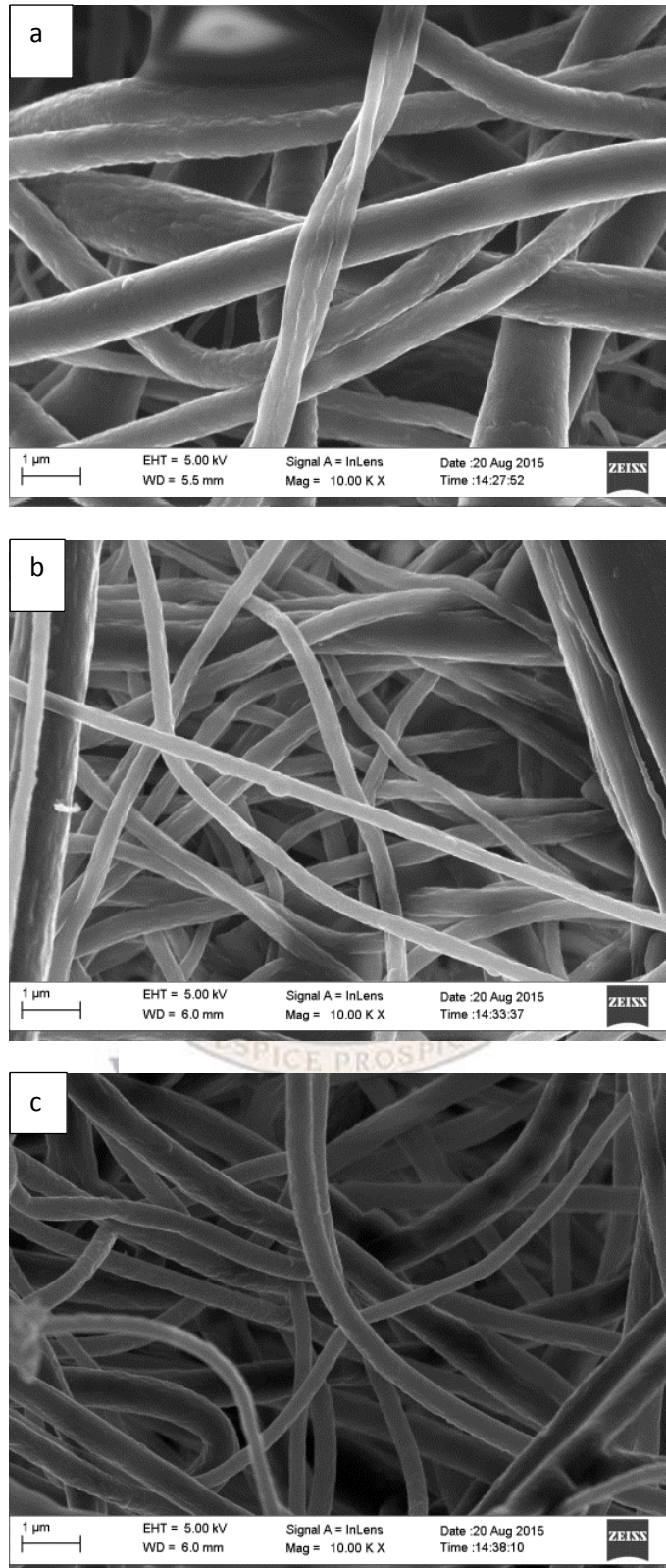


Figure 5.9. SEM micrograph of PS nanofibre modified at 2, 3, and 4 hr time intervals (a) PS-DGA-3-2, (b) PS-DGA-3-3 and (c) PS-DGA-3-4 (conc - 3 g; fibre weight - 0.109 g)

Figure 5.9 above depicts the SEM morphology of PS-DGA-3-2 (462 nm), PS-DGA-3-3 (475 nm) and PS-DGA-3-4 (485 nm) functionalised at different contact time of 2, 3 or 4 hrs. Individual PS nanofibre diameters were smooth and uniform even after the modification process; the PS nanofibre mats obtained are very similar to that of the neat PS fibres, however, there is an increased fibre diameter over time after fibre modification which may be due to DGA attachment or swelling by the solvent solution during the reaction. PS-DGA-3-3 (Figure 5.9.(b)) selected for further adsorption studies did not show any damage to the nanofibre and there was no evidence of adjacent fibre segments conglutinating to each other at any points, in agreement with the FTIR studies. All the modified fibres did not show any serious cracks or degradation with their surfaces still smooth, but the mean diameters increased up to 4 h of modification time. The known poor mechanical properties of PS sorbents make them prone to damage (Wu et al. 2016) but as revealed from the morphologies shown by SEM, the fibres remained smooth and still retained their fibre strength even up to 4 h of functionalisation time.

5.1.6 Morphology of modified PET as a function of DGA ligand concentration and reaction time

The surface morphology of PET nanofibres were determined using High Resolution Scanning Electron Microscopy (HRSEM) technique described in the experimental procedure given in Chapter 3, Section 3.4.2. This characterisation technique was applied in order to monitor any changes in the morphology of the surface of PET nanofibres during their functionalisation steps with DGA chelating moieties. The HRSEM analyses were carried out on both pristine and modified nanofibre mats. The PET nanofibres mats analysed in this case were those obtained after surface modification as a function of ligand concentration as described in Chapter 3, Section

3.3.2 and 3.3.3 where electrospun PET nanofibre (0.100 g) was first pre-wetted with ethanol and immersed in a solution containing different mass concentration of 1, 1.5, 2 and 3 g diglycolic anhydride and at different time interval of 30 mins, 1, 2, 3 and 4 hours. Morphologies of the pristine and the modified PET nanofibre (PET-DGA) mats at different DGA concentrations are shown in Figure. 5.10. and Figure 5.11 respectively

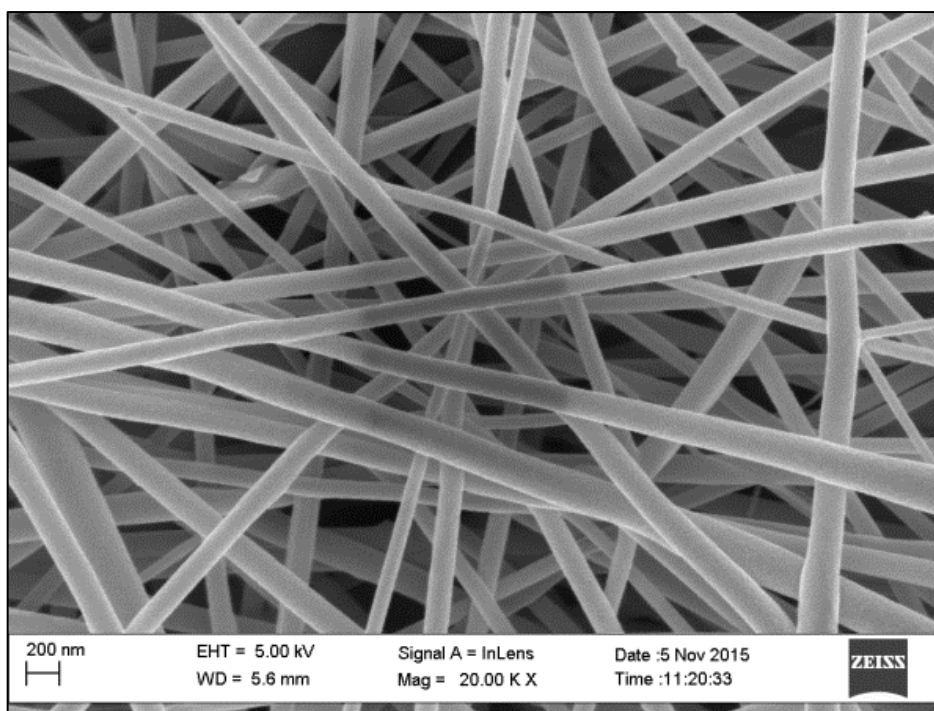


Figure 5.10. SEM micrograph of pristine PET nanofibre (PET concentration - 10 wt %; voltage - 17 kV; solution flow rate - 1.0 mL/h; collector distance - 20 cm)

Figure 5.10 depicts the pristine PET nanofibre used in the study. It showed a beadless and smooth fibre morphology. Figure 5.11 illustrates the SEM micrograph of modified PET nanofibres using 1.5, 2 or 3 g DGA chelating ligand.

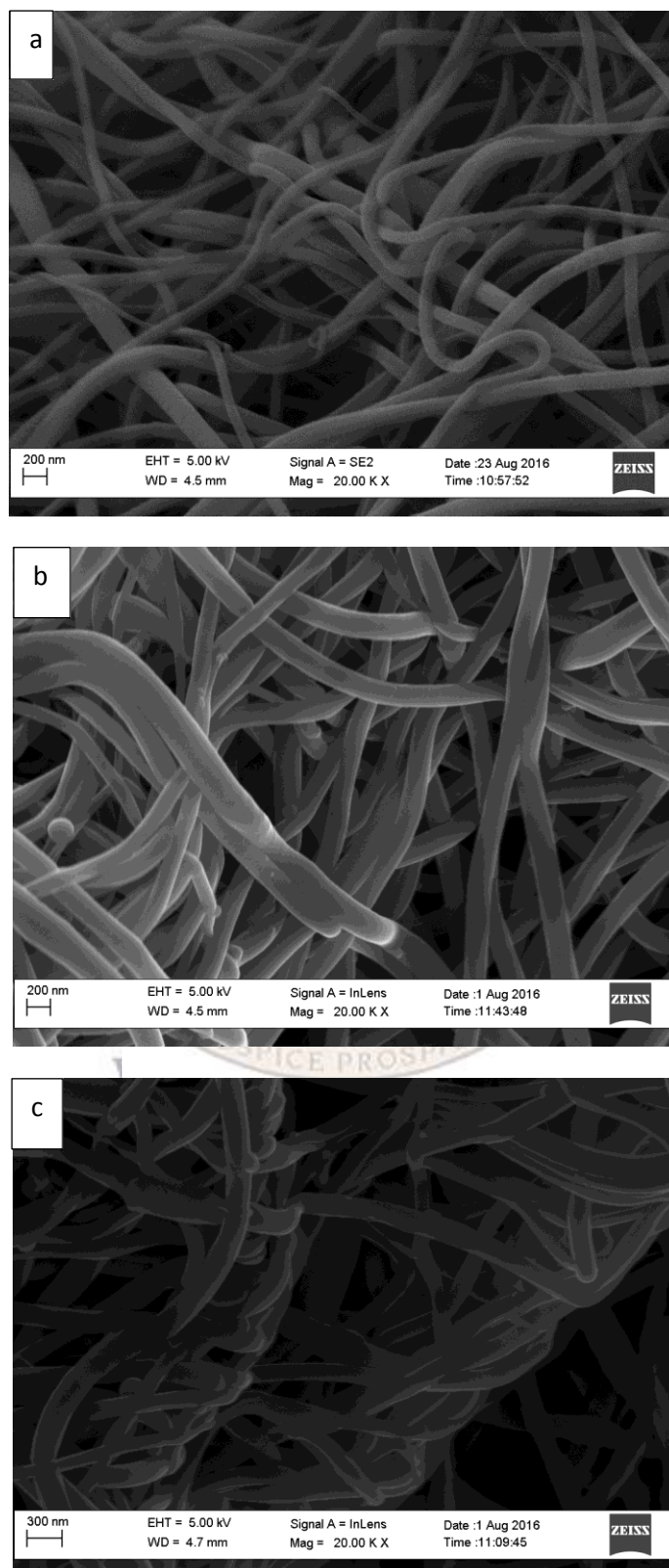


Figure 5.11. SEM micrograph of (a) PET-DGA-1.5 (1.5 g) (b) PET-DGA-2 (2 g) and (c) PET-DGA-3 (3 g) (time - 3 h; fibre weight - 0.102 g)

Figure 5.11 a–c depicts the effects of DGA ligand concentration modification on the nanofibre morphology of PET (122 nm). Before being placed in the solutions, the nanofibres were smooth and straight, but with an increase in concentration of the ligand during modification, the nanofibres became intertwined and entangled. Thus, higher concentration of DGA chelating ligand led to a 7 nm increase in the nanofibres' diameter when compared with PET-DGA-1.5 (129 nm).

The micrographs also show cross-linked fibres as the DGA concentration was increased, leading to nanofibres with a fully cross-linked matrix as revealed in PET-DGA-3 (168 nm) (Figure. 5.11 (c)), and it further showed that an increased ligand concentration may be detrimental to the morphology of the nanofibres due to excessive crosslinking that may subsequently affect the performance of the nanofibre adsorbent mats in adsorption due to reduced surface area. Cross-linking can enhance the resistance of polymers against acids and chemicals (Chen et al. 2008; Justi et al. 2005), and therefore, chemical cross-linking by the ligand may increase the resistance of PET nanofibre adsorbent against acid, alkali and chemicals.

The tendency for the crosslinking reaction to occur is directly related to increasing the content of DGA chelating moieties in the modification solution. It was concluded that the concentration of DGA used for sample PET-DGA-2 (164 nm) (Figure 5.11 b) was suitable to modify the surface of the nanofibres for adsorption purposes and this is supported by the previous FTIR results (Figure 5.5 (d)) which showed that at DGA content of 2 g, the PET nanofibre support has been modified. Further HRSEM analyses as shown in Figure 5.12 were done on the PET-DGA-2 nanofibre samples in order to determine the effect of the DGA functionalisation reaction time on the nanofibre morphology.

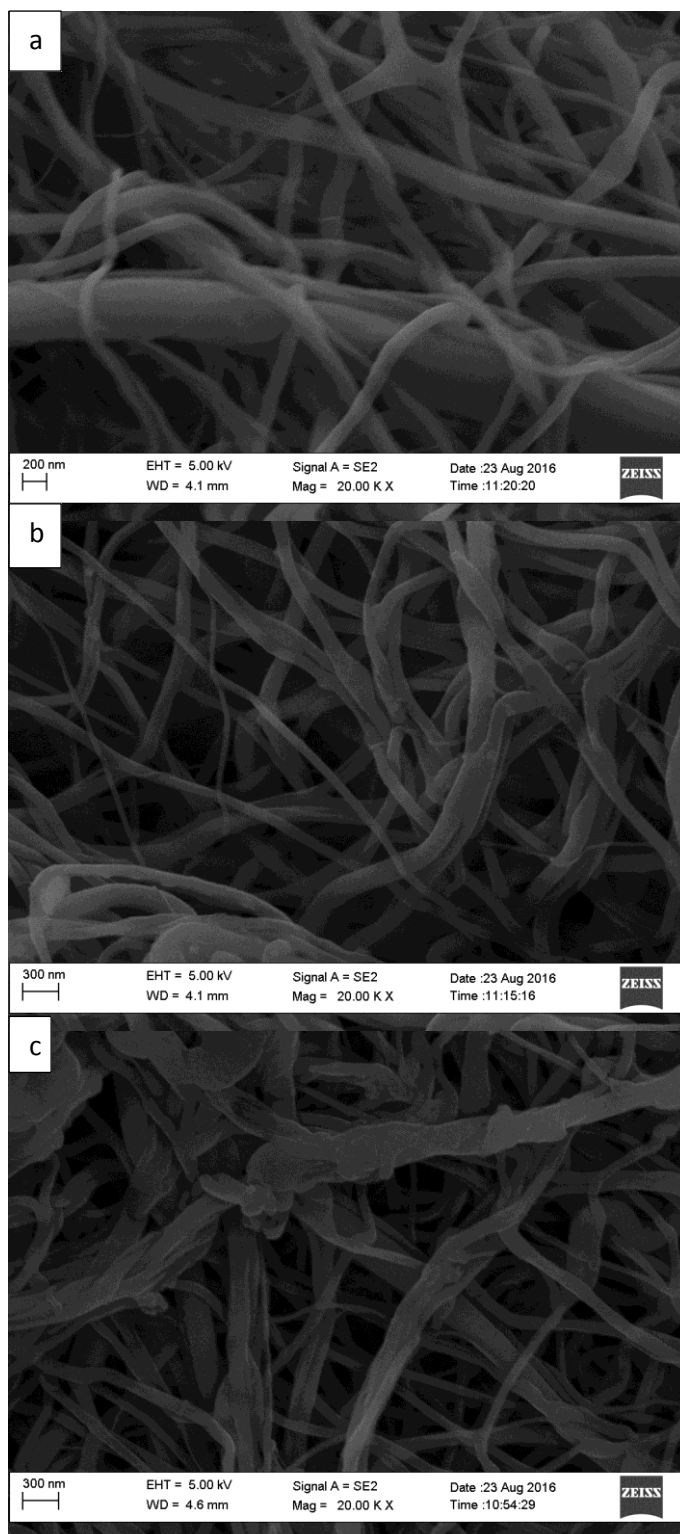


Figure 5.12. SEM micrograph of (a) PET-DGA-2-2 (2 hr), (b) PET-DGA-2-3 (3 hr) and (c) PET-DGA-2-4 (4 hr) (DGA conc - 2 g (0.017 mol); fibre weight - 0.102 g).

Figure 5.12 (a-c) depicts the modification of PET after different reaction times of the PET sample with 2 g DGA ligand and the surface of the PET nanofibre mat showed fibre crosslinking due to the increased time in the solution which increased crosslinking by the ligand. Figure 5.12 (c) depicts a nanofibre with increased crosslinking after 4 h of modification time. PET-DGA-2-3 (Figure 5.12b) that had been exposed to the DGA reaction for 3 h was selected as the appropriate sample as the reaction at 3 h only showed mild crosslinking of the nanofibre.

A contraction and consequent thickening of the fibres is noticed, with adhesion of fibres in the mat with PET-DGA-2-3. It was concluded that sufficient modification with DGA can be obtained after 3 h of reaction time and the integrity of the fibres will still be intact. At 4 h reaction time, the fibres were significantly damaged and lost their cylindrical shape. Increased crosslinking could increase the hydrophobicity of the nanofibre, for instance, Dong et al. (2015) utilised hydrophilic poly (vinyl alcohol) polymer to fabricate a super hydrophobic nanofibre membrane via electrospinning of PVA due to chemical cross-linking by glutaraldehyde and surface fluorination via low surface energy fluoroalkylsilane. It is concluded that modified PS-DGA-3-3 and PET-DGA-2-3 nanofibre adsorbents obtained using SEM and FTIR analysis has been endowed with abundant DGA groups and unique morphologies without defects. The PS-DGA-3-3 and PET-DGA-2-3 nanofibre will further be investigated in the following sections.

5.1.7 Structural properties of PS-DGA-3-3

To investigate the structural changes caused during modification, nanofibres were characterised by X-ray diffraction. X-ray diffractometry (XRD) is a technique for characterising the crystalline nature of various solids. It provides information on

identity of phases as described in Chapter 3 Section 3.4.4. The XRD patterns of PS and modified PS-DGA-3-3 samples are shown in Figure 5.13 to examine if the modification caused any structural changes to the nanofibres.

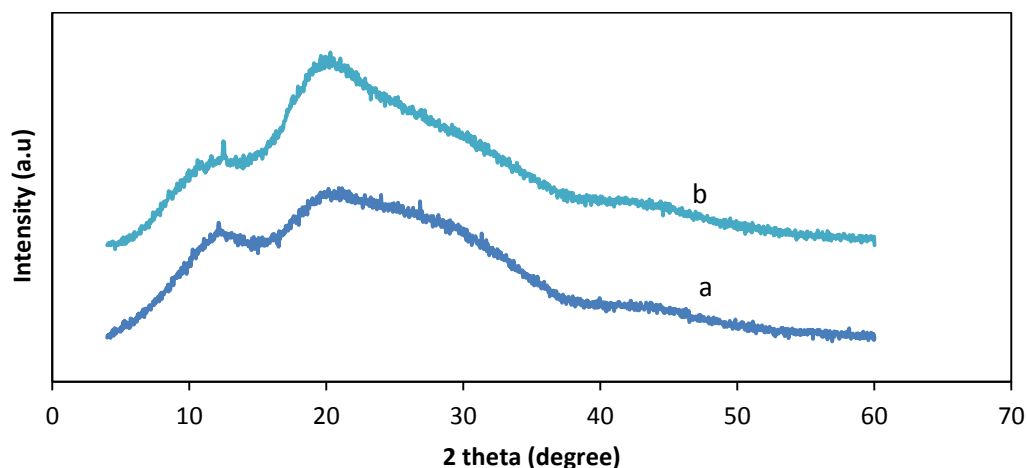


Figure 5.13. XRD of (a) PS and (b) PS-DGA-3-3

Figure 5.13 (a) showed a broad peak at 11.9° and 19.70° (2θ) which corresponds to the presence of the amorphous form of polystyrene for the nanofibre as shown by the broad and wide peaks of the nanofibre. Typically the narrower and more intense the peak, the more ordered the nanofibre sample is and broad peaks are usually associated with small particle size or a disordered material, lacking regular repeating order.

After modification of the PS nanofibre with DGA ligand, the PS-DGA-3-3 peak intensity was increased and implied that the PS-DGA-3-3 nanofibre increased in ordering after DGA modification whereas the observed diffraction pattern for PS mainly showed broad peaks. Generally, this would suggest that PS nanofibres are less ordered but the backbone of PS nanofibre supported the attachment of the DGA ligand which accounted for the increased peak definition. This result indicated the

transition from a less ordered PS nanofibre phase prior to functionalisation to a more ordered structure after the functionalisation.

Rathna et al. (2013) reported that in the process of electrospinning the polymer chains have less than the required time to form an orderly array because of the simultaneous processes of evaporation of solvent and solidification of elongated nanofibres which may inhibit ordering of the subunits and favours their amorphous nature. Electrospinning could not have altered the polymer structure and would have inhibited regular ordering therefore, the increased ordering could possibly be due to the functionalisation by the DGA chelating ligand and this further supported the successful modification of DGA on the PS nanofibre backbone.

5.1.8 Structural properties of PET-DGA-2-3

To investigate the structural changes caused during modification, PET nanofibres were characterised by X-ray diffraction. This was to determine if there was a change in ordering of PET and PET-DGA-2-3. The XRD procedure is described in Chapter 3 Section 3.4.4. The X-ray diffraction patterns of the pristine PET and modified PET-DGA-2-3 samples are shown in Figure 5.14.

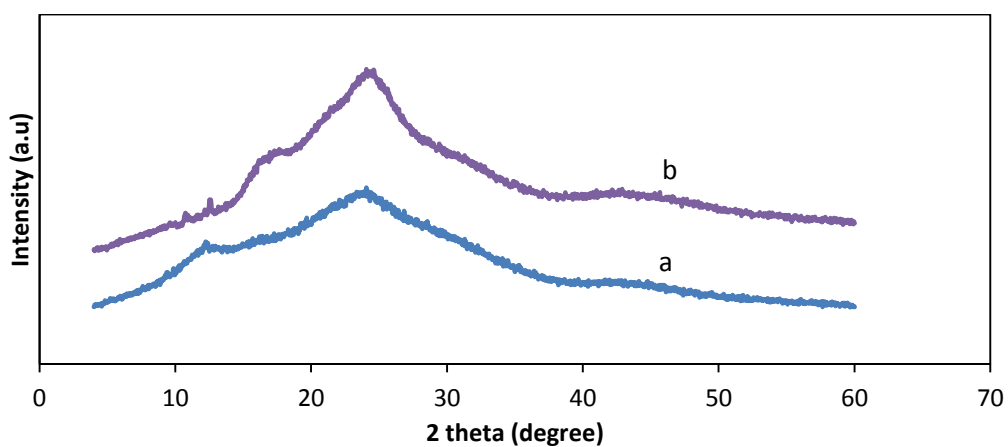


Figure 5.14. XRD graphs of (a) PET and (b) PET-DGA-2-3

Figure 5.14 (a) depicts a broad peak at 23.98° (2θ) which corresponds to the presence of relatively orderly subunits of PET nanofibre. Hadjizadeh et al. (2011) had reported that electrospun PET mats can exhibit both amorphous and crystalline peaks which were attributed to the semi-crystalline structure of the PET polymer in their study. After chemical modifications, the arrangement of polymer chains is strongly affected. The grafting of chemical groups induced the intercalation of molecules that increased the ordered arrangement of the polymer structure. As a consequence the crystallinity of the modified polymer is strongly increased and the intensity of the peaks increased and this detectable peak corresponds to the peak at 24.6° . Figure 5.14 (b) records more defined peaks which can be identified in the diffractogram of the spectrum of PET-DGA-2-3 which depicts a more intense band at $2\theta = 24.6^\circ$ and shoulders on the peaks at $2\theta = 12^\circ$ and $2\theta = 17^\circ$ for DGA functionalised nanofibre which were not visible in the pristine PET nanofibre. The peak at $2\theta = 24.6^\circ$ and 17° corresponds to the (1 0 1) plane of DGA indicate semi crystallinity which is attributed to the repeating hydroxyl groups.

PET forms a phase which has an intermediate structure between regular ordering and amorphousness as shown in Figure 5.14 (a), but the modification increased the peak intensity giving rise to sharper peaks indicating that the DGA chelation moieties had increasingly ordered the PET nanofibre backbone structure. Therefore, Figure 5.14 (a) showed PET nanofibres were relatively less ordered while Figure 5.14 (b) showed PET-DGA-2-3 displayed greater ordering that was induced by functionalisation. In general, when a polymer contains an ordered repeating structure, then the XRD peaks are sharper and their intensities are higher, whereas for an amorphous polymer they are broad (Kim et al. 2004). This trend could be

observed to increase in terms of peak intensity for the PET-DGA-2-3 nanofibre and this supported the successful modification of DGA on the PET nanofibre backbone.

The effect of chemical groups was further confirmed by Guimarães et al. (2007) who reported in a study of the synthesis and characterisation of polyesters derived from glycerol and phthalic acid that the XRD pattern suggested the presence of rigid aromatic rings, which stemmed from the phthalic acid, and led to more rigid structures, which was more prone to crystallise the polymer chains despite that the differential scanning calorimetry (DSC) curves gave no evidence for crystallinity of the polymers.

5.1.9 Thermal profile of modified PS-DGA-3-3

In this study, thermal gravimetric analysis of PS nanofibres was carried out in order to determine the PS nanofibres' thermal stability and to confirm their thermal resistance for further experiments. The modified fibre must be thermally and chemically stable in practice in order to allow long term utility. Therefore, there should be no significant change in their thermal properties and chemical structures after repeated use at operational temperatures. The thermal stability of the pristine and PS-DGA-3-3 samples was investigated by thermo gravimetric analysis under N₂ atmosphere and the procedure was described in Chapter 3 Section 3.4.3. Samples were heated from room temperature to 800 °C at a heating rate of 20 °C/min. The obtained thermal gravimetric profile of the pristine nanofibres and PS-DGA-3-3 nanofibre are shown in Figure 5.15 depicting the thermal loss at different temperatures. The degradation data obtained from the TG thermograms in Figure 5.15 are given in Table 5.2.

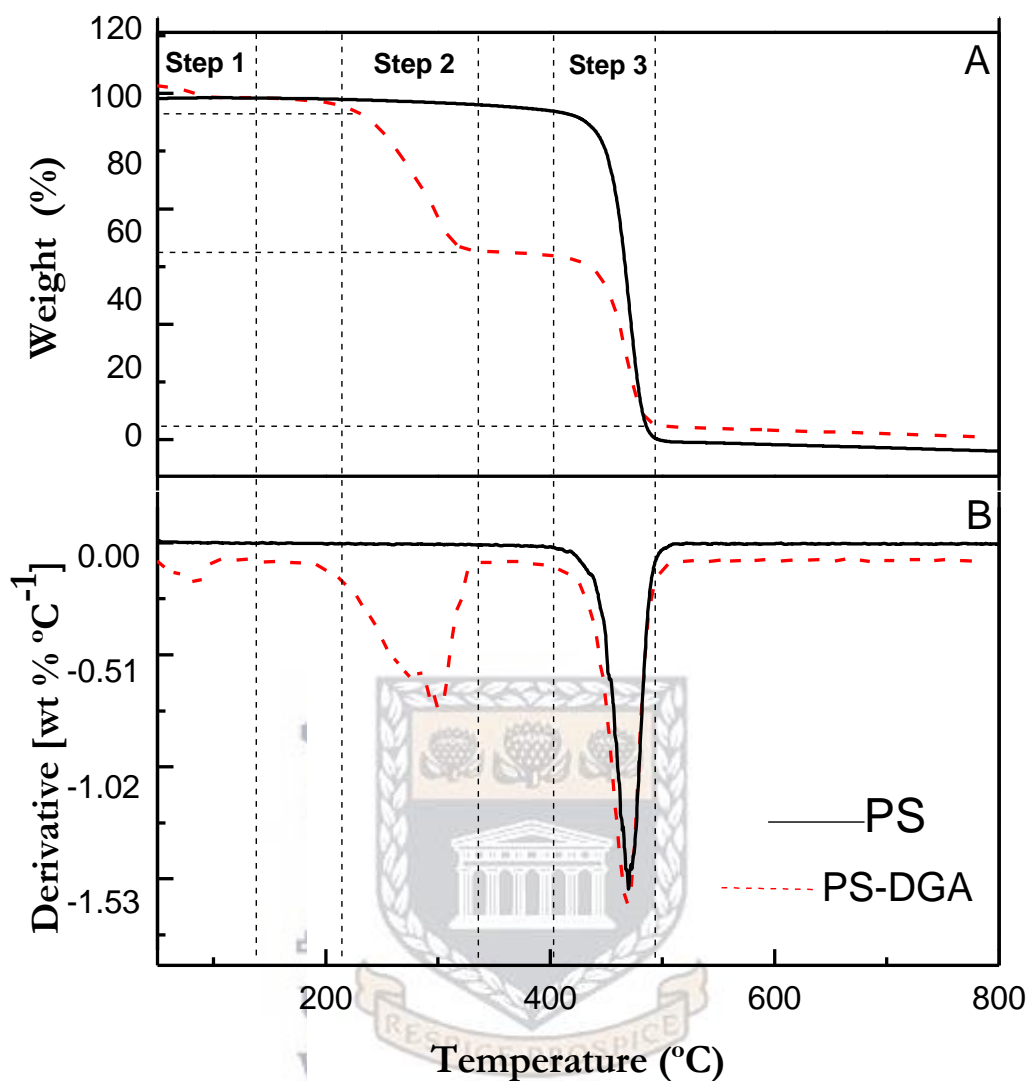


Figure 5.15. (a) TGA profile (b) TGA derivatives of pristine PS and PS-DGA-3-3

Table 5.2. TG analysis data of PS and PS-DGA-3-3

	Degradation interval (°C)	Mass loss (%wt)
PS	392-487	98%
Solvent	80-100 (Step 1)	5%
PS-DGA-3-3	215-350 (Step 2)	43%
PS-DGA-3-3	405 -498 (Step3)	52%

Figure 5.15 (a) presents the thermal gravimetric analysis of electrospun PS nanofibre and the thermal profile shows that PS nanofibres only start losing their thermal

stability at temperatures around 392 °C and are completely pyrolysed at 487 °C. It can be concluded that the pristine polystyrene nanofibre had high thermal durability. As can be seen from Figure.5.15, the TG curve of PS is sharp and occurs in one step whereas the TG curve for PS-DGA-3-3 had three steps. The degradation with two steps for the PS-DGA-3-3 is an indication of the independent decomposition of components (PS nanofibre; DGA functionalities) in the modified nanofibre adsorbent.

The TGA results presented in Fig. 5.15 (b) shows that PS-DGA-3-3 lost a small amount of mass at 80-100 °C which is due to solvent. Oxygen-containing functional groups of DGA result in water adsorption and consequently, some mass loss below 100 °C was observed for PS-DGA-3-3 (Figure. 5.15 b). Thereafter it lost weight rapidly as the temperature was increased above 200 °C. The sample showed a considerable weight loss between 215 and 350 °C, which corresponds to CO, CO₂, and steam release from the labile oxygen containing functional groups. The other mass loss between 405 and 498 °C can be attributed to the degradation of more stable oxygen functionalities.

The DGA attached to PS chains was degraded between 200 – 490 °C in two steps. The first weight loss is related to the decomposition of oxygen functionalities and the second weight loss is assigned to the loss of attached PS chains similar to results obtained by Roghani-Mamaqani (2015) for graphene-attached PS with oxygen-containing functional groups. PS and PS-DGA-3-3 reached a char value of about 40.5 wt. % at 500 °C. The result showed good attachment of DGA onto PS and confirmed the successful attachment and thermal stability of the attached ligand.

To estimate the mass of ligand immobilised per gram of PS-DGA-3-3, the following explanation and estimation were made from the TGA profile (See Appendix i); and as can be seen from Figure 5.15, the amount of DGA adsorbed onto PS nanofibre degraded in step 2 and step 3 indicating that the DGA was immobilised on the PS nanofibre while PS degraded in only one step. The maximum capacity of DGA on PS nanofibre was 0.827 g g^{-1} . It should be concluded that, the achieved PS-DGA-3-3 nanofibre mat would show unique structures that will contain abundant etheric oxygen and $> \text{C}=\text{O}$ groups, which will be beneficial to the adsorption of REEs. PS-DGA-3-3 nanofibre therefore possesses abundant etheric oxygen and carbonyl ($> \text{C}=\text{O}$) groups which enhanced the removal and selectivity towards trivalent lanthanides.

5.1.10 Thermal profile of modified PET-DGA-2-3

In this study, thermal gravimetric analysis of PET and modified PET-DGA-2-3 nanofibres was carried out in order to determine the nanofibres' thermal stability and confirm their thermal resistance for further applications such as adsorption at different temperatures. The thermogravimetric analysis was performed under N_2 atmosphere and the procedure was detailed in Chapter 3 Section 3.4.3. Samples were heated from room temperature to $800 \text{ }^\circ\text{C}$ at a heating rate of $20 \text{ }^\circ\text{C}/\text{min}$. The obtained thermal gravimetric profile of the pristine PET nanofibres and modified nanofibre (PET-2-3) are shown in Figure 5.16. The degradation data obtained from the TG thermograms in Figure 5.16 are given in Table 5.3.

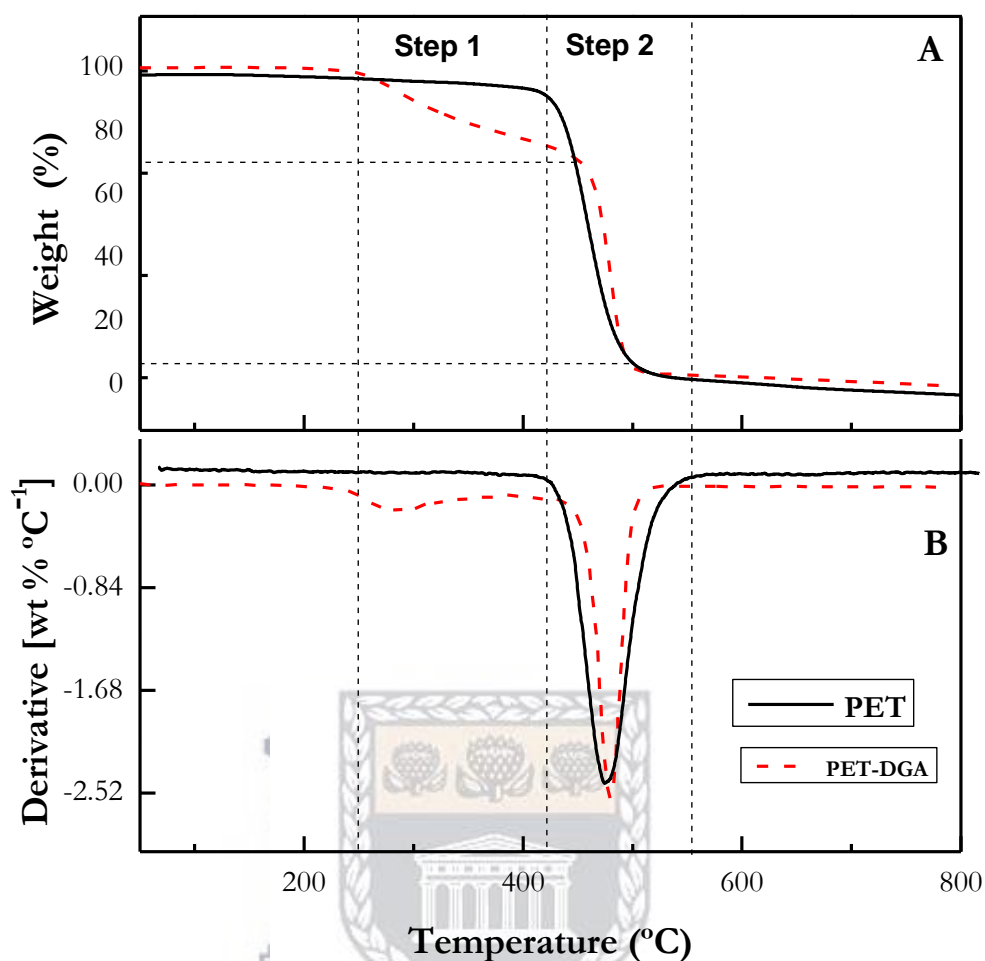


Figure 5.16. (a) TGA profile (b) TGA derivatives of PET and PET-DGA-2-3

Table 5.3. TG analysis data of PS and PET-DGA-2-3

	Degradation interval (°C)	Mass loss (% wt)
PET	403-501	90%
PET-DGA-2-3	242-446 (Step 1)	31%
PET-DGA-2-3	446-502 (Step 2)	69%

Figure 5.16 (a) presents the thermal gravimetric analysis of pristine PET nanofibres showing a single stage thermal decomposition at 403-501 °C during pyrolysis. According to the thermal profile curve, PET nanofibres only start losing their thermal stability at temperatures around 378 °C with 20% char left losing about 80%

weight at 434 °C due to the strong chemical structure. PET is a class of synthetic polyesters widely used in functional applications because of its excellent thermal and mechanical properties (Mahalingam et al. 2015). Figure 5.16 (b) showed that the TGA thermograms of PET-DGA-2-3 nanofibres slowly began to decompose at 226 °C (31 %) and completely pyrolysed at 446 °C with minimal char left. The TGA profile revealed that a two-step thermal degradation was observed for the modified PET-DGA-2-3 while the gradual loss of the DGA moiety indicates strong bonds between PET and DGA allowing high thermal stability after DGA modification and confirmed the successful attachment of the ligand.

The thermal stability is probably due to the DGA crosslinked nanofibres which usually make polymeric matrices more resistant to degradation when compared to the pristine polymer. It means that PET-DGA-2-3 nanofibres will be stable in the working temperature region for adsorption applications and in the temperature range of modification. It can be concluded that the PET-DGA-2-3 nanofibres have sufficient thermal durability because the lower limit of decomposition temperature of 226 °C was much higher than any working temperature region for the adsorbent during modification and in use.

The conversion of diglycolic acid groups on PET nanofibre mats was determined by gravimetric determination using the TGA profile (see appendix ii). The calculated conversion of DGA groups represents the amount of the ligand (DGA) molecules that was grafted onto the solid support (PET nanofibre mats). The optimum PET-DGA-2-3 nanofibre mats with excellent physical flexibility of the nanofibre were obtained with 0.449 g g⁻¹ conversion of DGA groups on the surface of PET nanofibres after the optimum reaction time.

5.1.11 Nitrogen adsorption–desorption of PS-DGA-3-3

The surface area and pore size of the PS nanofibre and PS-DGA-3-3 was studied using Brunauer–Emmett–Teller (BET) analysis which involves the physical adsorption of N_2 gas molecules on a solid surface. The aim of N_2 BET adsorption–desorption characterisation was to investigate the relationship and influence of pore size, pore volume and surface area of the nanofibres treated with chelating ligand compared to the pristine nanofibre. To create more suitable porous supports, it is of importance to understand the change of porosity and surface area caused by the immobilisation of the ligand on the nanofibre. This procedure was described in Chapter 3 Section 3.4.5. The porous properties of the pristine PS and PS-DGA-3-3 nanofibre adsorbents are shown in Figure 5.17.

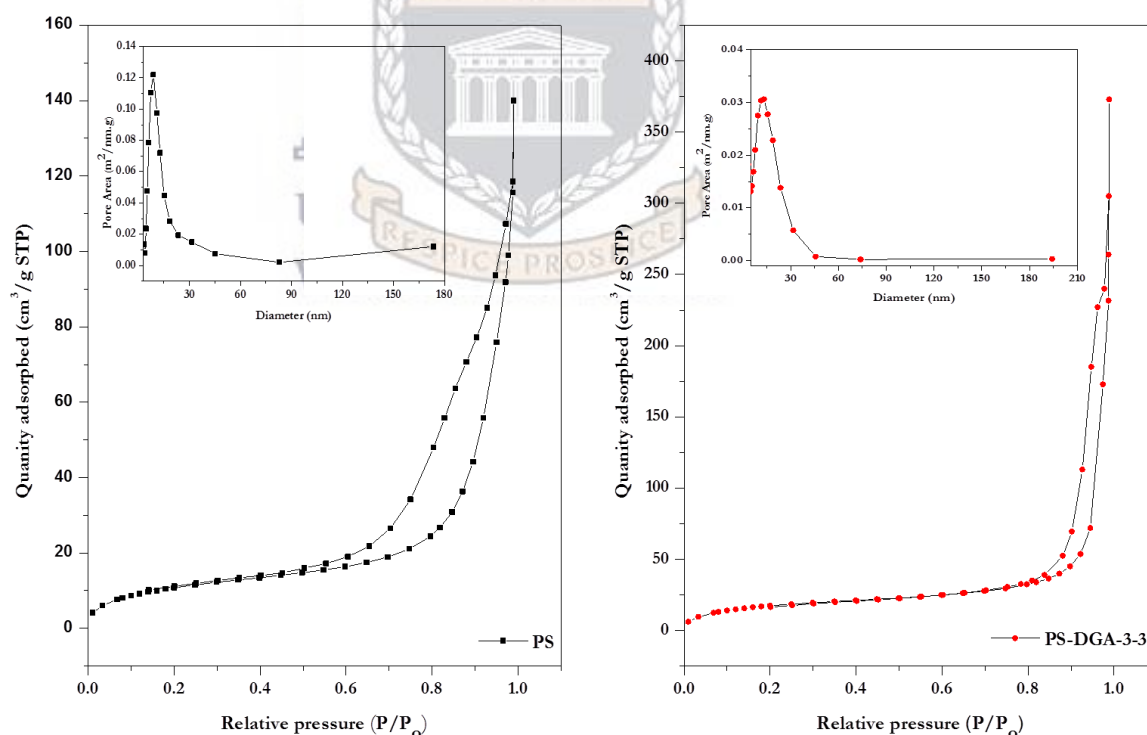


Figure 5.17. N_2 adsorption–desorption isotherm for (a) PS and (b) PS-DGA-3-3. (Inset) Pore size distribution of PS and PS-DGA-3-3

Figure 5.17 depicts the N₂ adsorption–desorption isotherm for PS, showing a large uptake of nitrogen due to capillary condensation at relative pressure (P/P_0) in the range of 0.6 - 0.99 indicating multiform pore distribution while PS-DGA-3-3 has hysteresis loop at relative pressure of >0.8 . According to Figure 5.17 (inset), it is shown that the pore size distribution of unmodified PS nanofibre was mainly centred around 20 nm, it is revealed that the pore size distribution of modified nanofibre was similar in size but depicts dependency on the DGA content.

The BET surface area of PS-DGA-3-3 ($67.3 \text{ m}^2/\text{g}$) was higher than that of the pristine PS ($41.3 \text{ m}^2/\text{g}$). The average pore size between fibres of surface modified PS-DGA-3-3 was higher than that of untreated nanofibre and was associated with crosslinking between ligand and the nanofibre matrix and creation of mesopores between adjacent nanofibres. The average pore diameter of the pristine nanofibres was measured to be 8.86 nm with a uniform pore size distribution in the range of 1–18 nm. The differential pore area distribution plots against pore size for PS-DGA nanofibre adsorbent and the measured average pore diameter of the nanofibres was 13.2 nm with a uniform pore size distribution in the range of 6–23 nm.

The nitrogen adsorption–desorption isotherm for the PS-DGA-3-3 nanofibre shown in Figure 5.17 can be assigned as a type IV isotherm, which was attributed to physical adsorption and also indicated a high affinity between gas and solid (Liang, Cao, Qian 2011; Min et al. 2012). The volume adsorbed for nitrogen adsorption–desorption isotherm of PS-DGA-3-3 nanofibre increased sharply at a relative pressure (P/P_0) of approximately 0.90, indicating capillary condensation, in pores between interconnected fibres.

Figure 5.17 (inset) showed the pore size distribution of PS-DGA-3-3 nanofibre and the value of pore diameter of fibres which indicated that the surface of PS-DGA-3-3 nanofibre was mesoporous. The large specific surface area and porous structure showed that the PS-DGA-3-3 nanofibre will have potential application in adsorption or separation. As shown, Figure 5.17 exhibited a hysteresis loop, i.e. the adsorption and desorption isotherms do not coincide over a certain region of external pressures which is typical for mesoporous adsorbents. At low pressures, first an adsorbate monolayer is formed on the pore surface, which is followed by the multilayer formation. The hysteresis loop Type H1 (Figure 5.17) is associated with porous materials known, from other evidence, to consist of agglomerates or compacts of approximately uniform spheres in fairly regular array, and hence to have narrow distributions of pore size, whereas in this study, the voids between adjacent or interconnected fibres were filled with N₂.

It can be concluded that the surface area of the adsorbent materials were increased after modification with DGA chelating groups when compared with the pristine nanofibre. This may be explained if it is assumed that the deep pockets formed between fibres of the PS-DGA are accessible to N₂, and this result is supported by the SEM observations obtained for PS-DGA-3-3. Generally, in the immobilisation, the support is a critical issue and the essential requirement for any carrier is the need to retain a large surface area.

5.1.12 Nitrogen adsorption–desorption of PET-DGA-2-3

The porous properties of nanofibres are influenced by the fibre surface treatment and the effect of fibre surface modification on pore size and surface area was investigated for the DGA modified PET nanofibre. The surface area and pore size of

the PET nanofibre and modified nanofibre were examined using N_2 adsorption and the results are depicted as shown in Figure 5.18.

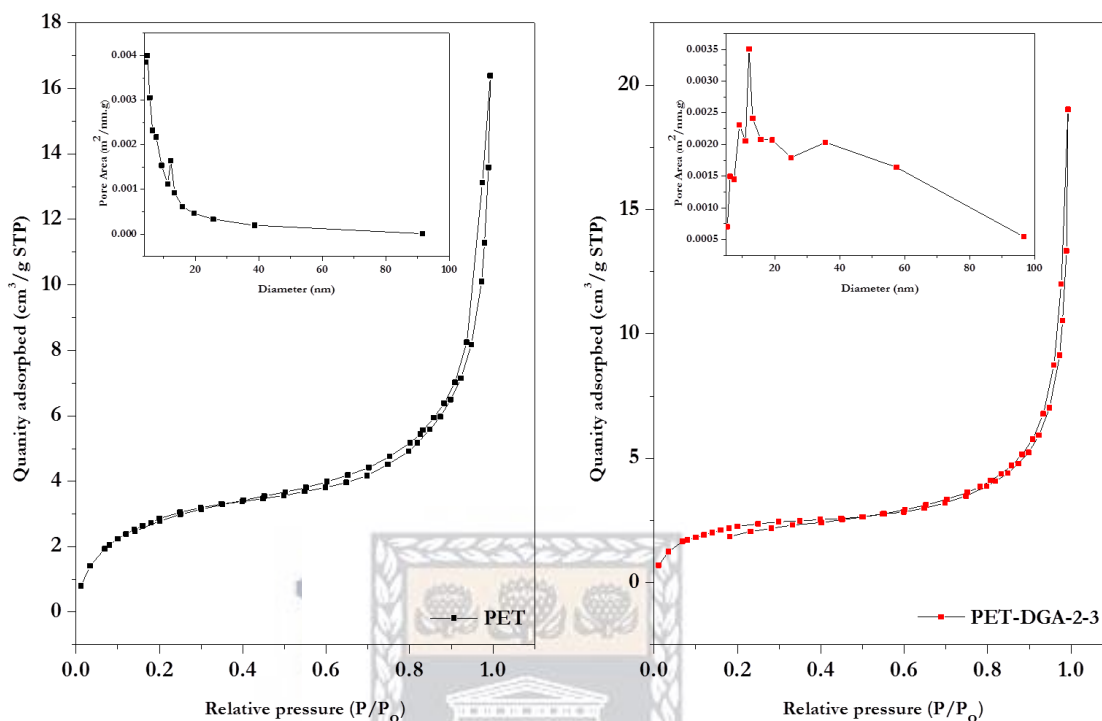


Figure 5.18. N_2 adsorption–desorption isotherm for (a) PET and (b) PET-DGA-2-3.

The surface properties of the PET-DGA-2-3 nanofibre (8.55 m²/g) were reduced after modification with DGA chelating groups when compared with the pristine PET (11.2 m²/g). Figure 5.18 shows the N_2 adsorption–desorption isotherm for PET and PET-DGA-2-3. The average pore size of modified nanofibre was increased from 56 Å to 66.2 Å according to Figure 5.18 (inset), and the increasing pore size could be due to the crosslinking of intersecting nanofibres which resulted in decreased nitrogen molecules adsorption in pores. Figure 5.18 can be assigned as a type II isotherm representing unrestricted monolayer-multilayer adsorption, which indicates a complete monolayer coverage and also indicating a high affinity between gas and solid (Min et al. 2012). The shapes of hysteresis loops which have often been identified with specific pore structures, shows a Type H3 loop (Figure 5.18), which

does not exhibit any limiting adsorption at high p/p° , but observed with aggregates of plate-like particles giving rise to slit-shaped pores. In this study, the hysteresis loop could be ascribed to pores created by crosslinking of fibres when modified.

There was a decrease in the surface area from 11.2 m²/g, to 8.5 m²/g and pore volume from 0.0156 cm³/g, to 0.0142 cm³/g, when PET-DGA-2-3 was compared with the pristine PET. The surface area and the pore volume were in agreement with the SEM micrograph of the PET-DGA-2-3 crosslinked structure. The DGA ligand was primarily immobilised on the surface of fibres and caused crosslinking of fibres. The voids between fibres were in the mesoporous range.

5.1.13 Material stability of PS-DGA-3-3 adsorbent in HNO₃ and EDTA

After the surface modification of PS nanofibres, a study of the stability of DGA chelating moieties grafted on the surface of nanofibres and the regeneration ability of the adsorbents was investigated. This is to determine the stability of the nanofibres in acid or basic solutions. A functionalised nanofibre was contacted with different concentrations of HNO₃ or EDTA for 1 hour to simulate the conditions used for batch desorption experiments as detailed in Chapter 3 Section 3.3.4. Figure 5.19 depicts the pristine PS nanofibre and PS-DGA-3-3 functionalised nanofibre shaken in 10 mL HNO₃ of different molar concentrations.

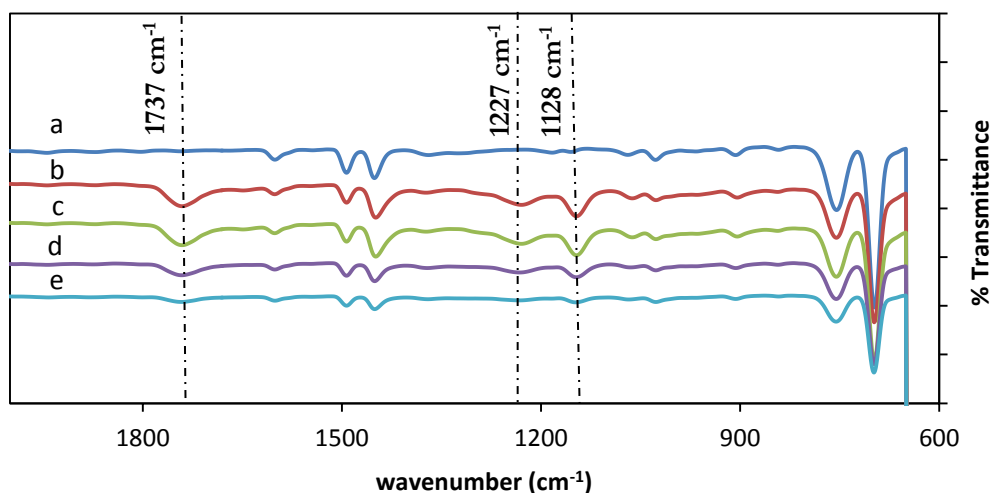


Figure 5.19. FTIR Spectra of a) Pristine PS nanofibre, b) PS-DGA-3-3, c) 1 M HNO_3 , d) 1.5 M HNO_3 , and e) 2 M HNO_3 , (Vol – 10 mL; time - 1 hr; rpm - 240)

It was expected that the FTIR spectra of the as made PS-DGA-3-3 nanofibres and the acid-treated functionalised nanofibres should be nearly identical to prove that the ligand remained intact after short-term acid-contact. It can be seen in Figure 5.19 (c – d) that the peak positions and shapes were consistent before and after the nitric acid regeneration test up to a concentration of 1.5M solutions, but the peaks almost disappeared after using 2M nitric acid solution, especially the shoulder at 1227 cm^{-1} as depicted by Figure 5.19 (e). These results indicated that chemical structure of the PS-DGA-3-3 was not adversely affected by any chemical degradation up to 1.5 M nitric acid after 1 hr exposure. Figure 5.20 below depicts the result of PS-DGA-3-3 nanofibres shaken in 10 mL EDTA of different molar concentrations for 1 hr to simulate the conditions used for batch sorption and regeneration experiments.

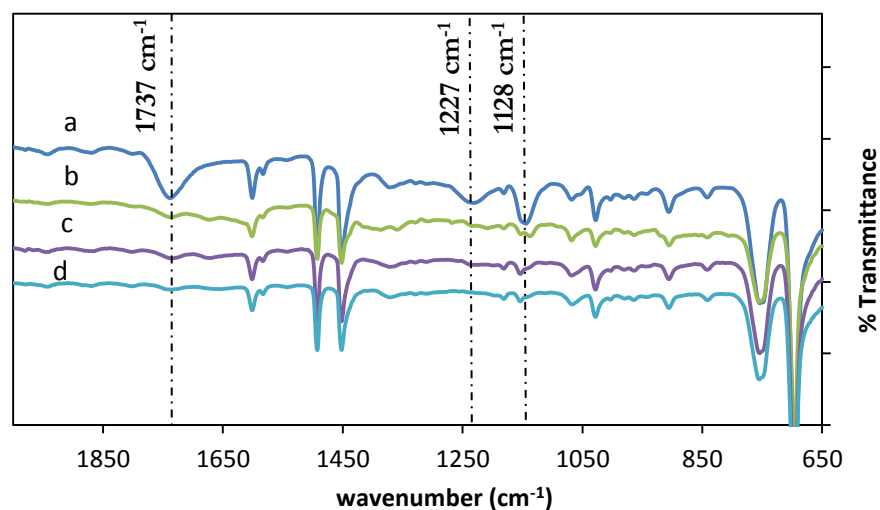


Figure 5.20. FTIR Spectra of a) PS-DGA-3-3 b) 0.05 M EDTA, c) 0.1 M EDTA and d) 0.25 M EDTA (vol – 10 mL; time - 1 hr; rpm - 240)

It can be seen in Figure 5.20 (a) that the peak positions and shapes of the carbonyl ($\text{C}=\text{O}$) group in PS-DGA-3-3 were present at 1737 cm^{-1} , 1128 cm^{-1} and 1227 cm^{-1} and were consistent with the expected peak positions before the EDTA regeneration test but were eroded from the nanofibres by all the different EDTA concentrations after washing except the peak at 1128 cm^{-1} which shifted slightly and became weak. Figure 5.20 (b-d) confirmed that the DGA functional groups were eroded off the nanofibre after EDTA treatment and EDTA regeneration may not be suitable for regenerating the PS-DGA-3-3 nanofibre adsorbent. These results indicated that chemical structure of the PS-DGA-3-3 was adversely affected by chemical degradation after EDTA contact and exposure. However, the major PS nanofibre peak at 1454 cm^{-1} which is the -CH_2 bending peak of the polymer support remained intact indicating that the PS nanofibres itself was not affected by the regeneration. Therefore, 1M HNO_3 was selected as the regenerant for PS-DGA-3-3 rather than EDTA.

5.1.14 Material stability of PET-DGA-2-3 nanofibre in HNO₃ and EDTA

A study of the stability of DGA chelating moieties grafted on the surface of the PET nanofibre and the regeneration ability of the adsorbents is presented as detailed in Chapter 3 Section 3.3.4. Figure 5.21 presents the result of PET-DGA-2-3 nanofibres shaken in different molar concentrations of HNO₃ to simulate the conditions used for batch regeneration experiments.

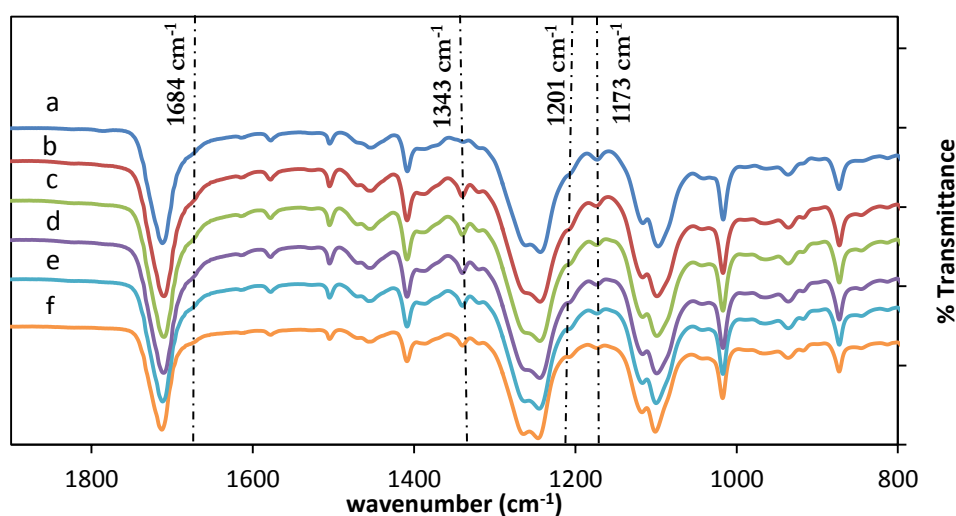


Figure 5.21. FTIR Spectra of a) Pristine PET; b) PET-DGA-2-3; c) 0.5 M HNO₃, d) 1 M HNO₃, e) 1.5 M HNO₃ and f) 2M HNO₃. (Vol - 10 mL HNO₃; time - 1 hr; rpm -240)

Figure 5.21 shows the FTIR spectra of the pristine PET nanofibre and the acid-contacted PET-DGA-2-3 functionalised nanofibre were identical up to 2 M concentration of HNO₃ indicating that the ligand remained intact during 1 hr of acid-contact. The peak positions assigned to the DGA chelating ligand anchored on the nanofibre support are consistent before and after acid treatment with nitric acid for 1 hr up to 2 M indicating the strong chemical stability of the DGA chelating ligand on the nanofibre which may have been assisted by the crosslinking effect. These results indicated that the chemical structure of the DGA ligand upon PET

would not be affected by chemical degradation during regeneration with nitric acid and would therefore be stable during acid use in the regeneration process. Figure 5.21 below presents the result of PET-DGA-2-3 nanofibres shaken in different molar concentrations of EDTA to simulate the conditions used for batch sorption and regeneration experiments.

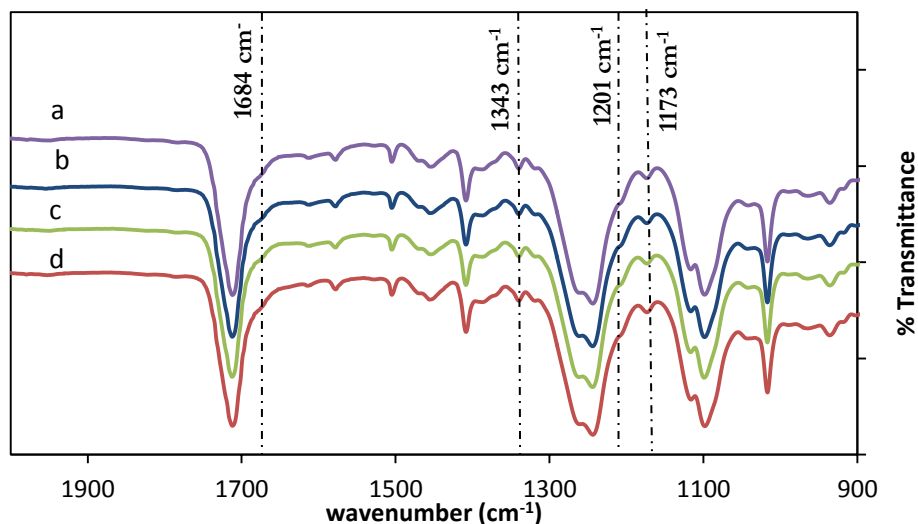


Figure 5.22. FTIR Spectra of a) PET-DGA-2-3, b) 0.05 M EDTA d) 0.1 M EDTA and f) 0.25 M EDTA (vol - 10 mL EDTA; time - 1 h; rpm - 240)

Figure 5.22 (b-d) showed that the peak positions assigned to the DGA chelating ligand on the nanofibre support are consistent before and after treatment with EDTA for 1 hr in the various concentration tested indicating a strong chemical stability of the DGA chelating ligand on the PET nanofibre. Cross-linking of fibres can enhance the resistance of polymers against acids and chemicals, therefore the stability properties of PET-DGA-2-3 may have increased due to increased nanofibre crosslinking effect during modification. Hence, both HNO_3 and EDTA solutions can be employed for regeneration of PET-DGA-2-3. The activity of the ligand will be preserved during use because the DGA ligands are stable on PET in both acidic and

basic conditions and the desorbed sorbent could be generated for reuse after washing in ultrapure water and drying.

5.2 Summary

Introducing functional groups by attaching DGA to the surfaces of electrospun nanofibre (PS and PET) was investigated and successful grafting was confirmed by FTIR, SEM, TGA, XRD and BET analytical techniques. SEM and FTIR confirmed the unique morphology of the DGA modified PS (PS-DGA-3-3) nanofibre and, confirmed abundant carbonyl and etheric oxygen atom groups. PS-DGA-3-3 was achieved with an optimum amount of 3 g (0.026 mol) of the DGA ligand and contact time of three hours for stable nanofibre adsorbent. XRD result indicated the PS-DGA-3-3 transition from a less ordered PS nanofibre phase prior to functionalisation to a more ordered structure after the functionalisation process.

FT-IR confirmed the modification reactions between PET and DGA using 2 g (0.017 mol) DGA ligand concentration after 3 h reaction contact time which yielded PET-DGA-2-3 nanofibre adsorbent. HRSEM studies also showed crosslinked nanofibre morphology which increased their resistance to chemical and thermal degradation and the nanofibres were preserved after modifications. The FT-IR results confirmed that the DGA modified PET nanofibres retained their chemical functionalities even when subjected to treatments with nitric acid and EDTA during stability testing.

The thermal degradation curve for PS-DGA-3-3 occurred in three steps, the first step was due to solvent while the DGA attached to PS was degraded between 200 - 450 °C in two steps, the first weight loss is related to the decomposition of oxygen functionalities and the second weight loss is assigned to the loss of attached DGA

moieties. TGA investigations revealed PET-DGA-2-3 nanofibres began to decompose at 226 °C and pyrolysed completely at 446 °C which revealed two - step degradation indicating strong bonds between PET and DGA which allowed high thermal stability after DGA modification. The amount of DGA on PS nanofibre was 0.82691 g g⁻¹ for PS-DGA-3-3 while the optimum PET-DGA-2-3 nanofibre mats with excellent physical flexibility of the nanofibre were obtained, with 0.449 g g⁻¹ DGA groups on the surface of PET nanofibres after the optimum reaction time. Hence PS could accommodate nearly double the amount of DGA than PET nanofibres

The BET adsorption surface area of modified PS-DGA-3-3 resulted in an increase in the BET surface area from 41.3 m²/g to 67.3 m²/g. Nitrogen adsorption–desorption investigation when PET-DGA-2-3 was compared to the pristine PET showed a decrease in the surface area from 11.2 m²/g, to 8.5 m²/g and pore volume from 0.0156 cm³/g, to 0.0142 cm³/g, however, there was an increase in the average pore sizes from 56.0 (Å) to 66.2 (Å). The study of the stability of DGA chelating moieties grafted on the surface of nanofibres and the regeneration ability of the adsorbents was investigated and 1M HNO₃ was selected as the regenerant of choice for PS-DGA-3-3.

The functionalised PET-DGA-2-3 has higher thermal and chemical stability when compared to PS-DGA-3-3. The PET-DGA-2-3 was also stable in both HNO₃ and EDTA when compared to PS-DGA-3-3 due to increased nanofibre crosslinking effect during modification, but the PS-DGA-3-3 had much more DGA ligands deposited on the nanofibre mats than the PET-DGA-2-3. PS-DGA-3-3 nanofibre therefore possess more abundant etheric oxygen and carbonyl (> C=O) groups than

the PET-DGA-2-3 which will enhance the removal and selectivity towards trivalent lanthanides. The performance of the synthesised nanofibres will be further tested for their adsorption capacities in Chapter Six.



CHAPTER SIX

ADSORPTION STUDY OF Ce^{3+} AND Nd^{3+} ON THE CHELATING PS-DGA-3-3 OR PET-DGA-2-3 NANOFIBRES

6 INTRODUCTION

Chapter six discusses the results of application of the polystyrene-diglycolic acid (PS-DGA-3-3) and polyethylene terephthalate-diglycolic acid (PET-DGA-2-3) modified nanofibres for the removal of Ce^{3+} and Nd^{3+} from a synthetic solution. Different batch experiments were conducted in order to optimise the experimental conditions of Ce^{3+} and Nd^{3+} extraction. This chapter is divided into three main sections. In the first section, adsorption parameters such as solution pH, contact time and initial concentration of Ce^{3+} and Nd^{3+} were optimised and the binding capacities determined. The optimisation of these parameters was carried out in such a way that one parameter was varied while others were kept constant during the adsorption experiments and at least two replicates were run in parallel for each experiment. After these adsorption experiments, the second section considered the modelling of sorption data obtained from different adsorption experiments with the Ce^{3+} and Nd^{3+} and the adsorption binding kinetics. Langmuir and Freundlich which are the most commonly used solid–liquid phase isotherms were used to describe the relationship between the metal ions in solution and the functionalised nanofibres. The third section of this chapter focused on the desorption and regeneration study of the adsorbent materials and their cycles of reusability while the selective separation of Ce^{3+} and Nd^{3+} were also examined in the section. All the experiments that were carried out are detailed in Chapter 3 Section 3.5.

6.1 Determination and optimisation of adsorption parameters of Ce^{3+} and Nd^{3+} binding capacity on modified nanofibre adsorbents

The objective of this section is the optimisation of the selected rare earth metals of Ce^{3+} and Nd^{3+} binding capacity by the modified nanofibre adsorbent as described in experimental procedure in Section 3.5.2, 3.5.3 and 3.5.4. The rate of cation removal from solutions is dependent on factors which include pH, contact time and concentration. The experiment determined the adsorption capacity of the modified nanofibres as adsorbents for Ce^{3+} and Nd^{3+} uptake from aqueous solution by varying parameters such as solution pH, contact time and initial concentration of Ce^{3+} and Nd^{3+} which were optimised and the binding kinetics determined. Lanthanide ion binding capacity experiments were conducted using the modified nanofibres PS-DGA-3-3 and PET-DGA-2-3 based on polystyrene or polyethylene terephthalate nanofibre supports respectively. The adsorption capacity of the chelating adsorbents was determined using the mathematical Equation 3.1 that was described in Chapter 3, Section 3.5.1.

6.1.1 Effect of solution pH using PS-DGA-3-3 nanofibre adsorbent

The effect of solution pH on Ce^{3+} or Nd^{3+} uptake by a chelating-ligand is usually a function of pH which affects the surface charge of adsorbents, the degree of ionisation and species of adsorbate. The pH experiments as described were carried out up to pH 6 in order to avoid precipitation of the Ce^{3+} and Nd^{3+} . The experiments were carried out up to pH 6 in order to avoid precipitation of the Ce^{3+} and Nd^{3+} . The experiments were carried out in 10 mL of 100 mg/L Ce^{3+} or Nd^{3+} solution on PS-DGA-3-3 nanofibres (0.0075 g) by manually adjusting (with 0.1 M HNO_3 or NaOH solution) the solution to the desired pH value starting from pH 1.0; 2.0; 3.0; 4.0; 5.0; and 6.0 as described in the experimental procedure in Chapter 3 Section 3.5.2. The

results obtained from the study of the effect of the solution pH upon Ce^{3+} or Nd^{3+} uptake are shown in Figure 6.1. Each metal ion was tested separately and was therefore not a competitive adsorption and at least two replicates were run in parallel for each experiment.

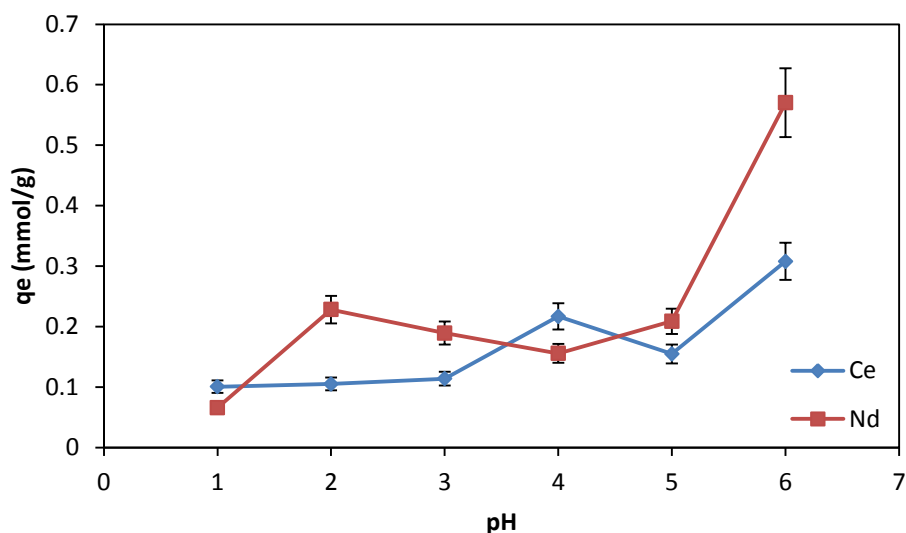


Figure 6.1. Effect of pH on the removal efficiency (%) of Nd^{3+} ; Ce^{3+} from aqueous solution by PS-DGA-3-3 nanofibres (Ce^{3+} or Nd^{3+} concentration - 100 mg/L; contact time - 120 min; adsorbent dosage - 0.0075 g)

Figure 6.1 showed the pH for optimum adsorption when the material (PS-DGA-3-3) was subjected to 100 mg/L of either metal ion solutions at pH 1, 2, 3, 4, 5 and 6. Removal of Ce^{3+} or Nd^{3+} is known to increase after pH above 7 which is due to the formation of insoluble metal hydroxides. The metal uptake below pH 2 was negligible, as the energetics and kinetics favours proton attachment on the adsorption sites. According to Figure 6.1, there was an initial low adsorption capacity of Ce^{3+} at low pH values, because the active sites of PS-DGA-3-3 nanofibre adsorbents are mostly protonated. Consequently, limited active sites are available for metal ion adsorption. As the pH rises, the concentration of H^+ ions decreases leading to the decrease of protonation and an increase of available sites for metal ions to

adsorb. Also, the adsorption capacity increased with increasing pH and reached the maximum amount of 0.308 and 0.570 mmol/g for Ce^{3+} or Nd^{3+} at pH 6, respectively. In the adsorption process, optimising the initial pH of the solution is an essential parameter to investigate adsorption capacity as depicted in Figure 6.1. The effects of pH on Ce^{3+} or Nd^{3+} adsorption capacity were evaluated in the range of 2 - 6 and the pH of 6 was used to monitor the adsorption for Ce^{3+} or Nd^{3+} from synthetic aqueous solutions for subsequent adsorption studies in order to avoid metal hydroxide formation. In some previous studies, precipitation was observed at pH higher than 6 (Niu et al. 2007; Eser et al. 2012) and it was noted that precipitation was observed at pH values higher than 6 for REEs in solutions. Thus the experiments above pH of 7 were not considered in this study.

6.1.2 Effect of solution pH using PET-DGA-2-3 nanofibre adsorbent

The effect of solution pH on Ce^{3+} or Nd^{3+} uptake by PET-DGA-2-3 chelating adsorbent was studied because the complexation of metal ions by a chelating-ligand is a function of the pH. The pH experiments were described in the experimental procedure in chapter 3, section 3.5.2 and were considered up to pH 6 in order to avoid precipitation of the Ce^{3+} or Nd^{3+} . The experiments were carried out in 10 mL of 100 mg/L Ce^{3+} or Nd^{3+} solution respectively on PET-DGA-2-3 nanofibres (0.0075 g) by manually adjusting the pH with 0.1 M HNO_3 or NaOH solution starting from pH 1.0; 2.0; 3.0; 4.0; 5.0; and 6.0. The results obtained from the study of the effect of the solution pH upon Ce^{3+} or Nd^{3+} uptake using PET-DGA-2-3 are shown in Figure 6.2. Each metal ion was tested separately and the experiment was therefore not focussed on competitive adsorption and at least two replicates were run in parallel for each experiment.

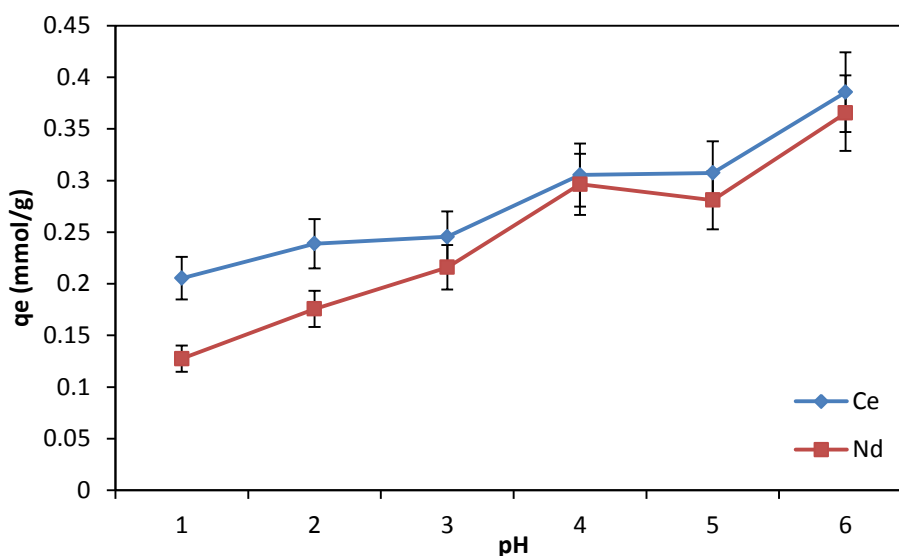


Figure 6.2. Effect of pH on the removal efficiency (%) of Nd^{3+} ; Ce^{3+} from aqueous solution by PET-DGA-2-3 nanofibres (Ce^{3+} or Nd^{3+} concentration - 100 mg/L; contact time - 60 min; adsorbent dosage - 0.0075 g)

The effect of pH on adsorption was optimised by investigating its influence on uptake of Ce^{3+} or Nd^{3+} metal ions as shown in Figure 6.2. Adsorption of the two metal ions respectively was observed to increase with an increase in pH up to pH 4 with a decrease up to pH 5 and a gradual increase to pH 6 for either Nd^{3+} or Ce^{3+} respectively. The adsorption capacity increased with an increasing pH value and reached the maximum amount of 0.386 and 0.365 mmol/g for Ce^{3+} or Nd^{3+} at pH 6, respectively. The low adsorption of metal ions observed at pH 1 and 2 may be explained by the high concentration of protons at lower pH competing with metal ions for the active sites on the modified PET-DGA-2-3 surface. At higher pH values, there is a high degree of de-protonation (proton abstraction) which results in stronger complexing ability of the PET-DGA-2-3 and hence greater metal ion sorption. The metal ion solutions were reported to precipitate as insoluble hydroxides beyond pH 7 from literature (Wang et al. 2006; Pathak and Choppin

2007). In this regard, pH 6 was chosen as the optimum pH for Ce^{3+} as well as Nd^{3+} adsorption using the PET based adsorbent.

In the case of the two functionalised nanofibre adsorbent materials (PS-DGA-3-3 and PET-DGA-2-3), it can be seen that there was an increase in adsorption capacity with an increase in pH and this trend is well reported in literature for other adsorbents. Generally, adsorbents have low capacity at low pH levels and a higher pH is favourable for the deprotonation of hydroxyl groups on the sorbent surface (Luo et al. 2006). Increased deprotonation results in the increase of the negatively charged sites, and then the release of linked H^+ from the adsorbent is greater, consequently more active sites become available for binding with metal ions due to the decrease of protons (H^+) attached to the ligand surface. Because of the release of H^+ from the surface, the surface of the nanofibre was more negatively charged, which enhanced electrostatic attraction between the sorbent surface and the metals; however, Ce^{3+} or Nd^{3+} , which are positively charged, could easily bind to negatively dissociated forms of active groups or may form metal complexes with surface groups, and this resulted in an increase in the adsorption capacity as the pH increases (Sarı et al. 2007; Younis et al. 2014).

Neodymium ion species in the aqueous solution evaluated in a study by Park, Tavlarides (2010) using a phosphorus based sol-gel adsorbent showed that Nd^{3+} was the main species in acidic solution, and formation of $Nd(OH)^{2+}$ occurred above pH 6. Similar pH-dependent adsorption of lanthanides (III) was also observed by other researchers (Wang et al. 2006; Pathak and Choppin 2007).

6.1.3 Effect of contact time on PS-DGA-3-3

The effect of contact time on Ce^{3+} or Nd^{3+} uptake by the polystyrene based nanofibre adsorbent (PS-DGA-3-3) was studied over different contact times of 1, 2, 3, 4, 5, 10, 15, 20, 40 and 60 min with sampling at each interval. One important factor and an objective in the metal removal using nanofibre adsorbents is the improved rate at which the materials would adsorb the metal cations from the solutions as well as the shorter time required to reach equilibrium. The efficiency of an adsorbent for metal ions species is determined by its adsorption rate, with a good adsorbent being fast and quantitative. Therefore, the kinetic experiments were performed using 100 mg/L (see experimental procedure in Section 3.5.3) at the optimum pH previously determined at values of 6 since these pH values were chosen to be a suitable pH for the Ce^{3+} or Nd^{3+} uptake on the PS-DGA-3-3 adsorbent. The results obtained from the study of the effect of contact time on Ce^{3+} or Nd^{3+} uptake by PS-DGA-3-3 are shown in Figure 6.3. Each metal ion was tested separately and the experiment was therefore not testing competitive adsorption.

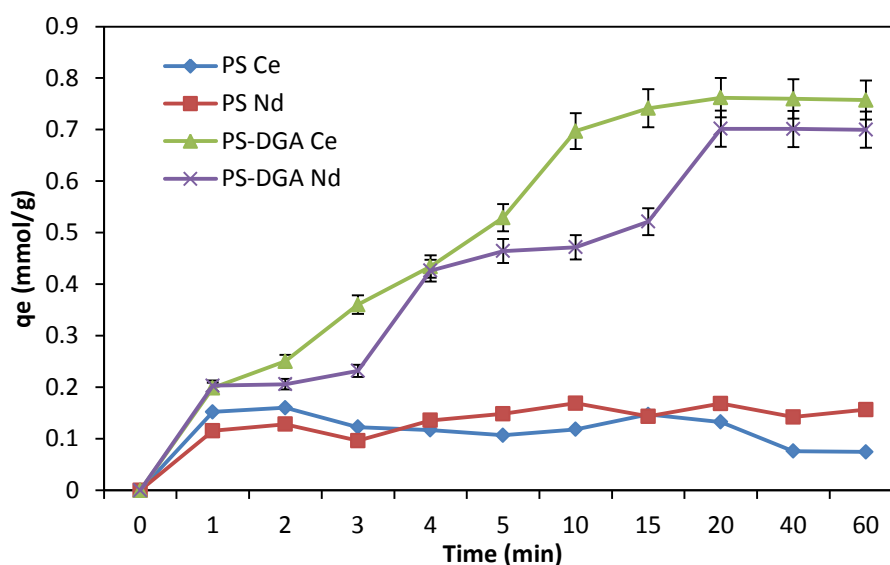


Figure 6.3. Effect of contact time on the removal efficiency of Ce^{3+} ; Nd^{3+} from aqueous solution by Pristine PS and PS-DGA-3-3 nanofibre (Ce^{3+} or Nd^{3+} concentration - 100 mg/L; pH - 6; adsorbent dosage - 0.0075 g)

The effect of contact time on adsorption of Ce^{3+} and Nd^{3+} metal ions onto PS-DGA-3-3 nanofibre adsorbent and pristine PS is depicted in Figure 6.3 which showed that high adsorption was attained within 10 minutes for the two metals using PS-DGA-3-3 respectively. It was found that the adsorption of Ce^{3+} or Nd^{3+} ions increased with contact time and equilibrium was achieved at 20 min. Within the first 20 min, the amount adsorbed reached 0.762 mmol/g Ce^{3+} (which was 90.5 %) and 0.702 mmol/g Nd^{3+} (which was about 91.4 %) of the available metal ion concentration present in the solution. As depicted in Figure 6.3, more than 90% adsorption of the available Ce^{3+} metal ions was achieved within 20 minutes whereas Nd^{3+} removal was slightly slower and lower within the 20 minutes experimental process.

PS-DGA-3-3 had a fast and high adsorption attributed to the amount of the DGA (0.8269 g g^{-1}) immobilised on PS-DGA-3-3 when compared with the pristine PS (0.1603 mmol/g). The two metal ions' adsorption onto the nanofibre adsorbent did

not change with increased time after twenty minutes of contact time. Therefore, twenty minutes was set as the necessary time needed to attain equilibrium for the nanofibre adsorbents. The fast adsorption during the first 10 min was related to the high amount of vacant surface sites of nanofibre adsorbent available for the adsorption of the metal ions (see kinetic study in section 6.2.1).

Many sorption sites are available in the initial stage on the surface of the nanofibres for Ce^{3+} or Nd^{3+} binding, where after the adsorption rate dropped off slightly due to diffusional constraints of low adsorbate concentration to the available sorption sites. Thus, for adsorption experiments, 60 minutes of contact time was considered enough to establish the equilibrium. The high adsorption rate can also be attributed to the high surface area and numerous binding sites of PS-DGA-3-3 and after 20 mins, no further adsorption occurred on the adsorbent because of limited supply of metal ions in solution as more than 90 % of the adsorbate was removed from solution as shown by experiments at a higher concentration in Section 6.1.5. The Ce^{3+} and Nd^{3+} adsorption rates were high, which showed the PS-DGA-3-3 nanofibre has the potential for practical use. The amount of Ce^{3+} or Nd^{3+} adsorbed onto the adsorbent increased rapidly during the initial 10 min. The short time thereafter needed to reach equilibrium suggests that the PS-DGA-3-3 has very high adsorption efficiency and has a great potential in Ce^{3+} or Nd^{3+} uptake.

6.1.4 Effect of contact time on PET-DGA-2-3

The effect of contact time on Ce^{3+} or Nd^{3+} uptake by the PET based nanofibre adsorbent (PET-DGA-2-3) was studied over different contact times of 1, 2, 3, 4, 5, 10, 15, 20, 40 and 60 min with sampling at each time interval in order to determine the rate of the Ce^{3+} or Nd^{3+} uptake. The experiment were performed using 100

mg/L (see experimental procedure in Chapter 3 Section 3.5.3) at the optimum pH values of 6 chosen to be a suitable pH for optimum adsorption with the PET based adsorbent. The results obtained from the study of the effect of contact time on Ce^{3+} or Nd^{3+} uptake respectively are shown in Figure 6.4. Each metal ion was tested separately and the experiment was therefore not testing competitive adsorption.

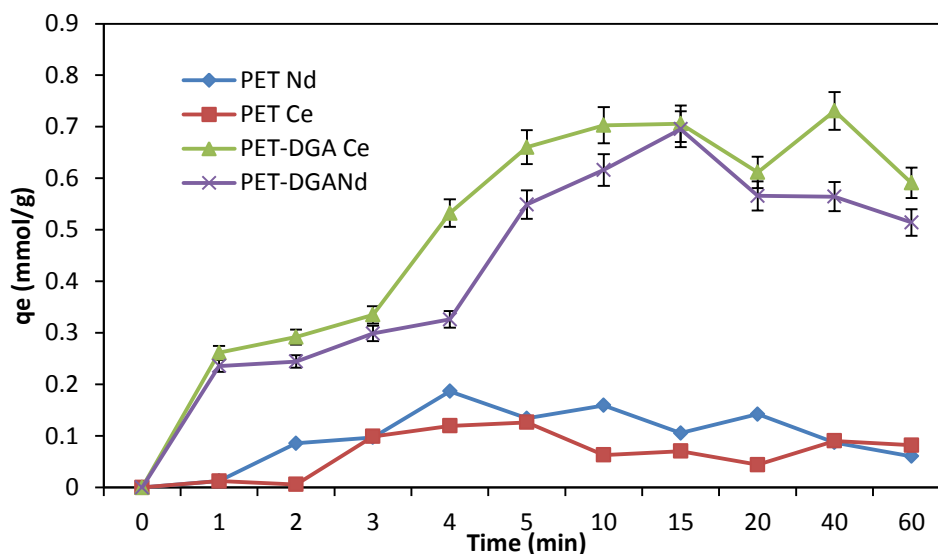


Figure 6.4. Effect of contact time on the removal efficiency of Ce^{3+} ; Nd^{3+} from aqueous solution by Pristine PET and PET-DGA-2-3 nanofibre (Ce^{3+} or Nd^{3+} concentration - 100 mg/L; pH - 6; adsorbent dosage - 0.0075 g)

As shown in Figure 6.4, the metal uptake was rapid within the first 10 minutes, thereafter there was an increase in the adsorption binding capacity which peaked at 15 mins and started a decline for Nd^{3+} but fluctuated slightly for Ce^{3+} before final decline. The decline was initially noticed after the initial rapid adsorption up to 15 mins where equilibrium was reached with the available metal ion concentrations. This decline may probably due to the total uptake of the available metal ions in solution by the adsorption sites while several available sites still remained unoccupied. Figure 6.6 also confirmed that there were no fluctuations when the solute was over supplied.

Over 90% of total adsorption of Ce^{3+} or Nd^{3+} occurred within the first 15 min, which was reached at 0.706 mmol/g Ce^{3+} and 0.695 mmol/g Nd^{3+} respectively. At the start of the experiment, the ions selectively occupied the active sites on the adsorbent and as the contact time increased the active sites on the adsorbent were occupied by the limited solute present in solution and the rate of adsorption became gradually slower to reach a plateau within 15 min. The fast initial metal adsorption was attributed to the greater concentration gradient, large surface area available and numerous available binding sites to be occupied and very little mass transfer resistance expected and therefore the uptake rate was very high within the initial 10 mins. In comparing the pristine PET with PET-DGA-2-3, the fast adsorption was attributed to the amount of the DGA (0.449 g g^{-1}) immobilised on PET-DGA-2-3. Therefore, the two advantages of unique nanofibre structure and high DGA loading gave the PET-DGA-2-3 nanofibre excellent adsorption capability for REEs. For practical consideration 60 mins time was presumed to represent the equilibrium time for the adsorption of metal ions (see kinetic study in section 6.2.2). The experiments evaluating the concentration of adsorbate are presented in Section 6.1.5 and 6.1.6 for PS-DGA-3-3 and PET-DGA-2-3 respectively.

The surface modification of PS or PET nanofibres with DGA was therefore found to enhance the binding capacities of the available Ce^{3+} or Nd^{3+} uptake. The Ce^{3+} or Nd^{3+} uptake for both PS-DGA-3-3 and PET-DGA-2-3 nanofibre adsorbent showed fast binding capacities obtained rapidly within 10 minutes in this study which may be due to the high surface area and many surface binding sites that the nanofibres adsorbent possessed combined with the suitability of the chelating DGA ligand towards lanthanide uptake. Therefore, the two nanofibre adsorbent materials (PS-

DGA-3-3 and PET-DGA-2-3) are very suitable nanofibre materials that can be used for recovery and uptake of Ce^{3+} or Nd^{3+} due to the rapid kinetics.

6.1.5 Effect of equilibrium concentration of Ce^{3+} or Nd^{3+} on PS-DGA-3-3

Experiments to determine the effect of rare earth metal ion concentration were performed over a range of Ce^{3+} or Nd^{3+} equilibrium concentrations (a range from 60 to 180 mg/L (see experimental procedure in chapter 3 section 3.5.4) at the optimum pH values of 6 (see Figure 6.1) previously determined for PS-DGA-3-3 nanofibre adsorbent at a contact time of 60 min (see Figure 6.3). The obtained experimental results of the effect of initial concentration of Ce^{3+} or Nd^{3+} on adsorption of PS-DGA-3-3 nanofibre adsorbents are shown in Figure 6.5. Each metal ion was tested separately and the experiment was therefore not testing competitive adsorption.

This experiment was conducted to determine the maximum uptake capacity of the adsorbent in an unlimited supply of metal ion solution because REEs being recovered exist in different concentrations depending on the sources of metal ions. It was also necessary to determine the total capacity and the available binding sites. Thus, the behaviour of the adsorbent for removal of Ce^{3+} or Nd^{3+} from aqueous solution was investigated as a function of their concentrations at constant temperature ($25 \pm 0.1^\circ C$) using different initial metal concentrations from 60 to 180 mg/L, while keeping all other parameters constant. The sorption results of Ce^{3+} or Nd^{3+} using functionalised nanofibres are shown in Figure 6.5.

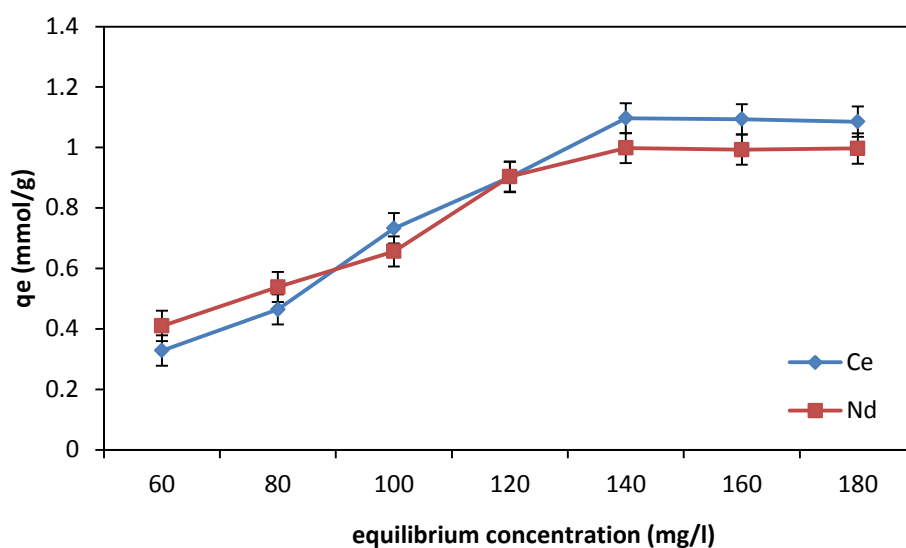


Figure 6.5. Effect of equilibrium metal concentrations on adsorption of Nd^{3+} ; Ce^{3+} onto PS-DGA-3-3 nanofibre (contact time - 90 min; pH - 6; adsorbent dosage - 0.0075 g /10 mL)

As can be seen in Figure 6.5, the adsorption capacities of the metal ions increased rapidly as the initial concentration increased and then the uptake of the Ce^{3+} reached a maximum as the concentration increased to 140 mg/L to obtain equilibrium. This increase in uptake with increasing concentration up to 140 mg/L may be related to the large surface area and many available binding sites upon both inter and intra fibrous pores in the nanofibres. The maximum adsorption capacities of Ce^{3+} and Nd^{3+} ions on the PS-DGA-3-3 chelating nanofibre membranes were 1.09 mmol/g and 0.998 mmol/g respectively indicating that the available sites was fully satisfied.

Generally, for both elements the adsorption capacities increased with increasing amounts of metal concentrations up to a maximum of 140 mg/L where after, all the available sites were fully saturated and no further adsorption could take place. The adsorption of the Ce^{3+} or Nd^{3+} increased with an increase of metal ions concentration from 60 mg/L to 140.0 mg/L and remained constant up to 180.0 mg/L. This suggests that the Ce^{3+} and Nd^{3+} adsorption upon the available active sites

by PS-DGA-3-3 could strongly depend on the available sites due to the nanofibre large surface area and contact time. From the investigation, at 100 mg/L, there were more available sites for the metal ion, but on increasing the concentration, there was an increased adsorption up to 140 mg/L.

6.1.6 Effect of equilibrium concentration of Ce^{3+} or Nd^{3+} on PET-DGA-2-3

Experiments to determine the effect of rare earth metal ion concentration upon adsorption were performed over a range of Ce^{3+} or Nd^{3+} from 40 to 180 mg/L on PET-DGA-2-3 at the optimum pH values of 6 and contact time of 60 min. The experiments were performed as described in the experimental procedure in Chapter 3 Section 3.5.4. The results showing the effect of initial concentration of Ce^{3+} or Nd^{3+} uptake on PET-DGA-2-3 nanofibres adsorbent are shown in Figure 6.6. Each metal ion was tested separately and was therefore not a competitive adsorption.

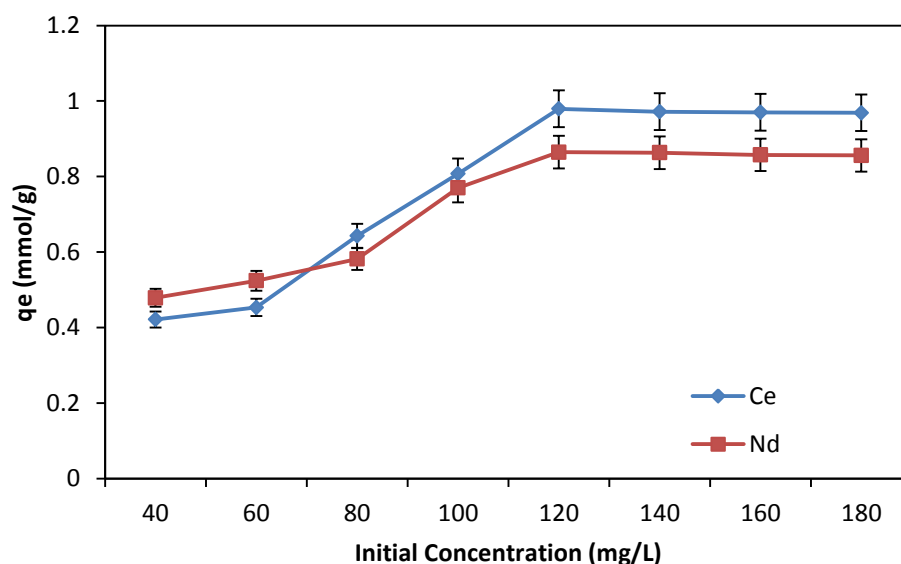


Figure 6.6. Effect of equilibrium metal concentrations on adsorption of Ce^{3+} ; Nd^{3+} onto PET-DGA-2-3 nanofibre (contact time - 100 min; pH - 6; adsorbent dosage - 0.0075 g /10 mL)

The effect of equilibrium concentration of Ce^{3+} or Nd^{3+} on their adsorption was investigated using a concentration range 40 - 180 mg/L and Figure 6.6 showed that as the concentration was increased beyond 120 mg/L, the available adsorption sites on the surface of the PET-DGA-2-3 nanofibres became saturated. The adsorption of Ce^{3+} or Nd^{3+} reached a plateau state at a concentration of ca. 120 mg/L. The maximum adsorption capacities of Ce^{3+} or Nd^{3+} ions on the PET-DGA-2-3 chelating nanofibre membranes were 0.969 mmol/g, and 0.857 mmol/g respectively.

The adsorption of Ce^{3+} or Nd^{3+} was observed to increase for all initial concentrations until equilibrium was attained for both PS-DGA-3-3 and PET-DGA-2-3. This type of adsorption behaviour is typical of the specific adsorption process in which the adsorption rate is greatly dependent on the available number of adsorption sites on the surface of the adsorbent with no diffusional constraints and the metal ion adsorption is therefore controlled by the number of available ligands on the adsorbent's surface. The results showed that the maximum adsorption upon PS-DGA-3-3 for Ce^{3+} or Nd^{3+} was obtained at a concentration of 140 mg/L, and a concentration of 120 mg/L for PET-DGA-2-3. The loading capacities of the nanofibre adsorbent for Ce^{3+} or Nd^{3+} were calculated from Equation (3.1). In comparing the two adsorbent, the maximum loading capacity of PS-DGA-3-3 for Ce^{3+} or Nd^{3+} were found to be 1.09 and 0.998 mmol/g and it was observed to have a better adsorption capacity compared to PET-DGA-2-3 with 0.969 mmol/g, and 0.857 mmol/g respectively for Ce^{3+} or Nd^{3+} .

6.2 Adsorption isotherm models

The equilibrium adsorption isotherm is essential in describing the interaction between the adsorbate and adsorbent, and is important in the design of adsorption systems. Adsorption isotherms indicate how the adsorbates (metal ions) interact with

adsorbents and how adsorption uptakes vary with adsorbate concentrations at given pH values and temperatures. The two most commonly used isotherms, namely the Freundlich and Langmuir isotherms have been adopted here to describe the adsorption characteristics of PS-DGA-3-3 and PET-DGA-2-3 nanofibre adsorbent. The linearisation according to the Langmuir and Freundlich adsorption isotherms were therefore examined and the correlation coefficient (R^2) was calculated to evaluate the fit of the two models.

6.2.1 Adsorption isotherm models for PS-DGA-3-3

The fitting of experimental adsorption isotherm data into linearised plots are depicted in Fig. 6.7 and Fig. 6.8 for Langmuir and Freundlich isotherms models respectively while the extrapolated theoretical parameters for the models are provided in Table 6.1.

6.2.1.1 Langmuir isotherm

Langmuir isotherm (Langmuir 1916) model is expressed in the form of the following equation:

$$\frac{1}{q_e} = \frac{1}{q_m} + \frac{1}{bq_m C_e} \dots\dots\dots\text{Equation 6.1}$$

where q_m is the amount of adsorbate at complete monolayer coverage (mg/g), which gives the maximum sorption capacity of sorbent and b (L/mg) is the Langmuir isotherm constant that relates to the energy of adsorption calculated from the slope and intercept of the plot $1/q_e$ vs. $1/C_e$. Figure 6.7 depicts the adsorption isotherm of PS-DGA-3-3 nanofibre adsorbent with (a) Ce (b) Nd linearised according to the Langmuir equations.

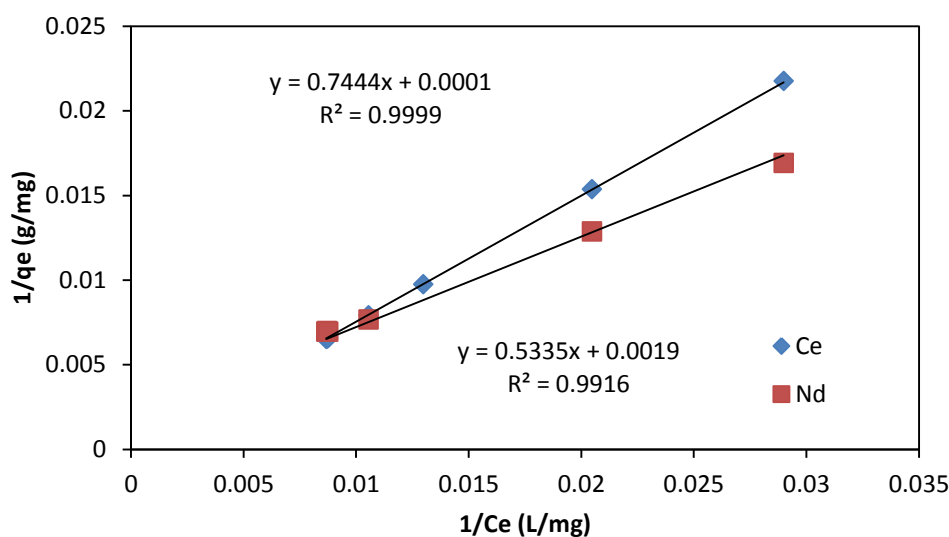


Figure 6.7. Adsorption isotherm of PS-DGA-3-3 nanofibre adsorbent for Ce^{3+} ; Nd^{3+} linearised according to Langmuir equations.

The values of the correlation coefficient R^2 for the Langmuir equation were 0.9999 or 0.9916 for Ce^{3+} or Nd^{3+} respectively which suggested that the adsorption of the two rare earth metal ions on the PS-DGA-3-3 nanofibre followed the Langmuir adsorption isotherm.

The Langmuir model (Langmuir 1916) advocates 3 major conditions viz (i) no interaction among the molecules in the monolayer, (ii) the sorption of adsorbate molecules in one adsorbing site does not influence the adsorption of other molecules in neighbouring sites, and (iii) the intermolecular attraction forces between the adsorbate molecules in the monolayer and the ones in the solution decrease drastically with distance (Foo and Hameed 2010; Ng et al. 2003).

6.2.1.2 Freundlich isotherm

The well-known Freundlich isotherm is an empirical equation employed to describe heterogeneous systems. The linear form of the Freundlich isotherm (Freundlich 1906b) is written as the following equation:

$$\ln q_e = \ln k_f + \frac{1}{n} \ln C_e \dots\dots\dots \text{Equation 6.2}$$

where q_e is the amount of metal ion adsorbed per unit weight of the sorbent (mg/g), C_e the equilibrium concentration in solution (mg/L), k_f (mg/g), a measure of adsorption capacity, and $1/n$, the adsorption intensity, were calculated from the slope and intercept of the plot $\ln q_e$ vs. $\ln C_e$. The values of $1/n$ lying between 0 and 1 confirm favourable conditions for adsorption.

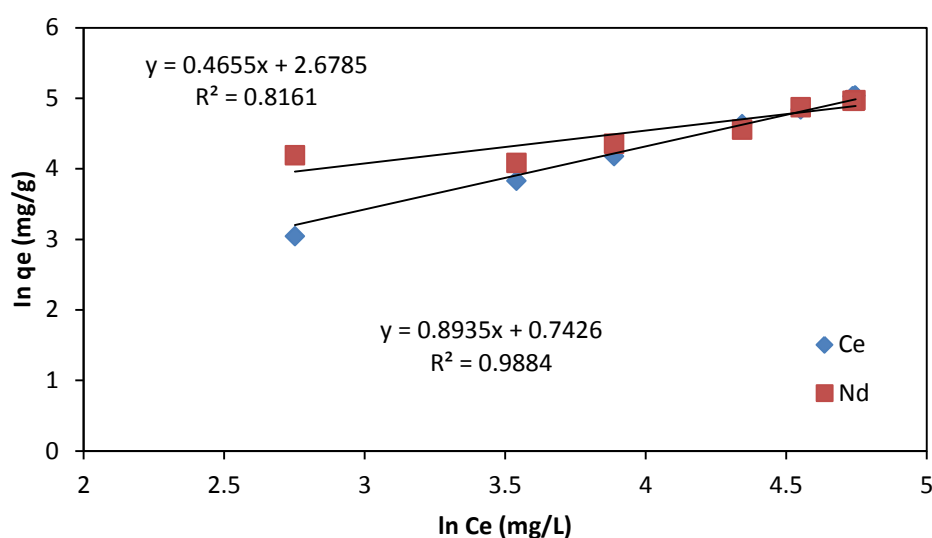


Figure 6.8. Adsorption isotherm of PS-DGA-3-3 nanofibre adsorbent of Nd^{3+} ; Ce^{3+} linearised according to the Freundlich equation.

The Freundlich isotherm R^2 values for the PS-DGA-3-3 are 0.988 and 0.816 for Ce^{3+} or Nd^{3+} respectively which are relatively high force indicating the applicability of the Freundlich isotherm and thus it could be also inferred that the adsorption of the Nd adsorbate on the nanofibres may not entirely follow the 3 strict rules of Langmuir, but the metal ions may adsorb on a somewhat heterogeneous surface of the nanofibres chemically fabricated by the PS-DGA-3-3 functionalisation.

Contrary to Langmuir, the Freundlich isotherm advocates the formation of a multilayer of the adsorbing molecule or/and heterogeneous distribution onto the

surface of the adsorbent (Freundlich 1906a). This model presupposes that the amount of adsorbates collected onto the adsorbent is directly proportional to its concentration in the solution and not constant at a given concentration (Ng et al. 2003). The PS-DGA-3-3 nanofibres show similar trends for both metals with these sorption isotherms. A comparison of the parameters obtained from the plots of Langmuir and Freundlich isotherms for Ce^{3+} or Nd^{3+} adsorption on the PS-DGA-3-3 nanofibres is shown in Table 6.1

Table 6.1. Parameters obtained from the plot of Langmuir and Freundlich isotherms for Ce^{3+} or Nd^{3+} adsorption using PS-DGA-3-3.

	Langmuir isotherm		Freundlich isotherm				
	q_e (exp) mg/g	R^2	b_1 (L/mg)	q_e (mg/g)	R^2	n	$k_f [(mg/g) (mg/L)^{1/n}]$
Nd^{3+}	144.007	0.992	0.00356	146.206	0.816	2.148	14.563
Ce^{3+}	152.077	0.999	0.00013	152.493	0.988	1.119	2.101

From Table 6.1, the n values 1.11 and 2.15 for Ce^{3+} and Nd^{3+} of the Freundlich isotherm were in the range of $n > 1$ for the rare earth metal ions revealing their favourable adsorption. From this comparison, it can be seen that the values of the correlation coefficient R^2 of the Ce^{3+} or Nd^{3+} estimated from the Langmuir equation was higher than that estimated from the Freundlich equation, indicating that the Langmuir equation gives a better fit of the experimental data than the Freundlich equation.

The maximum Langmuir absorption capacities (q_e) for Ce^{3+} and Nd^{3+} were 152.5 mg/g (1.09 mmol/g) and 146.2 mg/g (1.01 mmol/g) respectively. This number is very close to the measured experimental values of 152.0 mg/g (1.09 mmol/g) for Ce^{3+} ; and 144.0 mg/g (0.998 mmol/g) for Nd^{3+} at the C_e of 140 mg/L, indicating the

dependability of q_e value (Table 6.1). The value of K_f (2.101 and 14.6) and n (1.11 and 2.19) for Ce^{3+} and Nd^{3+} respectively are determined from the linear plot of $\ln q_e$ versus $\ln C_e$ (Fig. 6.8) and by considering the values of the Freundlich constant (n) it can be observed that the adsorption of both metal ions are favourable.

6.2.2 Adsorption isotherm models for PET-DGA-2-3

The fitting of experimental adsorption isotherm data into linearised plots for PET-DGA-2-3 are depicted in Fig. 6.9 and Fig. 6.10 for Langmuir and Freundlich isotherms models respectively while the extrapolated theoretical parameters for the models are provided in Table 6.2.

6.2.2.1 Langmuir isotherm

The Langmuir model was derived to describe the adsorption of a sorbate on a homogeneous, flat surface of an adsorbent and each adsorptive site can be occupied only once in a one-on-one manner. The plot of experimental adsorption isotherm data for both metals into linearised form for the Langmuir isotherms models are depicted in Figure. 6.9.

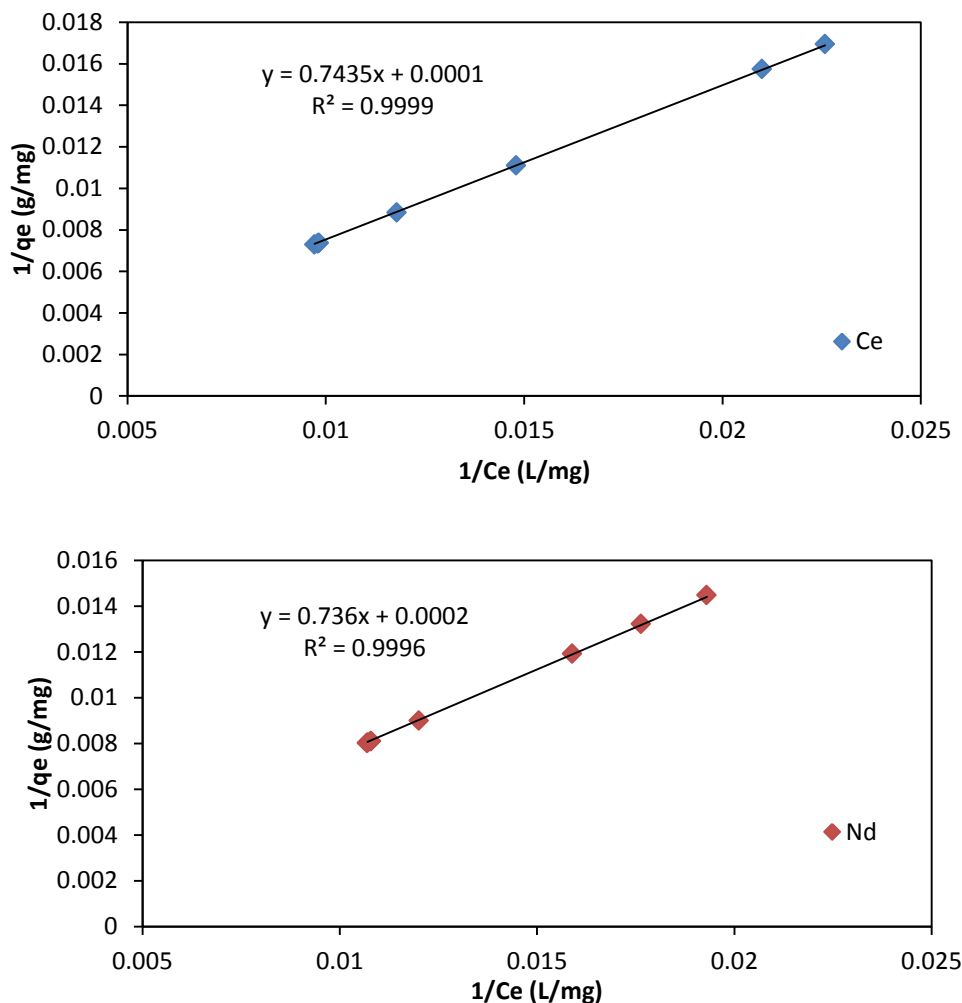


Figure 6.9. Adsorption isotherm of PET-DGA-2-3 nanofibre adsorbent of Ce³⁺; Nd³⁺ linearised according to Langmuir equations.

According to the obtained results shown in Figure 6.9, the adsorption data of the Ce³⁺ and Nd³⁺ ions on the PET-DGA-2-3 nanofibre fitted particularly well with the Langmuir model, as indicated by the high values of the correlation coefficient (R^2 over 0.999), thus, monolayer adsorption occurred on the PET-DGA-2-3 nanofibre for both metals. Parameters in Fig. 6.9 are summarised in Table 6.2. The Langmuir adsorption model is based on the assumption that the maximum adsorption corresponds to a saturated monolayer of adsorbate molecules on the adsorbent surface. Thus, adsorption occurs uniformly on the active sites of the adsorbent, and

once an adsorbate occupies a site, no further adsorption will take place at this site (Chen et al. 2009).

6.2.2.2 Freundlich isotherm

The well-known Freundlich isotherm is an empirical equation employed to describe heterogeneous systems. The plot of experimental adsorption isotherm data for both metals into linearised plots for the Freundlich isotherm models are depicted in Fig. 6.10.

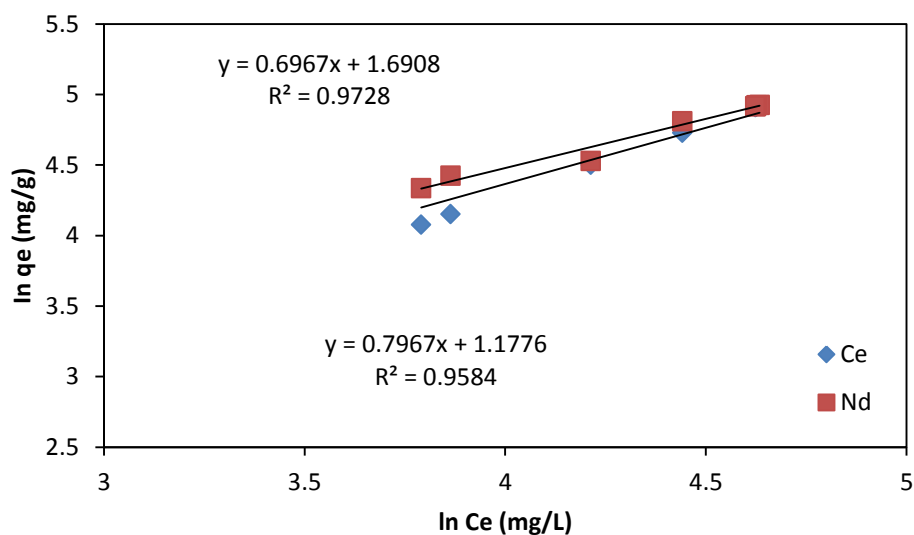


Figure 6.10. Adsorption isotherm of PET-DGA-2-3 nanofibre adsorbent for Nd^{3+} ; Ce^{3+} linearised according to the Freundlich equation.

The fact that the Freundlich adsorption isotherm shows relatively high values in the adsorption process could possibly be as a result of heterogeneous distribution of adsorption sites on PET-DGA-2-3 and different metal binding sites from the diglycolic anhydride (DGA). The Freundlich adsorption equation predicts that the solute concentrations on the adsorbent will increase so long as there is an increase in the solute concentration in the aqueous solution.

Table 6.2. Parameters obtained from the plot of Langmuir and Freundlich isotherms for Ce³⁺ or Nd³⁺ adsorption for PET-DGA-2-3.

	Langmuir isotherm				Freundlich isotherm		
	q _e (exp) mg/g	R ²	b1 (L/mg)	q _e (mg/g)	R ²	n	k _f [(mg/g) (mg/L) ^{1/n}]
Nd ³⁺	123.669	0.9996	0.00027	123.915	0.973	1.435	5.424
Ce ³⁺	135.762	0.9999	0.00013	136.554	0.958	1.255	3.247

As shown in Table 6.2, the maximum adsorption capacities of Ce³⁺ and Nd³⁺ ions on the PET-DGA-2-3 chelating nanofibre membranes are 136.6 mg/g (0.975 mmol/g) and 123.9 mg/g (0.859 mmol/g) respectively from the Langmuir isotherm which values were close to the measured experimentally obtained results. The maximum adsorption capacity (q_e) obtained by Langmuir isotherm for Ce³⁺ was also higher than the values found for Nd³⁺. The comparison of determination coefficients (i.e., R²) for the different systems shows that the Langmuir equation was a better fit and generally gave higher coefficients than the Freundlich equation. For this investigation, PS-DGA-3-3 performed better than PET-DGA-2-3 when the maximum Langmuir adsorption capacities (q_e) were compared.

6.3 Comparison of the functionalised nanofibre absorption capacity with other absorbents

The sorption properties of the nanofibre adsorbents for Ce³⁺ and Nd³⁺ were compared to the sorption capacities of commercial or alternative sorbents also fitted by the Langmuir model which is usually adopted in the studies of absorbents for the extraction of REEs. Table 6.3 summarises the comparison of adsorption capacities of various absorbents for Nd³⁺ while Table 6.4 summarises the adsorption capacity of various absorbents for Ce³⁺. Due to the different surface and bulk properties, it is

very difficult to perform a really fair comparison. However, this data still provided the useful information at least on the order of magnitude of removal of the metal ions.

Table 6.3. Comparison of sorption capacities of different sorbents for Nd³⁺.

Sorbent	Metal	pH	time (h)	Adsorption capacity (mg/g)	Reference
Mordenite containing tuff	Nd(III)	3	24	11.77	Kozhevnikova and Tsybikova 2008
Yeast cells	Nd(III)	1.5	24	10–12	Vlachou et al. 2009
Microorganisms	Nd(III)	1.5	2	136.7	Palmieri et al. 2000
Aminomethylphosphonic acid modified chitosan	Nd(III)	5	7	30.32	Elsalamouny et al. 2017a
Calcium alginate–poly glutamic acid	Nd(III)	3.5	24	237.99	Wang et al. 2014
Phosphoric acid on silica matrix	Nd(III)	6	24	160	Park and Tavlarides 2010
Fumarated polystyrene microspheres	Nd(III)	5	0.4	39.7	Elsalamouny et al. 2017b
Aspartic acid grafted Cellulose	Nd(III)	5	3	81.2	Galhoum et al. 2017
Extractant impregnated alginate microcapsules	Nd(III)	4	20	149.3	Zhang et al. 2011
Sargassum sp. algal biomass	Nd(III)	5	1	101	Oliveira and Garcia Jr 2009
EDTA and DTPA-functionalised chitosan	Nd(III)	4	3	72–80	Roosen and Binnemans 2014
Acrylic resin (110 resin)	Nd(III)	6	72	315	Xiong et al. 2015
Functionalised magnetic nano-particles	Nd(III)	6	0.5	25	Miraoui et al. 2016
PS-DGA-3-3	Nd(III)	6	0.4	146.2	This work
PET-DGA-2-3	Nd(III)	6	0.4	123.9	This work

Table 6.4. Comparison of sorption capacities of different sorbents for Ce³⁺.

Sorbent	Metal	pH	time (h)	Adsorption capacity (mg/g)	Reference
4-dodecyl-6-((4-(hexyloxy)phenyl)diazanyl)benzene-1,3-diol on mesoporous silica nano-composite	Ce(III)	2.5	2	150.37	Awual et al. 2015
Platanus orientalis leaf powder	Ce(III)	4	1	32.05	Sert et al. 2008
chitosan/polyvinyl/Alcohol/3-mercaptop Beads	Ce(III)	5	6	251.41	Najafi Lahiji et al. 2016
Amino Phosphate Nano TiO ₂	Ce(III)	6	1.5	21.39	Shojaei et al. 2016
Pinus brutia leaf powder	Ce(III)	5	0.4	17.24	Kütahyalı et al. 2010
Arthrospira cyanobacteria	Ce(III)	5.5	1	38.2	Sadovsky et al. 2016
hybrid nano-material	Ce(III)	5	3.5	130	Yavarpour et al. 2015
PS-DGA-3-3	Ce(III)	6	0.4	152.5	This work
PET-DGA-2-3	Ce(III)	6	0.4	136.6	This work

The q_e value of PS-DGA-3-3 and PET-DGA-2-3 is competitive with and outperforms other adsorbents when compared with the previously reported adsorbents. Even though some materials such as phosphoric acid functionalised adsorbents (Park and Tavlarides 2010), calcium alginate–poly glutamic acid (Wang et al. 2014), Chitosan/Polyvinyl Alcohol/3-mercaptopropyltrimethoxysilane Beads (Najafi Lahiji et al. 2016) or impregnated alginate microcapsules (Zhang et al. 2011) showed significantly higher sorption levels than those obtained with PS-DGA or PET-DGA,

but the modification and synthesising is more complexity. These new nanofibre adsorbents have sorption capacities at least comparable to more conventional sorbents and even better than some adsorbents.

Different experimental conditions make the comparison of sorption performance very complex; however, table 6.3 and 6.4 has shown that the sorbents made in this study had comparable sorption properties for the binding of selected REEs in slightly acidic to neutral solutions. Some of the reported materials may have significantly higher sorption properties but also had very elongated times to achieve equilibrium. Generally, PS-DGA-3-3 and PET-DGA-2-3, have very comparable sorption properties and very rapid kinetics for the selected REEs used in this study. The main advantages of the present adsorbents are the very fast kinetics of sorption (see Section 6.1.4) associated with their nano size, large surface areas and the loaded ligand, as well as relatively simple mode of preparation.

6.4 Kinetic study of nanofibre adsorbent (PS-DGA-3-3 and PET-DGA-2-3)

It has been found that the adsorption process could be governed by diverse types of mechanisms such as mass transfer, diffusional control, chemical reaction and pore diffusion. In order to clarify the adsorption process, two reaction-based kinetic models were used. The reaction-based kinetic models are known as either pseudo-first-order or pseudo-second-order. In the pseudo-first-order model, all phases of the adsorption process involving external diffusion, internal diffusion and adsorption are integrated. It is also supposed that the driving force for the adsorption is the changing rate of occupation of adsorption sites which is directly proportional to the number of unoccupied sites. This pseudo-first-order kinetic model, known as the Lagergren equation (Lagergren 1898), can be expressed in its linearised form as:

$$\ln(q_e - qt) = \ln q_e - k_1 t \dots\dots\dots\text{Equation 6.3}$$

where q_t and q_e , are the amounts of ion adsorbed at time t and at equilibrium (mmol/g), respectively, and k_1 is the rate constant of pseudo-first-order adsorption process (1/min). The plot of $\ln(q_e - q_t)$ versus t gives a straight line with a slope of $-k_1$ and an intercept of $\ln q_e$. The pseudo-second-order also considers the same assumptions as used in the pseudo-first-order model, but the rate of occupation of adsorption sites is proportional to the square of the number of unoccupied sites, while the overall rate of adsorption process is controlled by chemisorption. The pseudo-second-order kinetic model (Özacar and Şengül 2004):

$$\frac{t}{q_t} = \frac{1}{k_2 q_e^2} + \frac{1}{q_e} t \dots\dots\dots\text{Equation 6.4}$$

where k_2 is the equilibrium rate constant of pseudo-second-order sorption (g/mg min). The plot of t/q_t versus t gives a straight line with a slope of $1/q_e$ and an intercept of $1/(k_2 q_e^2)$. The kinetics of metal ion sorption is therefore an important parameter for designing sorption systems and is required for selecting the optimum operating conditions for the full-scale batch metal removal process. The adsorption pseudo-first-order and pseudo-second-order kinetic plots for the adsorption of Ce^{3+} or Nd^{3+} metal ions are shown in Figures 6.11 and 6.12 respectively and all the obtained kinetic parameters are summarised in Table 6.5.

6.4.1 Kinetic studies for PS-DGA-3-3

The effect of time on Ce^{3+} or Nd^{3+} metal ions adsorption onto PS-DGA-3-3 was previously performed and the results were shown in Figure 6.3. The pseudo-first-order kinetic model and pseudo-second-order kinetic model were applied to the experimental data to analyse the adsorption kinetics and were depicted in Figure 6.11 and 6.12 respectively. Metal uptake on the PS-DGA-3-3 adsorbent increased

very rapidly in the first 15 mins, and then become almost stable, denoting attainment of equilibrium before 15 mins. These changes in metal uptake may be due to the fact that, initially, all adsorbent sites were vacant and the solute concentration was high. After 20 min, only a very low increase in the metal uptake was observed because there were few available metal ions remaining in solution for adsorption. Various models can describe the transient behaviour of a batch adsorption process. Most adsorption kinetics have been reported as pseudo-first-order and some as pseudo-second-order kinetic processes. The results for the kinetic studies are shown in Figure 6.11 for the pseudo first order reaction and Figure 6.12 for pseudo second order reactions for PS-DGA-3-3.

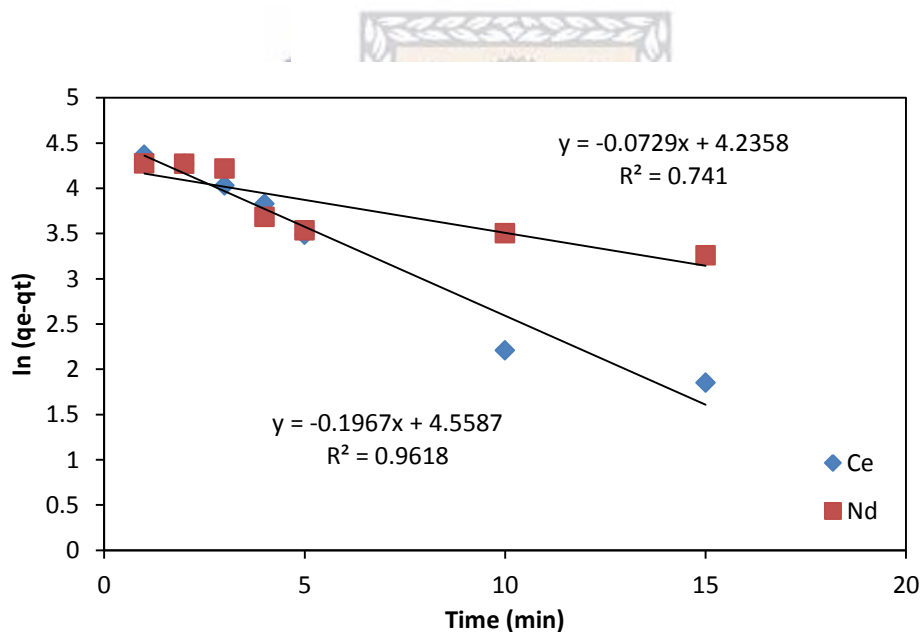


Figure 6.11. Adsorption kinetics of Nd^{3+} ; Ce^{3+} based on the pseudo-first-order model for PS-DGA-3-3

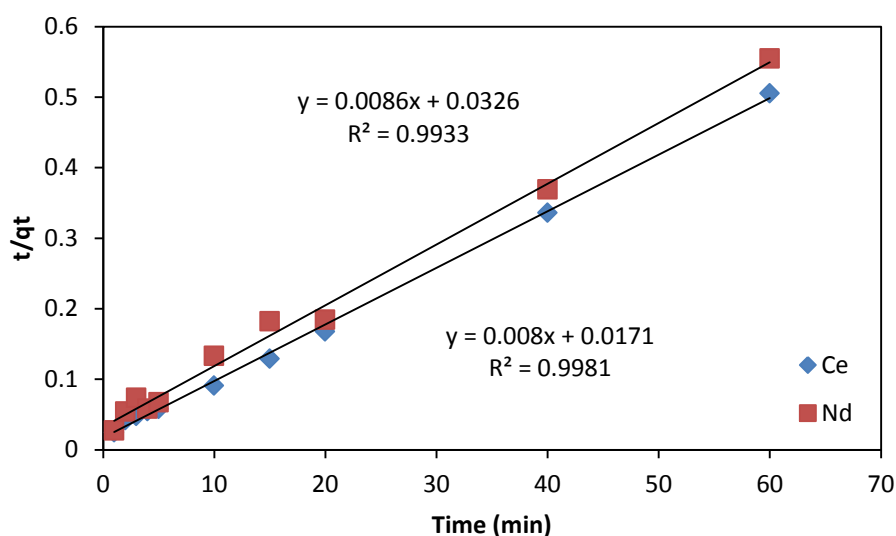


Figure 6.12. Adsorption kinetics of Nd^{3+} ; Ce^{3+} based on the pseudo-second-order model for PS-DGA-3-3

The kinetic data of Ce^{3+} or Nd^{3+} metal ions adsorption onto PS-DGA-3-3 nanofibre adsorbent were predicted by these kinetic models and the corresponding fitting parameters are summarised in Table 6.5.

Table 6.5. Comparison of the kinetics constants for the sorption of for Ce^{3+} or Nd^{3+} on PS-DGA-3-3

PS-DGA	Pseudo-first-order equation			Pseudo-second-order equation		
	q_e (mg/g)	k_1 (1/min)	R^2	q_e (mg/g)	k_2 (g/mg min)	R^2
Nd^{3+}	69.117	0.0729	0.741	116.279	0.00227	0.9933
Ce^{3+}	95.459	0.1967	0.9618	125	0.00374	0.9981

Table 6.5 above presents the constants of kinetic models for the adsorption of Ce^{3+} or Nd^{3+} on PS-DGA-3-3. The pseudo-second-order correlation coefficients (R^2 0.9981) for Ce^{3+} and (R^2 0.9933) for Nd^{3+} were higher than that of the pseudo-first-order model (R^2 0.9618) for Ce^{3+} and (R^2 0.741) for Nd^{3+} indicating that the correlation coefficient obtained for the pseudo-second-order kinetic model is greater

than 0.99 for both metals which is also higher than values for pseudo-first order and indicates that the pseudo-second order equation fits the experimental data well. Table 6.5 showed that the theoretical q_e values of the pseudo-second-order kinetic model are similar to the experimental values obtained in the study. The pseudo-second-order kinetic model provides the best correlation with the experimental data for the sorption of Ce^{3+} or Nd^{3+} onto PS-DGA-3-3 thus explaining the adsorption kinetics of Ce^{3+} or Nd^{3+} onto PS-DGA-3-3. The pseudo-second-order kinetic model assumes that the PS-DGA-3-3 surface is homogenous and contains the reactive groups which bind the metal ions, with the operating sorption mechanism being chemisorption, involving valency forces through sharing or exchange of electrons between metal ions and PS-DGA-3-3. The observed rapid kinetics have significant practical importance as this will facilitate the scale up of the process to smaller reactor volumes ensuring efficiency and economy.

6.4.2 Kinetic studies for PET-DGA-2-3

Based on the results of the contact time study, the adsorption kinetic data was analysed with both the pseudo-first-order model and the pseudo-second-order model. The trends of the two models can be seen in Figures 6.13 and 6.14 respectively. The adsorption kinetic plots for the adsorption of Ce^{3+} or Nd^{3+} metal ions are summarised and all the obtained kinetic parameters are depicted in Table 6.6.

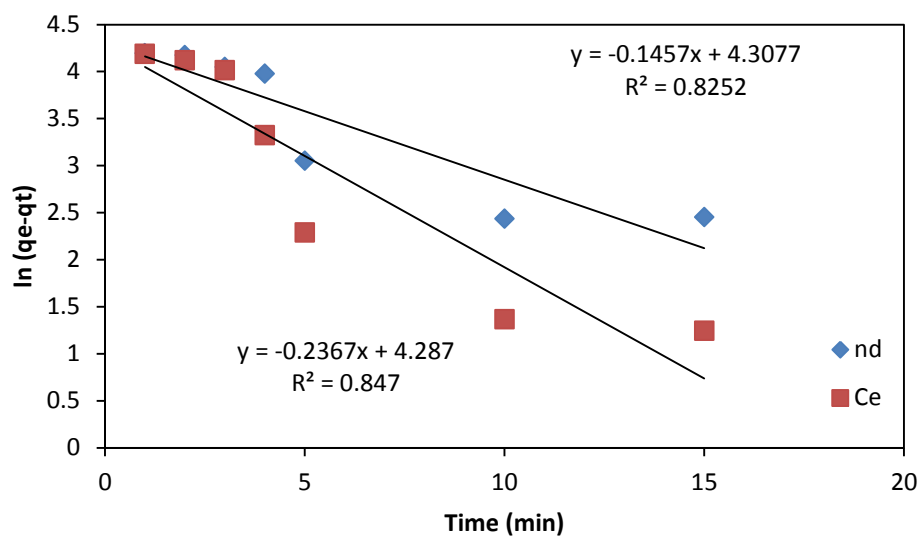


Figure 6.13. Adsorption kinetics of Nd^{3+} ; Ce^{3+} based on the pseudo-first-order model for PET-DGA-2-3

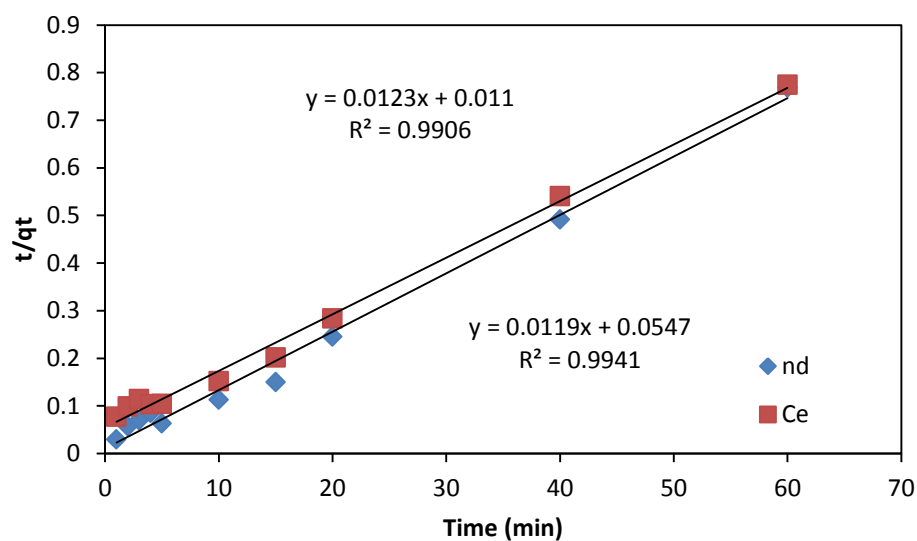


Figure 6.14. Adsorption kinetics of Nd^{3+} ; Ce^{3+} based on the pseudo-second-order model for PET-DGA-2-3

The analyses of the data obtained with the two models shown in Figures 6.13 and 6.14 is summarised and all the obtained kinetic parameters are listed in Table 6.6 below.

Table 6.6. The kinetics constants for the sorption of Ce^{3+} or Nd^{3+} on PET-DGA

PET-DGA	Pseudo-first-order equation			Pseudo-second-order equation		
	q _e (mg/g)	k ₁ (1/min)	R ²	q _e (mg/g)	k ₂ (g/mg min)	R ²
Nd ³⁺	74.2695	0.1457	0.825	81.3008	0.1375	0.991
Ce ³⁺	72.7479	0.2367	0.847	84.0336	0.0301	0.994

Table 6.6 showed coefficient (R^2) which was coherent with the pseudo-second-order equation. The pseudo-second-order correlation coefficients (R^2 0.994) for Ce^{3+} and (R^2 0.991) for Nd^{3+} were higher than that of the pseudo-first-order model (R^2 0.847) for Ce^{3+} and (R^2 0.825) for Nd^{3+} indicating that the pseudo-second-order model was more suitable for explaining the adsorption kinetics of Ce^{3+} or Nd^{3+} ions onto PET-DGA-2-3 nanofibre, which also revealed that chemisorption was the rate-determining step.

The results (the correlation coefficients R^2 listed in Table 6.6) clearly indicated that the adsorption kinetics closely followed the pseudo-second-order kinetic model rather than the pseudo-first-order kinetic model based on the obtained correlation coefficients (R^2). The results based on the obtained correlation coefficients (R^2), suggest that the overall rate of Ce^{3+} or Nd^{3+} adsorption by PET-DGA-2-3 is controlled by chemisorption as the rate-limiting step of the adsorption mechanism through sharing or exchanging electrons between the adsorbate and the adsorbent with no involvement of a mass transfer in solution.

The pseudo-second-order kinetic model also provided the best correlation of the experimental data in the studies carried out by Wang et al. (2012) on adsorption of Cu^{2+} and Ni^{2+} onto chelating fibres based on PET; on adsorption of Hg (II), Cu (II)

and Co(II) metal ions onto PET fibres (Monier and Abdel-Latif 2013) and on adsorption of Cr(VI) ions onto chelating fibres based on PET (Yiğitoğlu and Arslan 2009) which were studied and are all in agreement with the kinetic results found in this study.

6.5 Desorption and regeneration studies

Effective regeneration performance of an adsorbent is very important for its potential practical application. The experiments for desorption efficiency were carried out as set out in Chapter 3 Section 3.5.5. The experiments were carried out by using 1 M HNO₃ solution to regenerate the PS-DGA-3-3 or PET-DGA-2-3 nanofibres after adsorption of Ce³⁺ or Nd³⁺. After washing the mats with deionised water and drying in vacuum, the nanofibre mats were re-used in the three further adsorption - desorption cycles. The results of the desorption efficiency for Ce³⁺ and Nd³⁺ using PS-DGA-3-3 or PET-DGA-2-3 are shown in Table 6.7.

Table 6.7. Desorption efficiency for Ce³⁺ or Nd³⁺ from PS-DGA-3-3 and PET-DGA-2-3 for three cycles of adsorption-desorption (initial concentration - 100 mg/L; adsorbent dosage - 0.0075 g; stripping agent - 1 M HNO₃; desorption time - 60 min).

Recycle times	Desorption efficiency			
	(PS-DGA-3-3)		(PET-DGA-2-3)	
	Ce (%)	Nd (%)	Ce (%)	Nd (%)
1	98.7	97.6	98.6	91.3
2	98.5	95.3	97.9	91.1
3	96.7	92.1	96.5	90.1

As can be seen, the desorption efficiency for Ce³⁺ and Nd³⁺ reached 98.7 % and 97.6 % for the regeneration of the PS-DGA-3-3 and 98.6 % and 91.3 % for the regeneration rate of the PET-DGA-2-3 nanofibre. PS-DGA-3-3 maintained up to 92

% capacity for the removal of Nd^{3+} after 4 cycles but was able to maintain capacity for Ce^{3+} uptake up to 96.7 % of the initial concentration after four adsorption - desorption cycles. PET-DGA-2-3 uptake capacity was maintained over four cycles with capacity above 95% for Ce^{3+} and 90 % for Nd^{3+} without significant loss of their initial binding affinity. The nanofibres retained high uptake capacity after the third and the fourth cycles of adsorption–desorption. The main objective of the regeneration process is to restore the adsorption capacity of the exhausted adsorbent and to recover valuable components present in the adsorbed phase. These results compare favourably to the study by Galhoum et al. (2017) that used nitric acid (0.5 M solution) as regenerant to desorb Nd^{3+} from loaded sorbents.

The adsorption capacity of PET-DGA-2-3 remained almost constant for the four cycles of Nd^{3+} adsorption which indicated that there were no irreversible adsorption sites on the surface of the adsorbent, thus it could retain the original metal removal capacity after the successive adsorption–desorption process. The table also show that the regeneration was better achieved for PS-DGA-3-3 than PET-DGA-2-3 nanofibres since Ce^{3+} and Nd^{3+} uptake was maintained at a very high level after four repetitions of the adsorption–desorption cycles. This result indicated that PS-DGA-3-3 and PET-DGA-2-3 affinity nanofibres could be recycled conveniently at least four times without significant loss of their initial properties. Desorption studies help to elucidate the nature of the adsorption process and to recover the Ce^{3+} and Nd^{3+} from sorbents. Moreover, it is also important to be able to regenerate the sorbent so that it can be used again to adsorb metal ions, and thus develop a successful sorption process (Wan Ngah et al. 2002).

6.6 Selective adsorption

The experiments for selective adsorption were carried out as set out in Chapter 3 Section 3.5.6. Each metal ion (Ce^{3+} and Nd^{3+}) was tested separately in solutions and was therefore not a competitive adsorption. The experiments for selectivity using PS-DGA-3-3 and PET-DGA-2-3 nanofibres were executed in a 15 mL centrifuge tube containing 10 mL aqueous solution of a mixture of Ce^{3+} , Co^{2+} , Ni^{2+} and Sr^{2+} metal ions with the same concentration of each metal (100 mg/L), and a piece of nanofibre adsorbent of about 0.0075 g was inserted into the centrifuge tube containing the mixture to conduct the investigation of the selectivity of PS-DGA-3-3 and PET-DGA-2-3 toward REEs at pH of 6, chosen to be a suitable pH for optimum adsorption. Similarly, the adsorption of various metal ions in single ion solutions onto the PS-DGA-3-3 or PET-DGA-2-3 was also tested respectively. The amount of every metal ion adsorbed onto the PS-DGA-3-3 or PET-DGA-2-3 was evaluated and the results are summarised in Table 6.8 and Table 6.9 respectively. The selectivity coefficients (S) was described as set out in Chapter 3 Section 3.5.6 using Equation 3.7.

Table 6.8. Adsorption capacity of different metal ions in solution on PS-DGA-3-3 and their selectivity coefficients (S)

	Co^{2+}	Ni^{2+}	Sr^{2+}	Ce^{3+}
Single (mmol/g)	0.0469	0.0937	0.2118	0.7327
Mix (mmol/g)	0.0341	0.0852	0.0377	0.7159
S (Ce/M)	20.9801	8.4054	19.0055	1

Table 6.8 shows the adsorption capacities of different metal ions of PS-DGA-3-3. The PS-DGA-3-3 depicted better adsorption selectivity toward Ce^{3+} over other metal ions. The co-existence in solution of selected metal ions did not significantly interfere

with the adsorption of REEs binding to PS-DGA-3-3 as can be deduced from the higher selectivity coefficient. Table 6.9 also shows the adsorption capacities of different metal ions onto PET-DGA-2-3

Table 6.9. Adsorption capacity of different metal ions in solution on PET-DGA-2-3 and their selectivity coefficients

	Co ²⁺	Ni ²⁺	Sr ²⁺	Ce ³⁺
Single (mmol/g)	0.0686	0.2342	0.1965	0.8075
Mix (mmol/g)	0.0341	0.0870	0.1166	0.7131
S (Ce/M)	20.8972	8.1960	6.1170	1

It can be seen from Table 6.9 that the amount of Ce³⁺ adsorbed in the presence of interfering ions was 0.71 mmol g⁻¹, which is slightly lower than that (0.89 mmol g⁻¹) in single ions solution, attributable to the competitive adsorption from other miscellaneous metal ions present in solution, such as Co²⁺, Ni²⁺ and Sr²⁺ which could have led to a slight change in adsorption equilibrium. The lowest and highest selective adsorption coefficient was 20 for S_{Ce/Co} and 6 for S_{Ce/Sr}, respectively, revealing that the PET-DGA-2-3 showed much higher selectivity toward Ce³⁺ in the modelled solution than to the other metals investigated.

Ce³⁺ was selected for the experiments because both equilibrium and dynamic experiments showed that the nanofibre adsorbents had very similar sorption properties for the two REEs (Ce³⁺ and Nd³⁺) indicating that a selective separation of individual REEs may be difficult at the metal-binding equilibrium due to their close sorption capacities as shown previously in Table 6.1 and 6.2 for PS-DGA-3-3 and PET-DGA-2-3 respectively. Their individual differences were therefore not large enough and would therefore require more enrichment steps to achieve metal separation between these two REEs. In the recovery process of rare earth elements

from low grade ores and scrap, selective separation of dilute rare earth metal ions from solutions containing high concentrations of base metal ions such is required. PS-DGA and PET-DGA will therefore be useful for separation and recovery of REEs from base metals.

6.7 Chapter Summary

Chapter six discusses the results of the application of the polystyrene-diglycolic acid (PS-DGA-3-3) and polyethylene terephthalate-diglycolic acid (PET-DGA-2-3) modified nanofibres for the removal of Ce^{3+} and Nd^{3+} in synthetic solution. Different batch experiments were conducted in order to optimise the experimental conditions of Ce^{3+} or Nd^{3+} extraction. Adsorption parameters such as solution pH, contact time and initial concentration of Ce^{3+} and Nd^{3+} were optimised and the binding capacities determined. The modelling of sorption data obtained from different adsorption experiments with the Ce^{3+} and Nd^{3+} were performed and adsorption binding kinetics determined. The desorption and regeneration study of the adsorbent materials and their cycles of reusability including the selective separation of Ce^{3+} and Nd^{3+} were examined in this section.

The results of the different batch experiments conducted in order to optimise the effect of solution pH on the experimental conditions showed that the adsorption capacity for (Ce^{3+} and Nd^{3+}) increased with increasing pH value and the optimised pH of 6 was therefore selected for monitoring their adsorption on PS-DGA-3-3 and PET-DGA-2-3. The maximum Langmuir absorption capacities (q_m) for Ce^{3+} and Nd^{3+} were 152.5 mg/g (1.09 mmol/g) and 146.2 mg/g (1.01 mmol/g) respectively. This number is very close to the measured experimental values of 152.0 mg/g (1.09 mmol/g) for Ce^{3+} ; and 144.0 mg/g (0.998 mmol/g) for Nd^{3+} at the concentration of

140 mg/L indicating the dependability of q_e value and a higher sorption capacity, to PET-DGA-2-3 chelating nanofibre at 136.6 mg/g (0.975mmol/g) and 123.9 mg/g (0.859 mmol/g) for of Ce^{3+} and Nd^{3+} respectively which was achieved at a maximum concentration of 120 mg/L. Sorption isotherms were well fitted by the Langmuir equations for PS-DGA-3-3 and PET-DGA-2-3 chelating nanofibre with the values of the correlation coefficient R^2 (>0.99) being higher than for the Freundlich equation.

Kinetic profiles were well fitted by the pseudo-second order rate equation which coefficient (R^2) greater than 0.99 and higher than values obtained for pseudo-first order modelling for both PS-DGA-3-3 and PET-DGA-2-3. The PS-DGA-3-3 pseudo-second-order correlation coefficients (R^2 0.9981) for Ce^{3+} and (R^2 0.9933) for Nd^{3+} were higher than that of the pseudo-first-order model (R^2 0.9618) for Ce^{3+} and (R^2 0.741) for Nd^{3+} indicating that the pseudo-second order equation fits the experimental data well. Similarly, the pseudo-second-order model was more suitable for explaining the adsorption kinetics of Ce^{3+} or Nd^{3+} ions onto the PET-DGA-2-3 nanofibre adsorbent. The equilibrium was reached within 20 minutes of contact time, the fast adsorption during the first 4 min was related to the high amount of vacant surface sites of nanofibre adsorbent available for the adsorption of the metal ions while 60 minutes was adopted as the optimum time required for the adsorption to take place.

The highest selective adsorption coefficient was 20 for S Ce/Co , 19 for S Ce/Sr and 6 for S Ce/Sr respectively revealing that the PS-DGA-3-3 showed high selectivity toward Ce^{3+} with the lowest S Ce/Ce of 1 in the modelled solution than the other metals (Co^{2+} , Ni^{2+} and Sr^{2+}) investigated and also performed better than PET-DGA-

2-3 in selective adsorption. Ce^{3+} and Nd^{3+} can be readily desorbed from loaded sorbents using 1 M solution of nitric acid and the sorbents can be re-used with negligible loss in sorption performance for a minimum of 3 sorption/desorption cycles.



CHAPTER SEVEN**CONCLUSIONS, NOVELTY AND RECOMMENDATIONS****7 INTRODUCTION**

This chapter presents all the obtained findings and their conclusions. The novelty in the study and recommendations are presented in the second section of this chapter. Electrospinning, grafting of functional groups, chemical characterisations and adsorption procedures were carried out in order to achieve the objectives of this research. Many previous processes show limited applicability due to their small surface area and slow adsorption rate, which are also a disadvantage in the regeneration step. In comparison, this study develops a route for adsorption which has many material advantages such as low fibre weight, high porosity, low basis weight, cost effectiveness, large surface area, metal binding strength, regeneration of adsorbent, selective separation, reusability and less waste accumulation after usage.

7.1 Conclusions

This study provided answers to the following research questions;

- a. What are the optimum conditions for the polymers to be electrospun into nanofibres?

The optimum electrospinning conditions for the experiments were obtained under the following operating conditions: PS (concentration - 15 wt %; voltage - 17 kV; solution flow rate - 0.8 mL/h and collector distance - 15 cm) and PET (concentration - 10 wt %; voltage - 17 kV; solution flow rate - 1.0 mL/h and collector distance - 20 cm).

- b. Can these nanofibres be successfully functionalised with the selected ligands?

Yes, FTIR spectra of functionalised polystyrene nanofibres (PS-DGA-3) confirmed the stretching vibration peak of the carbonyl (-C=O) group at 1737 cm^{-1} , 1128 cm^{-1} and 1227 cm^{-1} on the polymer support while the peak at 1454 cm^{-1} which represented the -CH_2 bending peak of the polymer support remained intact confirming the nature and structure of PS nanofibre support.

FTIR spectra also confirmed the changes observed in PET structures when functionalised with DGA. A new peak at 1343 cm^{-1} was noted in the modified nanofibre which was assigned to the vibration peak of the carbonyl (-C-O) group from DGA. The C-O bond vibrations show that diglycolic groups have been successfully added to the PET skeleton of PET-DGA modified adsorbent (PET-DGA-2). SEM, TGA, XRD and BET analytical techniques also confirmed the introduction of functional groups to PET electrospun nanofibre support.

- c. How can the ligand binding be enhanced on the nanofibres?

The ligand binding was enhanced on the nanofibres as shown by results of experiments conducted to determine the optimum reaction time for the surface modification of PS and PET nanofibres and the concentration of DGA chelating ligand required for the modifications of electrospun PS and PET nanofibre. The obtained results confirmed the optimum amount of DGA as 3 g (0.026 mol) and the reaction time of 3 hours for PS-DGA and 2 g (0.017 mol) and 3 h modification time for PET-DGA was sufficient to enhance more groups on the surface of nanofibre which were characterised by FTIR, SEM, TGA, XRD and BET techniques.

d. How stable is the ligand on the nanofibres?

The study of the stability of DGA chelating moieties grafted on the surface of PS and PET nanofibres adsorbents was investigated and the results indicated that the chemical structure of the PS-DGA-3-3 was not adversely affected by any chemical degradation up to a concentration of 1.5 M nitric acid for 1 h exposure but EDTA caused instability, removing the ligand from the nanofibres. The grafted ligand on the PS-DGA-3-3 was removed by chemical degradation after EDTA contact and exposure. However, nitric acid and EDTA solution did not affect the bond between the ligand and PET in the case of PET-DGA-2-3 after 1 h exposure. The ligand is better adhered to the nanofibres on PET-DGA-2-3 than PS-DGA-3-3.

e. What are the adsorbents' capacity

The PS-DGA-3-3 maximum Langmuir absorption capacities (q_e) for Ce^{3+} or Nd^{3+} were 152.5 mg/g (1.09 mmol/g) or 146.2 mg/g (1.01 mmol/g) respectively while the maximum Langmuir absorption capacities on PET-DGA-2-3 chelating nanofibre were 136.6 mg/g (0.975 mmol/g) and 123.9 mg/g (0.859 mmol/g) for Ce^{3+} and Nd^{3+} respectively from the Langmuir isotherm. The new nanofibre adsorbents have sorption capacities at least comparable to more conventional sorbents and even better than some adsorbents reported in literature.

f. Which combination of polymer/ligand will be most effective for REE metal removal?

The Langmuir absorption capacities indicated that PS-DGA-3-3 affinity nanofibre was most effective for Ce^{3+} and Nd^{3+} at 152.5 mg/g (1.09 mmol/g) and 146.2 mg/g (1.01 mmol/g) at the pH of 6. The values of PS-DGA-3-3 and PET-DGA-2-3 are

competitive with that of other absorbents when compared with literature. The maximum capacity of DGA on PS nanofibre was 0.827 g g^{-1} which was responsible for the better performance of the PS-DGA-3-3 nanofibre when compared with the PET-DGA-2-3 obtained with 0.449 g g^{-1} conversion of DGA groups on the surface of PET nanofibres after the optimum reaction time. PS-DGA-3-3 nanofibre therefore possess more abundant etheric oxygen and carbonyl ($> \text{C}=\text{O}$) groups which enhanced the removal and selectivity towards trivalent lanthanides.

- g. How effectively will these functionalised nanofibres recover different REE metals from the model aqueous solution?

The PS-DGA-3-3 and PET-DGA-2-3 nanofibre depicted enhanced selectivity and showed significantly higher affinity toward Ce^{3+} over other metal ions such as Co^{2+} , Ni^{2+} and Sr^{2+} in a complex solution. The co-existence of these selected metal ions did not significantly interfere with the adsorption of REEs binding to PS-DGA-3-3 or PET-DGA-2-3, as could be seen from the selectivity coefficient adsorption experiments.

- h. What is the effect of change in pH, time, and concentration on the adsorption of REEs by the new functionalised PS and PET nanofibres?

Results obtained with PS-DGA-3-3 showed that as the pH value rises, and the concentration of H^+ ions decreases, the adsorption capacity increased with increasing pH value. Adsorption reached the maximum amount of 0.308 and 0.570 mmol/g for Ce^{3+} or Nd^{3+} at pH 6 respectively. The effect of contact time on adsorption of Ce^{3+} and Nd^{3+} metal ions onto PS-DGA-3-3 nanofibre adsorbent showed that high adsorption capacities were attained within a few minutes and equilibrium was

reached within 20 minutes for each of the two metal solutions respectively. The total adsorption of Ce^{3+} or Nd^{3+} metal ions was obtained within 1 h and the results showed that sorption sites were still available for adsorption but limited by the solute availability during the binding experiments. The maximum adsorption capacities of Ce^{3+} or Nd^{3+} ions on the PS-DGA-3-3 chelating nanofibre were 1.09 mmol/g or 0.99 mmol/g respectively at the initial metal concentrations of 140 mg/L.

The adsorption capacity of PET-DGA-2-3 increased with an increasing pH value and reached the maximum amount of 0.386 and 0.365 mmol/g for Ce^{3+} or Nd^{3+} at pH 6, respectively. The metal uptake was rapid within the first 10 minutes before reaching quasi equilibrium conditions at 10 minutes for either Ce^{3+} or Nd^{3+} , thereafter; there was an increase in the adsorption binding capacity which peaked at 15 mins and started a decline for Nd^{3+} but fluctuated slightly for Ce^{3+} and over 90% of total adsorption of Ce^{3+} or Nd^{3+} occurred within the first 15 min, which was reached at 0.706 mmol/g Ce^{3+} and 0.695 mmol/g Nd^{3+} respectively. The adsorption of Ce^{3+} or Nd^{3+} reached a plateau state at a concentration of ca. 120 mg/L. The maximum adsorption capacities of Ce^{3+} or Nd^{3+} ions on the PET-DGA-2-3 chelating nanofibre membranes were 0.969 mmol/g or 0.857 mmol/g respectively.

i. Can these adsorbent be regenerated?

The possibility to regenerate the synthesised nanofibre for reuse is one of the most important factors considered to achieve much more feasibility and cost effectiveness for this process. The desorption efficiency for Ce^{3+} or Nd^{3+} reached 98.7 % and 97.6 % for the regeneration of the PS-DGA-3-3 and 98.6 % or 91.3 % for the regeneration of the PET-DGA-2-3 nanofibre without significant loss of their initial binding affinity over three cycles. Overall, PS-DGA-3-3 performed better and its

removal capacity was maintained up to 92 % for Nd^{3+} and up to 96.7 % for Ce^{3+} after three adsorption–desorption cycles but the removal capacity of PET-DGA-2-3 capacity was somewhat lower after three cycles, at 90 % for Nd^{3+} and 96.5% for Ce^{3+} . The nanofibres retained high removal capacity at the second and the third cycles of adsorption–desorption. Ce^{3+} was selected for the experiments because both equilibrium and dynamic experiments showed that the nanofibre adsorbents had very similar sorption properties for the two REEs indicating that a selective separation of individual REEs may be difficult at the metal-binding equilibrium due to their close sorption capacities.

7.2 Novelty

This study has been able to improve the capacity of PS and PET nanofibres by chemically attaching the DGA chelating ligand to the surface to afford a strong affinity for REEs especially for Ce^{3+} and Nd^{3+} and for the fast adsorption capacities which were achieved within the first 20 min and which was related to the high amount of surface sites available on the nanofibre adsorbent for the adsorption of the metal ions. The results of regeneration and stability of the functionalised nanofibres materials revealed that PS and PET nanofibres after modification with DGA chelating ligand were strongly bonded and proved to be suitable materials for Ce^{3+} and Nd^{3+} removal even from a mixed metal matrix.

As far as could be ascertained, no studies have been conducted on the surface modification of PS and PET nanofibres using DGA chelating ligand for Ce^{3+} and Nd^{3+} adsorption from aqueous solution. No studies have investigated the regenerability and stability of the grafted DGA ligand moieties on the PS and PET nanofibres using different regenerating agents such as EDTA and HNO_3 . This study revealed that HNO_3 is the most suitable regenerating agent for PS-DGA-3-3 and

PET-DGA-2-3 adsorbents without detaching the grafted ligand moieties from the surface of nanofibres. PET-DGA-2-3 adsorbent was also stable in EDTA after the stability studies. The study also demonstrated that PS-DGA-3-3 and PET-DGA-2-3 adsorbents had better adsorption selectivity toward REE (Ce^{3+}) than other metal ions (Co^{2+} , Ni^{2+} and Sr^{2+}) and that the co-existence of these selected metal ions did not significantly interfere with the adsorption of REEs binding therefore making these materials very suitable selective chelating adsorbents for existing industrial separations.

7.3 Recommendations

The study recommends a further study of the extraction behaviour of the ligands and the grafted systems for the selective extraction of some other REEs in order to explore or understand the grafted ligand influence on the selective extraction of any selected REEs. This study also recommends further selectivity studies using the PS-DGA-3-3 and PET-DGA-2-3 nanofibres to separate between individual REE's metal ions. This study also recommends further investigations on the adsorption behaviour of the nanofibre adsorbents in order to clarify the REE ion adsorption mechanism and also determine what mode of chelation conferred the high adsorption and selectivity for REE ions.

This study also recommends that further stability investigation should be conducted on the polystyrene nanofibre after modification to determine the effect of crosslinking on the adsorbent or trying out some other different modification strategies for the chemical attachment of the ligand to the nanofibre support. It will be interesting to test the properties and the crosslinking effect of PS and PET after modification by comparing the regeneration and stability after modification to those of other modification derivatives to better understand what is responsible for the

ligand stability. The critical role of the support may further be discernible by comparing the effect of a linker group attachment between the support and ligand to confirm if this will also increase the stability and adsorption capacity.



REFERENCES

- Abbasi A, Lindqvist-Reis P, Eriksson L, Sandström D, Lidin S, Persson I, Sandström M. 2005. Highly hydrated cations: Deficiency, mobility, and coordination of water in crystalline nonhydrated scandium (III), yttrium (III), and lanthanoid (III) trifluoromethanesulfonates. *Chemistry-A European Journal* 11(14):4065-77.
- Abbasizadeh S, Keshtkar AR, Mousavian MA. 2013. Preparation of a novel electrospun polyvinyl alcohol/titanium oxide nanofiber adsorbent modified with mercapto groups for uranium (VI) and thorium (IV) removal from aqueous solution. *Chemical Engineering Journal* 220:161-71.
- Abdolahifard M, Bahrami SH, Malek R. 2011. Surface modification of PET fabric by graft copolymerization with acrylic acid and its antibacterial properties. *ISRN Organic Chemistry* 2011 (265415): 1-8. doi:10.5402/2011/265415.
- Abdouss M, Shoushtari AM, Haji A, Moshref B. 2012. Fabrication of chelating diethylenetriaminated pan micro- and nano-fibers for heavy metal removal. *Chemical Industry & Chemical Engineering Quarterly* 18(1):27-34.
- Abreu RD and Morais CA. 2014. Study on separation of heavy rare earth elements by solvent extraction with organophosphorus acids and amine reagents. *Minerals Engineering* 61:82-7.
- Agrawal Y, Kaur H, Menon S. 1999. Poly (styrene-p-hydroxamic acids): Synthesis, and ion exchange separation of rare earths. *Reactive and Functional Polymers* 39(2):155-64.
- Ahad I, Bartnik A, Fiedorowicz H, Kostecki J, Korczyc B, Ciach T, Brabazon D. 2014. Surface modification of polymers for biocompatibility via exposure to extreme ultraviolet radiation. *Journal of Biomedical Materials Research Part A* 102(9):3298-310.

- Aksu Z. 2002. Determination of the equilibrium, kinetic and thermodynamic parameters of the batch biosorption of nickel (II) ions onto chlorella vulgaris. *Process Biochemistry* 38(1):89-99.
- Alexandratos SD and Crick DW. 1996. Polymer-supported reagents: Application to separation science. *Industrial & Engineering Chemistry Research* 35(3):635-44.
- Aliabadi M, Irani M, Ismacili J, Najafzadeh S. 2014. Design and evaluation of chitosan/hydroxyapatite composite nanofiber membrane for the removal of heavy metal ions from aqueous solution. *Journal of the Taiwan Institute of Chemical Engineers* 45(2):518-26.
- Alonso E, Sherman AM, Wallington TJ, Everson MP, Field FR, Roth R, Kirchain RE. 2012. Evaluating rare earth element availability: A case with revolutionary demand from clean technologies. *Environmental Science & Technology* 46(6):3406-14.
- Amin M, Alazba A, Manzoor U. 2014. A review of removal of pollutants from water/wastewater using different types of nanomaterials. *Advances in Materials Science and Engineering* 825910: 1-24. doi:10.1155/2014/825910.
- Ansari SA, Pathak P, Mohapatra PK, Manchanda VK. 2011. Chemistry of diglycolamides: Promising extractants for actinide partitioning. *Chemical Reviews* 112(3):1751-72.
- Awual MR, Hasan MM, Shahat A, Naushad M, Shiwaku H, Yaita T. 2015. Investigation of ligand immobilized nano-composite adsorbent for efficient cerium (III) detection and recovery. *Chemical Engineering Journal* 265:210-8.
- Bachman GB, Hellman H, Robinson K, Finholt R, Kahler E, Filar L, Heisey L, Lewis L, Micucci D. 1947. A new method of preparing substituted vinyl compounds. depolymerization studies on vinyl polymers. 1, 2. *The Journal of Organic Chemistry* 12(1):108-21.

- Bahramzadeh A, Zahedi P, Abdouss M. 2016. Acrylamide-plasma treated electrospun polystyrene nanofibrous adsorbents for cadmium and nickel ions removal from aqueous solutions. *Journal of Applied Polymer Science* 133(5).
- Bartolome L, Cho BG, Do Hyun Kim, Imran M, Al-Masry WA. 2012. Recent developments in the chemical recycling of PET. In: *Material Recycling - Trends and Perspectives*. Dimitris S. Achilias (Eds). INTECH Open. 1-148. DOI: 10.5772/2003
- Bauer D, Diamond D, Li J, Sandalow D, Telleen P, Wanner B. 2010. US Department of Energy critical materials strategy. US Department of Energy Technical Report. <https://www.osti.gov/scitech/biblio/1000846>.
- Baumgarten PK. 1971. Electrostatic spinning of acrylic microfibers. *Journal of colloid and interface science* 36(1):71-9.
- Beachley V and Wen X. 2009. Effect of electrospinning parameters on the nanofiber diameter and length. *Materials Science and Engineering: C* 29(3):663-8.
- Bessbousse H, Rhlalou T, Verchere J, Lebrun L. 2009. Novel metal-complexing membrane containing poly (4-vinylpyridine) for removal of Hg (II) from aqueous solution. *The Journal of Physical Chemistry B* 113(25):8588-98.
- Bhardwaj N and Kundu SC. 2010. Electrospinning: A fascinating fiber fabrication technique. *Biotechnology advances* 28(3):325-47.
- Bhattacharyya A, Mohapatra P, Roy A, Gadly T, Ghosh S, Manchanda V. 2009. Ethyl-bis-triazinylpyridine (et-BTP) for the separation of americium (III) from trivalent lanthanides using solvent extraction and supported liquid membrane methods. *Hydrometallurgy* 99(1):18-24.
- Binnemans K, Jones PT, Blanpain B, Van Gerven T, Yang Y, Walton A, Buchert M. 2013. Recycling of rare earths: A critical review. *Journal of Cleaner Production* 51:1-22.

- Birkholz M, Freixa Z, van Leeuwen PW. 2009. Bite angle effects of diphosphines in C–C and C–X bond forming cross coupling reactions. *Chemical Society Reviews* 38(4):1099-118.
- Biswas M and Chatterjee S. 1983. Chemical modification of polystyrene—IV. electrophilic substitution of polystyrene with cis-1, 2, 3, 6 tetrahydrophthalic anhydride. *European Polymer Journal* 19(4):317-20.
- Biswas M and Chatterjee S. 1982. Chemical modification of polystyrene. I. electrophilic substitution of polystyrene with aromatic anhydrides. *Journal of Applied Polymer Science* 27(10):3851-7.
- Blanchette JA and Cotman Jr JD. 1958. Synthesis of polyfunctional Polymers. *Journal of Organic Chemistry* 23(8):1117-22.
- Blissett R, Smalley N, Rowson N. 2014. An investigation into six coal fly ashes from the united kingdom and poland to evaluate rare earth element content. *Fuel* 119:236-9.
- Bode-Aluko CA, Perea O, Ndayambaje G, Petrik L. 2017(a). Adsorption of toxic metals on modified polyacrylonitrile nanofibres: A review. *Water, Air, & Soil Pollution* 228(1):35.
- Bode-Aluko CA, Perea O, Fatoba O, Petrik L. 2017. Surface-modified polyacrylonitrile nanofibres as supports. *Polymer Bulletin* 74(6): 2431-42
- Boerio F, Bahl S, McGraw G. 1976. Vibrational analysis of polyethylene terephthalate and its deuterated derivatives. *Journal of Polymer Science: Polymer Physics Edition* 14(6):1029-46.
- Breda S, Reva I, Fausto R. 2008. Molecular structure and vibrational spectra of 2 (5H)-furanone and 2 (5H)-thiophenone isolated in low temperature inert matrix. *Journal of Molecular Structure* 887(1):75-86.
- Bruckenstein S and Miller B. 1977. Unraveling reactions with rotating electrodes. *Accounts of Chemical Research* 10(2):54-61.

- Brunauer S, Emmett PH, Teller E. 1938. Adsorption of gases in multimolecular layers. *Journal of American Chemical Society* 60(2):309-19.
- Buchko CJ, Chen LC, Shen Y, Martin DC. 1999. Processing and microstructural characterization of porous biocompatible protein polymer thin films. *Polymer* 40(26):7397-407.
- Castor SB and Hedrick JB. 2006. Rare earth elements. *Industrial Minerals Volume, 7th Edition: Society for Mining, Metallurgy, and Exploration, Littleton, Colorado* :769-92.
- Çelik İ, Kara D, Karadaş C, Fisher A, Hill SJ. 2015. A novel ligandless-dispersive liquid–liquid microextraction method for matrix elimination and the preconcentration of rare earth elements from natural waters. *Talanta* 134:476-81.
- Chan C, Ko T, Hiraoka H. 1996. Polymer surface modification by plasmas and photons. *Surface Science Reports* 24(1-2):1-54.
- Chang X, Yang X, Wei X, Wu K. 2001. Efficiency and mechanism of new poly (acryl-phenylamidrazone phenylhydrazide) chelating fiber for adsorbing trace Ga, In, Bi, V and Ti from solution. *Analytica chimica acta* 450(1):231-8.
- Charalampides G., Vatalis K., Karayannis V. and Baklavaridis A. 2016. Environmental defects and economic impact on global market of rare earth metals. *IOP conference series: Materials science and engineering. IOP Publishing* 161: 012069 p.
- Chase G and Reneker D. 2004. Nanofibers in filter media. *Fluid/Particle Separation Journal* 16(2):105-17.
- Cháuque EFC, Dlamini LN, Adelodun AA, Greyling CJ, Catherine Ngila J. 2016. Modification of electrospun polyacrylonitrile nanofibers with EDTA for the removal of Cd and Cr ions from water effluents. *Applied Surface Science* 369:19-28.

- Chen A, Liu S, Chen C, Chen C. 2008. Comparative adsorption of Cu (II), Zn (II), and Pb (II) ions in aqueous solution on the crosslinked chitosan with epichlorohydrin. *Journal of Hazardous materials* 154(1):184-91.
- Chen S, Zou Y, Yan Z, Shen W, Shi S, Zhang X, Wang H. 2009. Carboxymethylated-bacterial cellulose for copper and lead ion removal. *Journal of Hazardous materials* 161(2):1355-9.
- Chen Z. 2011. Global rare earth resources and scenarios of future rare earth industry. *Journal of Rare Earths* 29(1):1-6.
- Chen Z, Hay J, Jenkins M. 2013. The thermal analysis of poly (ethylene terephthalate) by FTIR spectroscopy. *Thermochimica Acta* 552:123-30.
- Chen Z, Hay J, Jenkins M. 2012. FTIR spectroscopic analysis of poly (ethylene terephthalate) on crystallization. *European Polymer Journal* 48(9):1586-610.
- Chen Z, Mo X, Qing F. 2007. Electrospinning of collagen–chitosan complex. *Materials Letters* 61(16):3490-4.
- Chung DDL. 2013. Composite materials: Functional materials for modern technologies. (Eds) Springer-Verlag London Ltd.: Springer Science & Business Media. Technology & Engineering - 289 p
- Coşkun R. 2008. Synthesis of functionalized poly (ethylene terephthalate) fibers by grafting of crotonic acid/methacrylamide monomer mixture. *Reactive and Functional Polymers* 68(12):1704-14.
- Cossy C, Helm L, Merbach AE. 1989. High-pressure NMR study. 38. water-exchange mechanisms on the terbium to thulium octa-aqualanthanide (III) ions: A variable-pressure oxygen-17 NMR study. *Inorganic Chemistry* 28(14):2699-703.
- Cotton S. 2006. Introduction to the lanthanides. In *Lanthanide and Actinide Chemistry* (Eds). Chichester, UK: John Wiley & Sons, Ltd. DOI: 10.1002/0470010088.

- Cramariuc B, Cramariuc R, Scarlet R, Manea LR, Lupu IG, Cramariuc O. 2013. Fiber diameter in electrospinning process. *Journal of Electrostatics* 71(3):189-98.
- Crittenden B and Thomas WJ. 1998. Adsorption technology & design. *Technology & Engineering*. Butterworth-Heinemann, Oxford: 1-288.
- Cui W, Li X, Zhou S, Weng J. 2007. Investigation on process parameters of electrospinning system through orthogonal experimental design. *Journal of Applied Polymer Science* 103(5):3105-12.
- Danafar F, Fakhru'l-Razi A, Salleh MAM, Biak DRA. 2009. Fluidized bed catalytic chemical vapor deposition synthesis of carbon nanotubes—a review. *Chemical Engineering Journal* 155(1):37-48.
- Darko G, Chigome S, Tshentu Z, Torto N. 2011. Enrichment of cu(II), ni(II), and pb(II) in aqueous solutions using electrospun polysulfone nanofibers functionalized with 1-[bis[3-(dimethylamino)-propyl]amino]-2-propanol. *Analytical Letters* 44(11):1855-67.
- Das N and Das D. 2013. Recovery of rare earth metals through biosorption: An overview. *Journal of Rare Earths* 31(10):933-43.
- Davis ME and Davis RJ. 2012. *Fundamentals of chemical reaction engineering*. (Eds) Courier Corporation: Dover, Mineola. New York. 368 p
- Deb A, Ilaiyaraja P, Ponraju D, Venkatraman B. 2011. Diglycolamide functionalized multi-walled carbon nanotubes for removal of uranium from aqueous solution by adsorption. *Journal of Radioanalytical and Nuclear Chemistry* 291(3):877-83.
- Deitzel J, Kleinmeyer J, Harris D, Beck Tan N. 2001a. The effect of processing variables on the morphology of electrospun nanofibers and textiles. *Polymer* 42(1):261-72.
- Deitzel J, Kleinmeyer J, Hirvonen J, Tan NB. 2001b. Controlled deposition of electrospun poly (ethylene oxide) fibers. *Polymer* 42(19):8163-70.

- Demir MM, Yilgor I, Yilgor E, Erman B. 2002. Electrospinning of polyurethane fibers. *Polymer* 43(11):3303-9.
- Demirbas A. 2008. Heavy metal adsorption onto agro-based waste materials: A review. *Journal of Hazardous Materials* 157(2):220-9.
- Deng S, Bai R, Chen J. 2003. Behaviors and mechanisms of copper adsorption on hydrolyzed polyacrylonitrile fibers. *Journal of colloid and interface science* 260(2):265-72.
- Dharanivasan G, Rajamuthuramalingam T, Jesse DMI, Rajendiran N, Kathiravan K. 2015. Gold nanoparticles assisted characterization of amine functionalized polystyrene multiwell plate and glass slide surfaces. *Applied Nanoscience* 5(1):39-50.
- Djebara M, Stoquert J, Abdesselam M, Muller D, Chami A. 2012. FTIR analysis of polyethylene terephthalate irradiated by MeV he. *Nuclear Instruments and Methods in Physics Research Section B: Beam Interactions with Materials and Atoms* 274:70-7.
- Dodson J, Hunt A, Parker H, Yang Y, Clark J. 2012. Elemental sustainability: Towards the total recovery of scarce metals. *Chemical Engineering and Processing: Process Intensification* 51:69-78.
- Dolak I, Keçili R, Hür D, Ersöz A, Say R. 2015. Ion-imprinted polymers for selective recognition of neodymium (III) in environmental samples. *Industrial & Engineering Chemistry Research* 54(19):5328-35.
- Dong XC, Cao D, Shi Y, Fu ZF. 2013. Fast removal of cu (II) from aqueous solutions by PET nanofibrous membrane modified with acryamide. *Advanced Materials Research* 750-752:1343-6.
- Dong Z, Wang B, Ma X, Wei Y, Xu Z. 2015. FAS grafted electrospun poly (vinyl alcohol) nanofiber membranes with robust superhydrophobicity for membrane distillation. *ACS Applied Materials & Interfaces* 7(40):22652-9.

- Dorfner K. 1991. Ion exchangers. fourth ed. Walter de Gruyter. Mannheim., Germany: 1-1526.
- Doshi J and Reneker DH. 1995. Electrospinning process and applications of electrospun fibers. *Journal of Electrostatics* 35(2-3):151-60.
- Drost Danielle and Wang Rongchang. 2016. Rare earth element criticality and sustainable management. 4th international conference on sensors, measurement and intelligent materials 22015: pp 914-919.
- Du X and Graedel TE. 2011. Global in-use stocks of the rare earth elements: A first estimate. *Environmental Science & Technology* 45(9):4096-101.
- Dubey SS and Rao BS. 2011. Removal of cerium ions from aqueous solution by hydrous ferric oxide—a radiotracer study. *Journal of hazardous materials* 186(2):1028-32.
- Dupont D, Brullot W, Bloemen M, Verbiest T, Binnemans K. 2014. Selective uptake of rare earths from aqueous solutions by EDTA-functionalized magnetic and nonmagnetic nanoparticles. *ACS Applied Materials & Interfaces* 6(7):4980-8.
- EC-European Commission. 2010. Critical raw materials for the EU. Report of the ad-hoc working group on defining critical raw materials. <http://www.euromines.org/files/what-we-do/sustainable-development-issues/2010-report-critical-raw-materials-eu.pdf>.
- El-Didamony H, Ali M, Awwad N, Fawzy M, Attallah M. 2012. Treatment of phosphogypsum waste using suitable organic extractants. *Journal of Radioanalytical and Nuclear Chemistry* 291(3):907-14.
- El-Naggar AY. 2013. Thermal analysis of the modified and unmodified silica gels to estimate their applicability as stationary phase in gas chromatography. *Journal of Emerging Trends in Engineering and Applied Sciences* 4(1):144-8.

- Elsalamouny AR, Desouky OA, Mohamed SA, Galhoum AA, Guibal E. 2017a. Uranium and neodymium biosorption using novel chelating polysaccharide. *International Journal of Biological Macromolecules* 104:963-8.
- Elsalamouny AR, Desouky OA, Mohamed SA, Galhoum AA, Guibal E. 2017b. Evaluation of adsorption behavior for U (VI) and Nd (III) ions onto fumarated polystyrene microspheres. *Journal of Radioanalytical and Nuclear Chemistry* 314 (1): 429–437.
- Eser A, Tirtom VN, Aydemir T, Becerik S, Dinçer A. 2012. Removal of nickel (II) ions by histidine modified chitosan beads. *Chemical Engineering Journal* 210:590-6.
- Esmâ B, Omar A, Amine DM. 2014. Comparative study on lanthanum (III) sorption onto lewatis TP 207 and lewatis TP 260. *Journal of Radioanalytical and Nuclear Chemistry* 299(1):439-46.
- Fakirov S. 2016. Nano-size polymers: Preparation, properties, applications. (Eds) Springer Ag Switzerland pp 1-399.
- Fang J, Niu H, Lin T, Wang X. 2008. Applications of electrospun nanofibers. *Chinese Science Bulletin* 53(15):2265-86.
- Fayemi OE, Ogunlaja AS, Kempgens PFM, Antunes E, Torto N, Nyokong T, Tshentu ZR. 2013. Adsorption and separation of platinum and palladium by polyamine functionalized polystyrene-based beads and nanofibers. *Minerals Engineering* 53:256-65.
- Feng L, Li S, Li H, Zhai J, Song Y, Jiang L, Zhu D. 2002. Super-hydrophobic surface of aligned polyacrylonitrile nanofibers. *Angewandte Chemie* 114(7):1269-71.
- Feng S, Shen X, Ji Y. 2011. Submicron ion-exchange fibers of polystyrene and styrene-butadiene-styrene copolymer blends. *Journal of Macromolecular Science, Part B* 50(9):1673-81.

- Florek J, Mushtaq A, Larivière D, Cantin G, Fontaine F, Kleitz F. 2015. Selective recovery of rare earth elements using chelating ligands grafted on mesoporous surfaces. *RSC Advances* 5(126):103782-9.
- Fong H, Chun I, Reneker D. 1999. Beaded nanofibers formed during electrospinning. *Polymer* 40(16):4585-92.
- Foo K and Hameed B. 2010. Insights into the modeling of adsorption isotherm systems. *Chemical Engineering Journal* 156(1):2-10.
- Foo K and Hameed B. 2009. An overview of landfill leachate treatment via activated carbon adsorption process. *Journal of hazardous materials* 171(1):54-60.
- Forward KM, Flores A, Rutledge GC. 2013. Production of core/shell fibers by electrospinning from a free surface. *Chemical Engineering Science* 104:250-9.
- Freeman HM. 1989. *Standard handbook of hazardous waste treatment and disposal*. New York, NY (US); McGraw-Hill Book Company. <http://113.160.249.209:8080/xmlui/handle/123456789/14730>
- Freixa Z and Van Leeuwen PW. 2003. Bite angle effects in diphosphine metal catalysts: Steric or electronic? *Dalton Transactions* (10):1890-901.
- Frenot A and Chronakis IS. 2003. Polymer nanofibers assembled by electrospinning. *Current Opinion in Colloid & Interface Science* 8(1):64-75.
- Freundlich H. 1906a. Over the adsorption in solution. *Journal of Physical Chemistry* 57(385):e470.
- Freundlich U. 1906b. *Die adsorption in losungen*. (2nd Eds) Wilhelm Engelmann in Leipzig.
- Frontier Rare Earths. 2015. Zandkopsdrift - Africa's Leading Rare Earth Project [Internet]; c2015 [cited 2017 May/05]. Available from: <http://www.frontierrareearths.com/wp-content/uploads/2015/06/Frontier-Corporate-Presentation-June-2015.pdf>.

- Fu F and Wang Q. 2011. Removal of heavy metal ions from wastewaters: A review. *Journal of environmental management* 92(3):407-18.
- Galhoum AA, Hassan KM, Desouky OA, Masoud AM, Akashi T, Sakai Y, Guibal E. 2017. Aspartic acid grafting on cellulose and chitosan for enhanced Nd (III) sorption. *Reactive and Functional Polymers* 113:13-22.
- Galhoum AA, Mahfouz MG, Atia AA, Gomaa NA, Abdel-Rehem ST, Vincent T, Guibal E. 2016. Alanine and serine functionalized magnetic nano-based particles for sorption of Nd (III) and Yb (III). *Advances in environmental research* 5(1):1-18.
- Galhoum AA, Mahfouz MG, Abdel-Rehem ST, Gomaa NA, Atia AA, Vincent T, Guibal E. 2015. Diethylenetriamine-functionalized chitosan magnetic nano-based particles for the sorption of rare earth metal ions [Nd (III), Dy (III) and Yb (III)]. *Cellulose* 22(4):2589-605.
- Galster H. 1991. pH measurement: Fundamentals, methods, applications, instrumentation. VCH, Weinheim; New York pp 1-356.
- Garg K and Bowlin GL. 2011. Electrospinning jets and nanofibrous structures. *Biomicrofluidics* 5(1):013403.
- Gasser M and Aly M. 2013. Separation and recovery of rare earth elements from spent nickel–metal-hydride batteries using synthetic adsorbent. *International Journal of Mineral Processing* 121:31-8.
- Geng X, Kwon O, Jang J. 2005. Electrospinning of chitosan dissolved in concentrated acetic acid solution. *Biomaterials* 26(27):5427-32.
- Gerente C, Lee V, Cloirec PL, McKay G. 2007. Application of chitosan for the removal of metals from wastewaters by adsorption—mechanisms and models review. *Critical Reviews in Environmental Science and Technology* 37(1):41-127.

- Gładysz-Plaska A, Majdan M, Grabias E. 2014. Adsorption of La, Eu and Lu on raw and modified red clay. *Journal of Radioanalytical and Nuclear Chemistry* 301(1):33-40.
- Goon IY, Zhang C, Lim M, Gooding JJ, Amal R. 2010. Controlled fabrication of polyethylenimine-functionalized magnetic nanoparticles for the sequestration and quantification of free Cu^{2+} . *Langmuir* 26(14):12247-52.
- Gu S and Ren J. 2005. Process optimization and empirical modeling for electrospun poly (D, l-lactide) fibers using response surface methodology. *Macromolecular Materials and Engineering* 290(11):1097-105.
- Gugliuzza A. 2014. Smart membranes and sensors: Synthesis, characterization, and applications. Edited by Annarosa Gugliuzza. John Wiley & Sons. Hoboken, New Jersey. p 450.
- Guimarães DH, Brioude MdM, Fiúza RdP, Prado, Luis Antônio Sanches de Almeida, Boaventura JS, José NM. 2007. Synthesis and characterization of polyesters derived from glycerol and phthalic acid. *Materials Research* 10(3):257-60.
- Guo Y, Zhang S, Lai L, Wang G. 2015. Rare earth elements in oolong tea and their human health risks associated with drinking tea. *Journal of Food Composition and Analysis* 44:122-7.
- Gupta SS and Bhattacharyya KG. 2012. Adsorption of heavy metals on kaolinite and montmorillonite: A review. *Physical Chemistry Chemical Physics* 14(19):6698-723.
- Hadjizadeh A, Aji A, Bureau MN. 2011. Nano/micro electro-spun polyethylene terephthalate fibrous mat preparation and characterization. *Journal of the Mechanical Behavior of Biomedical Materials* 4(3):340-51.
- Haghi A and Akbari M. 2007. Trends in electrospinning of natural nanofibers. *Physica Status Solidi (a)* 204(6):1830-4.

- Hakkarainen M. 2002. Aliphatic polyesters: Abiotic and biotic degradation and degradation products. In: Degradable aliphatic polyesters. Advances in Polymer Science, Springer, Berlin, Heidelberg (157) p 113-138.
- Han L, Andraday AL, Davis JL, inventors; Porous and non-porous nanostructures and application thereof. US Patent 8,714,776 B2.
- Hart F. 1987. Scandium, yttrium and the lanthanides. In: Comprehensive coordination chemistry. the synthesis, reactions, properties and applications of coordination compounds. V. 3. main group and early transition elements. Pergamon Press; Oxford (UK) (3) p. 1059-1127.
- He W, Yong T, Teo WE, Ma Z, Ramakrishna S. 2005. Fabrication and endothelialization of collagen-blended biodegradable polymer nanofibers: Potential vascular graft for blood vessel tissue engineering. Tissue Engineering 11(9-10):1574-88.
- Hegemann D, Brunner H, Oehr C. 2003. Plasma treatment of polymers for surface and adhesion improvement. Nuclear Instruments and Methods in Physics Research Section B: Beam Interactions with Materials and Atoms 208:281-6.
- Helfferich F. 1965. Ion-exchange kinetics. V. ion exchange accompanied by reactions. The Journal of Physical Chemistry 69(4):1178-87.
- Ho Y. 2006. Review of second-order models for adsorption systems. Journal of hazardous materials 136(3):681-9.
- Hohman MM, Shin M, Rutledge G, Brenner MP. 2001. Electrospinning and electrically forced jets. I. stability theory. Physics of Fluids (1994-Present) 13(8):2201-20.
- Hokkanen S, Bhatnagar A, Sillanpää M. 2016. A review on modification methods to cellulose-based adsorbents to improve adsorption capacity. Water research 91:156-73.

- Hong G, Wang M, Li X, Shen L, Wang X, Zhu M, Hsiao BS. 2015. Micro-nano structure nanofibrous p-sulfonatocalix [8] arene complex membranes for highly efficient and selective adsorption of lanthanum (III) ions in aqueous solution. *RSC Advances* 5(27):21178-88.
- Hong G, Shen L, Wang M, Yang Y, Wang X, Zhu M, Hsiao BS. 2014. Nanofibrous polydopamine complex membranes for adsorption of lanthanum (III) ions. *Chemical Engineering Journal* 244:307-16.
- Horikawa T, Itoh M, Suzuki S, Machida K. 2004. Magnetic properties of the Nd–Fe–B sintered magnet powders recovered by yb metal vapor sorption. *Journal of Magnetism and Magnetic Materials* 271(2):369-80.
- Horwitz EP, McAlister D, Bond A, Barrans Jr RE. 2005. Novel extraction of chromatographic resins based on tetraalkyldiglycolamides: Characterization and potential applications. *Solvent Extraction and Ion Exchange* 23(3):319-44.
- Hou X, Amais RS, Jones BT, Donati GL. 2000. Inductively coupled plasma optical emission spectrometry. In *Encyclopedia of Analytical Chemistry*. John Wiley & Sons, Ltd p. 1–25. DOI: 10.1002/9780470027318.a5110.pub3.
- Huang M, Lu H, Li X. 2012. Synthesis and strong heavy-metal ion sorption of copolymer microparticles from phenylenediamine and its sulfonate. *Journal of Materials Chemistry* 22(34):17685-99.
- Huang Z, Zhang Y, Ramakrishna S, Lim C. 2004. Electrospinning and mechanical characterization of gelatin nanofibers. *Polymer* 45(15):5361-8.
- Huang Z, Zhang Y, Kotaki M, Ramakrishna S. 2003. A review on polymer nanofibers by electrospinning and their applications in nanocomposites. *Composites Science and Technology* 63(15):2223-53.
- Iannicelli-Zubiani EM, Cristiani C, Dotelli G, Stampino PG, Pelosato R, Mesto E, Schingaro E, Lacalamita M. 2015. Use of natural clays as sorbent materials for

- rare earth ions: Materials characterization and set up of the operative parameters. *Waste Management* 46:546-56.
- Ignatova M, Yovcheva T, Viraneva A, Mekishev G, Manolova N, Rashkov I. 2008. Study of charge storage in the nanofibrous poly (ethylene terephthalate) electrets prepared by electrospinning or by corona discharge method. *European Polymer Journal* 44(7):1962-7.
- Irani M, Keshtkar AR, Moosavian MA. 2012. Removal of cadmium from aqueous solution using mesoporous PVA/TEOS/APTES composite nanofiber prepared by sol-gel/electrospinning. *Chemical Engineering Journal* 200:192-201.
- Islam MS, Rahaman MS, Yeum JH. 2015. Phosphine-functionalized electrospun poly(vinyl alcohol)/silica nanofibers as highly effective adsorbent for removal of aqueous manganese and nickel ions. *Colloids and Surfaces A: Physicochemical and Engineering Aspects* 484:9-18.
- Jain V, Pandya R, Pillai S, Agrawal Y, Kanaiya P. 2007. Solid-phase extractive preconcentration and separation of lanthanum (III) and cerium (III) using a polymer-supported chelating calix [4] arene resin. *Journal of Analytical Chemistry* 62(2):104-12.
- Jain V, Handa A, Pandya R, Shrivastav P, Agrawal Y. 2002. Polymer supported calix [4] arene-semicarbazone derivative for separation and preconcentration of La (III), Ce (III), Th (IV) and U (VI). *Reactive and Functional Polymers* 51(2):101-10.
- Jain VK, Handa A, Sait SS, Shrivastav P, Agrawal YK. 2001. Pre-concentration, separation and trace determination of lanthanum(III), cerium(III), thorium(IV) and uranium(VI) on polymer supported o-vanillinsemicarbazone. *Analytica Chimica Acta* 429(2):237-46.
- Jal P, Patel S, Mishra B. 2004. Chemical modification of silica surface by immobilization of functional groups for extractive concentration of metal ions. *Talanta* 62(5):1005-28.

- Janssen LJJ and Koene L. 2002. The role of electrochemistry and electrochemical technology in environmental protection. *Chemical engineering journal* 85(2-3):137-46.
- Jarmelo S, Reva I, Lapinski L, Nowak M, Fausto R. 2008. Matrix-isolated diglycolic anhydride: Vibrational spectra and photochemical reactivity. *The Journal of Physical Chemistry A* 112(44):11178-89.
- Jarusuwannapoom T, Hongrojjanawiwat W, Jitjaicham S, Wannatong L, Nithitanakul M, Pattamaprom C, Koombhongse P, Rangkupan R, Supaphol P. 2005. Effect of solvents on electro-spinnability of polystyrene solutions and morphological appearance of resulting electrospun polystyrene fibers. *European Polymer Journal* 41(3):409-21.
- Jayaraman K, Kotaki M, Zhang Y, Mo X, Ramakrishna S. 2004. Recent advances in polymer nanofibers. *Journal of Nanoscience and Nanotechnology* 4(1-2):52-65.
- Jeon C and Kwon T. 2012. Desorption and regeneration characteristics for previously adsorbed indium ions to phosphorylated sawdust. *Environmental Engineering Research* 17(2):65-7.
- Jeoung E, Yeh Y, Nelson T, Kushida T, Wang L, Mout R, Li X, Saha K, Gupta A, Tonga GY. 2015. Fabrication of functional nanofibers through Post-Nanoparticle functionalization. *Macromolecular Rapid Communications* 36(7):678-83.
- Jha MK, Kumari A, Panda R, Kumar JR, Yoo K, Lee JY. 2016. Review on hydrometallurgical recovery of rare earth metals. *Hydrometallurgy* 165:2-26.
- Jover J, Fey N, Harvey JN, Lloyd-Jones GC, Orpen AG, Owen-Smith GJ, Murray P, Hose DR, Osborne R, Purdie M. 2012. Expansion of the ligand knowledge base for chelating P, P-donor ligands (LKB-PP). *Organometallics* 31(15):5302-6.
- Justi KC, Fávere VT, Laranjeira MC, Neves A, Peralta RA. 2005. Kinetics and equilibrium adsorption of Cu (II), Cd (II), and Ni (II) ions by chitosan

- functionalized with 2 [-bis-(pyridylmethyl) aminomethyl]-4-methyl-6-formylphenol. *Journal of Colloid and Interface Science* 291(2):369-74.
- Kajiya T, Aihara M, Hirata S. 2004. Determination of rare earth elements in seawater by inductively coupled plasma mass spectrometry with on-line column pre-concentration using 8-quinolinole-immobilized fluorinated metal alkoxide glass. *Spectrochimica Acta Part B: Atomic Spectroscopy* 59(4):543-50.
- Kampalanonwat P and Supaphol P. 2014. The study of competitive adsorption of heavy metal ions from aqueous solution by aminated polyacrylonitrile nanofiber mats. *Energy Procedia* 56:142-51.
- Kanani AG and Bahrami SH. 2011. Effect of changing solvents on poly (ϵ -caprolactone) nanofibrous webs morphology. *Journal of Nanomaterials* 2011(31):1-10. doi.10.1155/2011/724153.
- Kannan S, Moody MA, Barnes CL, Duval PB. 2008. Lanthanum (III) and uranyl (VI) diglycolamide complexes: Synthetic precursors and structural studies involving nitrate complexation. *Inorganic chemistry* 47(11):4691-5.
- Kansiz M, Domínguez-Vidal A, McNaughton D, Lendl B. 2007. Fourier-transform infrared (FTIR) spectroscopy for monitoring and determining the degree of crystallisation of polyhydroxyalkanoates (PHAs). *Analytical and Bioanalytical Chemistry* 388(5-6):1207-13.
- Karadaş C, Kara D, Fisher A. 2011. Determination of rare earth elements in seawater by inductively coupled plasma mass spectrometry with off-line column preconcentration using 2, 6-diacetylpyridine functionalized amberlite XAD-4. *Analytica chimica acta* 689(2):184-9.
- Kaur I, Sharma N, Kumari V. 2013. Modification of fiber properties through grafting of acrylonitrile to rayon by chemical and radiation methods. *Journal of Advanced Research* 4(6):547-57.

- Keller JU and Staudt R. 2005. Gas adsorption equilibria: Experimental methods and adsorptive isotherms. Springer Science & Business Media, New York USA p 1-421.
- Keshtkar A, Irani M, Moosavian M. 2013. Removal of uranium (VI) from aqueous solutions by adsorption using a novel electrospun PVA/TEOS/APTES hybrid nanofiber membrane: Comparison with casting PVA/TEOS/APTES hybrid membrane. *Journal of Radioanalytical & Nuclear Chemistry* 295(1):563-71.
- Keshtkar AR, Tabatabaefar A, Vaneghi AS, Moosavian MA. 2016. Electrospun polyvinylpyrrolidone/silica/3-aminopropyltriethoxysilane composite nanofiber adsorbent: Preparation, characterization and its application for heavy metal ions removal from aqueous solution. *Journal of Environmental Chemical Engineering* 4(1):1248-58.
- Khan MH, Liaqat K, Hafeez M, Fazil S, Riaz M. 2015. Extraction of cerium (IV) using di-n-butylsulfoxide in chloroform from nitric acid and determination with arsenazo (III) as chromogenic reagent. *South African Journal of Chemistry* 68(1):69-75.
- Ki CS, Gang EH, Um IC, Park YH. 2007. Nanofibrous membrane of wool keratose/silk fibroin blend for heavy metal ion adsorption. *Journal of Membrane Science* 302(1):20-6.
- Ki CS, Baek DH, Gang KD, Lee KH, Um IC, Park YH. 2005. Characterization of gelatin nanofiber prepared from gelatin-formic acid solution. *Polymer* 46(14):5094-102.
- Kidoaki S, Kwon IK, Matsuda T. 2005. Mesoscopic spatial designs of nano-and microfiber meshes for tissue-engineering matrix and scaffold based on newly devised multilayering and mixing electrospinning techniques. *Biomaterials* 26(1):37-46.
- Kim DS, Park HB, Rhim JW, Lee YM. 2004. Preparation and characterization of crosslinked PVA/SiO₂ hybrid membranes containing sulfonic acid groups for

- direct methanol fuel cell applications. *Journal of Membrane Science* 240(1):37-48.
- Kim G, Hwang Y, Ahn Y, Shin H, Lee J, Sung C. 2005. The morphology of electrospun polystyrene fibers. *Korean Journal of Chemical Engineering* 22(1):147-53.
- Kim K, Jeong L, Park H, Shin S, Park W, Lee S, Kim T, Park Y, Seol Y, Lee Y. 2005. Biological efficacy of silk fibroin nanofiber membranes for guided bone regeneration. *Journal of Biotechnology* 120(3):327-39.
- Kobya M. 2004. Removal of Cr (VI) from aqueous solutions by adsorption onto hazelnut shell activated carbon: Kinetic and equilibrium studies. *Bioresource Technology* 91(3):317-21.
- Koenig JL. 1999. *Spectroscopy of polymers*. (2nd Edition) Elsevier. New York USA. p 491.
- Koh H, Yong T, Chan C, Ramakrishna S. 2008. Enhancement of neurite outgrowth using nano-structured scaffolds coupled with laminin. *Biomaterials* 29(26):3574-82.
- Kolodyńska D and Hubicki Z. 2012. Investigation of sorption and separation of lanthanides on the ion exchangers of various types. In *Ion Exchange Technologies*. Ayben Kilislioglu (Ed). INTECH DOI: 10.5772/50857.
- Koltun P and Tharumarajah A. 2014. Life cycle impact of rare earth elements. *ISRN Metallurgy* 2014 (907536): 1-10 <http://dx.doi.org/10.1155/2014/907536>.
- Konishi Y, Shimaoka J, Asai S. 1998. Sorption of rare-earth ions on biopolymer gel beads of alginic acid. *Reactive and Functional Polymers* 36(2):197-206.
- Konishi Y, Asai S, Shimaoka J, Miyata M, Kawamura T. 1992. Recovery of neodymium and ytterbium by biopolymer gel particles of alginic acid. *Industrial & Engineering Chemistry Research* 31(10):2303-11.

- Koombhongse S, Liu W, Reneker DH. 2001. Flat polymer ribbons and other shapes by electrospinning. *Journal of Polymer Science Part B: Polymer Physics* 39(21):2598-606.
- Korovin V and Shestak Y. 2009. Scandium extraction from hydrochloric acid media by levestrel-type resins containing di-isooctyl methyl phosphonate. *Hydrometallurgy* 95(3):346-9.
- Koskenmaki DC and Gschneidner KA. 1978. Cerium. In *Handbook on the Physics and Chemistry of Rare Earths* 1:337-77. [https://doi.org/10.1016/S0168-1273\(78\)01008-9](https://doi.org/10.1016/S0168-1273(78)01008-9)
- Koski A, Yim K, Shivkumar S. 2004. Effect of molecular weight on fibrous PVA produced by electrospinning. *Materials Letters* 58(3):493-7.
- Kozhevnikova N and Tsybikova N. 2008. Sorption of neodymium (III) ions by natural mordenite-containing tuff. *Russian Journal of Applied Chemistry* 81(1):42-5.
- Krishnani KK, Meng X, Christodoulatos C, Boddu VM. 2008. Biosorption mechanism of nine different heavy metals onto biomatrix from rice husk. *Journal of Hazardous Materials* 153(3):1222-34.
- Ku Y and Jung I. 2001. Photocatalytic reduction of Cr (VI) in aqueous solutions by UV irradiation with the presence of titanium dioxide. *Water Research* 35(1):135-42.
- Kubota F, Shimobori Y, Baba Y, Koyanagi Y, Shimojo K, Kamiya N, Goto M. 2011. Application of ionic liquids to extraction separation of rare earth metals with an effective diglycol amic acid extractant. *Journal of Chemical Engineering of Japan* 44(5):307-12.
- Kuczynski B and Geyer R. 2010. Material flow analysis of polyethylene terephthalate in the US, 1996–2007. *Resources, Conservation and Recycling* 54(12):1161-9.

- Kumar SA, Pandey SP, Shenoy NS, Kumar SD. 2011. Matrix separation and preconcentration of rare earth elements from seawater by poly hydroxamic acid cartridge followed by determination using ICP-MS. *Desalination* 281:49-54.
- Kumar SS, Hidyatai N, Herrero JS, Irusta S, Scott K. 2011. Efficient tuning of the Pt nano-particle mono-dispersion on vulcan XC-72R by selective pre-treatment and electrochemical evaluation of hydrogen oxidation and oxygen reduction reactions. *International Journal of Hydrogen Energy* 36(9):5453-65.
- Kütahyalı C, Sert Ş, Cetinkaya B, Inan S, Eral M. 2010. Factors affecting lanthanum and cerium biosorption on pinus brutia leaf powder. *Separation Science and Technology* 45(10):1456-62.
- Kyzas GZ and Bikiaris DN. 2015. Recent modifications of chitosan for adsorption applications: A critical and systematic review. *Marine Drugs* 13(1):312-37.
- Laatikainen K, Udomsap D, Siren H, Brisset H, Sainio T, Branger C. 2015. Effect of template ion–ligand complex stoichiometry on selectivity of ion-imprinted polymers. *Talanta* 134:538-45.
- Ladizesky N and Ward I. 1995. A review of plasma treatment and the clinical application of polyethylene fibres to reinforcement of acrylic resins. *Journal of Materials Science: Materials in Medicine* 6(9):497-504.
- Lagergren S. 1898. About the theory of so-called adsorption of soluble substances. *Kungliga Svenska Vetenskapsakademiens Handlingar* 24(4): 1-39.
- Lakherwal D. 2014. Adsorption of heavy metals: A review. *International Journal of Environmental Research and Development* 4(1):41-8.
- Langmuir I. 1916. The constitution and fundamental properties of solids and liquids. part i. solids. *Journal of the American Chemical Society* 38(11):2221-95.
- Lee E, An AK, He T, Woo YC, Shon HK. 2016. Electrospun nanofiber membranes incorporating fluorosilane-coated TiO₂ nanocomposite for direct contact membrane distillation. *Journal of Membrane Science* 520:145-54.

- Lee JS, Choi KH, Ghim HD, Kim SS, Chun DH, Kim HY, Lyoo WS. 2004. Role of molecular weight of atactic poly (vinyl alcohol)(PVA) in the structure and properties of PVA nanofabric prepared by electrospinning. *Journal of Applied Polymer Science* 93(4):1638-46.
- Lee MS, Lee TS, Park WH. 2013. Highly hydrophobic nanofibrous surfaces generated by poly (vinylidene fluoride). *Fibers and Polymers* 14(8):1271-5.
- León-Bermúdez A and Salazar R. 2008. Synthesis and characterization of the polystyrene-asphaltene graft copolymer by FT-IR spectroscopy. *CT&F-Ciencia, Tecnología Y Futuro* 3(4):157-67.
- León-González ME and Pérez-Arribas LV. 2000. Chemically modified polymeric sorbents for sample preconcentration. *Journal of Chromatography A* 902(1):3-16.
- Leonor I, Kim H, Balas F, Kawashita M, Reis R, Kokubo T, Nakamura T. 2007. Functionalization of different polymers with sulfonic groups as a way to coat them with a biomimetic apatite layer. *Journal of Materials Science: Materials in Medicine* 18(10):1923-30.
- Lewin M. 1984. *Handbook of fiber science and technology volume 2: Chemical processing of fibers and fabrics--functional finishes*. CRC Press. Marcel Dekker INC New York USA. p. 1-509.
- Li L and Hsieh Y. 2005. Ultra-fine polyelectrolyte fibers from electrospinning of poly (acrylic acid). *Polymer* 46(14):5133-9.
- Li X, Feng H, Huang M. 2009. Strong adsorbability of mercury ions on aniline/sulfoanisidine copolymer nanosorbents. *Chemistry–A European Journal* 15(18):4573-81.
- Li X, Ma X, Sun J, Huang M. 2009. Powerful reactive sorption of silver (I) and mercury (II) onto poly (o-phenylenediamine) microparticles. *Langmuir* 25(3):1675-84.

- Li Y, Zhang J, Xu C, Zhou Y. 2016. Crosslinked chitosan nanofiber mats fabricated by one-step electrospinning and ion-imprinting methods for metal ions adsorption. *Science China Chemistry* 59(1):95-105.
- Li Z and Wang C. 2013. Effects of working parameters on electrospinning. In: *One-dimensional nanostructures*. Springer. Berlin, Heidelberg. p 15-28. [https://doi-10.1007/978-3-642-36427-3_2](https://doi.org/10.1007/978-3-642-36427-3_2).
- Li L, Li Y, Cao L, Yang C. 2015. Enhanced chromium (VI) adsorption using nanosized chitosan fibers tailored by electrospinning. *Carbohydrate polymers* 125:206-13.
- Li S, Yue X, Jing Y, Bai S, Dai Z. 2011. Fabrication of zonal thiol-functionalized silica nanofibers for removal of heavy metal ions from wastewater. *Colloids & Surfaces A: Physicochemical and Engineering Aspects* 380(1-3):229-33.
- Lian N, Chang X, Zheng H, Wang S, Dong Y, Lai S. 2005. Synthesis and efficiency of a chelating fiber for preconcentration and separation of trace Au (III) and Pd (IV) from solution samples. *Annali di Chimica* 95(9-10):677-83.
- Liang C and Krimm S, 1958. Infrared spectra of high polymers. VI. polystyrene. *Journal of Polymer Science* 27(115):241-54.
- Liang R, Cao H, Qian D. 2011. MoO₃ nanowires as electrochemical pseudocapacitor materials. *Chemical Communications* 47(37):10305-7.
- Lin K, Chua K, Christopherson GT, Lim S, Mao H. 2007. Reducing electrospun nanofiber diameter and variability using cationic amphiphiles. *Polymer* 48(21):6384-94.
- Liu X and Ma PX. 2009. Phase separation, pore structure, and properties of nanofibrous gelatin scaffolds. *Biomaterials* 30(25):4094-103.
- Liu X, et al. 2013. UV-assisted surface modification of PET fiber for adhesion improvement. *Applied Surface Science* 264(Supplement C):61-9.

- Lü Q, Huang M, Li X. 2007. Synthesis and heavy-metal-ion sorption of pure sulfophenylenediamine copolymer nanoparticles with intrinsic conductivity and stability. *Chemistry–A European Journal* 13(21):6009-18.
- Lu Y, Wu Z, Li M, Liu Q, Wang D. 2014. Hydrophilic PVA-co-PE nanofiber membrane functionalized with iminodiacetic acid by solid-phase synthesis for heavy metal ions removal. *Reactive and Functional Polymers* 82:98-102.
- Luo F, Liu Y, Li X, Xuan Z, Ma J. 2006. Biosorption of lead ion by chemically-modified biomass of marine brown algae *laminaria japonica*. *Chemosphere* 64(7):1122-7.
- Luo CJ, Nangrejo M, Edirisinghe M. 2010. A novel method of selecting solvents for polymer electrospinning. *Polymer* 51(7):1654-62.
- Ma M, Mao Y, Gupta M, Gleason KK, Rutledge GC. 2005. Superhydrophobic fabrics produced by electrospinning and chemical vapor deposition. *Macromolecules* 38(23):9742-8.
- Ma Z, Kotaki M, Yong T, He W, Ramakrishna S. 2005. Surface engineering of electrospun polyethylene terephthalate (PET) nanofibers towards development of a new material for blood vessel engineering. *Biomaterials* 26(15):2527-36.
- Maass S, Finsterwalder F, Frank G, Hartmann R, Merten C. 2008. Carbon support oxidation in PEM fuel cell cathodes. *Journal of Power Sources* 176(2):444-51.
- MacDiarmid A, Jones W, Norris I, Gao J, Johnson A, Pinto N, Hone J, Han B, Ko F, Okuzaki H. 2001. Electrostatically-generated nanofibers of electronic polymers. *Synthetic metals* 119(1-3):27-30.
- MacDiarmid AG. 2001. "Synthetic metals": A novel role for organic polymers (nobel lecture). *Angewandte Chemie - International Edition* 40(14):2581-90.
- Mahalingam S, Raimi-Abraham BT, Craig DQM, Edirisinghe M. 2015. Solubility–spinnability map and model for the preparation of fibres of polyethylene

- (terephthalate) using gyration and pressure. *Chemical Engineering Journal* 280:344-53.
- Maheswari MA and Subramanian M. 2004. Selective enrichment of U (VI), Th (IV) and La (III) from high acidic streams using a new chelating ion-exchange polymeric matrix. *Talanta* 64(1):202-9.
- Manoochchri M and Khalesi P. 2012. Synthesis and evaluation of ion imprinted mercapto-functionalized nano alumina as a selective sorbent for Nd (III) removal from water samples. *World Applied Sciences Journal* 19(2):215-22.
- Marder L, Bernardes AM, Zoppas Ferreira J. 2004. Cadmium electroplating wastewater treatment using a laboratory-scale electro dialysis system. *Separation and Purification Technology* 37(3):247-55.
- Massari S and Ruberti M. 2013. Rare earth elements as critical raw materials: Focus on international markets and future strategies. *Resources Policy* 38(1):36-43.
- Matloka K, Gelis A, Regalbuto M, Vandegrift G, Scott MJ. 2005. Highly efficient binding of trivalent f-elements from acidic media with a C₃-symmetric tripodal ligand containing diglycolamide arms. *Dalton Transactions* (23):3719-21.
- Matoso E, Kubota L, Cadore S. 2003. Use of silica gel chemically modified with zirconium phosphate for preconcentration and determination of lead and copper by flame atomic absorption spectrometry. *Talanta* 60(6):1105-11.
- McCann JT, Chen JI, Li D, Ye Z, Xia Y. 2006. Electrospinning of polycrystalline barium titanate nanofibers with controllable morphology and alignment. *Chemical Physics Letters* 424(1):162-6.
- Megelski S, Stephens JS, Chase DB, Rabolt JF. 2002. Micro-and nanostructured surface morphology on electrospun polymer fibers. *Macromolecules* 35(22):8456-66.
- Meier W, Bopp P, Probst M, Spohr E, Lin J. 1990. Molecular dynamics studies of lanthanum chloride solutions. *The Journal of Chemical Physics* 94(11):4672-82.

- Miaomiao T, Qiong J, Wuping L. 2013. Studies on synergistic solvent extraction of rare earth elements from nitrate medium by mixtures of 8-hydroxyquinoline with cyanex 301 or cyanex 302. *Journal of Rare Earths* 31(6):604-8.
- Michler GH. 2008. Electron microscopy of polymers. (SEM). In: *Electron Microscopy of Polymers*. Springer Laboratory. Springer, Berlin, Heidelberg. pp 87-120. https://doi.org/10.1007/978-3-540-36352-1_5.
- Middleton JC and Tipton AJ. 2000. Synthetic biodegradable polymers as orthopedic devices. *Biomaterials* 21(23):2335-46.
- Min M, Shen L, Hong G, Zhu M, Zhang Y, Wang X, Chen Y, Hsiao BS. 2012. Micro-nano structure poly (ether sulfones)/poly (ethyleneimine) nanofibrous affinity membranes for adsorption of anionic dyes and heavy metal ions in aqueous solution. *Chemical Engineering Journal* 197:88-100.
- Miraoui A, Didi MA, Villemin D. 2016. Neodymium (III) removal by functionalized magnetic nanoparticles. *Journal of Radioanalytical and Nuclear Chemistry* 307(2):963-71.
- Moghimi A and Abdouss M. 2012. Preconcentration of Ni (II) from sample water by modified poly (ethylene terephthalate)-grafted-acrylic acid/acryl amide fiber. *African Journal of Pure and Applied Chemistry* 6(8):110-8.
- Mohammad F. 2007. *Specialty polymers: Materials and applications*. (Eds) IK International Pvt Ltd - 588 p
- Mokhena T, Jacobs V, Luyt A. 2015. A review on electrospun bio-based polymers for water treatment. *Express Polymer Letters* 9(10):839-80.
- Moldoveanu GA and Papangelakis VG. 2012. Recovery of rare earth elements adsorbed on clay minerals: I. desorption mechanism. *Hydrometallurgy* 117:71-8.
- Moloney MG. 2008. Functionalized polymers by chemical surface modification. *J Phys D* 41(17):174006.

- Monier M and Abdel-Latif D. 2013a. Modification and characterization of PET fibers for fast removal of Hg (II), Cu (II) and Co (II) metal ions from aqueous solutions. *Journal of Hazardous Materials* 250:122-30.
- Monier M and Abdel-Latif D. 2013b. Synthesis and characterization of ion-imprinted chelating fibers based on PET for selective removal of hg 2. *Chemical Engineering Journal* 221:452-60.
- Morikawa K, Amano Y, Iwachido N, Fujiwara N, Takayama T, inventors; Porous graft copolymer particles, method for producing same, and adsorbent material using same. US Patent 14/692,986. US20150224472 A1.
- Musyoka S, Ngila C, Moodley B, Kindness A, Petrik L, Greyling C. 2011. Oxolane-2,5-dione modified electrospun cellulose nanofibers for heavy metals adsorption. *Journal of Hazardous Materials* 192(2):922-7.
- Naganawa H, Shimojo K, Mitamura H, Sugo Y, Noro J, Goto M. 2007. A new "green" extractant of the diglycol amic acid type for lanthanides. *Solvent Extraction Research and Development* 14:151-9.
- Najafi Lahiji M, Keshtkar AR, Moosavian MA. 2016. Adsorption of cerium and lanthanum from aqueous solutions by chitosan/polyvinyl alcohol/3-mercaptopropyltrimethoxysilane beads in batch and fixed-bed systems. *Particul Sci Technol* :1-11. <https://doi.org/10.1080/02726351.2016.1248262>
- Nakajima A and Baba Y. 2004. Mechanism of hexavalent chromium adsorption by persimmon tannin gel. *Water research* 38(12):2859-64.
- Narita H, Yaita T, Tamura K, Tachimori S. 1998. Solvent extraction of trivalent lanthanoid ions with N, N'-dimethyl-N, N'-diphenyl-3-oxapentanediamide. *Radiochimica Acta* 81(4):223-6.
- Narita H and Tanaka M. 2013. Separation of rare earth elements from base metals in concentrated HNO₃, H₂SO₄ and HCl solutions with diglycolamide. *Solvent Extraction Research and Development, Japan* 20:115-21.

- Naumov A. 2008. Review of the world market of rare-earth metals. *Russian Journal of Non-Ferrous Metals* 49(1):14-22.
- Ndayambaje G, Laatikainen K, Laatikainen M, Beukes E, Fatoba O, van der Walt N, Petrik L, Sainio T. 2016. Adsorption of nickel (II) on polyacrylonitrile nanofiber modified with 2-(2'-pyridyl) imidazole. *Chemical Engineering Journal* 284:1106-16.
- Neghlani PK, Rafizadeh M, Taromi FA. 2011. Preparation of aminated-polyacrylonitrile nanofiber membranes for the adsorption of metal ions: Comparison with microfibers. *Journal of Hazardous Materials* 186(1):182-9.
- Neto, Vicente de Oliveira Sousa, Raulino GSC, Paulo de Tarso, C Freire, Araújo-Silva MA, do Nascimento RF. 2013. Equilibrium and kinetic studies in adsorption of toxic metal ions for wastewater treatment. In *Ion Exchange, Adsorption and Solvent Extraction*. Naushad M and AlOthman (Eds) Nova Science Publishers Viewpoints 7:8.
- Ng J, Cheung W, McKay G. 2003. Equilibrium studies for the sorption of lead from effluents using chitosan. *Chemosphere* 52(6):1021-30.
- Ngah WW and Hanafiah, Megat Ahmad Kamal Megat. 2008. Removal of heavy metal ions from wastewater by chemically modified plant wastes as adsorbents: A review. *Bioresource technology* 99(10):3935-48.
- Nguyen D, Hwang Y, Moon W. 2016. Electrospinning of well-aligned fiber bundles using an end-point control assembly method. *European Polymer Journal* 77:54-64.
- Nicolet T. 2001. *Introduction to fourier transform infrared spectrometry*. Thermo Nicolet Corporation: Madison-USA. Information Booklet.
- Niu C, Wu W, Wang Z, Li S, Wang J. 2007. Adsorption of heavy metal ions from aqueous solution by crosslinked carboxymethyl konjac glucomannan. *Journal of Hazardous Materials* 141(1):209-14.

- Nogami M, Ismail I, Yamaguchi M, Suzuki K. 2003. Synthesis, characterization and some adsorption properties of TMMA chelating resin. *Journal of Solid State Chemistry* 171(1):353-7.
- Noll KE. 1991. *Adsorption technology for air and water pollution control*. CRC Press. p 376
- Nouri L, Ghodbane I, Hamdaoui O, Chiha M. 2007. Batch sorption dynamics and equilibrium for the removal of cadmium ions from aqueous phase using wheat bran. *Journal of Hazardous Materials* 149(1):115-25.
- O'Connell DW, Birkinshaw C, O'Dwyer TF. 2008. Heavy metal adsorbents prepared from the modification of cellulose: A review. *Bioresource technology* 99(15):6709-24.
- Ogata N, Shimada N, Yamaguchi S, Nakane K, Ogihara T. 2007. Melt-electrospinning of poly (ethylene terephthalate) and polyalirite. *Journal of Applied Polymer Science* 105(3):1127-32.
- Ogata T, Narita H, Tanaka M. 2016. Adsorption mechanism of rare earth elements by adsorbents with diglycolamic acid ligands. *Hydrometallurgy* 163:156-60.
- Ogata T, Narita H, Tanaka M. 2014. Immobilization of diglycol amic acid on silica gel for selective recovery of rare earth elements. *Chemistry Letters* 43(9):1414-6.
- Ogata T, Narita H, Tanaka M, Hoshino M, Kon Y, Watanabe Y. 2016. Selective recovery of heavy rare earth elements from apatite with an adsorbent bearing immobilized tridentate amido ligands. *Separation and Purification Technology* 159:157-60.
- Ogata T, Narita H, Tanaka M. 2015. Adsorption behavior of rare earth elements on silica gel modified with diglycol amic acid. *Hydrometallurgy* 152(0):178-82.
- Ohkawa K, Kim H, Lee K, Yamamoto H. 2004. Electrospun Non-Woven fabrics of poly (ϵ -caprolactone) and their biodegradation by pure cultures of soil filamentous fungi. *Macromolecular Symposia* 216(1):301-6.

- Olafadehan O, Jinadu O, Salami L, Popoola L. 2012. Treatment of brewery wastewater effluent using activated carbon prepared from coconut shell. *International Journal of Applied Science and Technology* 2(1):165-78.
- Oliveira RC and Garcia Jr Oswaldo. 2009. Study of biosorption of rare earth metals (La, Nd, Eu, Gd) by sargassum sp. biomass in batch systems: Physicochemical evaluation of kinetics and adsorption models. *Advanced Materials Research* 71-73: 605-608.
- Oliveira RC, Guibal E, Garcia O. 2012. Biosorption and desorption of lanthanum (III) and neodymium (III) in fixed-bed columns with sargassum sp.: Perspectives for separation of rare earth metals. *Biotechnology progress* 28(3):715-22.
- Olmos D, Martín E, González-Benito J. 2014. New molecular-scale information on polystyrene dynamics in PS and PS–BaTiO₃ composites from FTIR spectroscopy. *Physical Chemistry Chemical Physics* 16(44):24339-49.
- Oscik J. 1982. Adsorption, John Wiley & Sons, Inc, New York .
- Özacar M and Şengül IA. 2004. Two-stage batch sorber design using second-order kinetic model for the sorption of metal complex dyes onto pine sawdust. *Biochemical engineering journal* 21(1):39-45.
- Pai C, Boyce MC, Rutledge GC. 2009. Morphology of porous and wrinkled fibers of polystyrene electrospun from dimethylformamide. *Macromolecules* 42(6):2102-14.
- Pakade V, Cukrowska E, Darkwa J, Torto N, Chimuka L. 2011. Selective removal of chromium (VI) from sulphates and other metal anions using an ion-imprinted polymer. *Water SA* 37(4):529-38.
- Palmieri MC, Garcia O, Melnikov P. 2000. Neodymium biosorption from acidic solutions in batch system. *Process Biochemistry* 36(5):441-4.

- Panda N, Devi NB, Mishra S. 2013. Extraction of neodymium (III) using binary mixture of cyanex 272 and cyanex 921/cyanex 923 in kerosene. *Journal of Radioanalytical and Nuclear Chemistry* 296(3):1205-11.
- Parga JR, Cocke DL, Valenzuela JL, Gomes JA, Kesmez M, Irwin G, Moreno H, Weir M. 2005. Arsenic removal via electrocoagulation from heavy metal contaminated groundwater in la comarca lagunera mexico. *Journal of Hazardous Materials* 124(1):247-54.
- Park H and Tavlarides LL. 2010. Adsorption of neodymium (III) from aqueous solutions using a phosphorus functionalized adsorbent. *Industrial & Engineering Chemistry Research* 49(24):12567-75.
- Pathak P and Choppin G. 2007. Sorption of Am³ cations on suspended silicate: Effects of pH, ionic strength, complexing anions, humic acid and metal ions. *Journal of Radioanalytical and Nuclear Chemistry* 274(3):517-23.
- Paudyal H, Pangeni B, Ghimire KN, Inoue K, Ohto K, Kawakita H, Alam S. 2012. Adsorption behavior of orange waste gel for some rare earth ions and its application to the removal of fluoride from water. *Chemical Engineering Journal* 195:289-96.
- Pawlowski K, Belvin H, Raney D, Su J, Harrison J, Siochi E. 2003. Electrospinning of a micro-air vehicle wing skin. *Polymer* 44(4):1309-14.
- Pereao O, Bode-Aluko C, Ndayambaje G, Fatoba O, Petrik L. 2017. Electrospinning: Polymer nanofibre adsorbent applications for metal ion removal. *Journal of Polymers and the Environment* 25(4):1175-89.
- Pham QP, Sharma U, Mikos AG. 2006. Electrospinning of polymeric nanofibers for tissue engineering applications: A review. *Tissue Engineering* 12(5):1197-211.
- Polat H and Erdogan D. 2007. Heavy metal removal from waste waters by ion flotation. *Journal of Hazardous Materials* 148(1):267-73.

- Ponou J, Wang LP, Dodbiba G, Okaya K, Fujita T, Mitsuhashi K, Atarashi T, Satoh G, Noda M. 2014. Recovery of rare earth elements from aqueous solution obtained from vietnamese clay minerals using dried and carbonized parachlorella. *Journal of Environmental Chemical Engineering* 2(2):1070-81.
- Qu Y and Lian B. 2013. Bioleaching of rare earth and radioactive elements from red mud using penicillium tricolor RM-10. *Bioresource technology* 136:16-23.
- Rabie K. 2007. A group separation and purification of sm, eu and gd from egyptian beach monazite mineral using solvent extraction. *Hydrometallurgy* 85(2):81-6.
- Raghavan P, Lim D, Ahn J, Nah C, Sherrington DC, Ryu H, Ahn H. 2012. Electrospun polymer nanofibers: The booming cutting edge technology. *Reactive and Functional Polymers* 72(12):915-30.
- Rahal R, Annani F, Pellet-Rostaing S, Arrachart G, Daniele S. 2015. Surface modification of titanium oxide nanoparticles with chelating molecules: New recognition devices for controlling the selectivity towards lanthanides ionic separation. *Separation and Purification Technology* 147:220-6.
- Rahmani A, Mousavi HZ, Fazli M. 2010. Effect of nanostructure alumina on adsorption of heavy metals. *Desalination* 253(1-3):94-100.
- Ramakrishna S, Fujihara K, Teo W, Lim T, Ma Z. 2005. An introduction to electrospinning and nanofibers. World Scientific. 341 p.
- Ramakrishna S, Fujihara K, Teo W, Yong T, Ma Z, Ramaseshan R. 2006. Electrospun nanofibers: Solving global issues. *Materials Today* 9(3):40-50.
- Rao TP, Kala R, Daniel S. 2006. Metal ion-imprinted polymers—novel materials for selective recognition of inorganics. *Analytica chimica acta* 578(2):105-16.
- Rao TP, Praveen R, Daniel S. 2004. Styrene–divinyl benzene copolymers: Synthesis, characterization, and their role in inorganic trace analysis. *Critical Reviews in Analytical Chemistry* 34(3-4):177-93.

- Rathna G, Birajdar MS, Bhagwani M, Paul V. 2013. Studies on fabrication, characterization, and metal extraction using metal chelating nonwoven nanofiber mats of poly (vinyl alcohol) and sodium alginate blends. *Polymer Engineering & Science* 53(2):321-33.
- Razzaz A, Ghorban S, Hosayni L, Irani M, Aliabadi M. 2016. Chitosan nanofibers functionalized by TiO₂ nanoparticles for the removal of heavy metal ions. *Journal of the Taiwan Institute of Chemical Engineers* 58:333-43.
- Reddy BR, Kumar BN, Radhika S. 2009. Solid-Liquid extraction of terbium from phosphoric acid medium using bifunctional phosphinic acid resin, tulsion CH-96. *Solvent Extraction and Ion Exchange* 27(5-6):695-711.
- Reddy KH and Reddy AR. 2003. Removal of heavy metal ions using the chelating polymers derived by the condensation of poly (3-hydroxy-4-acetylphenyl methacrylate) with different diamines. *Journal of applied polymer science* 88(2):414-21.
- Ren Y, Abbood HA, He F, Peng H, Huang K. 2013. Magnetic EDTA-modified chitosan/SiO₂/Fe₃O₄ adsorbent: Preparation, characterization, and application in heavy metal adsorption. *Chemical Engineering Journal* 226:300-11.
- Reneker DH and Yarin AL. 2008. Electrospinning jets and polymer nanofibers. *Polymer* 49(10):2387-425.
- Reneker DH and Chun I. 1996. Nanometre diameter fibres of polymer, produced by electrospinning. *Nanotechnology* 7(3):216.
- Reneker DH, Yarin AL, Fong H, Koombhongse S. 2000. Bending instability of electrically charged liquid jets of polymer solutions in electrospinning. *Journal of Applied Physics* 87(9):4531-47.
- Repo E, Warchol JK, Kurniawan TA, Sillanpää MET. 2010. Adsorption of Co(II) and Ni(II) by EDTA- and/or DTPA-modified chitosan: Kinetic and equilibrium modeling. *Chemical Engineering Journal* 161(1–2):73-82.

- Rodríguez MPQ. 2000. Fourier transform infrared (FTIR) technology for the identification of organisms. *Clinical Microbiology Newsletter* 22(8):57-61.
- Rodríguez-Reinoso F. 1998. The role of carbon materials in heterogeneous catalysis. *Carbon* 36(3):159-75.
- Roghani-Mamaqani H. 2015. Grafting polystyrene with various graft densities through epoxy groups of graphene nanolayers via atom transfer radical polymerization. *Polymer Composites* 38(11):2450-8.
- Roosen J and Binnemans K. 2014. Adsorption and chromatographic separation of rare earths with EDTA-and DTPA-functionalized chitosan biopolymers. *Journal of Materials Chemistry A* 2(5):1530-40.
- Roosen J, Spooen J, Binnemans K. 2014. Adsorption performance of functionalized chitosan–silica hybrid materials toward rare earths. *Journal of Materials Chemistry A* 2(45):19415-26.
- Roosen J, Pype J, Binnemans K, Mullens S. 2015. Shaping of alginate–silica hybrid materials into microspheres through vibrating-nozzle technology and their use for the recovery of neodymium from aqueous solutions. *Industrial & Engineering Chemistry Research* 54(51):12836-46.
- Rošic R, Pelipenko J, Kocbek P, Baumgartner S, Bešter-Rogač M, Kristl J. 2012. The role of rheology of polymer solutions in predicting nanofiber formation by electrospinning. *European Polymer Journal* 48(8):1374-84.
- Rošic R, Pelipenko J, Kristl J, Kocbek P, Bešter-Rogač M, Baumgartner S. 2013. Physical characteristics of poly (vinyl alcohol) solutions in relation to electrospun nanofiber formation. *European Polymer Journal* 49(2):290-8.
- Roth H. 1954. Sulfonation products from polymers of styrene and vinyltoluene. *Industrial & Engineering Chemistry* 46(11):2435-9.

- Roulia M and Vassiliadis AA. 2008. Sorption characterization of a cationic dye retained by clays and perlite. *Microporous and Mesoporous Materials* 116(1):732-40.
- Ruparelia JP, Duttagupta SP, Chatterjee AK, Mukherji S. 2008. Potential of carbon nanomaterials for removal of heavy metals from water. *Desalination* 232(1-3):145-56.
- Rydberg J. 2004. *Solvent extraction principles and practice*. Rydberg J et al., 2nd Eds, revised and expanded. Marcel Dekker, New York. 480 p
- Saadeh HA, Shairah EAA, Charef N, Mubarak MS. 2012. Synthesis and adsorption properties, toward some heavy metal ions, of a new polystyrene-based terpyridine polymer. *Journal of Applied Polymer Science* 124(4):2717-24.
- Sacksteder C and Barry BA. 2001. Fourier transform infrared spectroscopy: A molecular approach to an organismal question. *Journal of Phycology* 37(2):197-9.
- Sadovsky D, Brenner A, Astrachan B, Asaf B, Gonen R. 2016. Biosorption potential of cerium ions using spirulina biomass. *Journal of Rare Earths* 34(6):644-52.
- Saeed K, Park S, Oh T. 2011. Preparation of hydrazine-modified polyacrylonitrile nanofibers for the extraction of metal ions from aqueous media. *Journal of applied polymer science* 121(2):869-73.
- Sahu T, Singh Bisht S, Ranjan Das K, Kerkar S. 2013. Nanocerium: Synthesis and biomedical applications. *Current Nanoscience* 9(5):588-93.
- Sakaki K, Sugahara H, Kume T, Ohashi M, Naganawa H, Shimojo K. 2015. Method for synthesizing rare earth metal extractant. Shin-Etsu Chemical Co., Ltd., Japan Atomic Energy Agency. Inventors US 9133100 B2.
- Sargeant TD, Guler MO, Oppenheimer SM, Mata A, Satcher RL, Dunand DC, Stupp SI. 2008. Hybrid bone implants: Self-assembly of peptide amphiphile nanofibers within porous titanium. *Biomaterials* 29(2):161-71.

- Sari A, Tuzen M, Cıatak D, Soylak M. 2007. Adsorption characteristics of Cu (II) and Pb (II) onto expanded perlite from aqueous solution. *Journal of Hazardous Materials* 148(1):387-94.
- Sarkar K, Gomez C, Zambrano S, Ramirez M, de Hoyos E, Vasquez H, Lozano K. 2010. Electrospinning to forcespinning™. *Materials Today* 13(11):12-4.
- Sasaki Y and Tachimori S. 2002. Extraction of actinides (III),(IV),(V),(VI), and lanthanides (III) by structurally tailored diamides. *Solvent Extraction and Ion Exchange* 20(1):21-34.
- Sasaki Y, Sugo Y, Suzuki S, Tachimori S. 2001. The novel extractants, diglycolamides, for the extraction of lanthanides and actinides in HNO₃-n-dodecane system. *Solvent Extraction and Ion Exchange* 19(1):91-103.
- Sasaki Y, Rapold P, Arisaka M, Hirata M, Kimura T, Hill C, Cote G. 2007. An additional insight into the correlation between the distribution ratios and the aqueous acidity of the TODGA system. *Solvent Extraction and Ion Exchange* 25(2):187-204.
- Schmidt N and Kodukula H. 1985. *Industrial waste management*. Lewis, Boca Raton, Fla .
- Schreuder-Gibson H, Gibson P, Senecal K, Sennett M, Walker J, Yeomans W, ZIEGLER D, TSAI PP. 2002. Protective textile materials based on electrospun nanofibers. *Journal of Advanced Materials* 34(3):44-55.
- Schweitzer GK and Pesterfield LL. 2010. *The aqueous chemistry of the elements*. Oxford University Press. New York. 448 p
- Seaman J. 2010. Rare earths and clean energy: Analyzing china's upper hand. Fellow in the Center for Asian Studies at the French Institute of International Relations.
http://www.iaea.org/inis/collection/NCLCollectionStore/_Public/42/052/42052647.pdf

- Selvan BR, Dasthaiah K, Suneesh A, Venkatesan K, Antony M, Gardas R. 2017. Diglycolic acid modified zirconium phosphate and studies on the extraction of Am (III) and Eu (III) from dilute nitric acid medium. *Radiochimica Acta* 105(4):275-83.
- Seredin VV, Dai S, Sun Y, Chekryzhov IY. 2013. Coal deposits as promising sources of rare metals for alternative power and energy-efficient technologies. *Applied Geochemistry* 31:1-11.
- Sereshti H, Amini F, Najarzadekan H. 2015. Electrospun polyethylene terephthalate (PET) nanofibers as a new adsorbent for micro-solid phase extraction of chromium (VI) in environmental water samples. *RSC Advances* 5(108):89195-203.
- Sert Ş, Kütahyalı C, İnan S, Talip Z, Çetinkaya B, Eral M. 2008. Biosorption of lanthanum and cerium from aqueous solutions by platanus orientalis leaf powder. *Hydrometallurgy* 90(1):13-8.
- Shah BA, Shah AV, Bhatt RR. 2007. Studies of chelation ion-exchange properties of copolymer resin derived from salicylic acid and its analytical applications. *Iranian Polymer Journal* 16(3):173-84.
- Shahram Forouz F, Ravandi S, Allafchian A. 2016. Removal of ag and cr heavy metals using nanofiber membranes functionalized with aminopropyltriethoxysilane (APTES). *Current Nanoscience* 12(2):266-74.
- Sharma S. 2013. Ferroelectric nanofibers: Principle, processing and applications. *Advanced Materials Letters* 4:522-33.
- Sharma DK, Li F, Wu Y. 2014. Electrospinning of nafion and polyvinyl alcohol into nanofiber membranes: A facile approach to fabricate functional adsorbent for heavy metals. *Colloids and Surfaces A: Physicochemical and Engineering Aspects* 457(0):236-43.

- Sheppard N, Guiseppi-Elie A, Webster J. 1999. pH measurement. *The Measurement, Instrumentation and Sensors Handbook*. Boca Raton: CRC Press.16p
- Shimamura M, Teramoto K, Yoshioka T, Tanaka M. 1989. Polystyrene-based functional fibers. *Handbook of Fiber Science and Technology* 3:209-52.
- Shimojo K, Naganawa H, Noro J, Kubota F, Goto M. 2007. Extraction behavior and separation of lanthanides with a diglycol amic acid derivative and a nitrogen-donor ligand. *Analytical Sciences* 23(12):1427-30.
- Shimojo K, Aoyagi N, Saito T, Okamura H, Kubota F, Goto M, Naganawa H. 2014. Highly efficient extraction separation of lanthanides using a diglycolamic acid extractant. *Analytical Sciences* 30(2):263-9.
- Shin DH, Ko YG, Choi US, Kim WN. 2004a. Synthesis and characteristics of novel chelate fiber containing amine and amidine groups. *Polymers for Advanced Technologies* 15(8):459-66.
- Shin DH, Ko YG, Choi US, Kim WN. 2004b. Design of high efficiency chelate fibers with an amine group to remove heavy metal ions and pH-related FT-IR analysis. *Industrial & Engineering Chemistry Research* 43(9):2060-6.
- Shojaei Z, Iravani E, Moosavian M, Torab-Mostaedi M. 2016. Removal of cerium from aqueous solutions by amino phosphate modified nano TiO₂: Kinetic, and equilibrium studies. *Iranian Journal of Chemical Engineering* 13(2):3-21.
- Shoushtari AM, Zargaran M, Abdouss M. 2006. Preparation and characterization of high efficiency ion-exchange crosslinked acrylic fibers. *Journal of Applied Polymer Science* 101(4):2202-9.
- Shukla S, Brinley E, Cho HJ, Seal S. 2005. Electrospinning of hydroxypropyl cellulose fibers and their application in synthesis of nano and submicron tin oxide fibers. *Polymer* 46(26):12130-45.

- Singh D, Singh H, Mathur J. 2006. Extraction of rare earths and yttrium with high molecular weight carboxylic acids. *Hydrometallurgy* 81(3):174-81.
- Sionkowska A. 2011. Current research on the blends of natural and synthetic polymers as new biomaterials: Review. *Progress in Polymer Science* 36(9):1254-76.
- Skoog DA, West DM, Holler FJ, Crouch SR. 2013. *Fundamentals of analytical chemistry*. 9th Eds. Nelson Education.
- Sohrin Y, Iwamoto S, Akiyama S, Fujita T, Kugii T, Obata H, Nakayama E, Goda S, Fujishima Y, Hasegawa H. 1998. Determination of trace elements in seawater by fluorinated metal alkoxide glass-immobilized 8-hydroxyquinoline concentration and high-resolution inductively coupled plasma mass spectrometry detection. *Analytica Chimica Acta* 363(1):11-9.
- Son WK, Youk JH, Lee TS, Park WH. 2004. Electrospinning of ultrafine cellulose acetate fibers: Studies of a new solvent system and deacetylation of ultrafine cellulose acetate fibers. *Journal of Polymer Science Part B: Polymer Physics* 42(1):5-11.
- Stankus JJ, Guan J, Fujimoto K, Wagner WR. 2006. Microintegrating smooth muscle cells into a biodegradable, elastomeric fiber matrix. *Biomaterials* 27(5):735-44.
- Strain I, Wu Q, Pourrahimi AM, Hedenqvist MS, Olsson RT, Andersson RL. 2015. Electrospinning of recycled PET to generate tough mesomorphic fibre membranes for smoke filtration. *Journal of Materials Chemistry A* 3(4):1632-40.
- Su W. 2013. Radical chain polymerization. In: *Principles of polymer design and synthesis*. Lecture Notes in Chemistry. Springer. Berlin, Heidelberg 82: 137 p.
- Subbiah T, Bhat G, Tock R, Parameswaran S, Ramkumar S. 2005. Electrospinning of nanofibers. *Journal of Applied Polymer Science* 96(2):557-69.

- Subotić B and Bronić J. 1986. Removal of cerium (III) species from solutions using granulated zeolites. *Journal of Radioanalytical and Nuclear Chemistry* 102(2):465-81.
- Sun T, Mai S, Norton D, Haycock JW, Ryan AJ, Macneil S. 2005. Self-organization of skin cells in three-dimensional electrospun polystyrene scaffolds. *Tissue Engineering* 11(7-8):1023-33.
- Sun Z, Zussman E, Yarin AL, Wendorff JH, Greiner A. 2003. Compound Core–Shell polymer nanofibers by Co-Electrospinning. *Advanced Materials* 15(22):1929-32.
- Suneesh A, Venkatesan K, Syamala K, Antony M, Vasudeva Rao P. 2012. Mutual separation of americium (III) and europium (III) using glycolamic acid and thioglycolamic acid. *Radiochimica Acta International Journal for Chemical Aspects of Nuclear Science and Technology* 100(7):425-30.
- Suneesh A, Jain R, Venkatesan K, Antony M, Bhanage B, Vasudeva Rao P. 2015. Novel diglycolamic acid functionalized iron oxide particles for the mutual separation of Eu (III) and Am (III). *Solvent Extraction and Ion Exchange* 33(7):656-70.
- Tabarzadi M, Abdouss M, Javanbakht M, Shoshtary S, Zargaran M, Dashtizadeh A. 2009. Production new chelating fibers of polyacrylonitrile for removing metal ions. *Materialwissenschaft Und Werkstofftechnik* 40(8):643-8.
- Tahaei P, Abdouss M, Edrissi M, Shoushtari A, Zargaran M. 2008. Preparation of chelating fibrous polymer by different diamines and study on their physical and chemical properties. *Materialwissenschaft Und Werkstofftechnik* 39(11):839-44.
- Tan S, Inai R, Kotaki M, Ramakrishna S. 2005. Systematic parameter study for ultra-fine fiber fabrication via electrospinning process. *Polymer* 46(16):6128-34.

- Tao X and Huiqing P. 2009. Formation cause, composition analysis and comprehensive utilization of rare earth solid wastes. *Journal of Rare Earths* 27(6):1096-102.
- Teo W and Ramakrishna S. 2006. A review on electrospinning design and nanofibre assemblies. *Nanotechnology* 17(14):R89.
- Teo W, Gopal R, Ramaseshan R, Fujihara K, Ramakrishna S. 2007. A dynamic liquid support system for continuous electrospun yarn fabrication. *Polymer* 48(12):3400-5.
- Teramoto K. 1991. Chemical modification of polystyrene surfaces by amidomethylation reaction with N-methylol-2-chloroacetamide. *Reactive Polymers* 15:89-101.
- Teramoto K and Nakamoto Y. 2002. Amidomethylation of vinyl aromatic polymers with N-methylol-2-chloroacetamide. *Polymer journal* 34(5):363-9.
- Thavasi V, Singh G, Ramakrishna S. 2008. Electrospun nanofibers in energy and environmental applications. *Energy & Environmental Science* 1(2):205-21.
- Theron S, Zussman E, Yarin A. 2004. Experimental investigation of the governing parameters in the electrospinning of polymer solutions. *Polymer* 45(6):2017-30.
- Tian G, Xu J, Rao L. 2005. Optical absorption and structure of a highly symmetrical neptunium (V) diamide complex. *Angewandte Chemie International Edition* 44(38):6200-3.
- Tian Y, Wu M, Liu R, Li Y, Wang D, Tan J, Wu R, Huang Y. 2011. Electrospun membrane of cellulose acetate for heavy metal ion adsorption in water treatment. *Carbohydrate Polymers* 83(2):743-8.
- Tolba AA, Mohamady SI, Hussin SS, Akashi T, Sakai Y, Galhoum AA, Guibal E. 2017. Synthesis and characterization of poly (carboxymethyl)-cellulose for enhanced La (III) sorption. *Carbohydrate Polymers* 157:1809-20.

- Tong S, Zhao X, Song N, Jia Q, Zhou W, Liao W. 2009. Solvent extraction study of rare earth elements from chloride medium by mixtures of sec-nonylphenoxy acetic acid with Cyanex301 or Cyanex302. *Hydrometallurgy* 100(1):15-9.
- Toutianoush A, El-Hashani A, Schnepf J, Tieke B. 2005. Multilayer membranes of p-sulfonato-calix [8] arene and polyvinylamine and their use for selective enrichment of rare earth metal ions. *Applied surface science* 246(4):430-6.
- Tse P. 2011. China's rare-earth industry. US: US Department of the Interior, US Geological Survey, Reston, Virginia. Open-File Report 2011–1042, 11 p.
- Tseng C, Lo S, Lo S, Chu PP. 2006. Characterization of Pt-Cu binary catalysts for oxygen reduction for fuel cell applications. *Materials chemistry and physics* 100(2):385-90.
- Uyar T and Besenbacher F. 2008. Electrospinning of uniform polystyrene fibers: The effect of solvent conductivity. *Polymer* 49(24):5336-43.
- Van Nguyen N, Iizuka A, Shibata E, Nakamura T. 2016. Study of adsorption behavior of a new synthesized resin containing glycol amic acid group for separation of scandium from aqueous solutions. *Hydrometallurgy* 165:51-6.
- Van Nguyen N, Lee J, Jeong J, Pandey B. 2013. Enhancing the adsorption of chromium (VI) from the acidic chloride media using solvent impregnated resin (SIR). *Chemical Engineering Journal* 219:174-82.
- Vander Hoogerstraete T and Binnemans K. 2014. Highly efficient separation of rare earths from nickel and cobalt by solvent extraction with the ionic liquid trihexyl (tetradecyl) phosphonium nitrate: A process relevant to the recycling of rare earths from permanent magnets and nickel metal hydride batteries. *Green Chemistry* 16(3):1594-606.
- Vander Hoogerstraete T, Wellens S, Verachtert K, Binnemans K. 2013. Removal of transition metals from rare earths by solvent extraction with an undiluted

- phosphonium ionic liquid: Separations relevant to rare-earth magnet recycling. *Green Chemistry* 15(4):919-27.
- Veleirinho B, Rei MF, Lopes-da-Silva J. 2008. Solvent and concentration effects on the properties of electrospun poly (ethylene terephthalate) nanofiber mats. *Journal of Polymer Science Part B: Polymer Physics* 46(5):460-71.
- Velu S, Watanabe S, Ma X, Song C. 2003. Regenerable adsorbents for the adsorptive desulfurization of transportation fuels for fuel cell applications. *American Chemical Society, Division of Fuel Chemistry Preprint Paper* 48(2):526-8.
- Vigneswaran S, Ngo HH, Chaudhary DS, Hung Y. 2005. Physicochemical treatment processes for water reuse. In: *Physicochemical treatment processes*. Lawrence K. Wang, Yung-Tse Hung, Nazih K. Shammam (Eds). *Handbook of Environmental Engineering* 3: 635-676. Humana Press Inc., Totowa, NJ.
- Vijayakumar G, Tamilarasan R, Dharmendirakumar M. 2012. Adsorption, kinetic, equilibrium and thermodynamic studies on the removal of basic dye rhodamine-B from aqueous solution by the use of natural adsorbent perlite. *Journal of Materials and Environmental Science* 3(1):157-70.
- Vlachou A, Symeopoulos B, Koutinas A. 2009. A comparative study of neodymium sorption by yeast cells. *Radiochimica Acta International Journal for Chemical Aspects of Nuclear Science and Technology* 97(8):437-41.
- Voice TC. 1989. Activated carbon adsorption. *Standard Handbook of Hazardous Waste Treatment and Disposal*, McGraw-Hill, New York :6.3.
- Wan Ngah W, Endud C, Mayanar R. 2002. Removal of copper (II) ions from aqueous solution onto chitosan and cross-linked chitosan beads. *Reactive and Functional Polymers* 50(2):181-90.
- Wan L, Liu Z, Xu Z. 2009. Surface engineering of macroporous polypropylene membranes. *Soft Matter* 5(9):1775-85.

- Wang C and Chen J. 2007. Studies on surface graft polymerization of acrylic acid onto PTFE film by remote argon plasma initiation. *Applied Surface Science* 253(10):4599-606.
- Wang C, Lee M, Wu Y. 2012. Solution-electrospun poly (ethylene terephthalate) fibers: Processing and characterization. *Macromolecules* 45(19):7939-47.
- Wang F, Zhao J, Wei X, Huo F, Li W, Hu Q, Liu H. 2014. Adsorption of rare earths (III) by calcium alginate–poly glutamic acid hybrid gels. *Journal of Chemical Technology and Biotechnology* 89(7):969-77.
- Wang J, Xu L, Cheng C, Meng Y, Li A. 2012. Preparation of new chelating fiber with waste PET as adsorbent for fast removal of Cu²⁺ and Ni²⁺ from water: Kinetic and equilibrium adsorption studies. *Chemical Engineering Journal* 193:31-8.
- Wang W, Yang Q, Sun L, Wang H, Zhang C, Fei X, Sun M, Li Y. 2011. Preparation of fluorescent nanofibrous film as a sensing material and adsorbent for Cu²⁺ in aqueous solution via copolymerization and electrospinning. *Journal of Hazardous Materials* 194:185-92.
- Wang X, Xu D, Chen L, Tan X, Zhou X, Ren A, Chen C. 2006a. Sorption and complexation of Eu (III) on alumina: Effects of pH, ionic strength, humic acid and chelating resin on kinetic dissociation study. *Applied Radiation and Isotopes* 64(4):414-21.
- Wang X, Li W, Meng S, Li D. 2006b. The extraction of rare earths using mixtures of acidic phosphorus-based reagents or their thio-analogues. *Journal of Chemical Technology and Biotechnology* 81(5):761-6.
- Wang C, Fang C, Wang C. 2015. Electrospun poly(butylene terephthalate) fibers: Entanglement density effect on fiber diameter and fiber nucleating ability towards isotactic polypropylene. *Polymer* 72:21-9.

- Wang L, Yang L, Li Y, Zhang Y, Ma X, Ye Z. 2010. Study on adsorption mechanism of Pb(II) and Cu(II) in aqueous solution using PS-EDTA resin. *Chemical Engineering Journal* 163(3):364-72.
- Wang X and Hsiao BS. 2016. Electrospun nanofiber membranes. *Current Opinion in Chemical Engineering* 12:62-81.
- Wannatong L, Sirivat A, Supaphol P. 2004. Effects of solvents on electrospun polymeric fibers: Preliminary study on polystyrene. *Polymer International* 53(11):1851-9.
- Watson J. 1999. Separation methods for waste and environmental applications. Marcel Dekker, NY. 616 p.
- Wenzel RN. 1936. Resistance of solid surfaces to wetting by water. *Industrial & Engineering Chemistry* 28(8):988-94.
- Werle M. 2008. Natural and synthetic polymers as inhibitors of drug efflux pumps. *Pharmaceutical Research* 25(3):500-11.
- Whitesides GM and Grzybowski B. 2002. Self-assembly at all scales. *Science* 295(5564):2418-21.
- Wojnárovits L, Földvály CM, Takács E. 2010. Radiation-induced grafting of cellulose for adsorption of hazardous water pollutants: A review. *Radiation Physics and Chemistry* 79(8):848-62.
- Wu D, Sun Y, Wang Q. 2013. Adsorption of lanthanum (III) from aqueous solution using 2-ethylhexyl phosphonic acid mono-2-ethylhexyl ester-grafted magnetic silica nanocomposites. *Journal of Hazardous Materials* 260:409-19.
- Wu H, Wu S, Wu I, Chang F. 2001. Novel determination of the crystallinity of syndiotactic polystyrene using FTIR spectrum. *Polymer* 42(10):4719-25.

- Wu J, An AK, Guo J, Lee E, Farid MU, Jeong S. 2017. CNTs reinforced superhydrophobic-oleophilic electrospun polystyrene oil sorbent for enhanced sorption capacity and reusability. *Chemical Engineering Journal* 314:526-36.
- Wu P, Wu X, Hou X, Young CG, Jones BT. 2009. Inductively coupled plasma optical emission spectrometry in the vacuum ultraviolet region. *Applied Spectroscopy Reviews* 44(6):507-33.
- Wu S, Li F, Wang H, Fu L, Zhang B, Li G. 2010. Effects of poly (vinyl alcohol)(PVA) content on preparation of novel thiol-functionalized mesoporous PVA/SiO₂ composite nanofiber membranes and their application for adsorption of heavy metal ions from aqueous solution. *Polymer* 51(26):6203-11.
- Wutticharoenmongkol P, Supaphol P, Srihirin T, Kerdcharoen T, Osotchan T. 2005. Electrospinning of polystyrene/poly (2-methoxy-5-(2'-ethylhexyloxy)-1, 4-phenylene vinylene) blends. *Journal of Polymer Science Part B: Polymer Physics* 43(14):1881-91.
- Xie F, Lin X, Wu X, Xie Z. 2008. Solid phase extraction of lead (II), copper (II), cadmium (II) and nickel (II) using gallic acid-modified silica gel prior to determination by flame atomic absorption spectrometry. *Talanta* 74(4):836-43.
- Xie F, Zhang TA, Dreisinger D, Doyle F. 2014. A critical review on solvent extraction of rare earths from aqueous solutions. *Minerals Engineering* 56:10-28.
- Xing X, Wang Y, Li B. 2008. Nanofibers drawing and nanodevices assembly in poly (trimethylene terephthalate). *Optics Express* 16(14):10815-22.
- Xiong C, Yuan M, Caiping Y, Chen S. 2009. Adsorption of erbium (III) on D113-III resin from aqueous solutions: Batch and column studies. *Journal of Rare Earths* 27(6):923-31.
- Xiong C, He R, Pi L, Li J, Yao C, Jiang J, Zheng X. 2015. Adsorption of neodymium (III) on acrylic resin (110 resin) from aqueous solutions. *Separation Science and Technology* 50(4):564-72.

- Yan G and Viraraghavan T. 2003. Heavy-metal removal from aqueous solution by fungus mucor rouxii. *Water research* 37(18):4486-96.
- Yang Y and Alexandratos SD. 2010. Mechanism of ionic recognition by polymer-supported reagents: Immobilized tetramethylmalonamide and the complexation of lanthanide ions. *Inorganic chemistry* 49(3):1008-16.
- Yang Y and Alexandratos SD. 2009. Affinity of polymer-supported reagents for lanthanides as a function of donor atom polarizability. *Industrial & Engineering Chemistry Research* 48(13):6173-87.
- Yang XJ, Livingston AG, Freitas dos Santos L. 2001. Experimental observations of nanofiltration with organic solvents. *Journal of Membrane Science* 190(1):45-55.
- Yavarpour S, Mousavi SH, Torab-Mostaedi M, Davarkhah R, Mobtaker HG. 2015. Effective removal of Ce (III) and Pb (II) by new hybrid nano-material: $\text{HnPMo}_{12}\text{O}_{40}@\text{Fe(III)}_x\text{Sn(II)}_y\text{Sn(IV)}_{1-x-y}$. *Process Safety and Environmental Protection* 98:211-20.
- Yığıtoğlu M and Arslan M. 2009. Selective removal of Cr (VI) ions from aqueous solutions including Cr (VI), Cu (II) and Cd (II) ions by 4-vinyl pyridine/2-hydroxyethylmethacrylate monomer mixture grafted poly (ethylene terephthalate) fiber. *Journal of Hazardous Materials* 166(1):435-44.
- Yoon H, Kim C, Chung KW, Lee J, Shin SM, Lee S, Joe A, Lee S, Yoo S. 2014. Leaching kinetics of neodymium in sulfuric acid of rare earth elements (REE) slag concentrated by pyrometallurgy from magnetite ore. *Korean Journal of Chemical Engineering* 31(10):1766-72.
- Yoon K, Hsiao BS, Chu B. 2008. Functional nanofibers for environmental applications. *Journal of Materials Chemistry* 18(44):5326-34.
- Yördem O, Papila M, Menciloğlu YZ. 2008. Effects of electrospinning parameters on polyacrylonitrile nanofiber diameter: An investigation by response surface methodology. *Materials & Design* 29(1):34-44.

- Younis AM, Kolesnikov AV, Desyatov AV. 2014. Efficient removal of La (III) and Nd (III) from aqueous solutions using carbon nanoparticles. *American Journal of Analytical Chemistry* 5(17):1273.
- Yuan X, Mak AF, Yao K. 2003. Surface degradation of poly (L-lactic acid) fibres in a concentrated alkaline solution. *Polymer degradation and stability* 79(1):45-52.
- Yuan X, Zhang Y, Dong C, Sheng J. 2004. Morphology of ultrafine polysulfone fibers prepared by electrospinning. *Polymer International* 53(11):1704-10.
- Zander NE. 2009. Chelating polymers and environmental remediation - Defense Technical Information Center (DTIC) document ADA495762. Dynamic Science Inc Phoenix AZ.
- Zaugg HE and Martin WB. 2011. A-amidoalkylations at carbon. In: *Organic reactions*. John Wiley & Sons, Inc. 14(2):52–269.
- Zhang C, Yuan X, Wu L, Han Y, Sheng J. 2005. Study on morphology of electrospun poly (vinyl alcohol) mats. *European Polymer Journal* 41(3):423-32.
- Zhang L, Menkhaus TJ, Fong H. 2008. Fabrication and bioseparation studies of adsorptive membranes/felts made from electrospun cellulose acetate nanofibers. *Journal of membrane science* 319(1):176-84.
- Zhang L, Wu D, Zhu B, Yang Y, Wang L. 2011. Adsorption and selective separation of neodymium with magnetic alginate microcapsules containing the extractant 2-ethylhexyl phosphonic acid mono-2-ethylhexyl ester. *Journal of Chemical & Engineering Data* 56(5):2280-9.
- Zhang S, Yang M, Liu H, Pan D, Tian J. 2013. Recovery of waste rare earth fluorescent powders by two steps acid leaching. *Rare Metals* 32(6):609-15.
- Zhang Y, Liu W, Wang Y, Tang N, Tan M, Yu K. 2002a. A novel supramolecular structure for a lanthanum picrate. *Journal of Coordination Chemistry* 55(11):1293-9.

- Zhang Y, Qian J, Ke Z, Zhu X, Bi H, Nie K. 2002b. Viscometric study of poly (vinyl chloride)/poly (vinyl acetate) blends in various solvents. *European Polymer Journal* 38(2):333-7.
- Zhang Y, Feng Y, Huang Z, Ramakrishna S, Lim CT. 2006. Fabrication of porous electrospun nanofibres. *Nanotechnology* 17(3):901.
- Zhao F, Repo E, Meng Y, Wang X, Yin D, Sillanpää M. 2016. An EDTA- β -cyclodextrin material for the adsorption of rare earth elements and its application in preconcentration of rare earth elements in seawater. *Journal of Colloid and Interface Science* 465:215-24.
- Zhao F, Repo E, Sillanpää M, Meng Y, Yin D, Tang WZ. 2015. Green synthesis of magnetic EDTA-and/or DTPA-cross-linked chitosan adsorbents for highly efficient removal of metals. *Industrial & Engineering Chemistry Research* 54(4):1271-81.
- Zhao S, Wu X, Wang L, Huang Y. 2004. Electrospinning of ethyl-cyanoethyl cellulose/tetrahydrofuran solutions. *Journal of Applied Polymer Science* 91(1):242-6.
- Zhao Z, Li J, Yuan X, Li X, Zhang Y, Sheng J. 2005. Preparation and properties of electrospun poly (vinylidene fluoride) membranes. *Journal of Applied Polymer Science* 97(2):466-74.
- Zhao J, Ding X, Meng C, Ren C, Fu H, Yang H. 2015. Adsorption and immobilization of actinides using novel SiO₂-ZrO₂-calcium alginate aerogels from high level liquid waste. *Progress in Nuclear Energy* 85:713-8.
- Zheng J, He A, Li J, Xu J, Han CC. 2006. Studies on the controlled morphology and wettability of polystyrene surfaces by electrospinning or electrospraying. *Polymer* 47(20):7095-102.

- Zheng P, Shen S, Pu Z, Jia K, Liu X. 2015. Electrospun fluorescent polyarylene ether nitrile nanofibrous mats and application as an adsorbent for Cu²⁺ removal. *Fibers and Polymers* 16(10):2215-22.
- Zhenggui W, Ming Y, Xun Z, Fashui H, Bing L, Ye T, Guiwen Z, Chunhua Y. 2001. Rare earth elements in naturally grown fern *dicranopteris linearis* in relation to their variation in soils in south-jiangxi region (southern china). *Environmental Pollution* 114(3):345-55.
- Zhu Z, Sasaki Y, Suzuki H, Suzuki S, Kimura T. 2004. Cumulative study on solvent extraction of elements by N, N, N', N'-tetraoctyl-3-oxapentanediamide (TODGA) from nitric acid into n-dodecane. *Analytica chimica acta* 527(2):163-8.
- Zong X, Kim K, Fang D, Ran S, Hsiao BS, Chu B. 2002. Structure and process relationship of electrospun bioabsorbable nanofiber membranes. *Polymer* 43(16):4403-12.
- Zuo W, Zhu M, Yang W, Yu H, Chen Y, Zhang Y. 2005. Experimental study on relationship between jet instability and formation of beaded fibers during electrospinning. *Polymer Engineering & Science* 45(5):704-9.

APPENDIX A

To estimate the mass of ligand immobilised per gram of PS nanofibre, the following explanation and estimation were made

Mass of PS-DGA-3-3 = 0.004749 g (mass weighed for TGA analysis)

Stage 1

Percentage mass loss at stage 1 (PS) = 0 %

Percentage mass loss at stage 1 (PS-DGA-3-3) = 5 % = 0.0002374g

Stage 2

Percentage mass loss at stage 2 (PS) = 0 %

Percentage mass loss at stage 2 (PS-DGA-3-3) = 43 % = 0.00202407g

Total mass loss from stage 1 and 2

5 % of initial mass loss (solvent) = 5 % of 0.004749 = 0.00023745 g

43 % of initial mass loss (PS-DGA-3-3) = 43 % of 0.004749 = 0.00204207 g

48 % of initial mass loss (PS-DGA-3-3) = 48 % of 0.004749 = 0.0022795 g

Mass of PS = Actual mass of PS-DGA-3-3 – Mass loss of 48 % DGA-2-3

The corrected mass of PS nanofibre

Actual mass of PS = initial weight of PS-DGA-3-3 – Mass of (DGA + Solvent)

Mass of PS = 0.004749 g – 0.0022795 g = 0.0024695 g

Therefore, for every 0.0024695 g of PS, 0.00204207 g of ligand (DGA) was immobilised

Therefore, for every 1 g of PS, 0.75437 g of ligand (DGA) was immobilised.

i.e 0.82691 g g⁻¹ DGA

APPENDIX B

To estimate the mass of ligand immobilised per gram of PET nanofibre, the following explanation and estimation were made from the TGA profile;

Mass of PET-DGA-2-3 = 0.004436 g (mass weighed for TGA analysis)

Percentage mass loss for Pristine PET = 0%

Percentage mass loss at PET-DGA-2-3 = 31%

Total mass loss of PET-DGA-2-3 = 31% of 0.004436 = 0.00137516 g (mass loss of DGA-2-3)

Therefore, 31 % of 0.004436 g was given off = 0.00137516 g of DGA

Mass of PET = Initial mass of PET-DGA-2-3 – Mass loss of DGA-2-3

Mass of PET = 0.004436 g – 0.00137516 g = 0.00306 g

The corrected mass of PET nanofibre 0.004436 g – 0.00137516 g = 0.00306 g

Therefore, for every 0.003061 g of PET, 0.00137516 g of ligand (DGA) was immobilised

Therefore, for every 1 g of PET, 0.44919 g of ligand (DGA) was immobilised.

i.e 0.44919 g g⁻¹ DGA